UNDERGROUND CABLE AMPACITY:
A FRESH LOOK AT ADDRESSING
THE FUTURE ELECTRIC GRID

by

Carson Bates

A dissertation submitted to the Faculty and the Board of Trustees of the Colorado School of Mines in partial fulfillment of the requirements for the degree of Doctor of Philosophy (Electrical Engineering).

Golden, Colorado

Date _____

Signed _____

Carson Bates

Signed _____

Dr. Pankaj Sen
Dissertation Advisor

Signed _____

Dr. Keith Malmedal
Dissertation Co-Advisor

Golden, Colorado

Date _____

Signed _____

Dr. Daniel Knauss
Professor and Head
Department of Electrical Engineering

ABSTRACT

Underground power cables serve a critical purpose in electric power applications and the electric grid. Many have experienced the frustration of a power outage resulting from a failed cable. This dissertation addresses underground electric power cable ampacity and provides analytical, experimental, and operational test results for underground cables. The motivation for this work stems from challenges facing the industry in determining cable ampacity due to the uncertainty in soil thermal resistivity and soil thermal stability. Analytical results compare multiple software models. Experimental results consist of radial temperature measurements of a buried cable at 3 heat rates for 5 to 21 days. Operational results include measurements of 1 kV DC combiner circuits installed at a 10 MW photovoltaic (PV) power plant.

There are numerous methodologies for calculating ampacity that can result in substantial differences. Some of these differences stem from the concern of soil dry-out described as soil thermal stability. This dissertation proposes a method to address using a soil parameter called the Non-Drying Heat Rate. Experimental results indicate that soil around a cable dries based on the magnitude of heat flux and length of time but not directly proportional to the cable diameter as proposed in the Law of Times. A set of experiments was performed on a direct buried cable to compare with the Neher-McGrath method and commercially available software programs. The results show the Neher-McGrath calculations and CYMCAP software outputs overestimated the measured temperature with a mean error of 4% ± 10% for the 6 experiments performed. Soil drying was not predicted to occur based on the non-drying heat rate measurements, and the experimental results confirmed this. A PV power plant design was used as a case study concluding that the measurements for the DC combiner cables were significantly lower than the calculated temperatures. It illustrates the need for an industry accepted standard that provides a clear methodology for addressing soil thermal resistivity and soil thermal stability.

This dissertation makes the following contributions:

1. Illustrates the need for an industry standard that addresses soil thermal stability
2. Proposes the non-drying heat rate method to address soil thermal stability
3. Indicates that the Neher-McGrath method is conservative by experimentation
4. Indicates no soil drying occurred during experimentation, as predicted by the non-drying heat rate method
5. Provides cable temperature measurements of an operational PV power plant

TABLE OF CONTENTS

LIST OF FIGURES

LIST OF TABLES

ACKNOWLEDGEMENTS

I am extremely grateful for the assistance I received throughout this academic pursuit. My sincere thanks go to: my Lord and Savior Jesus Christ—for the strength, knowledge, and wisdom necessary to complete this work; my wife, who encouraged me and graciously supported me with selfless love; my parents, who inspired me to pursue this degree and lovingly raised me through the years; my advisor, Dr. PK Sen, who engendered my passion for the electric power industry as an undergraduate and continued to share his knowledge and wisdom throughout this study; my co-advisor, Dr. Keith Malmedal, who mentored me in research, technical writing, experimentation—instilling confidence in me to begin this endeavor. This work would not have been possible without their sacrifices and support. Thank you.

CHAPTER 1
INTRODUCTION TO CABLE AMPACITY

Underground power cables serve a critical role in the electric grid. Many people can relate to the frustration of a power outage that can be a result of a failed cable. For some cases, the consequences are more severe including loss of equipment, material, production, and sometimes life. The term *cable* is used in this dissertation to describe an electric conductor, covered by insulation, buried underground. Cables are used extensively in all kinds of power distribution applications. Underground cables are becoming more common than overhead lines for power delivery at medium voltage (5 kV to 35 kV) particularly for new urban installations and new residential subdivisions. There are numerous reasons for this change such as: aesthetics, reduced land use, and less-frequent electrical faults due to weather, trees, or pests. In some cases, underground cables are safer than overhead lines since physical contact is more difficult and the conductor is protected with a grounded shield. Beyond this, technological advances have improved reliability, reduced cost, and eased installation difficulties prompting cities to standardize on underground cables for power delivery. Renewable generation power plants, such as wind and PV, utilize underground cables as standard. This has significantly increased the use since a typical wind farm may contain 200 miles of underground cable.

With increased installation comes increased emphasis on proper design for higher reliability. This is compounded with higher expectations from consumers, more stringent monitoring of the national reliability indices such as SAIDI and SAIFI[1], and penalizes utilities for poor performance. The wind and solar renewable generation industries (typically driven by developers or independent power producers—IPPs) have a different perspective than utilities but place equal or greater emphasis on the design of the cable installation. These facilities do not design for system growth that utilities commonly use. In addition, the cost of the installation is a major factor for financial viability of the project. Therefore, it is critical that the cables are properly engineered to minimize the cost while achieving the full design life of the facility, typically 20 to 30 years.

Many factors are involved in specifying a cable such as conductor material, conductor size, insulation thickness, and insulation type. This dissertation focuses on the conductor size because of its impact on ampacity. Cables are manufactured with a range of conductor sizes. For a given load, conductor size determines the heat rate of the cable primarily due to resistive

[1] SAIDI (System Average Interruption Duration Index) and SAIFI (System Average Interruption Frequency Index) are reliability metrics used by electric utilities to measure power outage duration and frequency of occurrence primarily for electric distribution networks (less than 46 kV)

losses, which are proportional the square of the current. Resistive losses are also commonly referred to as joule heating or I^2R losses ("I" is current Amperes and "R" is resistance in Ohms). Cable ampacity is defined according to the National Electrical Code (NEC) as "the maximum current, in amperes, that a conductor can carry continuously under the conditions of use without exceeding its temperature rating" [1, Sec. 100]. The term, "ampacity" is portmanteau used in the industry for current (Ampere) capacity combined as Amp-acity. There are other parameters that impact the cable construction. These include insulation thickness, shield type, jacket, and armor. However, these all relate primarily to the system operating voltage, installation method, and system grounding—specified early in the design and beyond the scope of this dissertation. Once the overall system design has been determined, the critical design value is ampacity for a conductor size or conductor size for a required operating current.

A design engineer typically determines the conductor size based on a required ampacity, but occasionally determines the ampacity based on a given conductor size. The ampacity must be greater than the continuous operating current or maximum operating current adjusted for load factor (see Section 9.1.3 Load Factor). Emergency loading—that is, current above the maximum continuous current typically four hours or less—is calculated based on the selected cable size and does not control the design. Short circuit current magnitude and duration for both the primary conductor and the shield can control the design, but the short duration requires calculation methods beyond the scope of this dissertation. Some site-specific data affecting cable ampacity cannot be adjusted while other parameters can. These are discussed in greater detail in this dissertation including burial depth, the spacing between cables, and backfill material. The following figures illustrate some common installation methods for typical 3-phase power cables. Figure 1.1 illustrates a single circuit, i.e. one 3-phase load connection. Conduit is used to provide additional protection to the cables and allow for cable replacement—provided the cable is not melted into the conduit as a result of an electrical fault. Direct buried cables reduce the cost of installation because the cables can be laid into position rather than pulled through the conduit. Figure 1.2 illustrates multiple 3-phase circuits, and Figure 1.3 illustrates circuits encased in concrete or fluidized backfill.

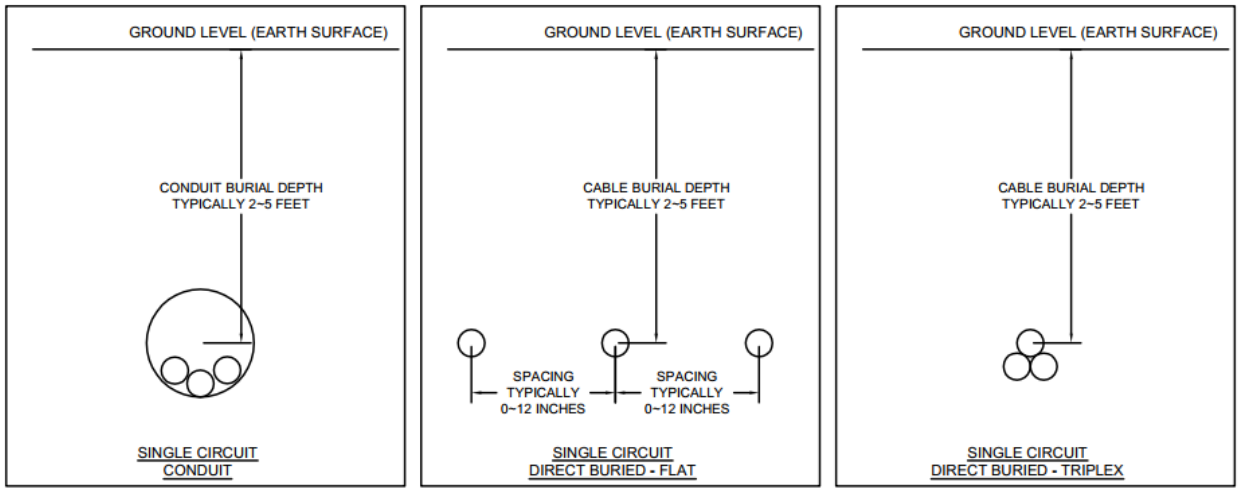

Figure 1.1 Typical cable installation details for single circuits

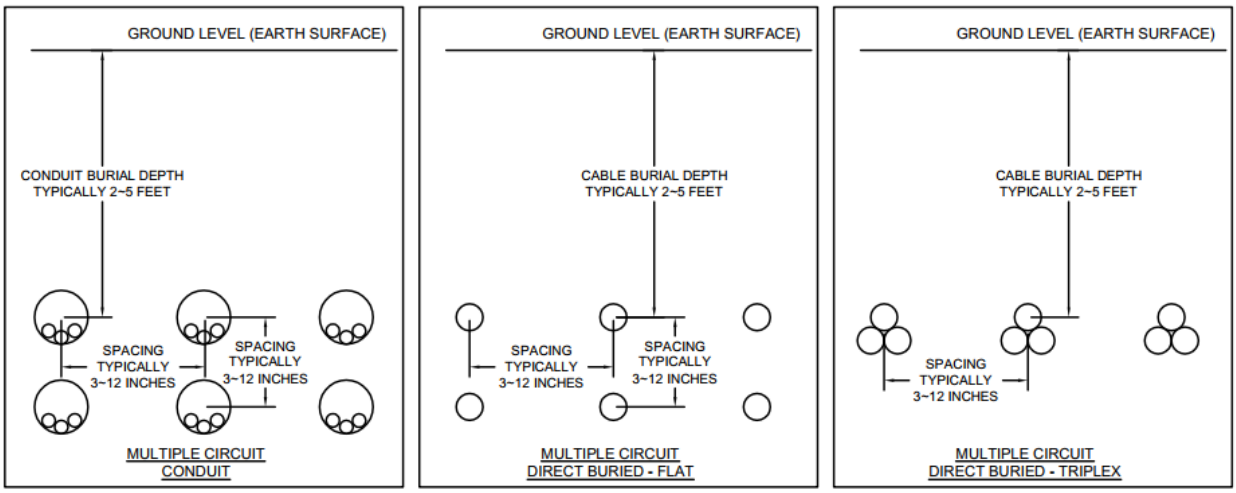

Figure 1.2 Typical cable installation details for multiple circuits

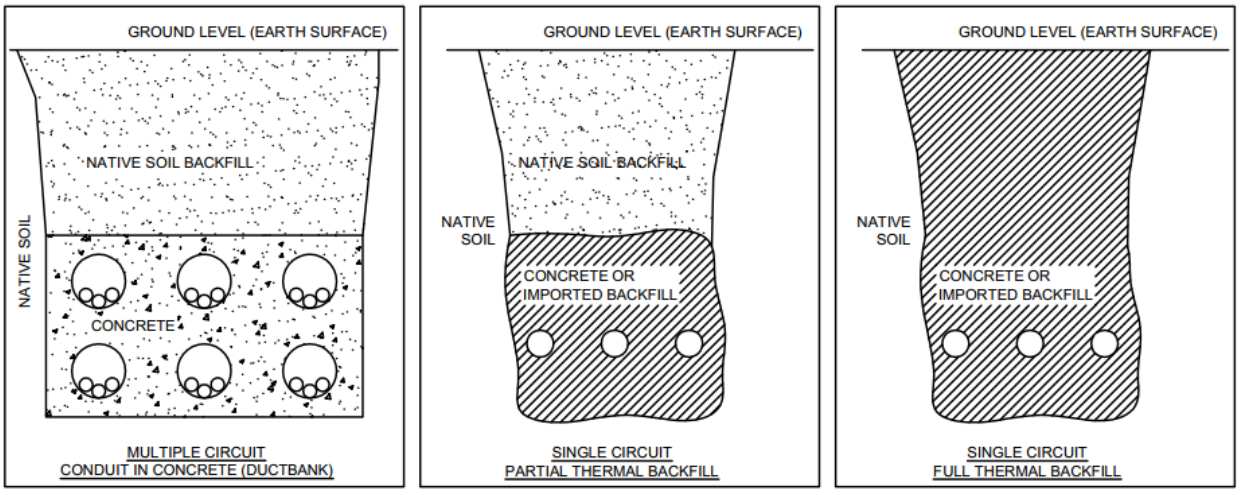

Figure 1.3 Typical cable installation details for concrete backfill

These figures give the impression that cable installation details are fairly simple. Frequently, however, the installation is more complicated due to multiple circuits as shown in the following figures.

Figure 1.4 Examples of complicated cable installations

Determining the ampacity for cables installed with multiple circuits is a challenge, and it's the engineer's job to determine the installation requirements such as spacing and depth. Installing multiple circuits, or even a single circuit carrying high current, requires significant heat dissipation to avoid operating temperatures that exceed the insulation temperature rating. Cables are typically buried for safety and to protect them from physical damage, but this has the negative effect of insulating them from the primary cooling method: ambient air. This insulating effect increases if the soil begins to dry out due to the heat generated by the cables.

The purpose of this dissertation is to address the effect of soil thermal resistivity on underground power cable ampacity and soil's tendency to dry as a result of heat generated by power cables. Though the concepts are applicable to all buried cables, medium (5 kV to 35 kV) and high voltage (greater than 35 kV) direct buried cables (cable in direct contact with the earth) are the focus due primarily to the greater impact of soil, the higher cost, and the greater importance of such installations.

1.1 History of Determining Cable Ampacity

The practice of determining cable ampacity has a long history, almost to the beginning of the electric power industry; one of the earliest sources is A. E. Kennelly in 1889. He primarily addressed it for the telegraph industry: “In August 1889, a report was made by one of the present writers to the Edison Electric Light Co., on ‘The Heating of Conductors by Electric Currents.’ The report was published in the minutes of the convention of the Association of Edison Illuminating Companies, at Niagara Falls, August 1889.” [2]. Other sources were published around the same time, but Kennelly became a key reference for future work on cable ampacity. Much of the original work examined cables in air and underground even though the heat transfer principles related to cables in air are significantly different than those underground. The heat for cables in air is primarily dissipated by convection and radiation. The heat for cables underground is primarily dissipated by conduction. This was not well understood at the time since the heat transfer field of study was still in development.

In June 2015, Holyk and Anders published a paper titled, “Power Cable Rating Calculations — A Historical Perspective” [3]. This paper provides significant details on the development of cable ampacity, both in air and underground, and provides a visual timeline of the key advances. This is shown in the following figures.

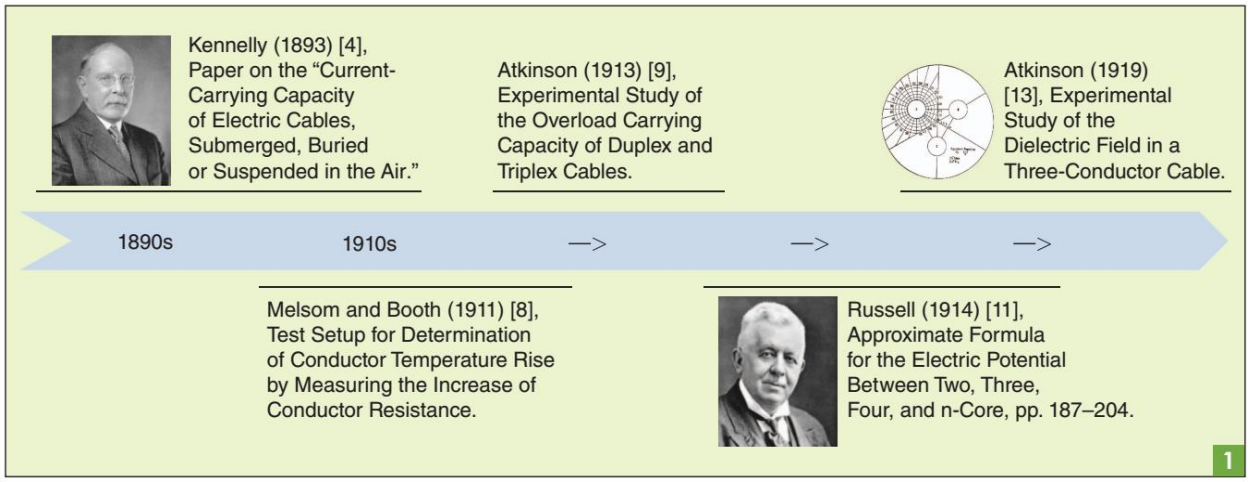

Figure 1.5 Ampacity calculation development timeline: 1890s to 1910s [3] © 2015, IEEE

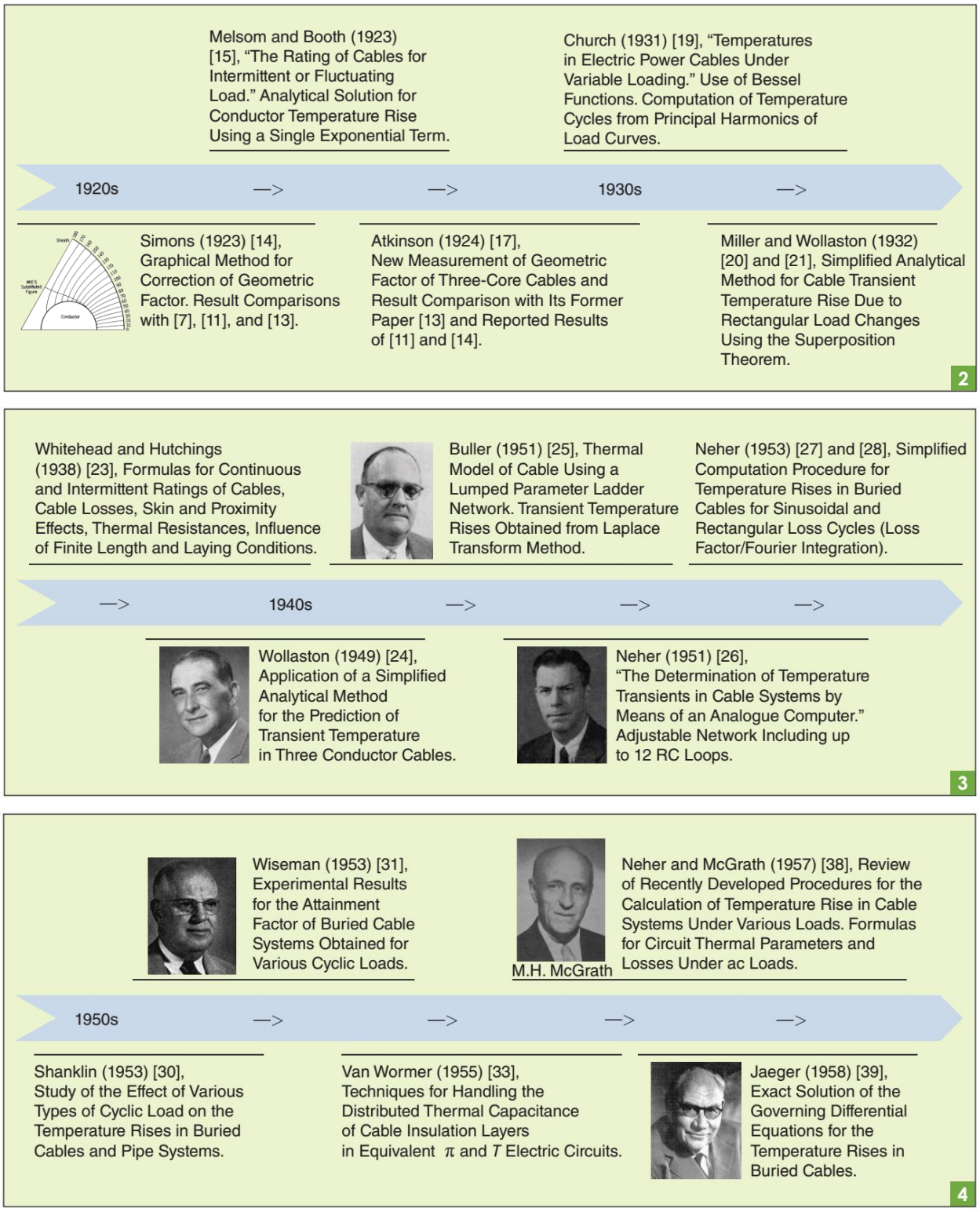

Figure 1.6 Ampacity calculation development timeline: 1920s to 1960s [3] © 2015, IEEE

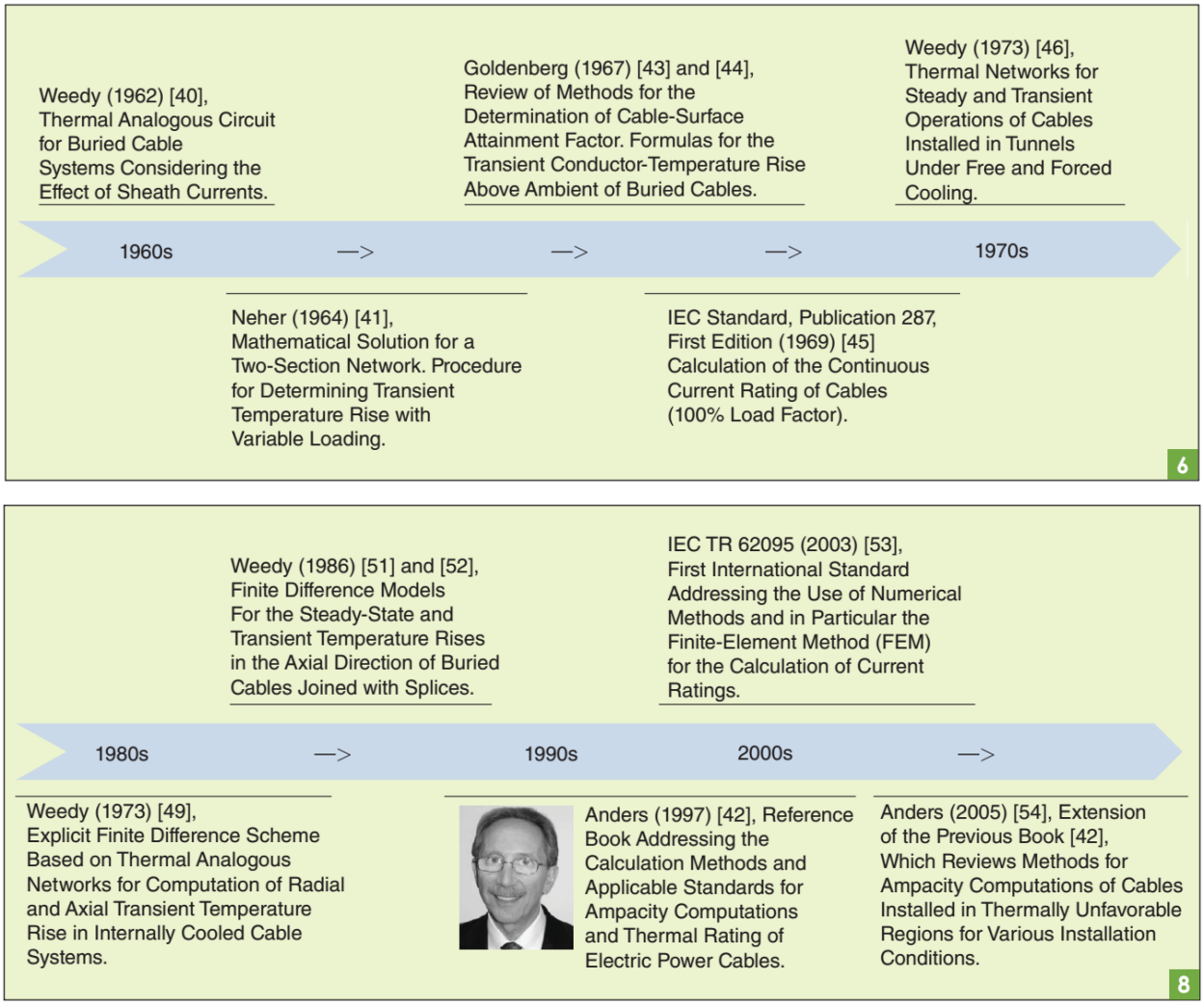

Figure 1.7 Ampacity calculation development timeline: 1960s to 2000s [3] © 2015, IEEE

Significant contributions to the underground cable ampacity problem include Kennelly's paper in 1893 [4] (after his first report in 1889 [2]), Simmons' paper in 1923 [5], Melsom and Booth's paper in 1923 [6], Whitehead and Hutchings' paper in 1938 [7], and the summary work of Neher and McGrath's paper in 1957 [8]. Absent from this list but key to ampacity determination is Simmon's group of papers entitled "Calculation of the Electrical Problems of Underground Cables" [9]. Once the summary paper by Neher and McGrath was published in 1957, the majority of cable ampacity calculations followed the analysis in that paper, and the renowned *Black Books* were generated [10]. These books list cable ampacities in table format for a variety of installation conditions (see Section 2.1.1 Black Books). Clearly, this met the needs of the industry in the United States because even today some engineers continue to use these for sizing cables. The next update related to continuous cable ampacity was made in the form of an IEEE standard — IEEE Std 835 [11]. Though this was an update, the ampacity

calculation method provided by Neher and McGrath—now commonly referred to as the Neher-McGrath method—was not altered. It primarily updated some of the cable construction parameters based on material and manufacturing developments (see Section 2.1.2 IEEE Std 835). This IEEE standard is quite comprehensive and voluminous. Because of this, it is the most frequently used reference by engineers for cable sizing—providing tables for a *quick look-up method* for a particular design rather than extensive calculations. A subset of the tables is given in the NEC [1, Sec. 300], and this results in the most significant use of this standard since NEC compliance is required for the majority of cable installations.

The state of the industry for determining ampacity predominantly involves the use of the IEEE Std 835 tables, often in the form of the NEC's republication of a limited number of cases. These tables adequately characterize heat transfer parameters for the cable construction but provide limited characterization of the surrounding medium of the cable even though this significantly impacts the ampacity. One significant parameter is the *soil thermal resistivity* (frequently shortened to *resistivity* in this dissertation unless otherwise noted—not to be confused with *electrical resistivity*). Far from comprehensive, only three values are given in the tables. Additionally, this does not consider the impact of *soil moisture*—a significant factor of soil resistivity. So, the most frequently used method for determining cable ampacity does not address the two most important factors that impact that very value: *soil thermal resistivity* and its dependence on moisture content, referred to as *soil thermal stability*.

Some attempts have been made to characterize the soil surrounding buried cables related to moisture content. One notable contribution was made by Groeneveld et. al [12] that provides a method for determining the propensity of soil to dry out. IEC 60287-1 does address soil dry out using this type of approach [13]. However, the parameters required for implementing the approach are based on the soil for a given location and are difficult to measure. As summarized by Anders, "strict mathematical explanations and physical models describing moisture migration phenomena are very complicated, and adequate evaluations of the quantities concerned have not yet been made" [14, p. 60]. The method to address soil dry out related to cable ampacity is not well-defined, at least in a manner that can be confidently used by engineers.

1.2 Importance of Ampacity

Ampacity is fundamentally a temperature limited design. Ideally, the conducting power from the generating source to the receiving load would be performed by a very small conductor. The conductor size for low-power devices is close to this ideal since it is primarily determined by

mechanical strength rather than ampacity. As the power requirements increase, ampacity becomes the dominant design factor. The cable must maintain a temperature within the temperature rating of the insulation, i.e. the cable size is limited by its ampacity. Temperature ratings for insulation types are defined by the manufacturer (see Section 2.2.2 Parameters Involving Thermal Resistance) with a typical continuous operating limit of 90°C.

"Using accurate cable ampacities is critical to electrical power system design. An optimally sized cable results in minimum cost and high reliability. Wind and solar power plants, in particular, strive to optimize cable design by using ampacities that closely match maximum generation without including a growth factor or other safety factor. Cable ampacities have been estimated over the years based on engineering assumptions and site conditions. Various configurations require different parameters and assumptions. Cables placed underground require information about the ambient earth temperature, cable separation distance, soil thermal resistivity, etc. If these parameters or assumptions are inaccurate, the resulting cable size will also be inaccurate. This may lead to cable overheating if the cable is undersized or increased cable cost if the cable is oversized" [15].

1.3 Factors of Ampacity

There are two parts to this temperature problem: heat removed from the cable and heat generated in the cable. The following figures illustrate an underground cable installation.

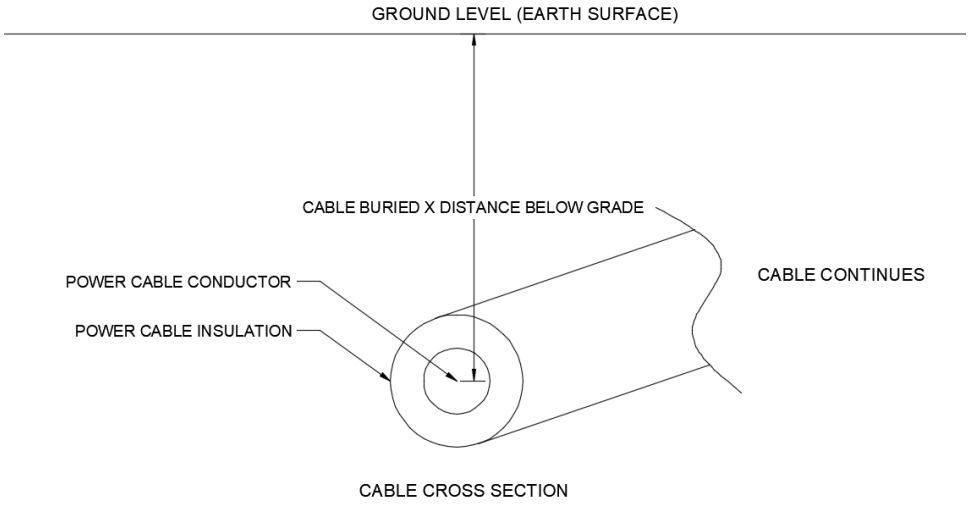

Figure 1.8 Cable cross section

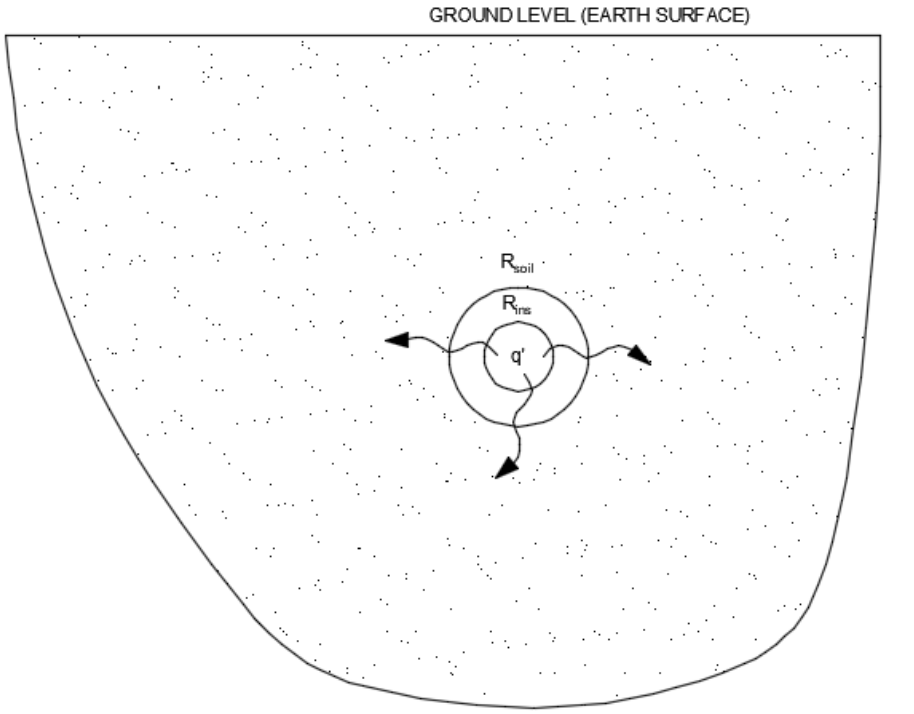

Figure 1.9 Cable cross section showing thermal characteristics

Heat transfer can occur through three primary modes: conduction, convection, and radiation [16]. Conduction is the only important mode by which heat is removed from an underground cable. It is limited by each material between the heat source and the heat sink. These materials generically include conductor covering materials (internal to the cable) and soil types (external to the cable). Each of these factors represents a resistance to heat that affects cable temperature rise. The parameter that characterizes the resistance to heat is referred to as thermal resistivity, or its inverse, thermal conductivity. Additional details of the following paragraphs are provided in Chapter 2.

Heat generated by the conductor is first impeded by the material covering the conductor, termed *insulation*. The conductor covering types, specified by the engineer and determined by cable manufacturers, do not substantially change for a given system design voltage. That is, the insulation thickness increases for increasing voltage at standard increments with material properties that are similar throughout the industry (see Section 2.2.2 Parameters Involving Thermal Resistance). The largest thermal resistance of the conductor covering is the insulation, followed by the jacket. The remaining components such as screens and shield wires do not significantly impact the resistance. These coverings provide benefits electrically, primarily by preventing faults, but they negatively impact the thermal performance of the cable. The thermal

resistance of materials used for cables cannot be significantly reduced without sacrificing other key features of a cable such as its electrical resistance, flexibility, and durability. So, these values change very little from one cable installation to another. The following figures show the basic components of a cable.

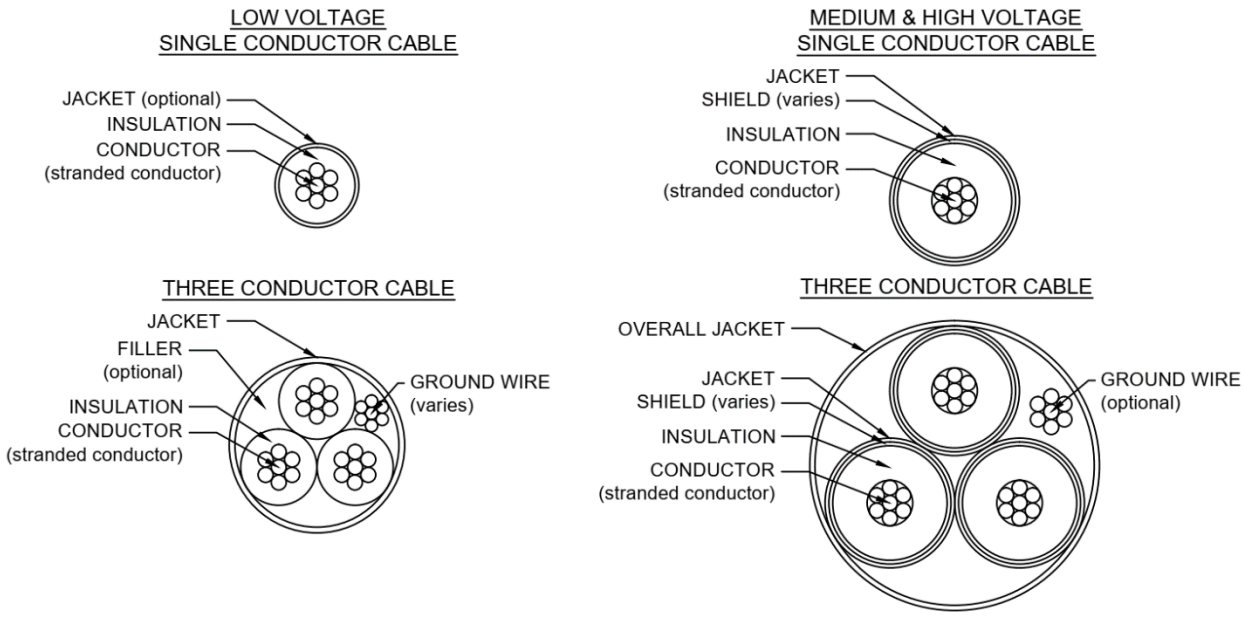

Figure 1.10 Cable components: low voltage and medium & high voltage

Conversely, soil parameters vary significantly from one installation to another. In addition, soil thermal resistance makes up a significant portion of the total thermal resistance from the heat source to the heat sink. For example, the soil thermal resistance for a direct buried 15 kV cable accounts for 70% to 90% of the total thermal resistance depending on the soil resistivity. Soil parameters include thermal resistivity, moisture content, and thermal stability. Moisture content is predominantly a function of the geographic installation location. For example, dry climates commonly found in the western United States create low soil moisture contents while wetter climates found in the eastern United States create high soil moisture contents. The minimum soil moisture content should be determined for each installation site, with typical ranges of 5%-10% water weight as a percentage of dry soil weight (see Section 2.2.2 Parameters Involving Thermal Resistance and Section 3.3.1 Site Specific Data Collection). Thermal resistivity depends on the soil type, compaction of the soil, and the moisture content. If imported backfill is used, it will also modify the thermal resistivity of the soil around the cable and must be measured for use in ampacity calculations. Soil thermal resistivity

has the largest range of values for all of the thermal resistances involved in an underground cable installation and is the focus of this dissertation.

Having summarized the thermal resistance to heat transfer, heat transfer will be addressed. Heat is dissipated from the cable (source) through the surrounding soil into the atmosphere (sink). Eventually, all heat flows into space since the core of the earth is actually a heat source and not a heat sink. This is intuitive in the winter when the air temperature is cooler than the soil temperature. It is not as intuitive in the summer when the air is warmer than the soil. In this case, the soil can be considered a thermal mass that will absorb the heat energy generated in the cable and then dissipate it to the air some time later, possibly even a few months later depending on air and soil temperatures. When determining ampacity, it is customary to use the soil temperature at the burial depth of the cable. The impact of the soil temperature is discussed in more detail in Chapter 2 Ampacity Calculation Methods.

Heat is generated in the cable by conductor resistive losses, dielectric losses, and shield losses. Heat can also be generated by duct or conduit losses—the medium surrounding the cable(s)—as in steel conduit or pipe-type cables. “In general, there are two type of losses generated in a cable: current-dependent losses and voltage-dependent losses” [14].

Of current-dependent losses, conductor resistive losses are the most obvious and largest heat source for most cable installations. These losses are a result of current through a resistance, commonly called “I^2R losses” or Joule heating. Resistance is determined by the conductor material, cross-sectional area, temperature, and skin effect. The conductor material for power cable applications is either copper or aluminum. Each of these materials has a resistivity (or the inverse: conductivity). According to Southwire’s, a well-known cable manufacturer, Power Cable Manual: “Conductivity is typically specified in percent. This percent is based on an International Annealed Copper Standard (IACS)” [17]. Therefore, the resistance for a given conductor is the same from one installation to another with limited deviation due to manufacturers’ tolerances. In addition to conductor losses, cables utilizing a shield, which includes most cables above 2.4kV, are heated by the resistive losses through the shield due to circulating currents. This can be more significant than the primary conductor losses for large separation between cables [18]. The magnitude of these shields losses depends on the shielding type (both material and cross-sectional area) and the grounding of the shield. Additional information on shield grounding, which can impact ampacity by 25% or more, can be found in IEEE Std 575 [19].

Voltage-dependent losses involve dielectric losses and charging current. Dielectric losses generate heat from the realignment of the insulation molecules caused by the alternating

electric field of the conductor. Charging current is generated by the capacitor created by the conductor and the shield separated by the insulation. Charging current losses are I^2R losses, as discussed in the previous paragraph, but are voltage dependent—generating heat when the cable is energized. Voltage dependent losses should be included for high voltage cables but can be neglected for operating phase-to-phase voltages of 15kV or less or up to 35kV and less for single circuits [11]. Both dielectric losses and charging current losses depend on the dielectric constant. Dielectric constants vary slightly between extruded insulation cable types as well as oil impregnated paper insulation. Typical values of dielectric constants are provided below [20].

Table 1.1 Dielectric constants

Material	Range ε_r	Typical ε_r
EPR	2.5 - 3.5	3.0
TR-XLPE2	1.0 - 2.6	2.3
Paper, impregnated	3.3 - 3.7	3.5

Heat transfer is determined by some general equations. Since cable ampacity is based primarily on conduction, the fundamental equation is derived from Fourier's law. According to Bergman, et. al [16], "Fourier's law is phenomenological; that is, it is developed from observed phenomena rather than being derived from first principles. Hence, we view the rate equation as a generalization based on much experimental evidence." The simplified equation is $q'=\Delta T/R'$, where q' is the heat rate per unit length (W/cm), ΔT is temperature difference (°C or K), and R' is thermal resistance per unit length (°C·cm/W). For a cylindrical wall, R' is determined by the following equation $R'_{cyl}=\rho/2\pi\cdot\ln(r_o/r_i)$ where ρ is the resistivity of the material (°C·cm/W) and r is the radius (cm), inner or outer, of the material boundary. For a cylinder in soil, the *shape factor* is used, which is an analytical solution to the heat diffusion equation. The assumption is a horizontal isothermal cylinder of length L, buried in a semi-infinite medium. There are two forms of this shape factor depending on the ratio of burial depth and cylinder diameter. Cable installations use a burial depth greater than 1.5 times the cable diameter, so the shape factor per unit length is $2\pi/\ln(4\cdot z/D)$ where z is the burial depth and D is the cable diameter [16]. This is shown in the following figure.

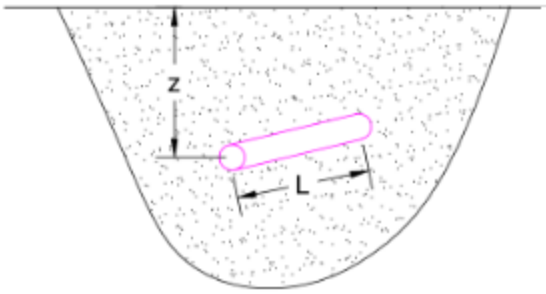

$$S = \frac{2\pi L}{\ln\left(\frac{4z}{D}\right)}$$

$$q = \frac{S}{\rho} * \Delta T$$

Figure 1.11 Buried cable shape factor

The resistance per unit length of the cable to the surface (R') is calculated by dividing the resistivity of the soil ρ (°C·cm/W) by the shape factor per unit length:

$$R' = \frac{\rho \cdot \ln\left(\frac{4z}{D}\right)}{2\pi} \left(\frac{°C \cdot cm}{W}\right)$$

When multiple cables are involved and heat is generated by the shield and insulation, the use of these equations becomes increasingly difficult. That is why empirically based methods have been used for many years, which are based on analytical models with few assumptions. More recently, the problem can also be solved numerically using finite element analysis as discussed in Chapter 5.

1.4 Failure Modes

A primary reason to accurately determine cable ampacity is to reduce cable failures from overheating and insulation breakdown. A failure is typically defined as a short circuit of the cable from one phase to another or from phase to ground; however, another failure is in open circuit condition experienced during a break in the cable. Significant research has been performed on cable failure modes. According to a NEETRAC (National Electric Energy Testing Research and Applications Center at Georgia Tech) report, "A power cable system fails when local electrical stresses are greater than the local dielectric strength of dielectric material(s). The reliability, and thus, the rate of failure of the whole system depend on the difference between the local stress and the local strength" [21]. Two self-explanatory figures from this same report are shown below, summarizing the various deteriorations.

Table 4: Aging and Degradation Mechanisms for Accessories of Extruded Cable

Type of Deterioration	Aging Process	Accessory Type	Typical Causes	Example
Dry Electrical	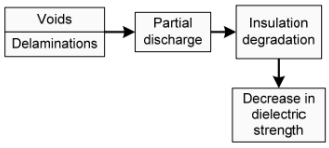	Joint, termination, separable connector	Manufacture defects, natural aging, poor workmanship	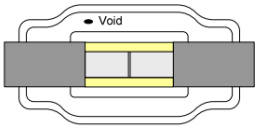
Electrical Interface	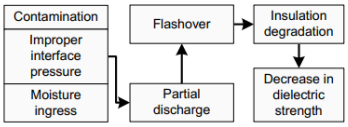	Joint, termination, separable connector	Moisture ingress, poor workmanship	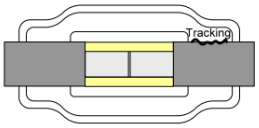
Electrical External	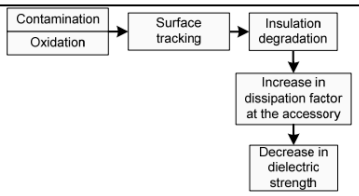	Termination	Pollution, Ultra Violet (UV) degradation	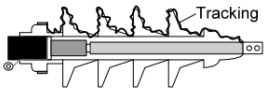
Thermal	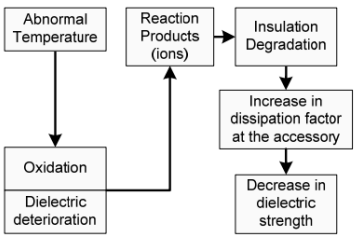	Joint, termination, separable connector	Excessive conductor current for a given environment and operating conditions, failed connectors	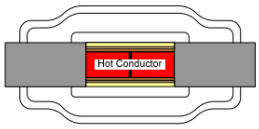

Figure 1.12 Cable accessory failure modes [21]

Table 2: Aging and Degradation Mechanisms for Extruded Cable

Type of Deterioration	Aging Process	Typical Causes	Example
Thermal	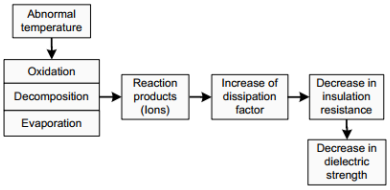	Excessive conductor current for a given environment and operating conditions	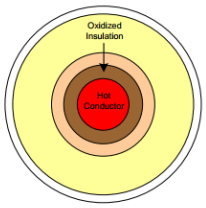
Dry Electrical	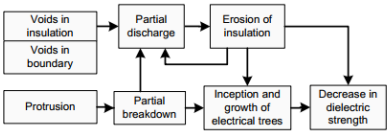	Manufacturing imperfections (i.e. voids, contaminants), mechanical damage	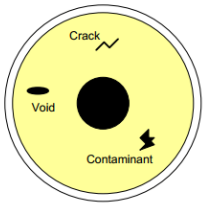
High Density of Small Water Trees	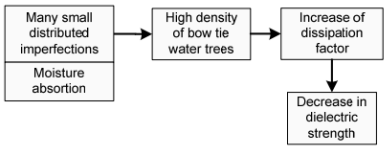	Moisture ingress (external and via conductor)	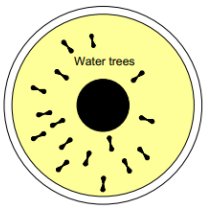
Large Water Trees	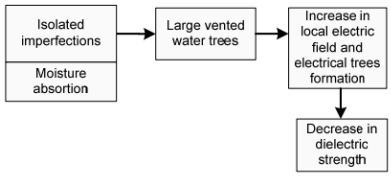	Moisture ingress	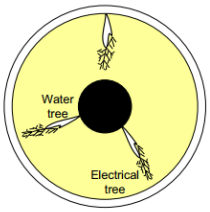
Chemical	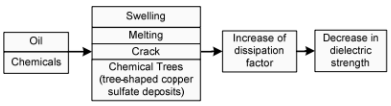	Petrochemical spills, transformer oil leaks, fertilizers	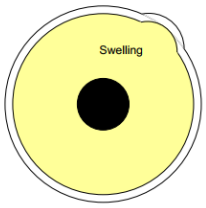
Neutral Corrosion	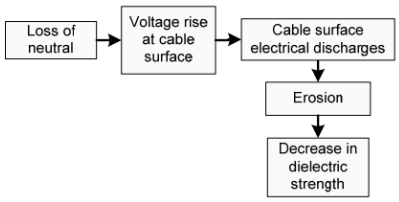	Unjacketed cable in soil that enhances copper (Cu) corrosion, jacketed cable with corrosive water ingress	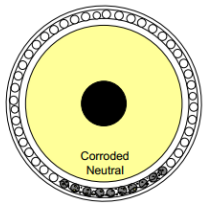

Figure 1.13 Cable insulation failure modes [21]

Note that the report states: “Mechanisms that lead to rapid failure (thermal runaway and extremely high local stresses from contaminants) are omitted as they bypass the degradation step and thus do not permit intervention” [21]. Thermal runaway is a concern related to cable ampacity and the soil thermal stability as discussed in more detail in Chapter 6 Soil Thermal Stability. Beyond the failure modes, cable reliability must also be considered. The following failure frequency statistics are provided by the NEETRAC report [21].

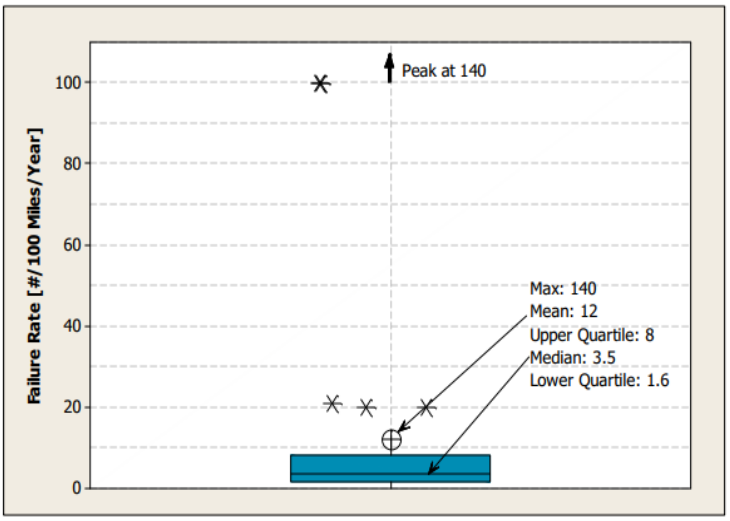

Figure 7: Estimate of North American MV Cable System Failure Rates

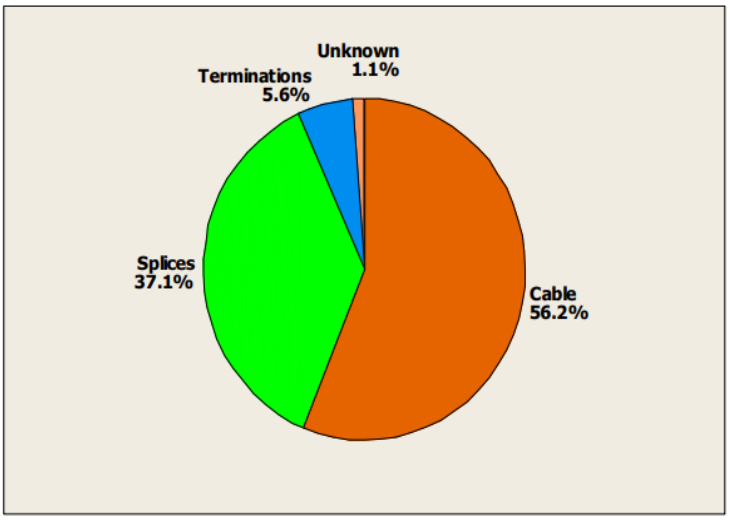

Figure 8: Estimated Dispersion of North American MV Cable System Failures by Equipment Type

Figure 1.14 Cable failure rates [21]

This indicates that splices and cables are a leading cause of failure, both of which are underground and are significantly impacted by temperature. For example, a study on a wind farm cable failure describes that the failure of a cable splice was caused by excessive temperature due to inadequate cable sizing [22].

CHAPTER 2

AMPACITY CALCULATION METHODS[2]

Engineers have calculated cable ampacity from the time cables were first manufactured. It's an important technical requirement. The method for determining the ampacity has developed over the years as described in Chapter 1. The modern calculation methods include the Neher-McGrath method (1957) [8], the IEC 60287-1 method (1982 and based on the Neher-McGrath method) [13], and finite element analysis (1997) [23]. However, it is a common practice for engineers to avoid calculations altogether by utilizing IEEE Std 835 (1994) that provides tabulated ampacities based on the Neher-McGrath method for a variety of conditions [11]. Some engineers still continue to use the so-called "Black Books" (1962), which are an older version of the IEEE Std 835.

The fundamental equation for the most commonly used ampacity calculation, the Neher-McGrath method is [8]:

$$I = \sqrt{\frac{T_c - (T_a + \Delta T_d)}{R_{dc}(1 + Y_c)R_{ca}}}\ kiloamperes$$

Where:

I = current [kA]

T_c = conductor temperature [°C]

T_a = ambient temperature [°C]

ΔT_d = dielectric loss temperature rise [°C] (neglected for operating voltage less than 35kV)

R_{dc} = dc resistance of conductor at temperature T_c [μΩ/ft]

Y_c = component of ac resistance resulting from skin effect and proximity effect

R_{ca} = effective thermal resistance between conductor and surrounding ambient [thermal ohm-feet, °C-ft/W]

The other commonly used calculation, developed based on and alongside the Neher-McGrath method—IEC 60287—is similar in result, but is shown with each of the components more separated [13].

$$I = \sqrt{\frac{\Delta\Theta - W_d[0.5\ T_1 + n\ (T_2 + T_3 + T_4)]}{RT_1 + nR\ (1 + \lambda_1)T_2\ +\ nR\ (1 + \lambda_1 + \lambda_2)(T_3 + T_4)}}$$

Where

[2] Parts of the material contained in the first section of this chapter were previously published in IEEE Transactions [15] Copyright © 2016, IEEE

I = current [A]

R = ac resistance of conductor at maximum operating temperature [Ω/m]

W_d = dielectric loss [W/m]

T_1 = thermal resistance between one conductor and sheath [K·m/W]

T_2 = thermal resistance of the bedding between sheath and armor [K·m/W]

T_3 = thermal resistance of the external serving (jacket) [K·m/W]

T_4 = thermal resistance between cable surface and the surrounding medium [K·m/W]

n = number of load-carrying conductors in the cable

λ_1 = ratio of losses in metal sheath to total losses in all conductors in the cable

λ_2 = ratio of losses in armoring to total losses in all conductors in the cable

2.1 Methods

2.1.1 Black Books [10]

The “Black Books”, entitled AIEE-IPCEA Power Cable Ampacities [10], were the first tabulated ampacities using the Neher-McGrath method and were published in 1962. This allowed an engineer to look up the appropriate cable size based on the current rather than calculating the cable size using Neher-McGrath calculations [8]. Considering the number of calculations needed to determine ampacity using the Neher-McGrath method, it is obvious why engineers would prefer using this simplified tabular method.

It is important to understand the assumptions used to create these tables. For example, one assumption used in the tables is that the ambient temperature of the earth is 20°C. Many locations in the Southwest USA experience maximum underground soil temperature of 25-30°C, which reduces the ampacity by 5-8% below the tabulated values, as determined by the Neher-McGrath equations. The tabular values must be adjusted for soil temperature by using methods included in the introductory pages of the Black Books [10].

Another assumption is that the cable depth is 36” and the cable spacing is 7.5”. If the burial depth was actually 18”, this would increase the ampacity by approximately 10%, and doubling the spacing would increase it by approximately 6%. Adjustment factors for these assumptions are not given in the tables, so the Neher-McGrath calculations must be done if conditions of depth or spacing vary from the assumptions. Furthermore, modern cables use different insulation material and thickness than those used in these older tables. These tables also assume the cables are not jacketed [10]. All of these assumptions may present difficulties for a modern user and, if differences are ignored, can result in cables that are sized too large or too small.

The key assumptions in these tables are listed below. The physical configuration is shown in the following figure:

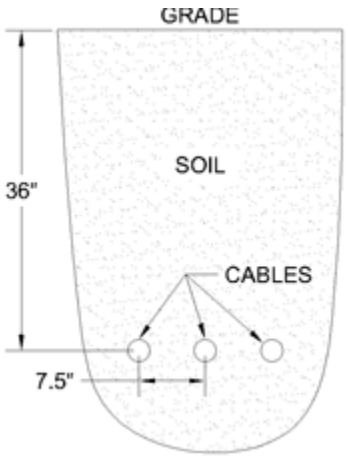

Figure 2.1 Example cable installation

- 20°C ambient earth temperature
- 90°C maximum conductor temperature
- Cable shields single point grounded
- 36” depth
- 7.5” spacing
- Generic rubber insulation
    - Thicker than modern insulations (XLPE or EPR) for equivalent voltage rating
    - Higher thermal resistivity (500°C·cm/W versus modern 350°C·cm/W)
    - Higher insulation power factor resulting in higher dielectric losses (3.5% versus modern 0.5%)

2.1.2 IEEE Std 835 [11]

In 1994, a new set of tabulated ampacities entitled “IEEE Std 835 Cable Ampacity Tables” was issued by the IEEE in order to: “update the cable constructions and design changes that had taken place since the original publication [of the Black Books]” [11]. While maintaining the fundamental calculations set forth by Neher-McGrath, the tables include updated information on cable properties and adjust some of the original assumptions. This includes assuming a 25°C ambient earth temperature and cable shields that are shorted, i.e. grounded at both ends, for most cable sizes. The standard also includes some step-by-step examples of the Neher-McGrath method with updates that address changes in assumptions of the original method [11]. The steps given assist an engineer in developing a spreadsheet to

calculate ampacity for any cable configuration, which eliminates the need for the tables except as a convenient check.

The key assumptions for these tables are given below:

- 25°C ambient earth temperature
- 90°C maximum conductor temperature
- Cable shields shorted
- 36” depth
- 7.5” spacing

2.1.3 Software Modeling

Commercially available computer software allows for the calculation of cable ampacity by modeling the cable properties and the physical configuration. The cables can be modeled with the intended design geometry and with the intended cable type. Programs utilize values of cable thermal resistivity as specified by IEEE Std 835 [11] for each material type (e.g. EPR is 350°C·cm/W), allowing the thickness and order of the components to be adjusted. Programs are typically advertised as using the Neher-McGrath method to determine ampacity, meaning the only assumptions necessary are those inherent to the Neher-McGrath method.

2.2 Neher-McGrath Method

The Neher-McGrath method is the cornerstone paper [8], [11], providing numerous equations that result in an estimate for a certain cable ampacity. Appendix A illustrates the use of these equations. The following sections summarize and discuss the parameters used. To provide clarity, the parameters involving heat generation will be described first, followed by the parameters involving thermal resistance. Figure 2.2 is helpful to consider while reading the following sections.

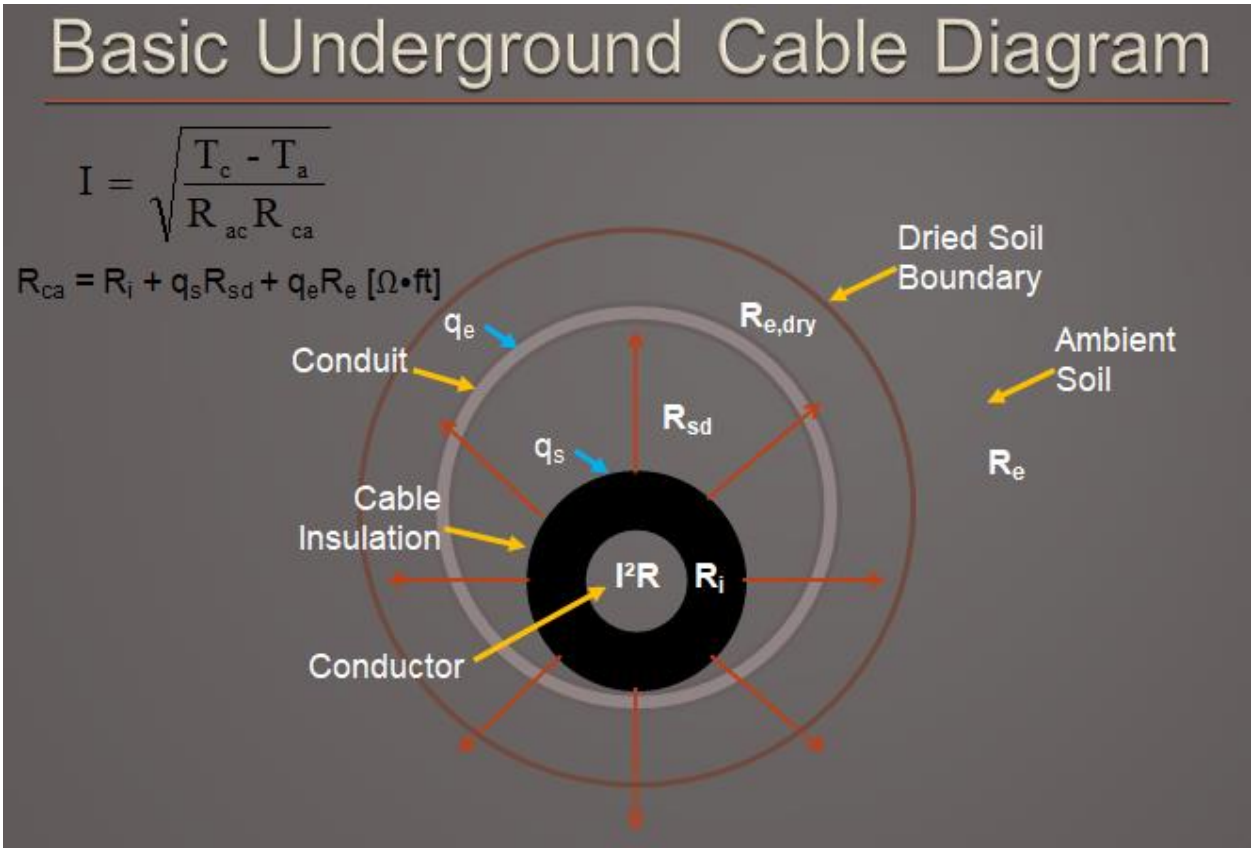

Figure 2.2 Diagram of basic cable thermal properties

2.2.1 Parameters Involving Heat Generation

The AC resistance of the cable is determined by adjusting the DC resistance for operating temperature, lay factor, and skin effect. The operating temperature correction is well understood and is specific to the conductor material—copper or aluminum. Typically, the temperature correction factor for the conductor resistance is determined using the insulation temperature rating. Most cables are rated for 90°C though some are rated for 105°C for medium voltage cables (5 kV and above) or even 75°C for low voltage cables (600V and less). It is possible to operate cables above these temperature limits for short durations, often referred to as emergency ratings. In addition, research has been done for insulations that withstand higher temperatures up to 150°C for continuous operation [24]. There is concern that jacket temperatures above the boiling point of water may cause excessive soil drying (discussed in Chapter 6), so the benefit may be limited to extending the emergency rating rather than continuous operation. Common insulation materials for medium and high voltage cables include cross-linked polyethylene (XLPE) and ethylene propylene rubber (EPR), and low voltage cables

include polyvinyl chloride (PVC) or XLPE. The following table provides the common manufacturer provided ratings for these insulations.

Table 2.1 Typical insulation continuous temperature ratings

Insulation	Continuous Temperature Rating
PVC	75°C or 90°C
XLPE	90°C or 105°C
EPR	90°C or 105°C

The *lay factor* accounts for conductor spiraling. Performed during the manufacturing process, the individual conductor strands used in most power cables are twisted. This increases the conduction path marginally and slightly increases the resistance per unit length. The *skin effect*, a result of the alternating current that generates magnetic fields internal to the conductor, decreases the effective conducting area (proportional to cross-sectional area and operating frequency) and marginally increases the effective resistance per unit length. In addition to the conductor internal skin effect, the same effect occurs between other current-carrying conductors—sometimes termed “proximity effect.” This effect depends on frequency, conductor size, number of strands in the conductor, and spacing between the conductors. While it is still considered in the calculation, it is typically not a significant factor especially considering the low operating frequency of the power system.

Medium and high voltage cables (5 kV and above) utilize shielding that generates appreciable heat and must be included in the ampacity calculation. The Neher-McGrath method accounts for this heat generated from circulating currents and eddy currents in the shield. Shield resistance is determined by the shield area and is adjusted for its operating temperature. This temperature must be estimated based on the conductor temperature and the expected temperature drop from the conductor to the shield due to the insulation. Though this is a difficult estimation to make a priori, it does not have a significant impact on the final ampacity. The skin effect is also used to adjust the effective shield resistance. Once the shield resistance is calculated, the induced currents are determined based on the mutual inductance between the primary conductor and the shield. In addition, the eddy currents circulating in the shield are calculated. Shields can be grounded at both ends, at one end only, or cross bonded. Shield grounding is discussed in detail in IEEE Std 575 [19]. Grounding at both ends provides a low impedance path for circulating currents, so it significantly reduces the ampacity.

One additional heat source is dielectric loss. It is only included for medium and high voltage cables since it is proportional to the square of the voltage, the insulation thickness, and the insulation capacitance properties. The NEC specifies that the dielectric loss can be neglected for single circuits less than 46kV [1, Sec. 310.60(C)].

Having addressed the heat sources and resistances, the final consideration is the load factor. It has a significant impact on the ampacity as shown in the following figure.

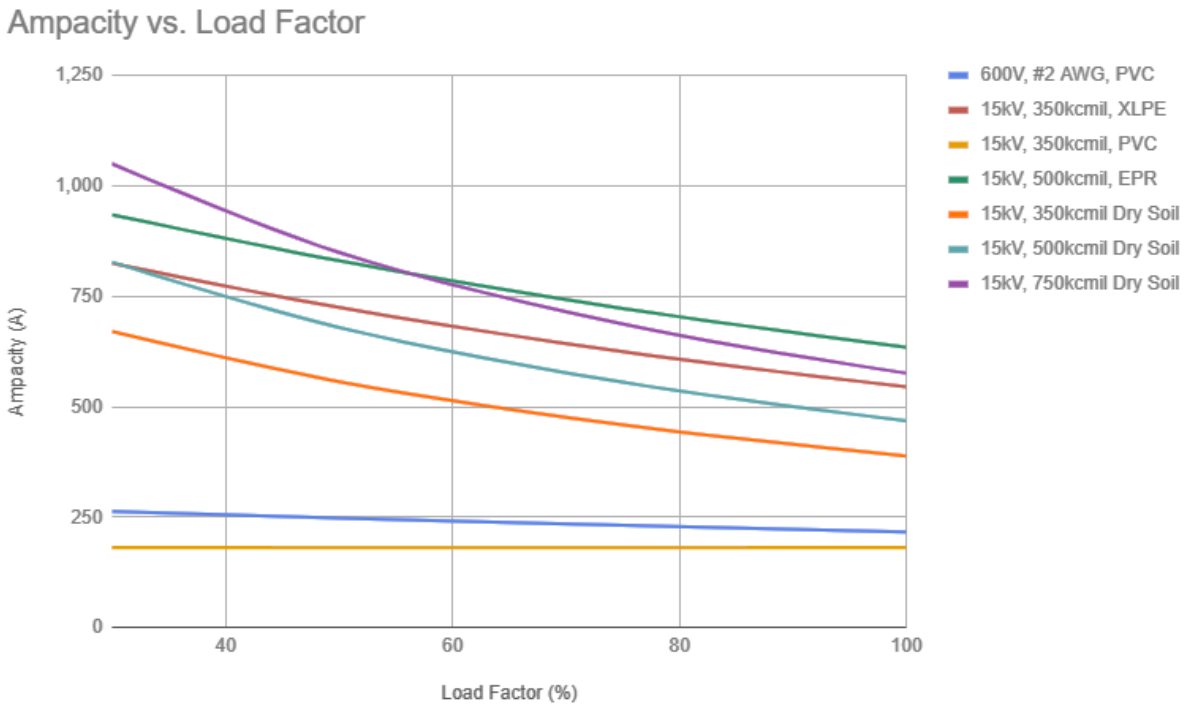

Figure 2.3 Ampacity versus load factor

The load factor impact is proportional to the ampacity, so designs with high current benefit the most from determining the lowest defensible load factor. Some designs may neglect to consider load factor possibly due to lack of understanding. A general definition of load factor is the ratio of the average current to the maximum current over a given period. The period may be assumed to be a 24-hour period, described as a daily-load factor. However, load factor is not well-defined in the original Neher-McGrath method [8]. It is only alluded to when it states, “In order to determine the maximum rise attained by a buried cable system under a repeated daily load cycle, the losses and resultant heat flows are calculated on the basis of the maximum load (usually taken as the average current for that hour of the daily load cycle during which the average current is highest, i.e. the daily maximum one-hour average load)” [8]. The term “daily” is used but is not stated as a requirement. Load factor is also not defined in IEEE Std 835

though it is listed in the tables [11]. It is not defined in the NEC either, though it provides several graphs and adjustment factors based on it, [1, Sec. Annex B]. A daily-load factor may not be appropriate for underground cables since the time constants are several days or longer. A weekly-load factor may be more appropriate, but a daily-load factor will yield more conservative ampacity calculations. One piece of software does consider load factors of different duration: daily, weekly, and yearly [25]. The impact of load factor on the calculations compared to a constant multi-day cable heating experiment is shown in Chapter 9 Experiments.

2.2.2 Parameters Involving Thermal Resistance

The remaining considerations of the Neher-McGrath method involve the thermal resistance for each section of the thermal circuit: cable insulation, cable jacket, air in duct or conduit (if applicable), duct or conduit wall (if applicable), concrete or backfill (if applicable), and earth (surrounding soil).

The cable insulation thermal resistance is based on the diameter (insulation thickness) and the intrinsic material thermal resistivity. The insulation diameter, or thickness, is based on the ICEA cable standards: ICEA S-95-658 (<2kV), S-96-659 (2kV-5kV) or S-93-639 (5kV-46kV). For example, 15kV cables at 100% insulation level are defined as a thickness of 175 mils. Medium voltage cables can use 100%, 133%, or 173% insulation levels that are primarily determined based on the system grounding. The most common insulation type is 100% used for grounded systems, while ungrounded systems utilize 133% (<1 hour fault clearing time) or 173% (indefinite fault clearing time) [17]. The NEC also provides a list of standard insulation thicknesses [1, Sec. 310.104]. The material thermal resistivity is not well-documented, but IEEE Std 835 provides a value of 350°C cm/W without explanation [11], so it is commonly used.

The cable jacket resistivity is similar to the cable insulation, depending on the thickness and material resistivity. The jacket thickness varies based on cable type, but standard jacket thicknesses are given in the NEC [1, Sec. 310.104]. Jacket material is typically PVC or low-density polyethylene (LDPE). The material thermal resistivity is not well documented, but IEEE Std 835 provides a value of 500°C cm/W for cable types of 3-6, which are the most commonly used today [11].

For cases where the cable is installed in duct, i.e. conduit, the resistance from the cable to the duct is dependent on the number of cables within the duct, the type of duct, and the mean temperature in the duct. Since it is difficult to determine the duct temperature without additional iterations and calculations, the method proposes an assumption of 60°C [8]. According to Sellers and Black, additional assumptions are also made in the Neher-McGrath method: “First, a

value for AT is assumed so that iterating for a correct value for the temperature is unnecessary...Second, the range of diameters is restricted to cable diameters between 1 and 4 inches when the cables are installed in ducts and between 3 and 5 inches for pipe-type cables. The complexity of the equation is further reduced by using several empirical relationships" [26]. These assumptions inherent to using a duct temperature of 60°C without iterating are often appropriate for standard cable installations. However, it is important to understand these underlying assumptions in the event they are not appropriate. Sellers and Black continue to describe the assumptions: "When determining the radiative heat transfer, the emissivity of the outer surface of the jacket and the inner surface of the duct are assumed to be equal. Also, the surface area of the inside of the duct is considered to be much larger than the surface area of the cable" [26]. The resulting temperature from radiative heat transfer combined with convective heat transfer is difficult to solve due to its nonlinearity. However, modern computer software is able to solve it numerically and could be used instead of the approximations made by the Neher-McGrath method especially when the assumptions deviate significantly.

The insulation resistance for the duct must also be included if applicable. This is treated in the same fashion as the cable jacket and insulation. The thickness of the duct is typically determined by the schedule type, e.g. Schedule 40, or the SDR, which is the ratio of the duct diameter to thickness. The resistivity is given as 480°C cm/W for "fiber duct" and 200°C cm/W for "transite duct" [8]. IEEE Std 835 restates the 480°C cm/W as the only duct material [11]. There isn't a source for this stated value.

The remaining thermal resistance includes the concrete or backfill material, if applicable, and the surrounding soil. The concrete or backfill material is handled in a unique fashion. The method uses a resistivity of the concrete or backfill for all of the surrounding soil and then adjusts it for a number of factors including: the number of cables in each duct, the number of ducts in the duct bank, the geometry of the duct bank, the resistivity of the surrounding soil and the concrete or backfill material, the diffusivity of the surrounding soil, the loss factor, and the mutual heating of other cables in the duct bank. All of this is included in one equation [8]. According to a paper entitled, "Refinements to the Neher-McGrath Model for Calculating the Ampacity of Underground Cables" [26]:

> "By utilizing the principle of superposition, and by restricting short-circuited shield operation to three conductor cables and three, single-conductor cables in a duct; therefore, equal heat generation in each cable, Neher McGrath show that the mutual heating factor is only a function of the installation geometry. This result greatly simplifies the model because the mutual heating factor is known once the

> cable geometry is specified. However, when the heat generated in all cables is not equal, the mutual heating parameter is also a function of the heat generation rates as well as the geometry. Therefore, when the heat generation in the cables vary, as it does when the circulating currents in the metallic shield are unequal, the value for F should be modified appropriately."

In addition to the simplification of the mutual heating of other cables, the geometry of the duct bank is simplified. "The surface of the duct bank is assumed to be transformed into an isotherm of radius Yb and the heat flow through the duct bank is assumed to be independent of angular direction" [26]. Also, the geometric factor is limited in its application to ratios of length to width from ⅓ to 3 [26]. Clearly, adjusting for a duct bank and the additional circuits within the duct bank adds significant complexity to the calculation. This is mostly due to the complexity of multiple heat sources. A common method used today to solve two-dimensional, multi-heat source problems is with finite element analysis using something like the finite difference method. This allows for handling the partial differential equations based on the fundamental heat transfer principles. Simplification of the fundamental heat transfer equations can also be accomplished by using the lumped parameter method. This generates a thermal circuit, which can be solved using standard electrical circuit techniques familiar to electrical engineers. The Neher-McGrath method attempts to simplify the thermal circuit into one resistance for each cable that is analyzed. This avoids solving simultaneous equations. At the time of the development of the method, reducing the number of calculations was critical because modern computers were not ubiquitous.

The final resistance is the earth or ambient soil around the cables, if not already accounted for in the duct bank calculation. As with all properties related to soil, each location on earth has unique soil properties and it is difficult to estimate what the value of any given property will be without digging down and testing it. IEEE Std 835 states it best: "the ratings for buried cables are significantly affected by the earth's portion of the thermal circuit and therefore correct knowledge of the effective soil thermal resistivity and soil thermal stability is paramount in establishing the correct rating for a buried cable system" [11]. The thermal resistivity can be measured according to IEEE Std 442 and involves driving a probe into the earth, injecting heat, and measuring the temperature rise [27]. Soil thermal resistivity varies by an order of magnitude, ranging from 50°C·cm/W to 500°C·cm/W. In addition to large variability from one location to another, the thermal resistivity varies throughout the year since it is strongly affected by the soil moisture content. Soil thermal stability is also mentioned in the quote from IEEE Std 835 above, but there is no IEEE standard method currently available to measure this parameter.

A proposed method for addressing this is provided in Chapter 4 Ampacity Calculation Method Including Soil Thermal Stability and is also discussed in Chapter 6 Soil Thermal Stability.

Selecting the proper soil resistivity is not trivial because of its dependence on moisture content. Soil thermal stability is a metric for “the ability of the soil to maintain its thermal resistivity in the presence of a heat source” [28]. An example of the range of resistivity values versus moisture content is shown in the following figure.

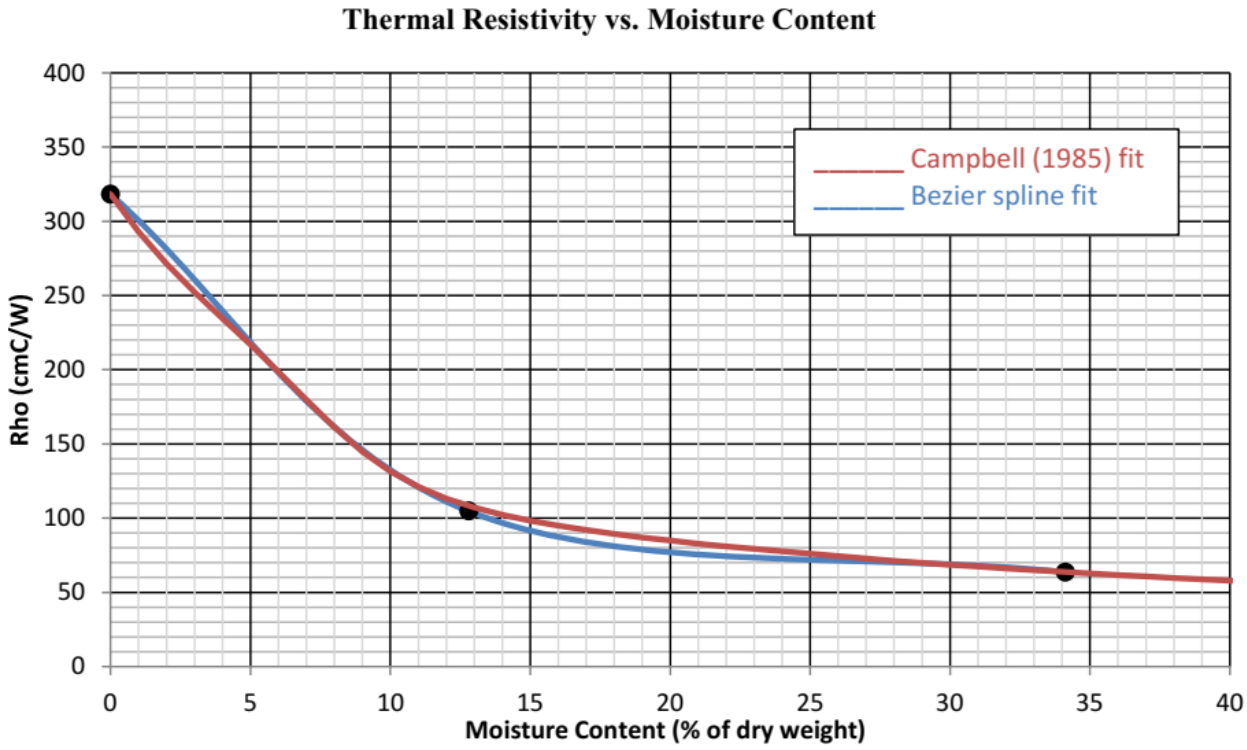

Figure 2.4 Example graph of thermal resistivity versus moisture content

This test, referred to as the thermal resistivity dry-out curve [29], is performed in a laboratory with a sample of the native soil because testing over a range of moisture contents in-situ would require modifying the moisture content of the native soil. The native soil moisture content varies through the year, so it is possible to measure the resistivity over time, but this is typically substituted for a laboratory test for cost and schedule reasons. This resistivity shows a range of 55 to 320°C·cm/W. There is no standard that specifies the specific value to use, so it is left to engineering judgement. Some engineers use the most conservative value, which occurs at 0% moisture content. This would occur if the soil around the cable were totally dry. Another engineer may consider this unrealistic and choose to use a resistivity based on typical soil moisture content in the area such as 15%. Another engineer may utilize the moisture content at the expected minimum moisture content in the area. It is difficult to obtain historic measurements of the soil moisture content at the specific location of the cable, but resources

are available through the Natural Resources Conservation Service that provide it for locations through the United States. This resource is entitled Soil Climate Analysis Network (SCAN) [30]. An example of the summary of this data is shown in the following figure.

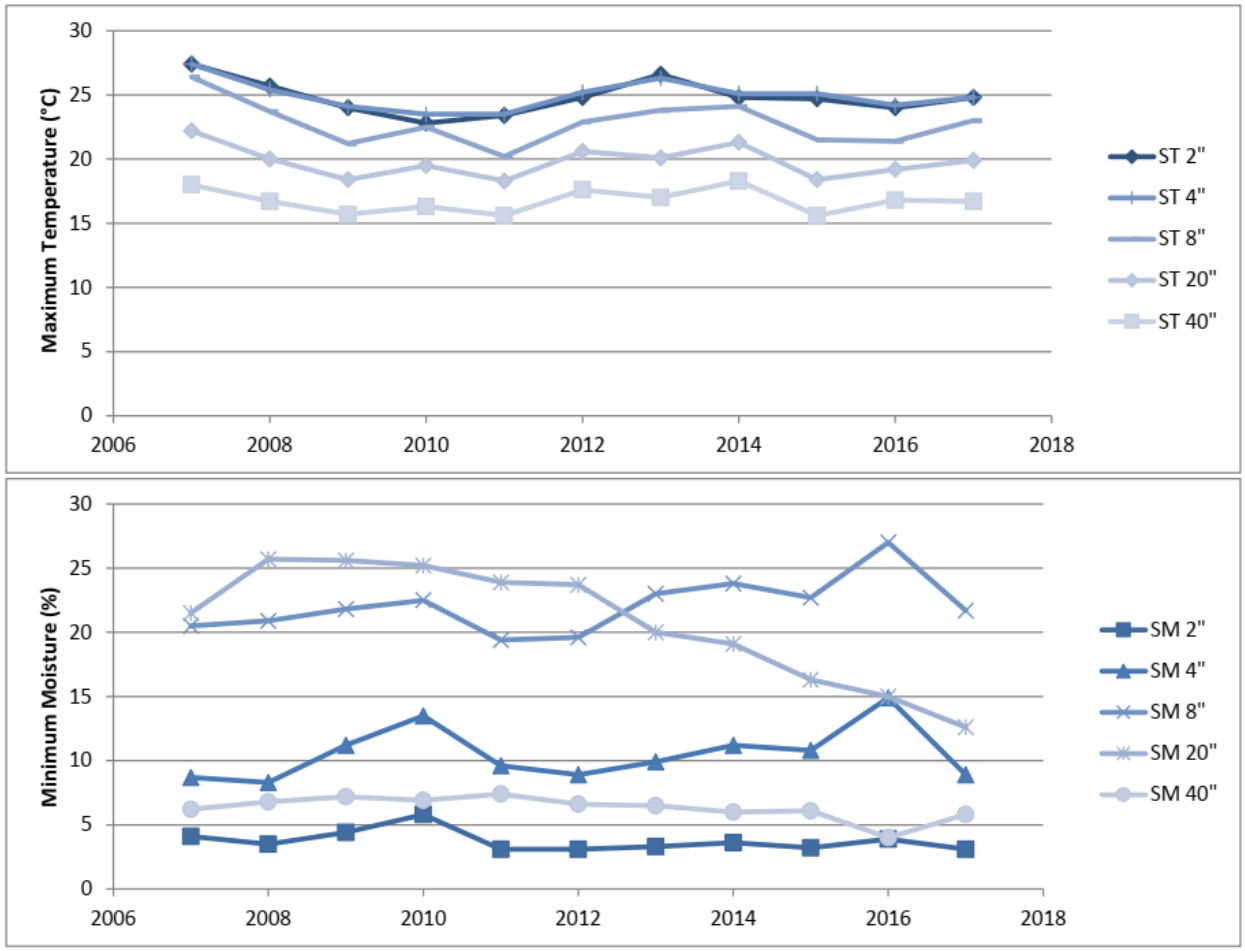

Figure 2.5 Historical maximum temperature and minimum temperature for example site

Using this data, the in-situ thermal resistivity can be adjusted with the laboratory measurements. This is done by determining a multiplier for the resistivity between the in-situ moisture content and the minimum moisture content from the lab measurements. Then, the in-situ resistivity is multiplied by this value to determine the expected resistivity at the minimum moisture content. An example of this is shown in the following tables.

Table 2.2 Soil resistivity lab tests example

Depth	**18"**			**36"**	
Parameter	ρ@4% M.C. [°C*cm/W]	M.C. [%]	ρ@M.C. [°C*cm/W]	M.C. [%]	ρ@M.C. [°C*cm/W]
TP-1	240	10.2	130	25.4	80
TP-2	140	14.5	50	5.6	-
TP-3	110	9.7	60	4.5	-
TP-4	140	17.7	95	17.7	130
TP-5	110	3.6	110	-	205
TP-6	95	4.3	95	4.3	-
Mean	165		106		
Stdev	70		46		
μ+σ	235		152		
Moisture Content Correction (Mean@4%/M.C.) = 1.55 for adjusting in-situ in Table 2.2					

Table 2.3 Soil resistivity in-situ tests example

Depth	**18"**		**36"**		**Comment**
Parameter	ρ [°C*cm/W]	M.C. [%]	ρ [°C*cm/W]	M.C. [%]	ρ=soil thermal resistivity M.C.=moisture content (% of dry weight)
BH-1	53	10.2	59	25.4	
BH-2	66	14.5	31	5.6	
BH-3	64	9.7	200 (5)	4.5	(5) excluded due to high error
BH-4	79	17.7	62	17.7	
BH-5	73	3.6	69	-	
BH-6	92	4.3	204 (5)	4.3	(5) excluded due to high error
Mean (18" & 36")	65	11			
Stdev (18" & 36")	16	7			
ρ=μ+σ (18" & 36")	65+16= 81				Resistivity plus 1 standard deviation to account for variability
Moisture Content Correction (Mean@4%/M.C.) = 1.55 from Table 2.1					
From Lab Tests	1.55				
ρ@4% [°C*cm/W]	65*1.55= 101				Resistivity corrected to minimum moisture content
ρ=μ+σ (18” & 36”)	81*1.55= 126				Final resistivity for use in ampacity calculation

The method of determining the soil thermal resistivity to be used for the ampacity calculations is not defined in a standard, such as one produced the IEEE, so engineers must use their judgement. As a result, engineers will calculate different ampacities for the same installation. Another example of this difficulty is shown in Chapter 11 Solar PV Power Plant Case Study.

2.3 IEC 60287-1

The International Electrotechnical Commission published the first version of the "Electric Cables - Calculation of The Current Rating" as IEC 287 1969, but has been updated multiple times to the most recent issue in 2006 as IEC 60287-1 [13]. The basic calculation for ampacity is essentially identical to the Neher-McGrath method, as described previously. The major difference is the inclusion of soil dry-out and more detail on losses. IEEE Std 835 actually references IEC 60287-1 for some of the loss calculations [11]. The addition of soil dry-out is not included in the Neher-McGrath method or IEEE Std 835. IEC 60287-1 standard references a working group report for the basis of the published equations [31]. This publication emphasizes the need to understand soil moisture as it relates to cable ampacity. It states the following in the introduction [31]:

> "The external thermal resistance of a buried cable plays an important part in the determination of its current carrying capacity, the temperature difference between a cable surface and ambient being in the region of 50 to 70 percent of the conductor temperature rise. Of all the factors which can influence the thermal resistivity of soil, its moisture content is one of the most important, particularly so because serious changes of moisture content in soil around a cable can be caused by heat from the cable itself. A reliable value of current carrying capacity can be allocated to a cable only if the thermal behaviour of its surrounding soil is taken into account."

The publication goes on to describe the method for accounting for soil dry-out. Critical temperature rise is the key value used in the method. This parameter is defined as the boundary radius between a layer of dry soil and the wet ambient soil. It is not well-defined and is stated as a "simple approach" in the publication, "A simple approach to the problem is to limit cable surface temperatures so that soil temperatures do not rise to levels at which significant migration is expected. This tends toward under-utilisation of cable materials and its economic justification usually depends on the relative value placed on the effort needed to obtain more complete soil information" [31]. Though the publication provides several examples, there is not a

defined method for determining the critical temperature. It simply illustrates the impact on ampacity with several assumed values. The publication does acknowledge work being performed by the IEEE Insulated Conductors committee by citing conference meeting minutes and published transactions investigating heat flux as the parameter for soil dry-out rather than temperature [32] [33]. The working group states, “Workers in this subject have proposed various critical parameters such as temperature gradient, temperature difference, and heat flux density,” and follows up by stating, “Until further information is available, it is proposed in this report to use a simple temperature rise above ground ambient as the critical factor which gives the position of the dry/moist boundary and to assume that the boundary is circular in shape” [31]. Addressing the cause of soil dry-out or moisture migration is a primary focus for this dissertation. It is important to note that IEC 60287-1 utilizes this critical temperature as the parameter impacting soil dry-out [13] and that the basis for selecting this parameter over others such as heat flux is due to lack of information.

An excellent comparison between IEC 60287-1 and the Neher-McGrath method is provided in Appendix F of Anders book [14, p. 417]. As stated, “Similarities in the approaches are not surprising since, during the preparation of the standard, Mr. McGrath was in touch with the Chairman of Working Group 10 of IEC Subcommittee 20A (responsible for the preparation of ampacity calculation standards)” [14]. Beyond the standard for ampacity calculation, there is a difference in the use of the calculation for generating standard ampacity tables. These tables provide a quick reference of calculated cable ampacity for specific installation details. IEEE Std 835 was produced based on the Neher-McGrath method [11]. This provides ampacity tables for a significant number of cable installations from 600V to 500kV. IEC 60502-2 provides tables but only up to 30kV [34]. It is clear the IEC expects engineers to perform the calculations for cables above 30kV rather than lookup values in a table. This is not unreasonable considering installations above 30kV are less frequent and involve more engineering support.

2.4 Development of IEEE P1254 Thermal Stability

A working group was formed within the IEEE Power and Energy Society Insulated Conductors Committee to address soil thermal stability in 2001. The working group began developing a standard on soil thermal stability, IEEE P1254, under an IEEE approved project authorization (PAR). This expired in 2016 due to difficulty in developing a consensus. However, there has been considerable effort exerted into developing an industry accepted method of characterizing soil thermal stability. The primary debate is related to defining stability in terms of temperature or heat rate. The original “Black Books” used a temperature limit for the cable

exterior, suggesting that soil stability is defined by temperature. However, heat rate appears to be the primary driving factor in terms of physical explanation and experimentation [32].

This IEEE standard, if it could be completed, would fill a large gap of knowledge and application in the industry by providing a consistent test method for determining stability, a method of addressing the impact of stability on cable ampacity calculations, and an assessment of the possibility of "thermal runaway." A consistent test method is currently lacking, at least in terms of an industry standard such as one issued by the IEEE or the American Society for Testing and Materials (ASTM). The current critical temperature of IEC 60287-1 does not provide enough guidance for a test method that can be readily applied [13]. Addressing the impact of stability on ampacity is difficult because a good metric for stability is missing. The fear of "thermal runaway" is fairly common in industry. The concept of "thermal runaway" is that cable heating dries the surrounding soil, which increases the soil thermal resistance and the cable temperature beyond its limit. There are not many publicly documented cases. However, the cases reported anecdotally involve poor backfill compaction (large backfill lifts or limited tamping between lifts), vegetation impact due to transpiration, and cables under seabeds assumed to have high moisture content and designed for higher heat rates. Thermal runaway can be properly addressed by characterizing thermal stability.

CHAPTER 3
STANDARD INDUSTRY PRACTICE[3]

3.1 Introduction

Using accurate cable ampacities is critical to electrical power system design. An optimally sized cable results in minimum cost and high reliability. Wind and solar power plants in particular strive to optimize cable design by using ampacities that closely match maximum generation without including a growth factor or other safety factor.

Cable ampacities have been estimated over the years based on engineering assumptions and site conditions. Various configurations require different parameters and assumptions. Cables placed underground require information about the ambient earth temperature, cable separation distance, soil thermal resistivity, etc. If these parameters or assumptions are inaccurate, the resulting cable size will also be inaccurate. This may lead to cable overheating if the cable is undersized or increased cable cost if the cable is oversized.

Underground cable ampacity is difficult to estimate because a primary factor determining ampacity—soil thermal resistivity—varies substantially from moist to dry conditions, which may occur depending on cable loading [28]. This paper compares the difference in results obtained when using various methods including one recently proposed in [28]. These methods will include cable ampacities calculated using the Neher-McGrath method, IEEE Cable Ampacity tables, and a commercially available computer program.

Each of these methods requires some values that must be collected at location where the cable will be installed. These include the soil thermal resistivity—also known as “rho” and measured in K·cm/W (°C·cm/W)—and the maximum expected ambient temperature, excluding cable heating, at the depth of the hottest cable. The soil thermal resistivity, while critical, may not be as readily available as the ambient temperature. IEEE Std 835 states:

> “In the past, when the thermal resistivity of the earth was not known a rho of 90 was recommended for rating the cable. However, the ratings for buried cables are significantly affected by the earth's portion of the thermal circuit and therefore correct knowledge of the effective soil thermal resistivity and soil thermal stability is paramount in establishing the correct rating for a buried cable system” [11].

[3] This chapter was previously published in IEEE Transactions [15].

Measuring the in-situ thermal resistivity is not a difficult process as described in [35], but it is frequently not performed. It is likely that a cable size will be selected that is either smaller or larger than optimal if this step is skipped.

3.2 Ampacity Calculation Methods

3.2.1 The Black Books

The “Black Books,” entitled AIEE-IPCEA Power Cable Ampacities [10], were the first tabulated ampacities using the Neher-McGrath method and were published in 1962. They allowed an engineer to look up the appropriate cable size based on design current rather than calculating the cable size using Neher-McGrath calculations in [8]. Considering the number of calculations needed to determine ampacity using the Neher-McGrath method, it is obvious why engineers would prefer using this simplified tabular method. These same tables are still used by some engineers today as their primary method of sizing underground cables.

It is important to understand the assumptions used to create these tables. For example, one assumption used in the tables is that the ambient temperature of the earth is 20°C. Many locations in the Southwest USA experience maximum underground soil temperature of 25-30°C, which reduces the ampacity by 5-8% below the tabulated values. The tabular values must be adjusted using methods included in the introductory pages of the Black Books.

Another assumption is that the cable depth is 36” and the cable spacing is 7.5”. If the burial depth was actually 18”, this would increase the ampacity by approximately 10%, and doubling the spacing would increase it by approximately 6%. Adjustment factors for these assumptions are not given in the tables, so the Neher-McGrath calculations must be done if conditions of depth or spacing vary from the assumptions. Furthermore, modern cables use different insulation material and thickness than those used in these older tables. Also, these tables assume the cables are not jacketed. All of these assumptions may present difficulties for a modern user and, if differences are ignored, can result in cables that are sized too large or too small.

The key assumptions in these tables are listed below.

- 20°C ambient earth
- 90°C maximum conductor temperature
- Cable shields single point grounded
- 36” depth
- 7.5” spacing
- Generic rubber insulation

- Thicker than modern insulations for equivalent voltage rating
- Higher thermal resistivity (500°C·cm/W versus modern 350°C·cm/W)
- Higher insulation power factor resulting in higher dielectric losses (3.5% versus modern 0.5%)

3.2.2 IEEE 835 Cable Ampacity Tables

In 1994, a new set of tabulated ampacities was issued by IEEE in order to: “update the cable constructions and design changes that had taken place since the original publication” [11]. While maintaining the fundamental calculations set forth by Neher-McGrath, the tables include updated information on cable properties and adjust some of the original assumptions. This includes assuming a 25°C ambient earth temperature and cable shields that are shorted (grounded at both ends) for most cable sizes. The standard also includes some step-by-step examples of the Neher-McGrath method with updates to address changes in assumptions of the original method. The steps given allow an engineer to develop a spreadsheet to calculate ampacity for any cable configuration, which eliminates the need for the tables except as a convenient check.

The key assumptions for these tables are given below.

- 25°C ambient earth
- 90°C maximum conductor temperature
- Cable shields shorted
- 36” depth
- 7.5” spacing

3.2.3 Computer Modeling

Commercially available computer software allows for the calculation of cable ampacity by modeling the cable properties and the physical configuration. The cables can be modeled with the intended design geometry and with the intended cable type. Programs utilize values of cable constituent thermal resistivity as specified by IEEE Std 835 [11] for each material type (e.g. EPR is 350°C·cm/W), allowing the thickness and order of the components to be adjusted. Programs are typically advertised as using the Neher-McGrath method to determine ampacity, meaning the only assumptions necessary are those inherent to the Neher-McGrath method.

3.2.4 Neher-McGrath Adaptation

The method proposed by [28] focuses on the thermal stability of the soil. All soils increase in resistivity as moisture content decreases. The suggested method addresses the

issue of moisture migration with a simple procedure to approximate the effective thermal resistance to ambient earth including the effects of drying. The non-drying heat rate (NHR) and the completely dried soil resistivity must be known in addition to the in-situ soil resistivity. These are used to calculate a dried soil diameter, which is then included in the Neher-McGrath method. The cable ampacity may be calculated with the aid of a spreadsheet, by hand, or by using a computer program that includes the capability of adding concentric layers of thermal resistance surrounding the cable. Another notable feature of this method is that it does not assume that the only heat transfer mechanism of the cable is conduction to ambient earth. Rather, it includes the effects of heat transfer by moisture moving through the soil.

3.3 Comparison

In order to highlight the differences between these methods, some examples are provided. Each example involves three single, copper conductors that are directly buried 36" underground as shown in Figure 3.1, which is the same configuration as figure "k" of IEEE Std 835 [11]. Also, each example involves single point grounded cables and the design requires an ampacity of at least 500 A at 15 kV with EPR insulation and tape shielding. A load factor of 100% is assumed.

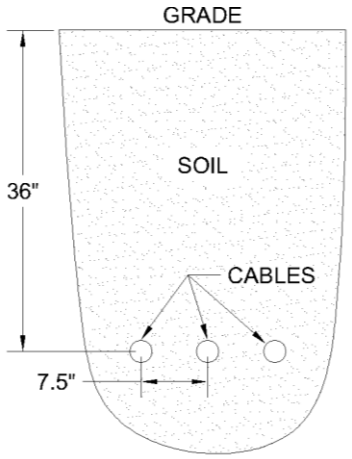

Figure 3.1 Cable Configuration

3.3.1 Site Specific Data Collection

To begin the design for the first example, the in-situ soil thermal resistivity and the moisture content must be measured. These can be found by following IEEE Std 442 [27] and ASTM D4643 [36]. For this example, the in-situ soil thermal resistivity has been measured at

90°C·cm/W at an in-situ moisture content of 8%. It is important that the soil resistivity be measured at the minimum soil moisture content because it has a large effect on the soil resistivity. In addition, both the moisture content and the resistivity should be measured at the depth that the cables will be installed.

Determining the minimum moisture content is often difficult because it may occur at any point during the year and it is impractical to measure the moisture content throughout the year when sizing cables. Also, the minimum moisture content will vary from year to year and the year in which the soil resistivity is measured for the design may be an abnormally high level. This would result in a low soil resistivity and a cable size that is too small during a drought.

A practical method to determine the approximate minimum soil moisture content involves using the data provided by the Soil Climate Analysis Network (SCAN) operated by the National Water and Climate Center [30]. This publicly available data provides soil moisture content and soil temperature for various soil depths up to 40" at locations across the United States. From this data, the minimum soil moisture content and maximum soil temperature can be found over a period of several years. A plot of the minimum soil moisture and maximum soil temperature over a given year at a depth of 40" below grade for the soil used in this example is show in the following figure:

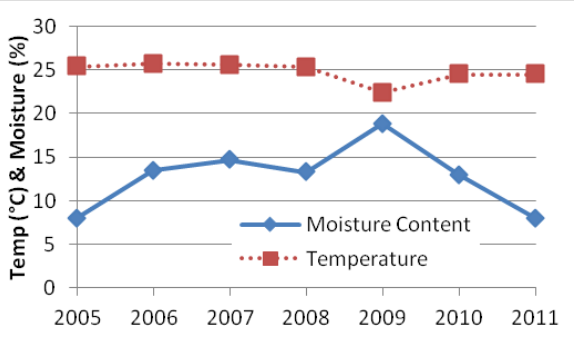

Figure 3.2 Max. soil temperature and min. moisture content per year

The maximum soil temperature and the minimum soil moisture content are the conditions that result in the lowest cable ampacity. Using these extremes will result in a conservative design. In the case of Figure 3.2, the lowest moisture content is 8% and the highest soil temperature is 25°C. Of course, the lowest moisture content may not occur concurrently with the highest soil temperature. A plot of the soil moisture content and the soil temperature over one year is shown in the following figure, which shows the maximum temperature occurring four months before the minimum moisture content.

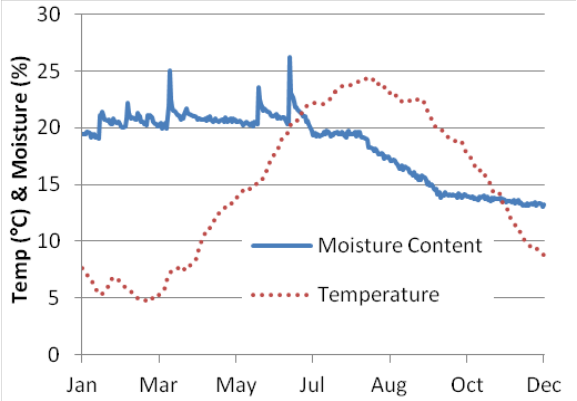

Figure 3.3 Soil temperature and moisture content over one year

Using this information, it is possible to use the moisture content and temperature which occur simultaneously rather than the yearly minimum moisture content and yearly maximum temperature. Multiple cases would need to be examined for each moisture content and temperature. The case that resulted in the lowest ampacity would determine the required cable size. The in-situ thermal resistivity is required for each moisture content used in the calculation. For example, after examining multiple cases, the minimum moisture content and maximum temperature that result in the minimum ampacity may occur in September compared to the maximum temperature occurring in July with the minimum moisture content in December. This is obviously more time consuming than using the minimum annual moisture content and maximum temperature, which will result in a more conservative design but may not differ significantly.

Another piece of information that is needed for the method proposed in [28] is the soil dry out curve, which is performed in a lab rather than in-situ. The lab test of the soil is shown in the following figure.

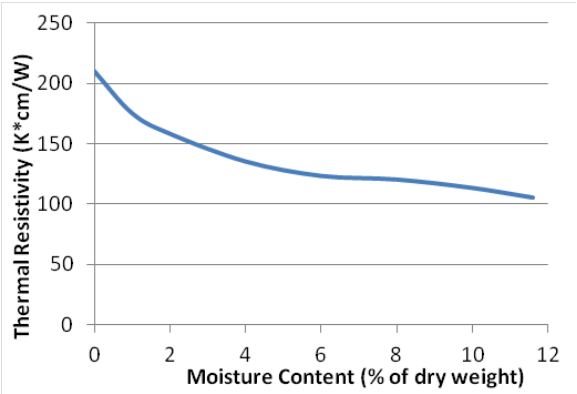

Figure 3.4 Soil dry out curve

This curve provides information on the soil thermal resistivity over a range of moisture contents, but it should not be used to replace the in-situ moisture content and thermal resistivity measurements. It is used for determining the dry soil resistivity. Laboratory tests allow for complete dehydration of the soil but do not permit ingress of moisture that would normally be experienced in-situ and, therefore, do not produce accurate measurements of the expected resistivity in the field. These laboratory results may provide higher resistivity values than measured in-situ because the surrounding soil moisture provides some cooling as it is heated by the cables [28].

3.3.2 Cable Sizing Example

After the soil data specific to the site has been determined, the ampacity can be found using various methods. Table 3.1 shows the calculated values of cable ampacity using four different methods, assuming the soil resistivity remains at 90°C·cm/W, i.e. the soil does not dry out.

Table 3.1 Ampacity with RHO-90

Method	Ampacity	Cable Size
Neher-McGrath	541A	350kcmil
Black Book P.210	534A	350kcmil
IEEE Std 835 P.465	519A	350kcmil
Computer Program	549A	350kcmil

All of these methods result in an equivalent cable size though there are slight discrepancies in the resulting ampacity. These differences can be attributed to the different assumptions used by each method as described earlier in this paper.

3.3.3 Soil Drying Consideration

The effect of soil drying can be checked by measuring the non-drying heat rate (NHR) as described in [28]. This example will use a value of 0.53 W/cm as the NHR measured using a standard probe diameter of 1.5875 cm, as per IEEE Std 442 [27]. In order to determine if soil drying occurs, the NHR can be compared to the cable heat rate. The cable heat rate is a calculated value in the Neher-McGrath method and can also be found using a computer program. The Black Books and IEEE Std 835 do not list the cable heat rate, but it could be calculated using the Neher-McGrath method if needed. The amount of heat a cable can generate before causing the soil to dry is a function of the diameter of the cable. The NHR found

using the standard probe must be adjusted for the cable diameter before it can be compared to the actual cable heat rate. This can be accomplished by first calculating the conductive heat flow rate of the test probe at the NHR using (3.1), which is (7) in [28].

$$\dot{q}_{c,probe} = \frac{2\pi(T_1 - T_2)}{\rho \ln\left(\frac{4L}{D_{probe}}\right)} \tag{3.1}$$

where

$\dot{q}_{c,probe}$ is the conductive heat rate at the NHR for the test probe (W/cm)

L is the length of the test probe (cm)

T_1 is the maximum temperature of the NHR test (°C)

T_2 is the ambient temperature of the NHR test (°C)

ρ is the in-situ soil thermal resistivity (using [27])

D_{probe} is the outside diameter of the test probe (cm)

The NHR for the cable diameter using the NHR measured with a test probe can be derived by beginning with (19) of [28], shown in the per unit length form in (3.2) below.

$$D_{cable} = \frac{D_{probe}\left(\dot{q}_{w,cable} + \dot{q}_{v,cable}\right)}{\dot{m}_{NHR,probe}(h_v + C_w \Delta T_{cable})} \tag{3.2}$$

where

D_{cable} is the outside diameter of the cable (cm)

$\dot{q}_{w,cable}$ is the heat rate due to inflowing water (W/cm)

$\dot{q}_{w,cable}$ is the heat rate due to water vapor (W/cm)

$\dot{m}_{NHR,probe}$ is the mass flow rate of water at the probe diameter (lb/sec·cm)

h_v is the latent heat of vaporization of water (1025 kJ/lb)

C_w is the specific heat of water (1.89 kJ/lb°C)

ΔT_{cable} is the temperature difference between ambient earth and the dried soil interface, which is the cable diameter in the case of the NHR (°C)

The mass flow rate of water is given in (13) of [28] as shown in the per unit length form in (3.3) below.

$$\dot{m}_{NHR} = \frac{\dot{q}_{NHR,cable} - \dot{q}_c}{h_v + C_w \Delta T} \tag{3.3}$$

where

$\dot{q}_{NHR,cable}$ is the total heat rate at the NHR for the cable (W/cm)

The heat absorbed by inflowing water and the heat transferred by water vapor is shown in (3.4), which is the per unit length form of (12) in [28].

$$\dot{q}_{w,cable} + \dot{q}_{v,cable} = \dot{q}_{NHR,cable} - \dot{q}_{c,cable} \tag{3.4}$$

where

$\dot{q}_{c,cable}$ is the conductive heat rate at the NHR for the cable (W/cm)

The conductive heat rate at the NHR for the cable can be found in terms of the NHR using the same assumption as in (3.1)—that the increase in total heat rate from the NHR at the probe diameter to the NHR at the cable diameter will result in a proportional increase in each component of the heat rate, i.e. the heat transferred by conduction, water, and vapor. This is shown in (3.5), which is the per unit length form of (20) in [28].

$$\dot{q}_{c,cable} = \frac{\dot{q}_{NHR,cable}}{\dot{q}_{NHR,probe}} \dot{q}_{c,probe} \tag{3.5}$$

The NHR for the cable diameter can now be calculated using (3.2), (3.3), (3.4), and (3.5) as shown in the following derivation:

Begin by inserting (3.3) into (3.2).

$$D_{cable} = \frac{D_{probe}\left(\dot{q}_{w,cable} + \dot{q}_{v,cable}\right)}{\frac{\dot{q}_{NHR,probe} - \dot{q}_{c,probe}}{h_v + C_w \Delta T_{probe}} (h_v + C_w \Delta T_{cable})} \tag{3.6}$$

The terms $h_v + C_w \Delta T_{cable}$ can be cancelled by $h_v + C_w \Delta T_{probe}$ if the same assumption is made as is made in [28]. Inserting (3.4) into (3.6) and cancelling the equivalent terms results in (3.7).

$$D_{cable} = \frac{D_{probe}\left(\dot{q}_{NHR,cable} - \dot{q}_{c,cable}\right)}{\dot{q}_{NHR,probe} - \dot{q}_{c,probe}} \tag{3.7}$$

Inserting (3.5) into (3.7) results in (3.8).

$$D_{cable} = \frac{D_{probe}\left(\dot{q}_{NHR,cable} - \frac{\dot{q}_{NHR,cable}}{\dot{q}_{NHR,probe}} \dot{q}_{c,probe}\right)}{\dot{q}_{NHR,probe} - \dot{q}_{c,probe}} \tag{3.8}$$

Rearranging the terms in (3.8) completes the derivation, which is shown as (3.9).

$$\dot{q}_{NHR,cable} = \frac{D_{cable}\left(\dot{q}_{NHR,probe} - \dot{q}_c\right)}{D_{probe}\left(1 - \frac{\dot{q}_{c,probe}}{\dot{q}_{NHR,probe}}\right)} \tag{3.9}$$

Using test data of T_1 = 36°C, T_2 = 20°C, and the IEEE Std 442 [27] standard probe dimensions yields the following $\dot{q}_{c,probe}$ based on (3.1).

$$\dot{q}_{c,probe} = \frac{2\pi(36°C - 20°C)}{90\frac{Kcm}{W} \cdot \ln\left(\frac{4 \cdot 120cm}{1.5875cm}\right)} = \frac{0.196W}{cm}$$

Using a cable diameter of 3.2 cm (compact stranded 350 kcmil) yields the following NHR that is corrected for the cable diameter using (3.9).

$$\dot{q}_{NHR,cable} = \frac{3.2cm\left(\frac{0.53W}{cm} - \frac{0.196W}{cm}\right)}{1.5875cm\left(1 - \frac{\frac{0.196W}{cm}}{\frac{0.53W}{cm}}\right)} = \frac{1.06W}{cm}$$

Now that the NHR is known for the cable diameter in question, a direct comparison can be made to the calculated cable heat flow rate needed in the design. The Neher-McGrath method yields values for the cable heat "W" that are the sum of the losses developed in a cable [32]. The value W is the sum of all of the other losses (Wc, Ws, Wp, and Wd), the most important of which will be the I2R losses. For a direct buried cable operating at 15 kV, the conduit losses (Wp) and dielectric losses (Wd) are zero. For this particular example, the cable heat rate, W or $\dot{q}_{cable}$, is equal to 0.373 W/cm. This is well under the 1.06 W/cm calculated for this soil, so soil drying is not expected to occur and no modification is needed to the calculations due to soil thermal instability [28].

3.3.4 Laboratory Testing Versus In-Situ Testing

A common concern when sizing cables is that the cable will heat up the surrounding soil enough to dry the soil. This would increase the temperature of the cable that would cause further drying of the soil that would cause an additional increase in temperature until the temperature rating of the insulation was exceeded. This is sometimes referred to as thermal runaway, but dramatic increases in temperature commonly associated with thermal runaway are not required in order to exceed the temperature rating of the cable. To avoid this problem, an engineer might choose to use a value of resistivity that is higher than the value measured in-situ.

If in-situ measurements are unavailable, the laboratory thermal measurements similar to those in Figure 3.4 may be needed. These are commonly higher than in-situ measurements and the designer may choose the highest value shown on the graph for safety.

For this example, a value of resistivity will be selected from the lab test based on the minimum moisture content of 8%. The other values are the same as those used in the first example. The value of resistivity found from the laboratory was approximately 120°C·cm/W. Using the same methods used in Table 3.1 results in the ampacities and cable sizes show in Table 3.2.

Table 3.2 Ampacity with RHO-120

Method	Current	Cable Size
Neher-McGrath	483A	350kcmil
Neher-McGrath	569A	500kcmil
Black Book P.210	485A	350kcmil
Black Book P.210	588A	500kcmil
IEEE Std 835 P.465	462A	350kcmil
IEEE Std 835 P.465	536A	500kcmil
Computer Program	489A	350kcmil
Computer Program	591A	500kcmil

Comparing Table 3.1 and Table 3.2 shows that all of the cables had to be increased in size from a 350 kcmil to a 500 kcmil cable in order to carry the desired 500 A design current. Using a cost of $9,900/1000 ft for 350 kcmil and $12,600/1000 ft for 500 kcmil, increasing the size from 350 kcmil to 500 kcmil would result in approximately 25% higher costs or $2,700 per 1000 feet. It is clear that if an in-situ test resulted in RHO=90 and laboratory tests resulted in RHO=120 (or the designer used an arbitrarily high value for rho) that the costs of the installation would be significantly affected. The higher cost of the in-situ measurement could easily be paid for in a situation such as this, and the desirability of accurate soil resistivity data is evident.

3.3.5 Sand Backfill Cable Sizing Example

Sand is often used to backfill cable trenches in a direct buried configuration. This protects the cables from damage that might otherwise occur if native backfill were used containing rocks or other debris. Protection against cable damage is required by section 300.5 of the National Electrical Code, which states, “Where necessary to prevent physical damage to the raceway or cable, protection shall be provided in the form of granular or selected material”

[1, Sec. 300.5]. Also, some cable manufacturers recommend that “sand or stone-free earth” be used “within 4 inches of the cable” [17].

Sand has poor thermal properties compared with many native soils when it is dry, and it dries with relatively low heat rates if the surrounding soil does not have high moisture content. For the next example, a value of resistivity equal to 90°C·cm/W is used for the in-situ soil with a moisture content of 8%. All other values are the same as in the first two examples. In addition, a dry resistivity of 350°C·cm/W is used for the surrounding sand layer and a NHR of 0.1 W/cm will be assumed. Converting the NHR at the test probe diameter to the cable diameter using (3.1), based on test data in sand, yields the following:

$$\dot{q}_{c,probe} = \frac{2\pi(25°C - 20°C)}{90\frac{Kcm}{W} \cdot \ln\left(\frac{4 \cdot 120cm}{1.5875cm}\right)} = \frac{0.061W}{cm}$$

Note that this equation uses the maximum temperature reached during the NHR test for sand as well as the thermal resistivity of sand.

$$\dot{q}_{NHR,cable} = \frac{3.2cm\left(\frac{0.1W}{cm} - \frac{0.061W}{cm}\right)}{1.5875cm\left(1 - \frac{\frac{0.061W}{cm}}{\frac{0.1W}{cm}}\right)} = \frac{0.20W}{cm}$$

Because the cable heat rate is 0.37 W/cm and the NHR of the sand surrounding the cable is 0.2 W/cm, soil drying will occur. Equation (3.8) can be used to determine the extent of drying.

$$D_{dry\ soil} = \frac{1.5875cm \cdot \frac{0.373W}{cm\left(1 - \frac{\frac{0.061W}{cm}}{0.1\frac{W}{cm}}\right)}}{\frac{0.10W}{cm} - \frac{0.061W}{cm}} = 5.9cm$$

This diameter of dried soil can be accounted for by adding its resistance to R_{ca}' as stated by [28] using (34) in the same reference and shown in (3.10) below.

$$R_{dry\ soil} = 0.012\rho_{dry\ soil}\log\left(\frac{D_{dry\ soil}}{D_{cable}}\right) \quad (3.10)$$

where

$R_{dry\ soil}$ is the resistance of the dried soil (thermal ohms)

$\rho_{dry\ soil}$ is the resistivity of the dry sand (°C·cm/W)

Solving for the resistance added by the dried sand yields:

$$R_{dry\ soil} = 0.012 \cdot \frac{350Kcm}{W} \cdot \log\left(\frac{5.9cm}{3.2cm}\right) = 1.12\Omega_{thermal}$$

The effective resistance of the earth portion of the circuit, R_e' in [8], must be recalculated for the new diameter of the dried soil. It can then be added to R_{ca}'. This yields a new ampacity of 504 A rather than the 541 A previously calculated in Table 3.1, which did not include the dried sand. It confirms that a 350 kcmil will be adequate to handle the design current of 500 A but is much less than the ampacities calculated in Table 3.1. This result is stated in Table 3.3.

Table 3.3 Ampacity with dried soil included

Method	Current	Cable Size
Adapted Neher-McGrath	504A	350kcmil

This method addresses the issue of soil drying and the possibility of thermal runaway by calculating an expected dried soil diameter rather than assuming the surrounding soil all dries to a larger resistivity, which would result in installing larger than necessary cables. The engineer may still include a factor of safety when sizing cables because of the large impact slight variations of soil resistivity have on the ampacity. However, this factor of safety no longer needs to include the risk of thermal runaway.

3.4 Conclusions

The assumptions in several methods for determining underground cable ampacity have been shown. The older Black Books use an ambient earth temperature of 20°C while the IEEE Std 835 tables use an ambient earth temperature of 25°C. However, the IEEE tables assume the cable shields are shorted while the Black Books assume the shields are single point grounded. Overall, IEEE Std 835 results in a lower ampacity than the Black Books.

Using the Neher-McGrath method, or a software program using that method, allows for calculating cable ampacities using various soil resistivities, ambient temperatures, and shield grounding configurations. This reduces the error in the calculated ampacity by eliminating the assumptions used in the tables.

Regardless of the method, it is often economical to perform an in-situ soil thermal resistivity measurement rather than attempting to utilize the lab thermal resistivity measurements. Performing an in-situ test also allows for the measurement of the NHR, which can be used in thermal stability calculations. Using a higher value of resistivity, whether because the actual value is uncertain or because of concerns for thermal instability, can result in

a larger cable size and a significant cost increase when compared to using measured in-situ values.

The method proposed in [28] calculates an effective dried soil diameter rather than assuming a complete thermal runaway. This allows for a more accurate assessment of the cable size while including the risk of drying soil. These effects of soil thermal stability are otherwise not included in the Neher-McGrath method or the tabulated ampacities. The result is a design that includes all factors relevant to determining cable ampacity and that minimizes cost by preventing oversized cables due to unknown or poorly defined parameters.

CHAPTER 4
AMPACITY CALCULATION METHOD INCLUDING SOIL THERMAL STABILITY[4]

4.1 Introduction

When a cable is buried in soil, whether direct buried or in an underground pipe, the heat generated by the I^2R losses in the cable must be carried away through the soil surrounding the cable. The rate at which this heat can be carried away determines the temperature the cable will reach during any loading condition. If this temperature becomes too great the cable can be damaged. The thermal resistivity of the soil surrounding the cable is the main factor in determining the rate at which heat can be conducted away from the cable, and therefore, the ultimate amount of current the cable can carry. Soil thermal resistivity is one of the most important values that an engineer must know to calculate the amount of current any particular cable can be allowed to carry. Once the thermal resistivity of the surrounding soil is known the Neher-McGrath method is commonly used to determine the amount of current a cable can carry without exceeding its allowable temperature [8].

4.2 Measurement of Soil Properties

Thermal resistivity is a measure of the ability of a material to resist the flow of heat. In the case of soil this property is commonly measured using either laboratory or field tests. Several soil tests are commonly performed to characterize a soil's properties. A soil sample is taken from the field and the in-place soil unit weight test gives the overall soil unit weight in lb/ft^3 as given in (4.1). The water content of the soil sample is also tested, and the results of this test gives the weight of water contained in the soil sample divided by the weight of dried soil and is given in percent as shown in (4.2).

$$Unit\ weight = \gamma = \frac{\frac{pounds\ of\ soil}{cubic\ foot\ of\ soil}\,lb}{ft^3} \tag{4.1}$$

$$\%Water\ content = \omega = \frac{Weight\ of\ water}{Weight\ of\ dry\ soil} = \frac{W_w}{W_s} \cdot 100\% \tag{4.2}$$

[4] This chapter was previously published in an IEEE IAS Magazine [37] © 2016, IEEE. Reprinted, with permission.

A soil's thermal resistivity is measured by inserting a heat generating thermal probe into the soil or soil sample (if done in a lab) and soil resistivity is measured as described in IEEE Std 442 "IEEE Guide for Soil Thermal Resistivity" [27] [38]. A known heat rate in W/cm is injected into the probe and a plot is made of the temperature of the probe/soil interface versus time. Figure 4.1 illustrates an idealized example of a dry out curve that may result from this type of test.

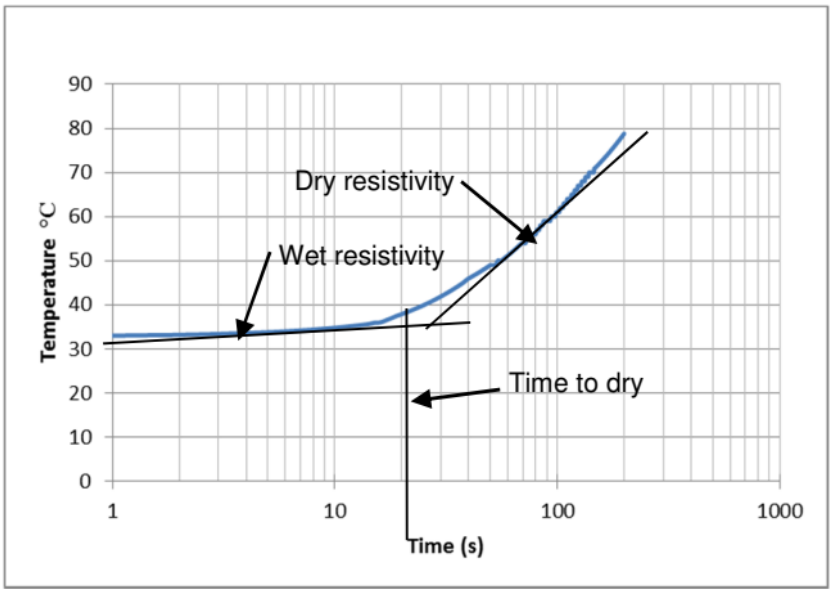

Figure 4.1 Soil drying curve

The graph in Figure 4.1 shows two fairly linear parts of this logarithmic temperature versus time curve. The part of the curve with the flatter slope represents the resistivity of the soil before it begins to dry. The part of the curve with the steeper slope represents the resistivity of the soil as the soil surrounding the probe dries. A soil's resistivity in each condition is proportional to the slope of the respective curves. In the either condition, wet or dry, the soil resistivity may be found using (4.3) [32].

$$\rho = \frac{4\pi}{q}\left[\frac{T_2 - T_1}{\ln\left(\frac{t_2}{t_1}\right)}\right] \tag{4.3}$$

Where

ρ = soil resistivity °C·cm/W

q = heat input in W/cm

T_1 = temperature at time t_1

T_2 = temperature at time t_2

Applying (4.3) to the case shown in Figure 4.1 the thermal resistivity on the wet part of the curve assuming 0.3 W/cm heat input is approximately 80°C·cm/W and the dry part of the curve the thermal resistivity is approximately 200°C·cm/W.

The effective drying time may also be found using this test. It will vary with heat input and soil moisture and will be the time measured to the knee point of the curve just before the resistivity of the soil changes as shown in Figure 4.1. The diameter of the probe and the heat input of the probe per unit length must also be recorded.

As the diameter of the heat source increases it is often claimed that the drying time will also increase. Some sources suggest that for a particular heat rate the drying time of the soil can be adjusted for a larger diameter heat source such as a cable using the measured drying time for the smaller diameter probe using (4.4) [32] [35] [20].

$$t_2 = t_p \left[\frac{D_2}{D_p}\right]^2 \tag{4.4}$$

Where

t_2 = soil time to dry with heat source diameter D_2

t_p = soil time to dry with probe diameter D_p

It is sometimes suggested that the time to dry for a particular diameter of cable being installed may be used to assess the stability of the soil resistivity [32]. However, the criteria used for such an assessment are difficult to define and caution is advised when using (4.4).

Laboratory tests are limited in the amount of information they can provide especially about moisture and its movement in the soil. Since the soil in the lab is not subject to natural moisture, it cannot provide information about water movement and the effect of that moisture movement on the heat source. It is reported that laboratory and field tests consistently provide differing results for the resistivity of soil [39]. The lab test may give a resistivity that is 2-3 times that of field tests.

While a curve similar to the one shown in Figure 4.1 is often used as an example of how soil resistivity is measured, when resistivity tests are performed in the field, curves of this nature will seldom be observed. In-situ tests will more frequently produce a curve similar to that shown in Figure 4.2 which shows data from the first 8 hours of a soil resistivity test taken with a 120 cm thermal probe with a heat input of 0.53 W/cm.

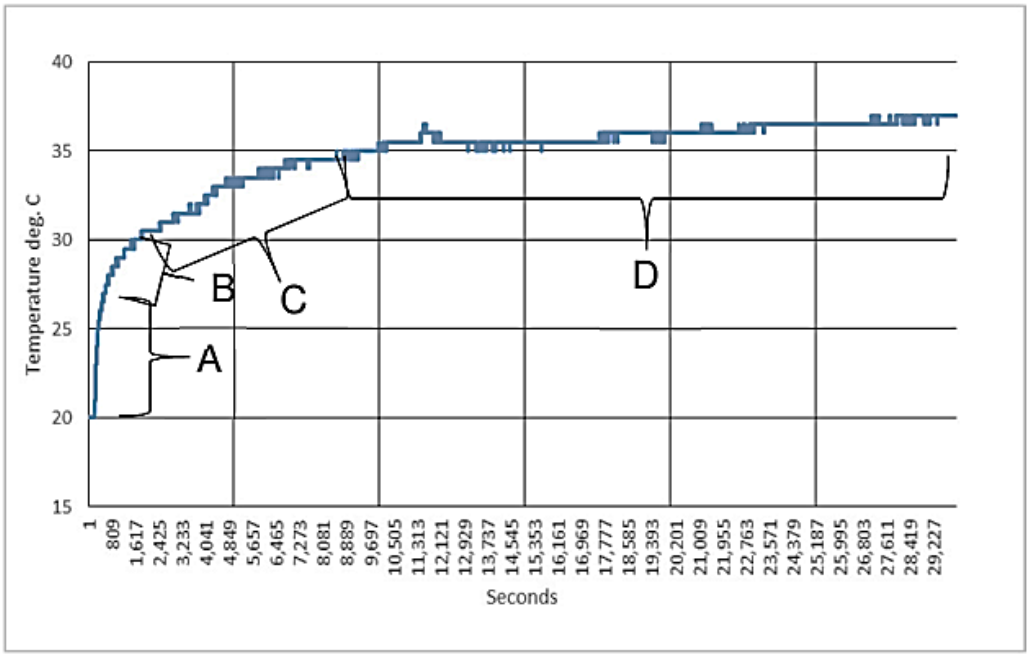

Figure 4.2 In-situ soil resistivity test results

There are four sections of data apparent from Figure 4.2. The following explanation is hypothesized to account for the measured data in this figure. Section “A” begins when heat is applied to the probe. The soil ambient temperature at this time is 20°C. This section is the transient portion of the heating test and lasts for approximately 10 minutes for the probe used. This represents the time the probe takes to heat up and cannot be used to determine the resistivity of the soil.

For clarity Sections “A” and “B” are extracted and plotted on a semi-log graph resulting in Figure 4.3.

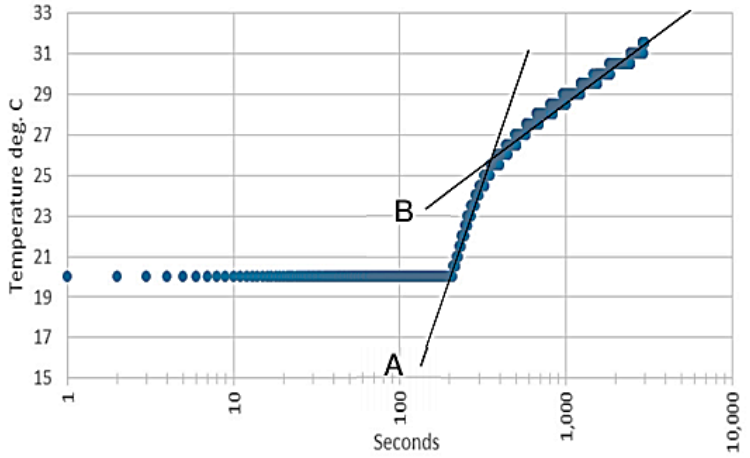

Figure 4.3 First 30 minutes of test

For the first ten minutes the probe and soil are heated producing slope “A” in this figure. After the probe has finished absorbing heat and reaches a quasi-steady state condition compared to the rate heat is being extracted by the soil, the slope of the graph changes from section “A” to section “B”. At this point the slope of the graphs is mainly due to heating the soil and the slope of “B” may be used with (4.3) to determine soil resistivity. This assumption can be made because the thermal time constant for the probe and soil interface is much smaller than the time constant of the soil itself.

The theory that permits using the slope of section “B” to determine the resistivity of the soil assumes an infinitely long line source of heat. As long as the thermal probe conducts heat in such a way that it approximates an infinitely long line heat source the slope of the resulting graph will be proportional to the soil thermal resistivity. However, at some point in time heat flow will no longer be one dimensional linear flow and will transition into two-dimensional heat flow. This transition region between one and two-dimensional heat flow is represented by Section “C” in Figure 4.2. This transition occurs approximately 45 minutes after the probe begins heating and lasts approximately 3 hours. During this time the soil is slowly heating and two-dimensional heat flow and end effects of the probe become important.

At the end of Section “C” and beginning of Section “D” the soil has reached a temperature of 36°C and becomes nearly constant. It then gradually increased at a rate beginning at about 1 degree/day increasing to slightly more than 2.5 degrees/day and decreasing once again to 0.5 degrees/day after 7 days. The soil finally achieved a constant temperature of 54°C at day 8. It stayed constant for the last 2 days of the test when the test was terminated. It is hypothesized that this gradual increase in temperature in Section “D” is due to a gradual reduction in moisture near the probe that resulted in the gradual increase in soil thermal resistivity near the probe thereby increasing the temperature of the probe. The soil finally achieved final equilibrium where this drying ceased, and the soil achieved its final resistivity for the heat rate used.

Using the slope of line “B” in Figure 4.3 the soil resistivity may be found using (4.3). It is suggested that when the in-field test is done and (4.3) is used to determine resistivity that T_1 is taken after approximately 10 minutes of heating (for most standard type probes) and T_2 is taken after approximately 25 minutes [27] later to avoid two-dimensional heating effects. In any case these values must be measured at two times when the data is as linear as possible but beyond the initial equipment controlled transient state. After 600 seconds T_1 was found to be 27.5°C and T_2 was measured at 30.5°C after 2100 seconds. The heat rate was 0.53 W/cm. Using (4.3) results in the following soil thermal resistivity.

$$\rho = \frac{4\pi}{q}\left[\frac{T_2 - T_1}{\ln\left(\frac{t_2}{t_1}\right)}\right] = \frac{4\pi}{0.53}\left[\frac{30.5 - 27.5}{\ln\left(\frac{2100}{600}\right)}\right] = 57°C \cdot \frac{cm}{W}$$

Now that the resistivity is known, an equation permitting the calculation of steady-state conductive heat flow from the thermal probe may be found using the appropriate conduction shape factor [16]. If a cylinder is inserted vertically into soil of a single thermal resistivity the common heat flow case shown in Figure 4.4 will result. This is the case of a vertical cylinder in a semi-infinite medium.

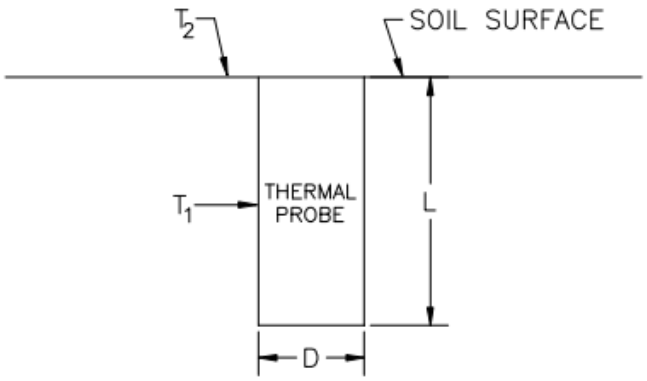

Figure 4.4 Thermal probe inserted vertically in soil

If the diameter and length of the probe, D and L, and soil thermal resistivity are known and the probe surface temperature T_1 is measured and soil surface temperature T_2 can be found under steady state conditions then a solution to the two-dimensional heat flow between the probe and the surface through an infinite soil layer bounded only at the surface may be found. It must be assumed that the thermal resistivity found is for a composite soil that can be assumed to be uniform, and the temperature T_2 will be assumed to be the ambient temperature of the soil at the depth of interest. During the time used for most testing, and at the soil depths of interest, these assumptions will be approximately true.

The shape factor for this condition where all dimensions are measured in centimeters and temperatures in degrees Celsius is [16]:

$$S = \frac{2\pi L}{\ln\left(\frac{4L}{D}\right)} \tag{4.5}$$

The thermal resistance of the soil for two-dimensional heat flow between the probe and the soil surface will be:

$$R = \frac{\rho}{S} = \rho \frac{\ln\left(\frac{4L}{D}\right)}{2\pi L} \tag{4.6}$$

Where

ρ = soil resistivity (°C·cm/W)

R = thermal resistance (°C/W)

S = shape factor from Equation 4.5

D = diameter of probe (cm)

L = length of probe (cm)

The equation for heat flow using the shape factor for this condition will be:

$$Q_c = \frac{\Delta T}{R} = \frac{S(T_1 - T_2)}{\rho} = \frac{2\pi L(T_1 - T_2)}{\rho \cdot \ln\left(\frac{4L}{D}\right)} Watts \tag{4.7}$$

The value of Q_c in (4.7), measured in Watts, is the amount of heat that is leaving the probe due to pure conduction in the soil.

The probe first achieves steady-state two-dimensional heat flow at the beginning of Section “D” of Figure 4.2. Assuming no change in soil thermal resistivity has yet occurred at this time, use (4.7) to find the heat flow due to conduction during this time period. The probe is 120 cm long, 1.5875 cm in diameter, T_1 was 36°C, and T_2 was soil ambient temperature—20°C.

$$Q_c = \frac{2\pi L(T_1 - T_2)}{\rho \cdot \ln\left(\frac{4L}{D}\right)} = \frac{2\pi(120\ cm)(36°C - 20°C)}{57\frac{°C \cdot cm}{W} \cdot \ln\left(\frac{4(120\ cm)}{1.5875\ cm}\right)} = 37\ Watts$$

Assuming the heat of conduction did not change with the final steady state condition after 8 days of testing the increase in soil resistivity may also be found using (4.7). Combining this equation for the 2 cases of different temperature changes but constant heat flow, the new thermal resistivity may be found using (4.8).

$$\rho_2 = \rho_1 \frac{\Delta T_2}{\Delta T_1} \tag{4.8}$$

For the case where the soil’s initial resistivity was 57°C·cm/W for the initial temperature change of 16°C, and the final temperature change after 8 days was 34°C, and assuming the heat of conduction through the soil did not change, the new apparent thermal resistivity would be:

$$\rho_2 = \rho_1 \frac{\Delta T_2}{\Delta T_1} = 57\frac{°C \cdot cm}{W}\left(\frac{34°C}{16°C}\right) = 121\frac{°C \cdot cm}{W}$$

From the measurements it appears that the soil has an initial resistivity to ambient earth of 57°C·cm/W and due to moisture changes near the probe the resistivity increases to 121°C·cm/W after several days of the application of 0.53 W/cm. It should be noted that the results shown are only valid for one soil moisture content and would be expected to change at other soil moisture contents. As the water content varies, as can be expected during the year in most locations, the resistivity of the soil will also vary [40].

More importantly, if the heat rate into the soil is increased, the soil will tend to dry more quickly near the heat source, changing the resistivity near the probe to a greater degree. The question that arises is which value of resistivity should be used in determining the ampacity of the underground cables? The moist value measured initially or the final dry value, or some intermediate value? It is clear that using the initial moist value will result in lower cable temperatures and using the final dry resistivity will result in much higher cable temperatures and lower allowable ampacities, and some intermediate value may be more accurate but more difficult to determine.

To answer this question, more than the soil resistivity must be measured. It is important to know if the soil will dry, and if so, how will this drying affect the soil resistivity and thus the cable ampacity calculations? The soil thermal stability must also be characterized so the design engineer can determine which value or values of thermal resistivity should be used and how they should be used. The question arises whether any useful information can be extracted from existing testing that will aid the engineer in determining the effects of soil drying on the cable ampacity.

4.3 Mechanism of Heat Transfer through Soil

Soil is made of solid particles in contact with each other at relatively small contact points as shown in Figure 4.5. The voids between the particles may contain either air or water. In dry soil the voids between particles are filled with air. Heat is conducted through the particles and between particles at the contact points. Some heat is also conducted through the air which has much more resistance to heat flow than the soil particles.

If the voids start to fill with water the effective contact area between particles increases resulting in increased conduction of heat. This reduces the resistivity of the soil. For this reason, an increase in water content means a decrease in soil resistivity and as the soil dries the resistivity will increase.

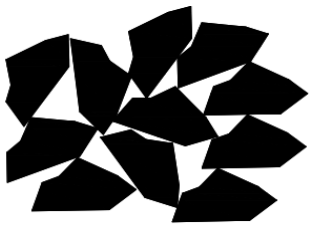

Figure 4.5 Soil particles with voids

If a heat source such as a current carrying cable is introduced into the soil the heat from the cable will cause the soil to dry out near the cable. As the soil dries its resistivity increases causing the temperature of the cable to increase. If the soil reaches some critical temperature and heat rate it may dry quickly allowing a type of thermal runaway condition where the dry soil increases in resistivity causing the cable temperature to increase which in turn more quickly forces the remaining moisture out of the soil. This is the basis of thermal instability that may occur which may cause the temperature of the cable to quickly increase until damage occurs.

There are two mechanisms by which moisture may move away from a heat source in soil. The first is movement in liquid form due to heat weakening surface tension between water and soil particles, and the second mechanism is due to vapor movement through the soil [41] [42]. Movement of moisture in the liquid state has been found to be a minor effect in the temperature change of cables [39] [43]. For this reason, only the second mechanism, the movement of vapor through the soil, will be considered as an effective enough mechanism to produce the type of drying seen in soils surrounding cables.

As the heat source heats, the surrounding soil the soil dries through evaporation. The water near the cable will vaporize and the increased pressure due to additional heating causes the vapor to move through the soil pores until it condenses in a cooler location [20]. As the water vapor leaves the area immediately surrounding the cable, water located farther from the cable flows back into the dried area due to the soil's hydraulic gradient as shown in Figure 4.6.

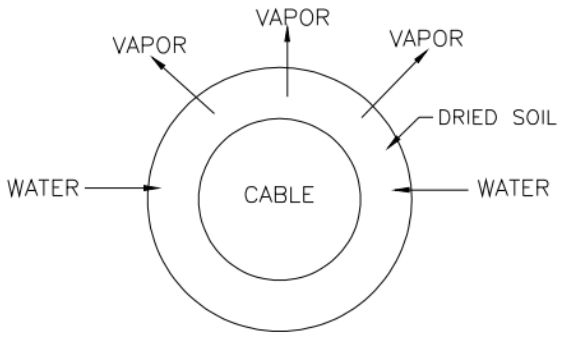

Figure 4.6 Vapor leaving and water entering a soil layer near a cable

If the rate that heat enters the soil is slow enough that the surrounding water can replenish the water that migrates away, then the resistivity of the soil will not change. If the heat source is large enough that water is vaporized and leaves the surroundings faster than the water can be replenished, then the soil will dry and increase the soil resistivity near the cable. If the soil never dries out use the wet value of resistivity as calculated in Figure 4.1, Figure 4.2 and Figure 4.3 for cable ampacity calculations. If the soil does dry out, then for some distance from the cable the dry value of soil resistivity must be used surrounded by soil at the moist resistivity value. In other words, the dry soil will form a cylindrical shell around the cable and be surrounded by moist soil. If the soil is partially dried, then it is suggested here that the use of a layer of some diameter of dried soil, surrounded by soil of the moist value of thermal resistivity, may still be used and will produce somewhat conservative results when determining cable ampacity. The question is: what is the diameter of this dried soil layer for a given heat rate?

4.4 Measuring Thermal Stability; Critical Heat Rate and Non-drying Heat Rate

After moist thermal resistivity is known the next requirement is to determine the rate at which water can flow into a dried area from the surrounding soil. Two heat rates are of interest:

1. Critical heat rate (CHR)
2. Non-drying heat rate (NHR)

The critical heat rate is the maximum heat rate at which the soil will not be dried completely and enter the area in Figure 4.1 beyond the “time to dry” line. This “time to dry” line is the time for the soil to reach a dried state. While this point is most easily seen in laboratory tests it may also occur in field tests that apply sufficiently high heat rates for a long enough period of time. Below the CHR the soil may begin to dry but will not dry to the point that the rapid increase in temperature shown in Figure 4.1 occurs. To find the value of the critical heat rate the heat input into the thermal probe could be increased in stages until a heat rate is found that is just sufficient to cause this rapid increase in resistivity.

To determine the critical heat rate in the lab the soil sample is divided into several equal parts and the time to dry is measured using a different heat rate input for each sample. A time to dry versus heat input graph is prepared as shown in Figure 4.7. The heat rate at which the graph become horizontal, showing soil would not dry at this input even after a long time, will be the critical heat rate [20].

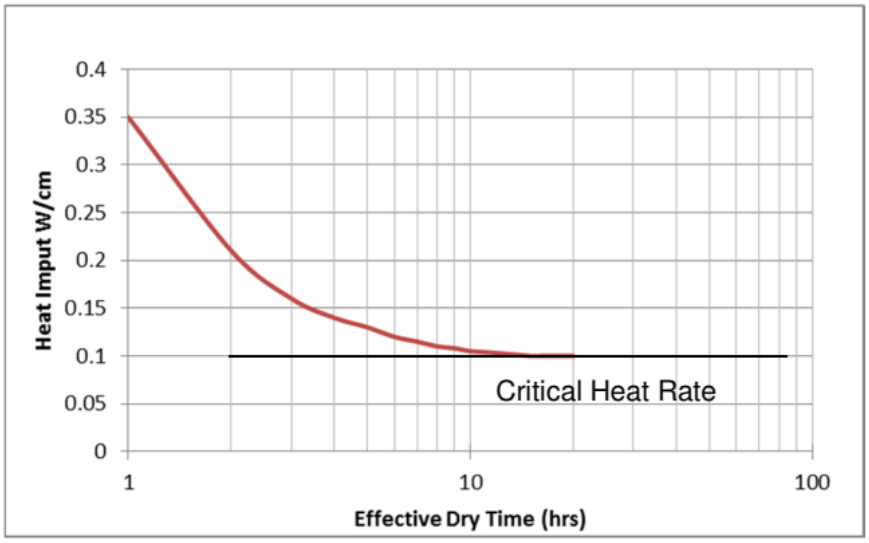

Figure 4.7 Thermal stability curve

The NHR is defined as the maximum heat rate at which the soil will not begin to dry. If the heat input used in the tests in Figure 4.2 had been slightly lower the temperature of the soil would have leveled off at 36°C and not increased. This would mean that the moisture leaving the area of the probe would be exactly balanced by the liquid flowing into the area around the probe; hence the soil would not dry. At and below the NHR it would be expected that soil resistivity would never change and the soil would not dry, so the temperature of the probe would be constant no matter how long heat was applied. The NHR can only be found in the field since it depends on the surrounding soil's natural vapor and liquid diffusivity levels and the moisture level and the soil's ability to supply moisture back to a drying area.

The rise in temperature in Section "D" of Figure 4.2 shows that the heat rate used was above the NHR since there was a gradual reduction in moisture and increase in resistivity. At exactly the NHR the water flowing back into the dried area would be returning at the maximum rate water could flow to a dried area through the soil. This would be the upper limit of the rate of moisture flow in the soil.

To find the NHR in the field start the probe at a low heat rate. If the temperature levels off after the transient portion of the curve and does not increase thereafter, the heat input must be at or below the NHR. Heat input may then be increased in stages until the point where the temperature begins to slowly trend upward as shown in Section "D" of Figure 4.2 occurs. If the temperature continues to trend up after the initial transient portion, it means that the soil is drying and changing in resistivity; therefore, the applied heat rate exceeds the NHR. To reduce the time it takes to determine the NHR, several thermal probes could be used simultaneously at different heat rates.

At the NHR, the moisture content near the heat source is in equilibrium and the mass of water leaving the area surrounding the heat source by evaporation will equal the mass of water entering the area. Were this not true the soil would dry. And if the NHR is known then the amount of moisture flowing back to the dried area would be the maximum the soil could supply. Using this knowledge will allow us to approximate the rate that water flows through the soil and the amount of soil that will dry at other heat rates.

4.5 Heat Flow from the Thermal Probe

For most cable ampacity calculations, it is usually assumed that all heat leaving the cable is due to conduction through the soil. However, if the soil is drying then the water leaving the soil must also be transferring heat and conduction is not the only method of heat transfer.

In the test shown in Figure 4.2 the heat input was 0.53 W/cm for a 120 cm probe this would be a total heat input of 63.6 W. However, from (4.7) the heat of conduction was found to be only 37 W. For the thermal probe used in this test the heat flow up the probe to the air was calculated to be approximately 1.5 W. This leaves 25.1 W unaccounted for. It is hypothesized that this heat is used to increase the temperature of the inflowing water from ambient soil temperature to the temperature of the probe. The continued heating vaporizes the water, which then leaves the area of the probe and draws liquid water into the dried area. To simplify the following, it is also assumed that a steady-state condition has developed where the existing water near the probe has already heated to a constant temperature. In addition, an equilibrium condition exists where the temperature gradients due to conduction in the soil have stabilized. Therefore, the only movement of heat is through conduction and the movement of water in liquid and vapor form. It is also assumed that the heat transfer due to convection and radiation in the soil is negligible.

The following discussion is based upon the hypothesis that there are only three ways heat transfer occurs from a heat source buried in the soil.

1. Conduction, which can be calculated if temperature and soil resistivity is known.
2. The latent heat of vaporization due to evaporation near the heat source followed by movement away from the source through the soil.
3. The heating of the water flowing back into the area from surrounding soil replacing the displaced vapor.

Equation (4.9) is the heat balance equation describing heat flow from the probe.

$$qL = Q_c + Q_w + Q_v \tag{4.9}$$

Where

q = heat rate into the probe (W/cm)

L = length of probe (cm)

Q_c = heat carried away by conduction (W)

Q_w = heat absorbed by inflowing water (W)

Q_v = heat carried away by vapor (W)

The heat absorbed by the inflowing water, Q_w, and leaving by evaporation, Q_v (assuming the temperature change of the water takes place as it moves from ambient earth to the heat source and evaporation takes place with no temperature change) is:

$$Q_w = C_w m_w \Delta T \tag{4.10}$$

$$Q_v = h_v m_v \tag{4.11}$$

Where

C_w = heat absorbed by inflowing water (4.18 J/g·°C = 1,890 J/lb·°C)

m_w = mass of water (kg/s or lb/s)

h_v = latent heat of vaporization of water (2,260 J/g = 1,025,000 J/lb)

m_v = mass of water evaporated in (kg/s or lb/s)

ΔT = change in temperature of inflowing water from ambient temperature (°C)

Combining (10) and (11) with (9):

$$qL - Q_c = C_w m_w \Delta T + h_v m_v = Q_w + Q_v \tag{4.12}$$

If the NHR is known, then determine the rate vapor is leaving the soil and water is returning by using the NHR for q in (4.12). At the NHR the soil will not dry no matter how long the heat source is applied because the mass of water leaving the soil as vapor will equal the mass of water flowing back as liquid preventing drying and any change in soil resistivity. For this condition where q=NHR then the mass of water entering the soil must equal the mass of vapor leaving the soil: $m_w=m_v=m_{NHR}$ resulting in (4.13).

$$Q_{NHR} - Q_c = C_w m_w \Delta T + h_v \mathrm{m_v}$$

$$Q_{NHR} - Q_c = \mathrm{m}(C_w \Delta T + h_v)$$

$$m_{NHR} = \frac{Q_{NHR} - Q_c}{C_w \Delta T + h_v} \tag{4.13}$$

This equation is the mass of either vapor leaving the soil or water returning to the dried area at equilibrium due to being at NHR, making $q \cdot L = Q_{NHR}$.

If it is assumed that ΔT, the change in temperature of the inflowing water, will be the temperature difference between the soil ambient temperature and the probe temperature then referring once again to Figure 4.4, (4.13) becomes Equation (4.14):

$$m_{NHR} = \frac{Q_{NHR} - Q_c}{C_w(\mathrm{T}_1 - \mathrm{T}_2) + h_v} \tag{4.14}$$

Where

m_{NHR} = mass of water or vapor (kg/s or lb/s at NHR)

Q_{NHR} = heat carried away by conduction (W)

T_1 = temperature of the probe (°C)

T_2 = ambient soil temperature (°C)

In order to get the flow rate per unit length, the result of (4.14) must be divided by the length of the probe.

It is clear from Figure 4.2 that the heat rate used for the test was slightly higher than the NHR. The heat rate used was probably not far above the NHR since the soil remained at 36°C for several hours and the subsequent increase in temperature was very slow. Understanding that using these values may be slightly non-conservative, if we estimate the NHR as 0.53 W/cm and Q_{NHR}=63.6 W and using (4.14) results in the following maximum flow of water through the soil.

$$m_{NHR} = \frac{63.6\ W - 37\ W}{1890\ {}^{J}/_{lb \cdot {}^{\circ}C}\,(36^{\circ}\mathrm{C} - 20^{\circ}\mathrm{C}) + 1{,}025{,}000\ {}^{\mathrm{J}}/_{\mathrm{lb}}} = 2.52 \cdot 10^{-5}\ {}^{lb}/_{s}$$

To get the mass flow rate per unit length of the probe, divide the result by the probe length of 120 cm.

$$\dot{m}_{NHR} = \frac{2.52 \cdot 10^{-5}\ {}^{lb}/_{s}}{120\ cm} = 2.1 \cdot 10^{-7}\ {}^{lb}/_{s \cdot cm}$$

This represents the maximum rate at which liquid water can flow back into a dried area. The soil will begin to dry if it is called upon to replenish the water at a rate greater than this. Using a density for water of 62.2 lb/ft^3 this would be $4 \cdot 10^{-7}$ ft^3/sec or 0.011 gal/hour.

If the moisture content of the soil during the determination of the NHR is known, and it is desired to find the flow rate at other moisture contents, the flow rate should increase or

decrease proportionally to the moisture content of the soil assuming the hydraulic gradient will increase or decrease in the same manner. So, the flow rate should be corrected for the minimum water content expected in the soil at a particular location.

4.6 Extent of Soil Drying

Referring once again to the test in Figure 4.2 the question arises that after the soil begins to dry and resistivity begins to increase in Section “D”, why does the temperature once again level off and quit rising after about 8 days? Why does the soil not continue to dry until it reaches its dry resistivity?

The moisture leaving the area of the thermal probe will migrate fastest from the warmest temperature next to the probe. To simplify analysis, it is assumed that the drying process will proceed in a manner that will completely dry a small annulus of soil next to the heat source and the diameter of this dried layer will gradually move outward as more soil dries. So, a completely dry layer is produced next to the probe surrounded by soil at its natural moisture level. The dried area will increase in size and the soil effective resistivity in relation to the probe will gradually increase.

The water replenishing the vapor that leaves the vicinity of the heat source flows into the dried area because of the hydraulic gradient that exists in the moist soil. It is assumed that this hydraulic gradient will remain constant in the interface between wet and dry soil during the drying process. Furthermore, it is assumed that the surrounding soil has sufficient moisture to replenish the dried area indefinitely without significantly affecting the ambient hydraulic gradient.

The maximum rate moisture can return to the dried area is determined using (14). This value of water flow would be the amount of water flowing into a dried volume equal to the volume of the heated probe. This water must flow through an area of soil equal to the surface area of the probe. However, as soil dries a small annulus of dried soil will be created between the probe and the moist soil as shown in Figure 4.8.

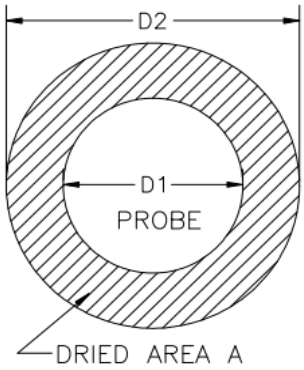

Figure 4.8 Dried soil surrounding probe

The drying process will increase the area through which moisture may flow back into the dried area. Where the original area was equal to πD_1 (for a unit length of probe) the new area after slight drying would be equal to πD_2.

Darcy's law describes the flow rate of a liquid through soil [44]. Darcy's law may be written as (15).

$$q = kiA \tag{4.15}$$

Where

q = flow rate

k = soil permeability

I = hydraulic gradient = head ÷ length of flow path

A = area through which water flows

Assuming the hydraulic gradient and permeability at the moist/dry interface will remain nearly constant, the only thing that will change as the dried soil area expands and moves away from the heat source is the area through which the replenishing water flows back into the dried area, and this area would increase as the diameter of the dried area increases. The drier the soil that exists and the farther we get from the heat source, the larger the area becomes through which water can flow back to the dried area. Comparing the flow rate between any two areas using Darcy's law:

$$\frac{q_1}{q_2} = \frac{kiA_1}{kiA_2} = \frac{A_1}{A_2} \tag{4.16}$$

Using the computed flow rate at the NHR as the flow rate at the original probe diameter and assuming the length of the dried area remains the same this becomes:

$$\frac{m_{NHR}}{\pi D_{probe}} = \frac{m_2}{\pi D_2} \tag{4.17}$$

Where

m_2 = flow rate (kg/s or lb/s) through D_2

D_2 = dried diameter (cm)

As the dried area increases in size, the flow rate of water into the dried area will also increase proportionally.

If the heat rate into the heat source is increased to some level above the NHR, the soil will dry radially outwards from the source until equilibrium is once again established between the mass of vaporized water and the amount of water that can return to the dried area. The circumference of the dried soil will increase until it is sufficiently large to allow the moisture entering the dried area to just equal the moisture being vaporized by the new heat rate. At this point the drying process will increase. This accounts for the stabilization of soil resistivity that was witnessed after an 8-day period during the test shown in Figure 4.2.

The rate that heat is leaving the soil due to moisture being raised from ambient temperature to the temperature at the wet/dry soil interface and leaving the area as vapor would be:

$$Q_w + Q_v = C_w m_w \Delta T + h_v m_v$$

If this occurs at the point where the diameter of the dry area has increased so a non-drying equilibrium is once again established, then the mass of water entering the soil equals the mass of water leaving and m_w=m_v=m, as shown in Equation (4.18):

$$m = \frac{Q_w + Q_v}{h_v + C_w \Delta T} \frac{lb}{sec} \tag{4.18}$$

Where

$m = m_w = m_v$ = flow rate of water or water vapor (lb/s)

Q_v = heat input available to vaporize water (W)

h_v = latent heat of vaporization of water (2,260 J/g = 1,025,000 J/lb)

Substituting (4.18) into (4.17) results in an equation for the diameter of dried soil D_2 that would result from moisture being vaporized by a heat rate equal to any arbitrary Q for the soil at which m_{NHR} and D_{probe} are known.

$$\frac{m_{NHR}}{\pi D_{probe}} = \frac{\frac{Q_w + Q_v}{h_v + C_w \Delta T}}{\pi D_2}$$

$$D_2 = \frac{D_{probe}(Q_w + Q_v)}{m_{NHR}(h_v + C_w \Delta T)} \tag{4.19}$$

If the heat rate is increased above the NHR, the diameter of the dried area of soil will increase and the temperature of the probe will increase due to the increase in soil resistivity next to the probe. An increase in heat rate would also be expected to increase the temperature at the moist/dry soil interface above that measured at the NHR. The increase in diameter would slightly decrease the resistivity between the moist/dry soil interface and ambient earth by increasing D in (4.17). Both of these effects would increase the heat conducted away from the heat source. However, the increase in temperature would also tend to increase the rate of evaporation from the moist/dry soil interface. It is unknown whether one effect will outweigh the other, i.e. whether the heat carried away by evaporation will increase more than the heat carried away by conduction, or whether the converse will be true.

This also means that ΔT is not precisely known for a new heat rate. However if we make the conservative assumption that the temperature of the water entering the moist/dry interface will increase at least as much as before the increase in heat rate, and furthermore assume that the heat transfer by conduction and heat transfer due to water movement will both increase at the same rate that the total heat rate increased, then we can solve (4.19) to determine the diameter of dried soil at the new heat rate using the following:

$$Q_c = \frac{Q_{new}}{Q_{NHR}} Q_{cNHR} \tag{4.20}$$

$$Q_w = \frac{Q_{new}}{Q_{NHR}} Q_{wNHR} \tag{4.21}$$

$$Q_v = \frac{Q_{new}}{Q_{NHR}} Q_{vNHR} \tag{4.22}$$

$$Q_w + Q_v = \frac{Q_{new}}{Q_{NHR}} (Q_{wNHR} + Q_{vNHR}) \tag{4.23}$$

Where

Q_c = heat transfer by conduction at the new heat input Q_{new}

Q_{cNHR} = heat transfer by conduction at Q_{NHR}

Q_w = heat transfer by inflowing water at the new heat input Q_{new}

Q_{wNHR} = Heat transfer by inflowing water at Q_{NHR}

Q_v = heat transfer by vapor at the new heat input Q_{new}

Q_{vNHR} = Heat transfer by vapor at Q_{NHR}

Q_{new} = new heat input to the probe

Using the example given earlier, if we doubled the heat rate into the probe from the NHR of 0.53 W/cm to 1.06 W/cm, for a change from 63.6 W to 127.2 W, this would also double the conduction rate from 37 W to 74 W leaving 50.2 W to be carried away by vaporization and heating of inflowing water (assuming 3 W lost to air in the probe). So, the new (Q_w + Q_v) = 50.2 W at the new heat rate using (4.23). The heat probe used in the testing had a diameter of 1.5875 cm. Using (4.19) to find the dried area:

$$D_2 = \frac{1.5875\ cm\ (50.2\ W)}{2.52 \cdot 10^{-5}\ {}^{lb}/_{s}\ \left(1890\ {}^{J}/_{lb\ .\ ^{\circ}C}\ (36^{\circ}\mathrm{C} - 20^{\circ}\mathrm{C}) + 1{,}025{,}000\ {}^{\mathrm{J}}/_{\mathrm{lb}}\right)} = 3\ cm$$

A dried area with a diameter of 3 cm would have resulted from this increase in heat rate. This would be a layer of dried soil of approximately 0.71 cm surrounding the probe on all sides.

If the volume of dried soil is known, and the maximum flow rate back into the soil is known, then the time for a dried area to completely return to its natural moisture level after the removal of the heat source can be found. If m_{NHR} is the maximum flow rate at the original probe diameter, and D_2 is the maximum diameter of the dried area, then the flow rate at the maximum diameter according to (4.17) would be:

$$m_2 = \frac{D_2 m_{NHR}}{D_{probe}}$$

The average flow rate back into the dried area will then be:

$$m_{avg} = \frac{m_{NHR} + m_2}{2} = \frac{1}{2}\left(m_{NHR} + \frac{D_2 m_{NHR}}{D_{probe}}\right) = \frac{m_{NHR}}{2}\left(1 + \frac{D_2}{D_{probe}}\right) \qquad (4.24)$$

If the in-place unit weight of soil and the moisture content of the soil are known, then the amount of water originally contained in the area of the soil around the probe may be found.

γ = unit weight of total soil sample (lb/ft³)

γ_w = weight of water per unit volume of soil sample (lb/ft³)

γ_s = weight of dry soil per unit volume of soil sample (lb/ft³)

ω = moisture content of the sample (%), Equation (4.2)

$$\gamma = \gamma_s + \gamma_w \tag{4.25}$$

$$\gamma_w = \omega\gamma_s$$

$$\gamma_s = \frac{\gamma_w}{\omega} \tag{4.26}$$

Substituting (4.26) into (4.25) and solving for the weight of water per total volume of soil:

$$\gamma = \frac{\gamma_w}{\omega} + \gamma_w = \gamma_w\left(1 + \frac{1}{\omega}\right) = \gamma_w\left(\frac{\omega + 1}{\omega}\right)$$

$$\gamma_w = \frac{\omega\gamma_s}{1+\omega}\ {lb\ water}/{ft^3 of\ total\ soil} \tag{4.27}$$

For a cylinder of dried soil 3 cm in diameter surrounding the probe that is 1.5875 cm in diameter and 120 cm long, the volume of the dried cylinder of soil would be:

$$V = \left(\frac{\pi D_2^2}{4} - \frac{\pi D_{probe}^2}{4}\right)L \tag{4.28}$$

$$V = \frac{\pi}{4}(3cm^2 - 1.5875cm^2)120cm = 610.7cm^3$$

If the soil unit weight was measured at 120 lb/ft³ (0.0042377 lb/cm³) and the moisture content was 12% the weight of water originally in the volume V of dried soil before it was dried would be from (4.27):

$$V\gamma_w = 610.7cm^3\frac{\gamma\omega}{1+\omega} = 610.7cm^3\frac{0.0042377\frac{lb}{cm^3}(12\%)}{1+12\%} = 0.277\ lb$$

Using (4.24) the average flow rate into the area would be:

$$m_{avg} = \frac{m_{NHR}}{2}\left(1 + \frac{D_2}{D_{probe}}\right) = \frac{2.52\cdot 10^{-5}\ {lb}/{s}}{2}\left(1 + \frac{3\ cm}{1.5875\ cm}\right) = 3.64\cdot 10^{-5}\ {lb}/{s}$$

This would result in a time to replenish the moisture in this area of dried soil of:

$$t = \frac{V\gamma_w}{m_{avg}} \tag{4.29}$$

$$t = \frac{0.277\ lb}{3.64 \cdot 10^{-5}\ {}^{lb}/_{s}} = 7609\ s = 2.11\ hours$$

So, it would take approximately 2 hours for the moisture to flow back into the area that was dried by the increased heat rate after the heat was removed.

4.7 Vertical Probe Test Results used for Horizontal Cables

The values we have measured using the vertical probe may be used for calculations for a horizontal cable buried in the earth. Both the soil resistivity and the maximum water flow rate will be the same for the vertical and horizontal heat source. Equations (4.5), (4.6), and (4.7) describe the heat flow from a vertical cylinder in a semi-infinite medium. Their counterparts for heat flow in from a horizontal cylinder of length L in a semi-infinite medium are:

$$S = \frac{2\pi L}{\ln\left(\frac{4z}{D}\right)} \tag{4.30}$$

$$R = \frac{\rho}{S} = \rho\frac{\ln\left(\frac{4z}{D}\right)}{2\pi L} \tag{4.31}$$

$$Q_c = \frac{2\pi L(T_1 - T_2)}{\rho \ln\left(\frac{4z}{D}\right)}\ W \tag{4.32}$$

Where

z = cable burial depth

D = cable diameter

Equation (4.32) is known as the short form of the Kennelly equation and is a valid approximation for cases where z is more than 1.5 times the cable diameter [39].

A comparison of (4.5), (4.6), and (4.7) with (4.30), (4.31) and (4.32) shows that they are identical if the depth of burial of the horizontal cable z is equal to the length L of the vertical probe. So, a cable of the same diameter as the probe buried at the depth equal to the length of

the probe and supplying the same heat rate should perform identically with the vertical probe. All heat rates, temperatures, and evaporation rates will be the same.

For a cable, however, both the diameter and the burial depth may vary from the vertical probe. This will change the amount of heat conducted away from the horizontal cable versus the amount of heat leaving through vaporization from the values computed. It is unlikely that the diameter of an underground cable will be less than the diameter of the vertical probe. If the underground cable of interest is larger than the vertical probe the result will be that the thermal resistance to ambient earth will decrease according to (4.31). This would mean that for the same heat rate used for the smaller diameter probe the temperature of the cable/soil interface would be less than the temperature of the probe. This lower temperature would tend to reduce the evaporation rate. This would decrease the heat carried away by vapor and increase the amount of heat conducted away resulting in an increase in the temperature of the cable/soil interface for any condition above the NHR. Increasing the diameter of the cable should decrease the temperature of the cable to some degree, but less than the value calculated using (4.32) with the same heat rate of conduction used in the probe. Furthermore, the rate of evaporation will also decrease to some degree. While it is unknown exactly how much conduction will increase or evaporation decrease, if the original values calculated for the vertical probe for both conduction and evaporation are used, a conservative result is expected. Using these assumptions, the diameter of dried soil calculated should be more than what will actually occur since the evaporation rate is reduced. It should also be noted that if the calculated diameter of dry soil is less than the diameter of the cable then the soil around the cable would be expected to never dry out at the heat rate used in the calculations.

If the depth of the cable in question were increased to be below the surface more than the length of the test probe, then according to (4.31) the thermal resistance to ambient earth will increase. If the heat rate of conduction was assumed to be equal to the heat rate of conduction for the probe, then the temperature of the cable/soil interface must increase from the temperature of the probe. This higher temperature will tend to increase the evaporation rate and increase the amount of heat carried away by water. Since more heat is being carried away by the water vapor, this leaves less heat needing to be transferred by conduction. This will in turn tend to reduce the heat transfer by conduction. A suggested approach is to use (4.32) to compute the heat transfer due to conduction from the buried cable, Q_{cNHR} using the original probe temperature for T_1 at the new cable depth z, and then modify Q_{cNHR} using (4.20) to get Q_c. Then the following heat balance equation is solved.

$$Q_{new} = Q_c + Q_w + Q_v$$

$$Q_w + Q_v = Q_{new} - Q_c \quad (4.33)$$

Where

Q_{new} = cable heat (W)

Q_c = Heat transfer by conduction calculated as described using (4.32)

This value $Q_w + Q_v$ determined using (4.33) can then be used in (4.19) to determine the diameter of dried soil for a cable deeper than the length of the probe. A cable buried at a depth less than the length of the probe should present the opposite case and using the original values computed for the probe should result in a conservative estimate for the diameter of dried soil. It should be noted that the equations for heat flow may not be accurate for depths of cable much less than the length of the probe. Use care when applying this method to shallow cables since actual temperatures may vary considerably from the assumptions made. Also, when long cables are involved, heat and moisture values can be converted to per unit length of cable by dividing by the probe length rather than working with bulk values.

4.8 Summary of Procedure

To find the thermal resistivity of the dried soil surrounding a direct buried cable at any expected heat rate, and the expected diameter of this dried soil around the cable, the procedure suggested herein is:

1. Determine soil in-place unit weight using (4.1) by any accepted method [45] [46] [47].
2. Determine water content ω using (4.2) by any accepted method [36] [48] [49].
3. Using the in-the-field thermal resistivity test equipment [27], start with a heat input of 0.1 W/cm. If the probe temperature reaches an equilibrium temperature and does not change for a period of 3 hours, increase the heat input by 0.1 W/cm to 0.2 W/cm. Repeat this process increasing by the same step size until the point where the temperature slowly increases and does not reach an equilibrium temperature in 3 hours. The highest heat input at which an equilibrium temperature is achieved is the assumed non-drying heat rate q_{NHR}. At this heat rate under steady-state temperature conditions, record: the heat input (q_{NHR}) and calculate Q_{NHR} by multiplying by probe length L; steady state probe temperature (T_1); beginning probe temperature (soil ambient temperature T_2).
4. Calculate the soil thermal resistivity using the data measured in Step 3 for the initial application of heat and using (4.3) (using T_2 at t_2=2400 seconds and T_1 at t_1=600 seconds

after the application of heat in this Equation). If the initial heat input in Step 3 does not produce a large enough temperature variation in the time suggested to produce an accurate result, then a separate thermal resistivity measurement will be needed. A heat input of between 0.5 and 0.8 W/cm is suggested for this test. (Note: The values of T_1 and T_2 used in this step are not the same values as those recorded in Step 3. See the method for calculating resistivity for these values).

5. At the steady state temperature reached at Q_{NHR} and using the data recorded in Step 3 calculate the heat carried away by conduction Q_c using (4.7). Use the results to compute the maximum mass of water flowing back to the dried area, m_{NHR}, using (4.14).
6. Find (Q_W+Q_V) at the non-drying heat rate (NHR) using (4.12). This value should be reduced by the heat loss in the system that is not transferred to the soil if it can be estimated.
7. Find the design heat rate in W/cm that will be injected into the soil by the cable [8]. This is calculated using the expected design current and cable resistivity. Determine the new value of heat transferred by water (Q_W+Q_V) using (4.23), and if necessary, (4.32) and (4.33).
8. Using the values calculated in Step 7 for (Q_W+Q_V), find the dried soil diameter at the new heat rate using (19). If the diameter of dried soil is less than the diameter of the cable, then soil drying will not occur at the heat rate used.
9. Determine the dry soil resistivity using the laboratory method [27] [50], or in field method if possible.
10. When preparing the soil thermal model to determine cable ampacity, model the soil resistivity surrounding the cable as a layer of dried soil with a resistivity determined in Step 9 and a diameter determined in Step 7. This will be surrounded by soil of ambient thermal resistivity as determined in Step 4. The final soil thermal model is shown in Figure 4.9.

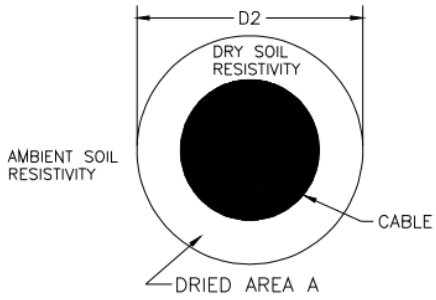

Figure 4.9 Diagram of thermal model

11. Add the thermal resistance of this dried soil layer to R_{ca}' (or to R_{sd} if conduit or electrical ducts are involved) in the Neher-McGrath equation. The value of thermal resistance to be added is computed using the equation:

$$R = 0.012\rho_{dry\ soil} \log\left(\frac{D_2}{D_1}\right)\ Ohm \cdot ft \quad (4.34)$$

Where

D_2 = computer maximum diameter of dried soil from Step 8

D_1 = diameter of the cable or conduit

$\rho_{dry\ soil}$ = resistivity of the dry soil from Step 9

The value used for D_e in the Neher-McGrath calculations would also change from the diameter of the beginning of the earth portion of the thermal circuit, to the diameter of the beginning of the earth circuit surrounding the dried soil, i.e. D_e is now D_2 stated above [8].

12. If it is desired to calculate the time it will take to replenish the moisture in this area of soil, an approximate value can be calculated using (4.29) and using the diameter of the cable rather than the diameter of the probe and the moisture rate per 1 cm length of cable.

4.9 Conclusions

The same field tests often used to determine soil thermal resistivity may provide additional information that can help to determine the amount of dried soil surrounding a cable that may be expected for varying heat rates. The thermal probe can be used to determine the non-drying heat rate of the soil being studied. This value in turn can be used to determine the maximum rate water can flow into a dried area of soil from the surrounding soil. When this is known then the diameter of soil around a cable that will dry can be determined for any heat input rate. This process will help the design engineer dramatically in properly sizing the cable. Currently, the engineer typically assumes a worst-case thermal runaway resistance, which results in cable sizes that may be too large.

The dried soil resistivity can sometimes be determined in the field but may need to be found using laboratory tests. When this is determined, then a thermal model can be built that includes the typical values used in Neher-McGrath calculations plus the thermal model of the worst-case dried soil layer that is expected at the heat rate of interest. This model will consist of the cable surrounded by the thermal resistance of the insulation and jacket, conduit if used, plus the thermal resistance of the dried soil of the diameter calculated, plus the thermal resistance of the unaffected soil surrounding the dried area. These values can then be included in the normal methods of determining cable ampacity [8].

CHAPTER 5
SOFTWARE MODELING TOOLS

There are several commercially available software packages that assist engineers in calculating underground power cable ampacity. These software packages implement the Neher-McGrath method [8] or IEC 60287-1 [13], providing results for both steady state and transient responses. As previously described, the calculations required for even a simple installation are numerous, on the order of 100 separate equations (shown in Appendix A). Adding additional cables to a simple installation dramatically increases the equations and often requires solving them iteratively. This propels engineers to utilize software to perform the calculations, freeing up time to optimize the design rather than painstakingly calculating each equation. Even during the early stages of computer development, the difficulty of performing these calculations was traded for the difficulties of programming and using a computer-based method. The Black Books published in the 1960s and described in a previous section of this work, were developed using the "Anaconda Wire and Cable Company's IBM 650 digital computer" and it took 8 years to complete the setup, work through issues and publish the results [10]. With modern computers, these calculations can be performed on the order of seconds. The processing power of a computer allows for additional calculations and numerical methods to be performed. For example, the finite difference method is used by CYMCAP to address gaps in the Neher-McGrath method when modeling multiple adjacent duct banks [51]

The most common software packages used for calculating ampacity are:

- Eaton CYME CYMCAP, cyme.com/software/cymcap
- ETAP Power Systems Analysis Software, etap.com
- PTW SKM Electrical Engineering Software, skm.com
- USi USAmp Prime Cable Ampacity, usi-power.com/software-applications-usamp
- CalcWare AmpCalc Cable Ampacity Software, calcware.com

These are ordered in the number of features and general popularity in industry based on perceived usage. The order or description below is not intended to convey recommendation by the author of one over the other. Also, many statements represent experience and opinion of the author rather than the marketing material provided by the vendor. They are also approximately ordered by cost, ranging from about $15,000 for CYMCAP (depending on purchased features) down to about $2,000 for AmpCalc. Each software provides ampacity calculations for user entered data, but each has unique capabilities. Some examples are listed here, but more detailed descriptions are provided in the following sections. CYMCAP offers

additional capabilities not typically found in ampacity software packages by allowing for multiple backfill materials around the cables, multiple casings (ducts) around cables, unfilled cable trench, and circuit crossings. ETAP allows for integrating with the project electrical power flow and using the calculated cable loading as the input to the ampacity problem. SKM recently added the ampacity feature to the base package it offers. Both ETAP and SKM allow for system power flow modeling, short circuit calculations, and other calculations beyond cable ampacity.

An interesting history of these software packages is provided by Francisco De Leon [52]:

> "The first and most advanced commercial program for cable ampacity calculations is CYMCAP. Its development started in the 1980's jointly by Ontario Hydro (Hydro One), McMaster University and CYME International, under the auspices of the Canadian Electricity Association (CEATI). CYMCAP is based on the IEC Standards and features a very friendly GUI (Graphical User Interface). Over 100 companies in close to 50 countries use CYMCAP. This program can compute steady state ampacities and transient ampacities. CYMCAP features a duct bank optimizer and the possibility to handle several duct banks with different thermal resistivities in the same installation.
>
> USAmp is next in the development ladder. It is based on the Neher-McGrath method for steady state ampacity calculations. It supports transients based on the CIGRE report [13]. It has a GUI, but data is entered and displayed mostly in tabular form. USAmp has been used to obtain the IEEE Standard tables published in [2].
>
> ETAP is another tabular program based on the Neher-McGrath method. It does not support transient ampacity calculations. There are other smaller programs such as: PCORP, Underground Cable Ampacity Calculator, etc. with rudimentary GUI's and calculation engines. Some are royalty free, with no documentation or technical support."

Since the publication of this quote by De Leon, ETAP has added transient ampacity calculations. This work focuses on using two software packages for cable ampacity, CYMCAP and ETAP, primarily because they were easily accessible during the development of this work.

5.1 CYMCAP

CYMCAP is focused on calculating cable ampacity. Other products of Eaton's CYME Power Engineering Software are available for performing additional power system design

calculations such as power flow analysis, coordination studies, or other studies. Because of the focus of CYMCAP is cable ampacity, it lends itself to quickly beginning the underground cable analysis. It also steps the user through entering the required cable data rather than relying on typical values. For example, the user is prompted to enter the critical, site specific parameters of ambient soil temperature and soil resistivity early in the analysis setup as shown in the following figure.

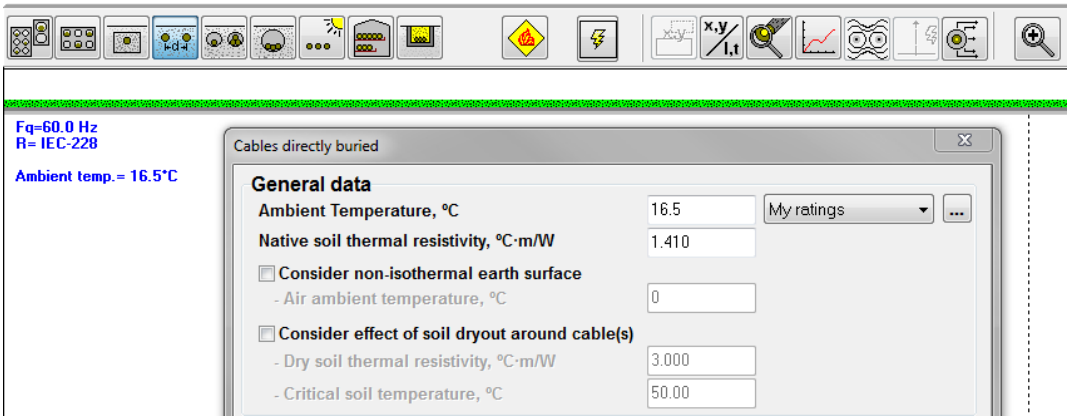

Figure 5.1 CYMCAP site specific parameters entry screenshot

It's also easy to adjust or add cable types to suit a specific application and/or match the manufacturer's data, as shown in the following figure.

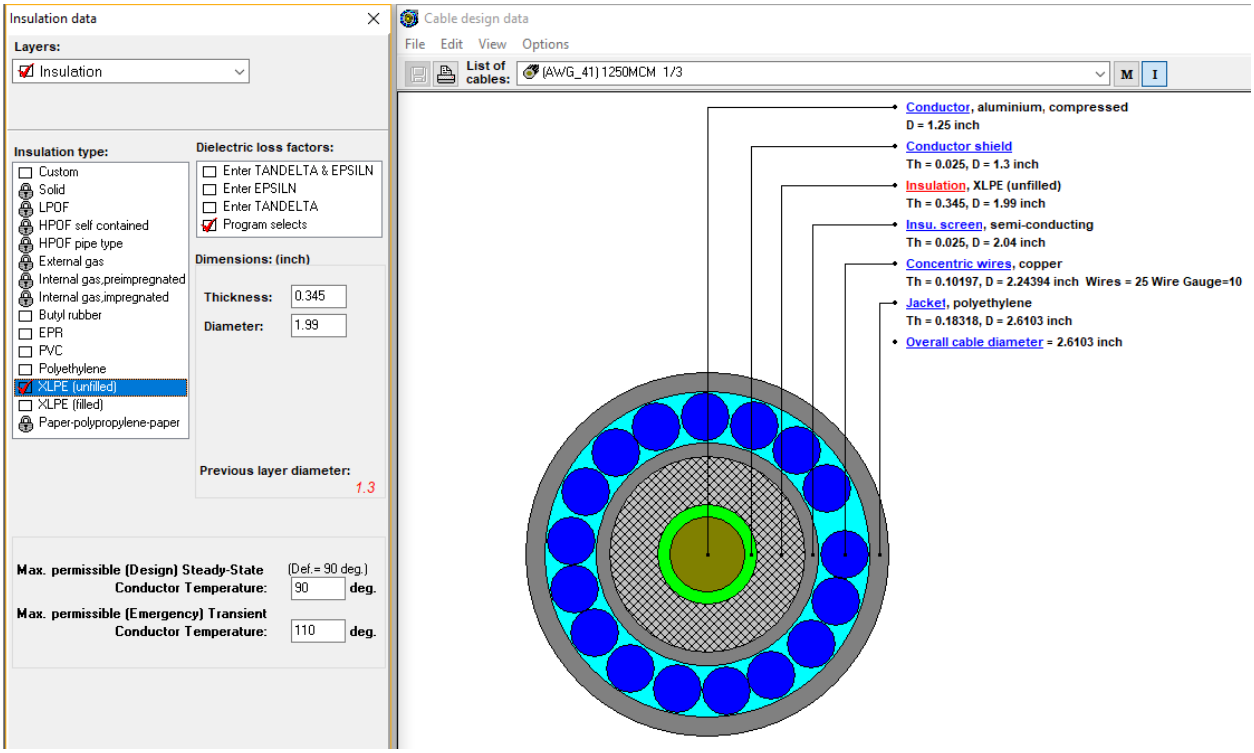

Figure 5.2 CYMCAP cable data entry screenshot

It can model multiple backfills, i.e. soils with different thermal properties. This is very useful for direct buried cables because it is common to have different thermal resistivity where the trench is dug, whether due to imported fill or lower compaction. CYMCAP can calculate the impact of moisture migration based on IEC 60287-1 (critical temperature rise) [13]. There are a few limitations of the software that stand out because of the focus of this dissertation. CYMCAP cannot model moisture migration for transient analysis or for non-native backfills. The IEC critical temperature rise method does not address these options, and so CYMCAP does not have a standard from which to build the model.

The inability to model moisture migration for transient analysis is an issue because the time constant for moisture migration may exceed the duration required for the cable to reach the temperature for soil-dry out. A workaround can be used to address this limitation. The calculation can be performed iteratively with the software using the calculated temperature from a transient simulation without considering moisture migration, and then performing the steady state calculation with moisture migration at the transient simulation maximum temperature.

The inability to model moisture migration for transient analysis is an issue because it is common to install a cable in a trench with backfill that is non-native, i.e. imported backfill. In this case, the moisture migration cannot be modeled directly. The calculation can be performed approximately, by adding an additional backfill area to the trench that is directly adjacent to the cables or conduit. The dimensions of this adjacent area (1.6 ft. by 1.6 ft.) is the estimated dried area, and it is set to the dry soil resistivity. This is demonstrated in the following figure.

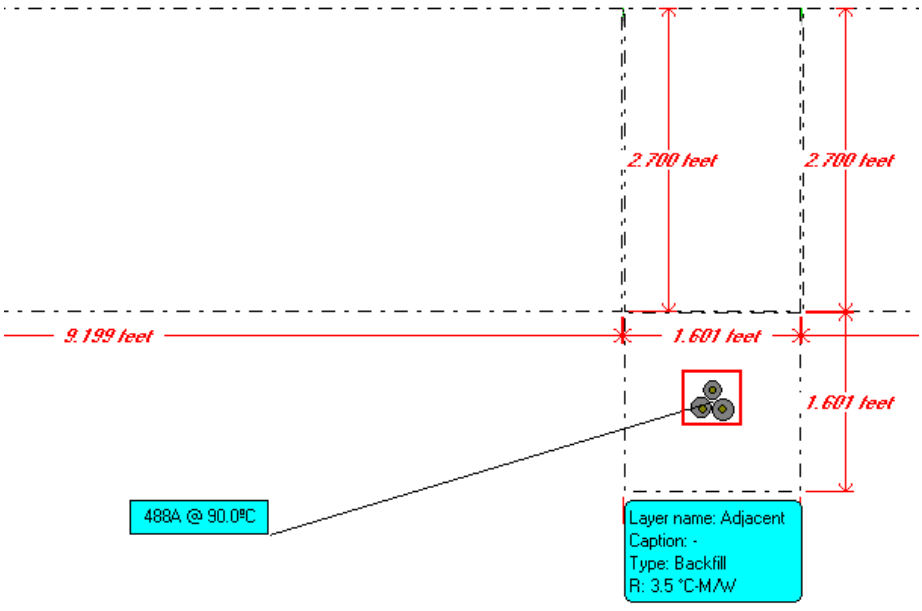

Figure 5.3 CYMCAP dried soil area approximation example

5.2 ETAP

ETAP is a computer software that provides calculation tools for multiple aspects of power system design: power flow, short circuit, arc flash, ground grid, harmonics power flow, and more [53]. Because of this, the underground raceway systems module easily incorporates cables that are already modeled in the project. It also allows for modeling the cable operating temperature based on the power flow study. Adjusting the thermal properties of the various cable layers is possible, but it must be done by finding the underlying data tables with Windows Explorer rather than the GUI provided in CYMCAP. It can model various soil resistivities and duct bank (conduit in concrete or soil and direct buried), but it cannot model soil dry out characteristics, i.e. it does not address thermal stability. It can model multiple duct banks at various depths and spacing, and it seems to do that in a more intuitive manner than CYMCAP.

Adding or adjusting cable resistivity data is difficult because a user must navigate outside of the program GUI and open the file with a spreadsheet editing tool such as Microsoft Excel. This added difficulty is likely to discourage most users from attempting or even being aware of this option. However, there are many cables in the standard library that are likely to be similar to the cable under study. Additionally, the specific cable layer information, such as the thickness of the conductor screen or insulation resistivity, does not have a large impact on the ampacity because the thickness and insulation material are similar between all cables of a specific voltage class. So, the difficulty in adjusting the cable parameters may not be as critical as one might expect.

Results are generated rapidly for Neher-McGrath modeling, and it also performs transient analysis. However, it cannot model soil dry-out, i.e. thermal stability, without simulating an extra layer around the cable. The dried soil thickness can be added to the cable jacket or to a surrounding duct bank [54]. Overall, ETAP works well for steady state modeling with typical cables used in low and medium voltage applications in duct bank or direct buried.

Entering the dimensional data for direct buried cases is somewhat difficult because the burial depth must be inferred based on the so called “location” that appears like a 5” conduit but is only used to place cables in and does not add thermal resistivity. This is shown in the following figure.

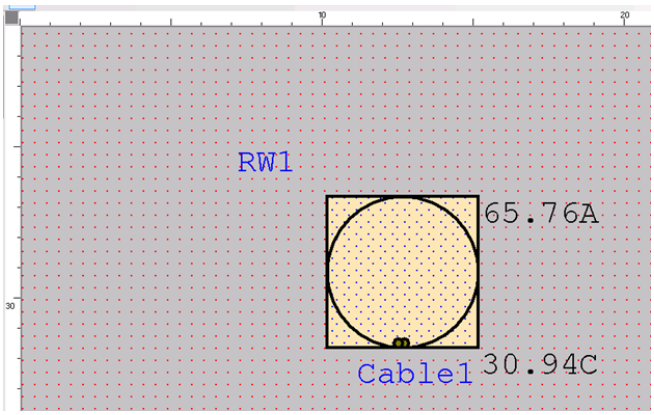

Figure 5.4 ETAP direct buried cable example screenshot

The standard cable library includes many cable types of various voltage and construction details. These can be edited or appended as shown in the following figure.

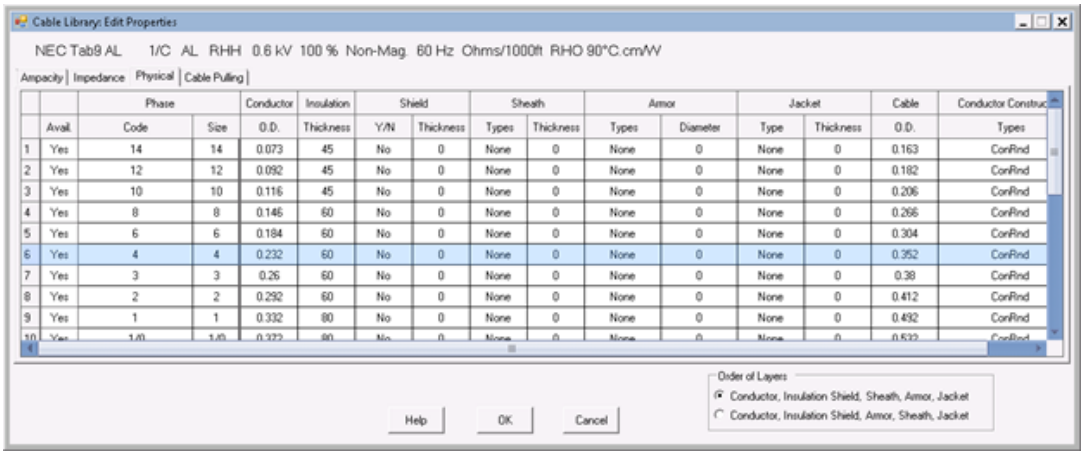

Figure 5.5 ETAP cable parameter entry screenshot

After entering the trench dimensions and cable construction, the operating current or maximum temperature can be specified. The operating current can be determined from the power flow model in the same software. This is a beneficial feature if the user is designing a large duct bank with dozens of circuits because it reduces the likelihood of mis-entering data, reduces data entry time, and automatically updates if the load changes. The operating current entry screen is shown in the following figure.

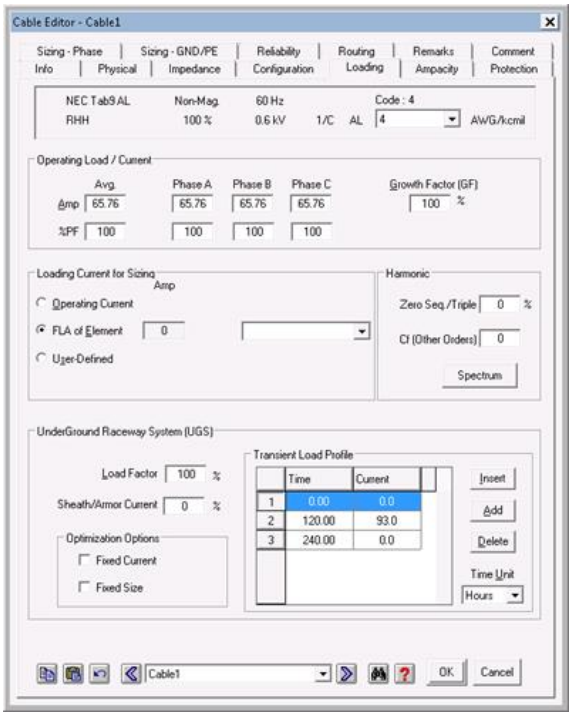

Figure 5.6 ETAP operating current entry screenshot

5.3 USAmp Prime

The original USAmp program was redone by USi to provide a graphical user interface. It provides many of the features offered in other programs including [55]:

- Computing steady-state and transient ampacities and temperatures for multiple cables with equal or unequal loading.
- Modeling duct banks, pipe cables, extruded cables, directly buried cables, casings, or mixtures thereof.
- Modeling steam lines or other extraneous heat sources.
- Modeling aerial cable installations with enhanced pictorial interface.
- Computing short-circuit rating of conductors, shields, and armor.

Cable installation types can be modeled as directly buried in a trench, duct bank, or casing. It is designed to be compliant with IEC 60287 (steady state ampacity), IEC 60853 (transient ampacity), and IEC 60949 (short circuit ampacity) standards. It facilitates entering all cable parameters including conductor, shields, insulation, and jackets easier than any other program compared in this chapter. One limitation is that the spacing of directly buried cable cannot be less than about 2 inches. In other words, cable diameters less than about an inch cannot be modeled as touching each other. This posed a problem for modeling the case study described in Section 10.3 USAmp Prime.

The interface is fairly simple to use and get started as shown in the following figure:

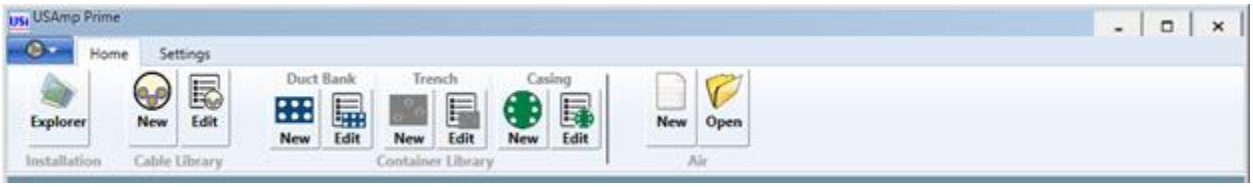

Figure 5.7 USAmp Prime startup screenshot

Modeling the cable parameters is guided by the interface and provides an image of the cable that is to scale to make it easy to account for the cable details as shown in the following figure:

Figure 5.8 USAmp Prime cable data entry screenshot

The cable installation method is specified from the selection of typical software options including duct bank, trench, and casing. After selecting the installation method, the user is prompted to define the location of each potential cable location, not the cable itself, as shown in the following figure:

Figure 5.9 USAmp Prime cable location entry screenshot

As stated before, it is not possible to model these locations closer than a couple of inches. It gives an error as shown in the following figure:

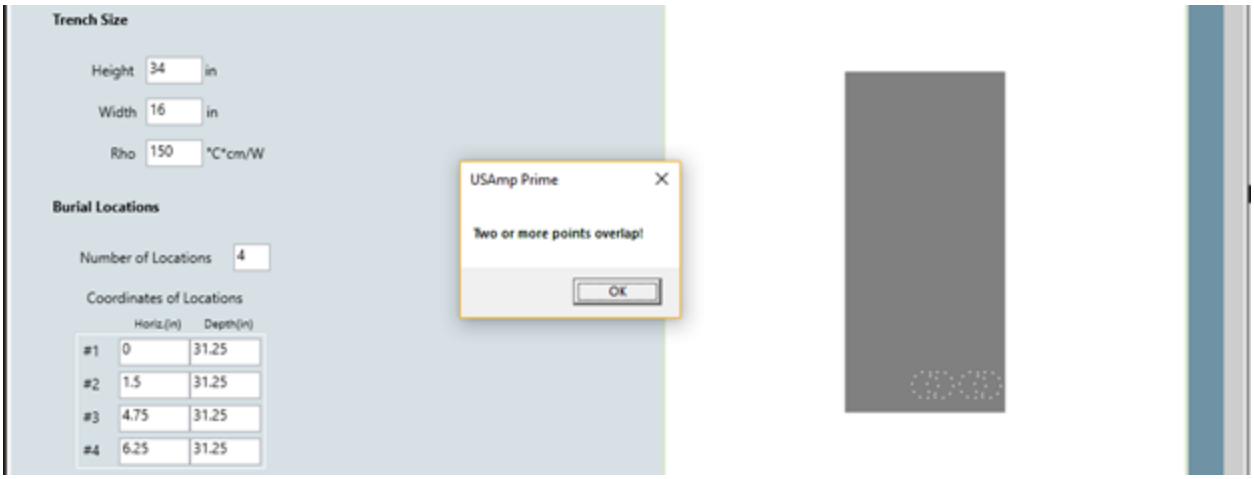

Figure 5.10 USAmp Prime location overlap error screenshot

The final analysis allows for defining the cable current, load factor, temperature rating, soil temperature, and pre-load temperature. It also allows for iterating through multiple parameters, such as thermal resistivity—a very useful tool since the exact values are rarely known.

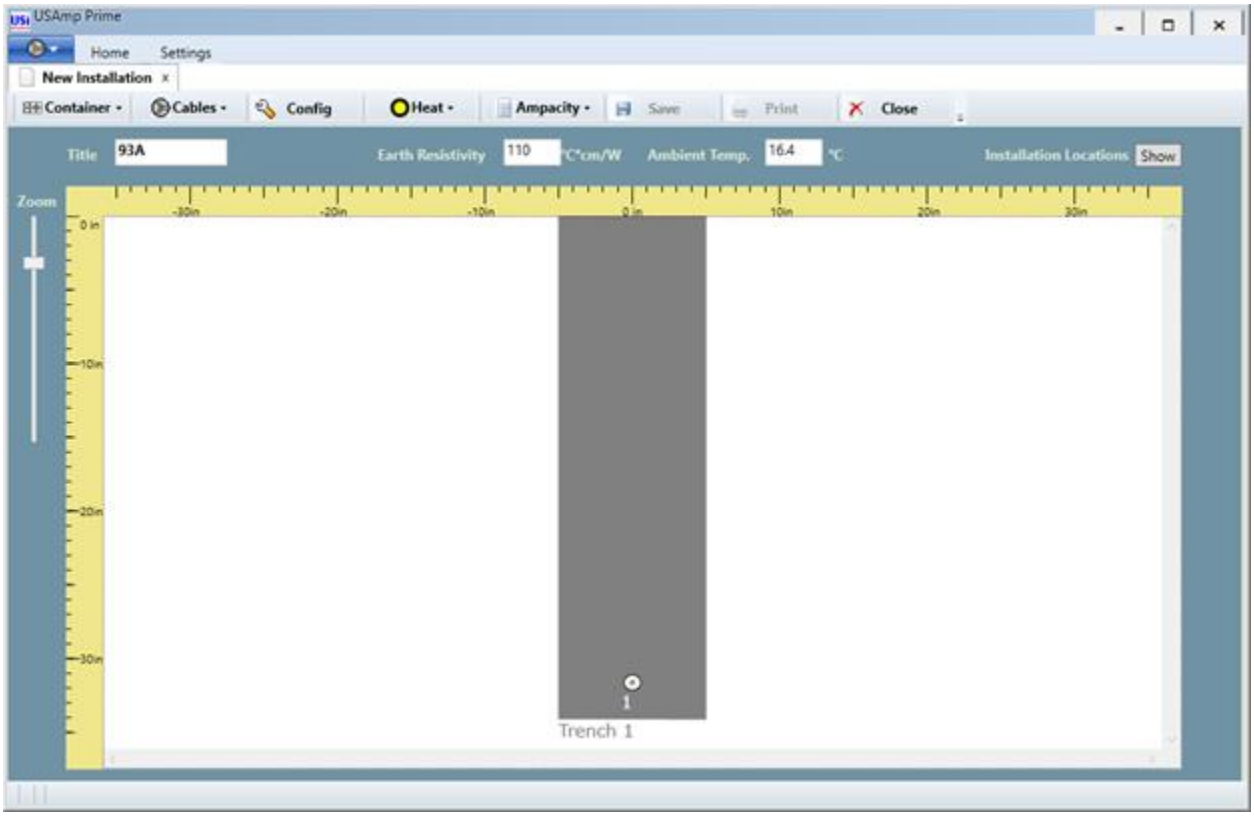

Figure 5.11 USAmp Prime current, resistivity, and soil temperature entry screenshot

The program does not appear to address thermal stability, i.e. moisture migration. In order to model a dry soil layer, it is necessary to add a layer to the cable representing the determined dried soil layer. The procedure for this is described in a paper by Bates, Malmedal, and Cain [54].

5.4 Finite Element Analysis

Finite element analysis or modeling has become the tool of choice for many engineering problems because of its flexibility and accuracy. The parameters can be directly specified rather than derived—for example, the earth surface boundary condition can be specified with a convective condition rather than assuming an isothermal condition to more accurately model the cable installation. Historically, the cost has been in computation time, but this has decreased significantly with the advancement of microprocessors and optimizations in software programming.

Finite element analysis can be subdivided into different methods including finite difference method, finite volume method, and finite element method. According to Sjodin of COMSOL, “Each method is quite similar in that it represents a systematic numerical method for solving PDEs. One important difference is the ease of implementation. A common opinion is that the finite-difference method is the easiest to implement and the finite-element method the most difficult. One reason for this may be that the finite-element method requires quite sophisticated mathematics for its formulation” [56]. According to Anders, “Even though both [finite-element and finite difference] methods have been applied to solve the heat conduction problem around loaded power cables, our view is that the finite-element method is better suited for this application” [14] p. 296.

ANSYS Mechanical software is capable of performing steady state and transient thermal analyses [57] using the finite element method. The software is not designed specifically for cable ampacity, but it is capable of modeling the physical and thermal properties of a cable installation. Because it is generic, setting up the model is not as straightforward as it is for the other software previously listed. Each physical layer of the cable must be drafted in CAD rather than simply entering cable information. Duct bank or conduit must be drafted in a similar fashion, specifying the exact dimensions rather than specifying the number and size of conduits. The earth must be modeled as a large surrounding volume with specific dimensions rather than simply entering a resistivity that extends to infinite. It is possible to model significant detail, but it is obviously time-consuming and difficult to determine exactly what must be modeled versus what can be simplified. After delineating the geometry, the material properties must be defined

including density, thermal resistivity, and specific heat. Most of this information can be found in cable reference books such as Rating of Electric Power Cables [14] or standards such as IEEE Std 835 [11].

CHAPTER 6
SOIL THERMAL STABILITY

Soil is defined as “the layer(s) of generally loose mineral and/or organic material that are affected by physical, chemical, and/or biological processes at or near the planetary surface, and usually hold liquids, gases and biota and support plants” [58]. This generic definition matches the interpretation and difficulty with characterizing soil for the purposes of cable ampacity calculations. Soil thermal resistivity plays a key role in determining underground cable ampacity and is calculated with one fixed number in the ampacity calculation. However, it is measured at a specific point with an approximate measurement area of a few inches. Even the shortest length of cable is on the order of feet, so a single measurement only accounts for a portion of the length. Most cable installations span more than several hundred feet. Since cables are manufactured with a uniform size, the design must be based off the maximum temperature over the installed length. It is difficult to determine where the maximum temperature occurs because it depends on the combination of parameters including: soil temperature, soil resistivity, cable burial depth, and any additional heat source. Soil temperature is fairly consistent for a large geographic area at a given depth, and the depth is controlled during installation based primarily on safety considerations. So, it is desirable to determine the maximum soil resistivity over the installed length of cable. This should be done using statistical analysis since it is impractical to measure the resistivity at intervals of 10 to 20 feet when the cable length is hundreds or thousands of feet long. Measurements at approximately 60-foot intervals have been performed for special areas [59]. It has been shown that a change in soil conditions can have an impact of 5-10% on the cable ampacity within 5 times the length to conduit diameter ratio (for a cable installed in conduit) and achieves a fixed derating value of 5-20% within 15 times the length to conduit diameter ratio [60].

In addition to the natural variability due to changing soil types over the installed length of cable, the moisture content of the soil is a significant factor for the soil resistivity. So, the resistivity varies with location and time. The moisture content changes in the soil due to a variety of factors including seasonal rain or snowfall, vegetation, water table, and cable heating. Seasonal rain or snowfall has an obvious effect on the soil moisture content. The migration of this moisture from the surface to the cable depth depends on the hydraulic gradient that may have a time constant of several days [32]. Vegetation affects the soil moisture by absorbing water through the root system, thereby reducing the soil moisture content. Certainly, the magnitude depends on the plant type, growing season, and root depth. The water table in some locations, which varies in depth throughout the year, can also be a factor if it is within several

feet of the cables. Finally, the cable heating impacts the moisture content by decreasing the water surface tension and increasing the vapor pressure at the cable surface [61]. According to Radhakrishna, et. al, “The rate of net moisture migration below the critical moisture level is determined by the heat flux imposed on the soil and the liquid and vapour permeabilities of soil” [62]. An excellent summary of the water potential is provided by a Geological Survey in a work entitled “Review of Some Elements of Soil-Moisture Theory” [63]. Remson and Randolph list 6 potentials that drive water in soil: gravitational, hydrostatic-pressure, osmotic-pressure, adsorption or adhesion, thermal gradient, and chemical [63]. The focus of this chapter is on the impact of the thermal gradient established by cable heating.

6.1 Time to Dry and the Law of Times[5]

An underground cable carrying current must dissipate heat to the surrounding soil. The rate at which this heat can be carried away is related to the thermal resistivity of the soil. The higher the thermal resistivity the more slowly heat can pass from the cable to the surroundings and the higher the operating temperature of the cable will be. There is a temperature limit for each cable type above which the cable or its insulation will sustain damage.

When cable sizes are chosen the value for the thermal resistivity of surrounding soil must be determined to calculate how much current any underground cable can carry before it will overheat. This value suggested for soil thermal resistivity, usually signified by ρ (Rho), in some cable ampacity tables, such as those in the National Electrical Code, is 90 °C·cm/W [1].

In the field, soil thermal resistivity may vary considerably from the values used in these tables making specific calculations necessary for many locations, especially where important or long underground cables are installed. While the method for calculating the ampacity of underground cable is simplified by assuming that soil thermal resistivity is the same for all soil types and locations, this assumption is not true.

The most important factor controlling thermal resistivity of soil is its moisture content. As soil dries out its thermal resistivity increases. The heat generated in a cable can cause moisture to leave the vicinity of the cable, drying the soil around the cable, raising the soil’s thermal resistance and impeding the flow of heat away from the cable. This causes the cable temperature to rise and may result in cable damage. The ability of soil to maintain a constant moisture level, and thus a constant thermal resistance, is known as soil thermal stability [20].

[5] The rest of this chapter was previously published in IEEE IAS Transactions [64]

6.2 The Law of Times

Many sources suggest that if the time it takes soil to dry around a heat source of a known diameter is measured, this time can be used to determine the time it will take soil to dry around a heat source of any other diameter [20][32][35][65].

Equation (6.1) is given by these sources for calculating this time to dry. This equation is known as the "Law of Times" [66].

$$\frac{t_1}{t_2} = \left(\frac{d_1}{d_2}\right)^2 \tag{6.1}$$

Equation (6.1) says that if we know the time t_1 it takes soil to dry at any particular heat rate using a heat source of diameter d_1, we can predict the time t_2 that it will take the soil to dry around a heat source of diameter d_2, assuming the same heat rate is used.

For example, if a soil sample was heated using a probe with a diameter of 0.122 inch (3.1mm), the standard heat probe suggested for thermal resistivity testing [27][50], and it was determined that the effective drying time was 15 minutes, and it was desired to predict the drying time in this soil at this same heat rate for a cable of 1 inch (25.4mm) diameter, the expected drying time would be:

$$\frac{15\ min.}{t_2} = \left(\frac{3.1\ mm}{25.4\ mm}\right)^2$$

$$t_2 = 1007\ minutes$$

So, this method claims that if it took 15 minutes to dry the soil around a 0.122-inch (3.1mm) source, it would take 1007 minutes (16 hours) to dry the soil around a cable 1-inch in diameter with the same heat rate. It is suggested that if the drying time calculated for the cable of interest is long enough, the soil can be considered thermally stable and drying of the soil will not be important in the operation of the cable.

While this method has the advantage of being simple to use, the question arises as to what theory it is based upon and whether it can yield accurate results. This paper will examine those questions.

6.3 The Theory of the Law of Times

One source [65] states when describing the origin of the Law of Times: "The response of a cable buried in the same soil with the same heat dissipation rate would be related to the probe

response through the Fourier number." While this is true in some contexts, a closer examination of the Fourier number calls into question whether this can be applied to heat leaving soil around the cable due to the movement of moisture out of the area and the inflow of moisture from the surrounding area [28]. The Fourier number F_{oh} is shown Equation (6.2) [16]:

$$F_{oh} = \frac{\alpha t}{L^2} \tag{6.2}$$

Where

α = thermal diffusivity (cm²/s)

L = length of thermal path (cm)

t = time (s)

Thermal diffusivity is defined as shown in Equation (6.3):

$$\alpha = \frac{k}{cp} = \frac{conductivity}{(specific\ heat)(density)} \tag{6.3}$$

The definition of the Fourier number, and the derivation of the Law of Times given in Section 7.15 of Ingersoll [66] both show that the law of times is used to determine how quickly a particular temperature will be reached at some distance from a heat source if the time needed to reach that temperature at a different distance from the heat source is already known. However, according to (6.2) and (6.3) and the derivation given in [66], the time calculated using the Law of Times is dependent upon the thermal conductivity, specific heat and density of the material being heated. If these parameters are known, then the Law of Times allows the calculation of the time required for any two points to reach the same temperature and states that these times are proportional to the square of their distances from the heat source and the material surrounding that source.

However, neither the Fourier number nor the Law of Times consider the effects of heat flow due to moisture migration. Furthermore, it does not address the time it takes for heat to vaporize moisture and for the moisture to leave the area of the heat source. The Law is concerned with temperature changes only due to heat flow by thermal conductivity and heat absorption due to the material's specific heat. It does not consider the parameter of heat loss by moisture migration. The question is therefore raised: since the Law of Times does not consider heat flow due to moisture migration, is it appropriate to use the Law of Times to try to predict soil stability as is suggested by some sources?

6.4 Experimental Testing of the Method

An experiment was performed to determine whether the Law of Times can be used to predict the drying time of soil. The experiment designed was a single factor, two level procedure with five replicates at each level. The factor tested was the diameter of the heat source and the production variable was the effective drying time of a soil sample.

Two thermal heat probes were prepared along the lines of the instructions given in IEEE and ASTM sources for testing soil thermal resistivity [27][50]. The only difference between the two probes was their diameter. One probe was 0.122” (3.1mm) in diameter and the second was 0.264” (6.7mm) in diameter.

The soil type used for the experiment was clean sand. A sample of sand was collected and mixed to achieve as homogeneous a mixture as possible. The sand was then divided into ten equal portions and placed into 10 identical 3-inch diameter by 7-inch polyvinyl chloride (PVC) cylinders to make 10 samples of sand in as nearly equal volumes and masses as possible. The cylinders were sealed in plastic to prevent moisture loss and were not unsealed until the day they were tested.

The cylinders were numbered from 1 to 10 and each cylinder was assigned a probe size at random. The 0.122” (3.1mm) probe was assigned to five of the samples and the 0.264” (6.7mm) probe was assigned to the other five cylinders. These assignments were made using a random number generator. Each cylinder was then assigned another random number which was used to determine the order in which the samples and their assigned probe sizes would be tested. The sample to be tested on a particular day was chosen, its probe was inserted into the sample, and heat was injected by the probe into the soil sample for a period of 14 hours. The temperature of the probe was measured during the testing period. The heat injected by each probe was held as constant as possible for each sample during the testing period.

The effective dry time was measured and recorded for each sample using the method suggested by several sources [20][32][35][65]. The measurements taken were also used to determine the soil resistivity before and after the effective dry time [27]. A typical graph of recorded data is shown in Figure 6.1.

The solid line is the temperature recorded over the 14-hour period. There are two slopes of interest shown in this Figure. The first starts at approximately 100 seconds and continues to approximately 1000 seconds. At that point the slope of the graphs changes and stays constant until approximately 3000 seconds. At that point a third slope begins and lasts until the end of the test.

The first slope between 100 and 1000 seconds can be used to determine the soil's beginning (wet) resistivity [27]. After the soil dries, the resistivity increases. This is represented by the change to the second slope between 1000 and 3000 seconds. From this second slope the effective dry soil resistivity can be determined. The transition point between the two slopes is the "effective dry time" of the soil sample at which point the soil changes from wet to dry resistivity. The final slope will slowly approach a steady state condition of constant temperature as the two dimensional and end effects of the heat source become important and the entire test apparatus reaches equilibrium in a two-dimensional heat flow configuration. This eventually will include the convection into the air around the test apparatus.

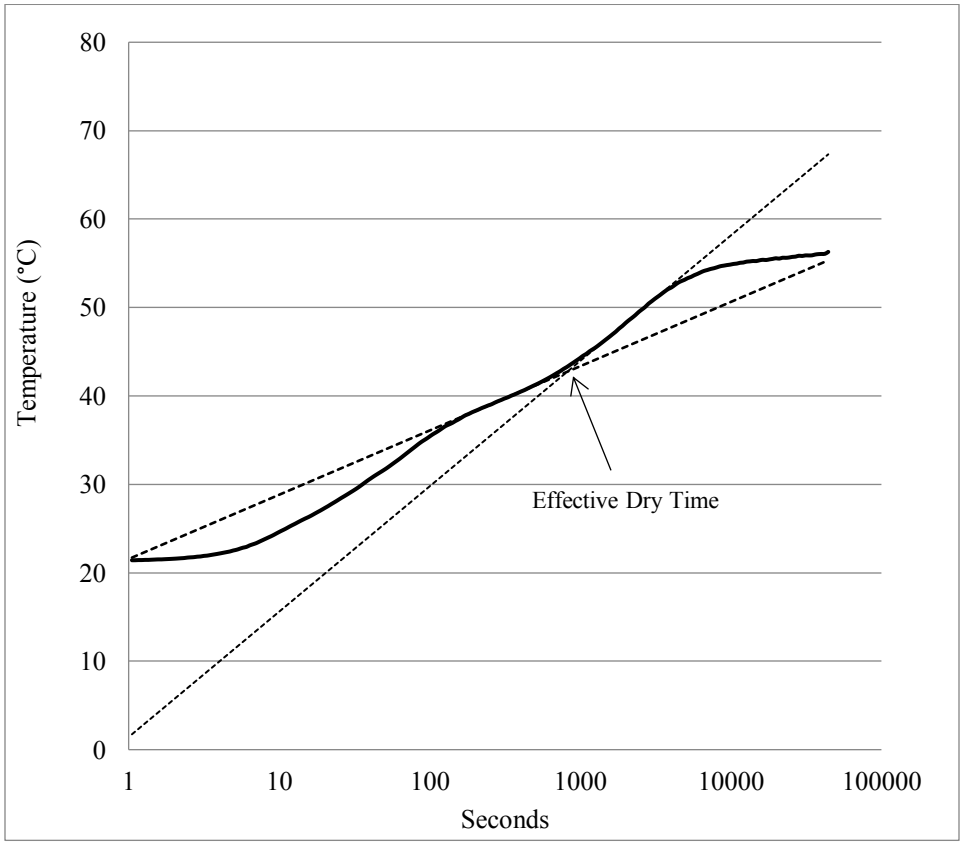

Figure 6.1 Graph of recorded data

The response variable measured for this experiment is the effective time to dry for each sample. The measurements taken during the testing are shown in Table 6.1 and Table 6.2.

Table 6.1 Measurement from tests

Sample Number	Testing Order	Soil Mass (g)	Heat Rate (W/cm)	Wet ρ (°C·cm/W)	Dry ρ (°C·cm/W)
1	6	729.4	0.4195	94.6	184.5
2	5	748.3	0.4213	90.5	170.7
3	9	757.7	0.3995	82.8	161.0
4	7	778.4	0.4229	85.5	155.3
5	10	765.7	0.4174	83.8	154.2
6	4	772.0	0.4169	76.2	170.5
7	3	734.1	0.4140	101.1	167.2
8	1	777.3	0.4159	61.9	120.5
9	8	740.9	0.4164	104.9	173.7
10	2	737.5	0.4152	89.0	162.0
AVERAGE		754.1	0.4160	87.0	162.0

Table 6.2 Measurement from tests

Sample Number	Probe Size (mm)	Water Lost (g)	Dry Time (sec)
1	6.7	10.9	818
2	6.7	11.8	758
3	3.1	14.5	591
4	6.7	14.6	655
5	6.7	12.7	685
6	3.1	14.9	631
7	6.7	12.1	767
8	3.1	12.6	774
9	3.1	11.0	758
10	3.1	12.2	744
AVERAGE		12.7	718

6.5 Analysis of Experimental Data

The drying time for the samples tested with each probe is shown in the first two columns of Table 6.3. The third column is the 0.264” (6.7mm) time measurements transformed using the Law of Times to the dry time predicted for a 0.122” (3.1mm) probe. In other words, column 3 is the time a 0.122” (3.1mm) probe should take to dry the soil according to (6.1) given the time to dry measurement for the 0.254” (6.7mm) probe in column 2.

Table 6.3 Time to dry measurement for each probe

0.122" (3.1mm) probe dry time (s)		0.264” (6.7mm) probe dry time (s)	0.264” (6.7mm) dry time adjusted to 0.122” (3.1mm) (s)
591		818	175
631		758	162
774		655	140
758		685	147
744		767	164
Avg.	699.6	736.6	157.6

The measurements for each probe are plotted in Figure 6.2 and a box plot of the data is shown in Figure 6.3.

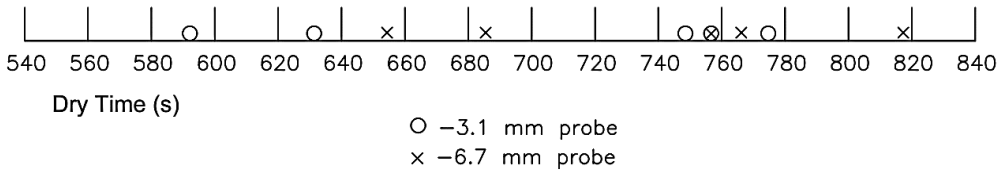

Figure 6.2 Plot of time to dry for each probe

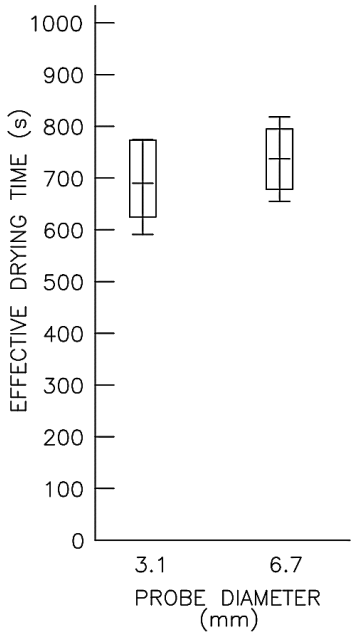

Figure 6.3 Box plot of data for each probe

A normal distribution plot was done for the data taken using each probe. This plot along with the best fit lines for the sampled points is shown in Figure 6.4. Figure 6.5 shows the normal distribution plot of the residuals from Table 6.3. It appears from these plots that the measurements and the residuals are reasonably normally distributed with similar variances.

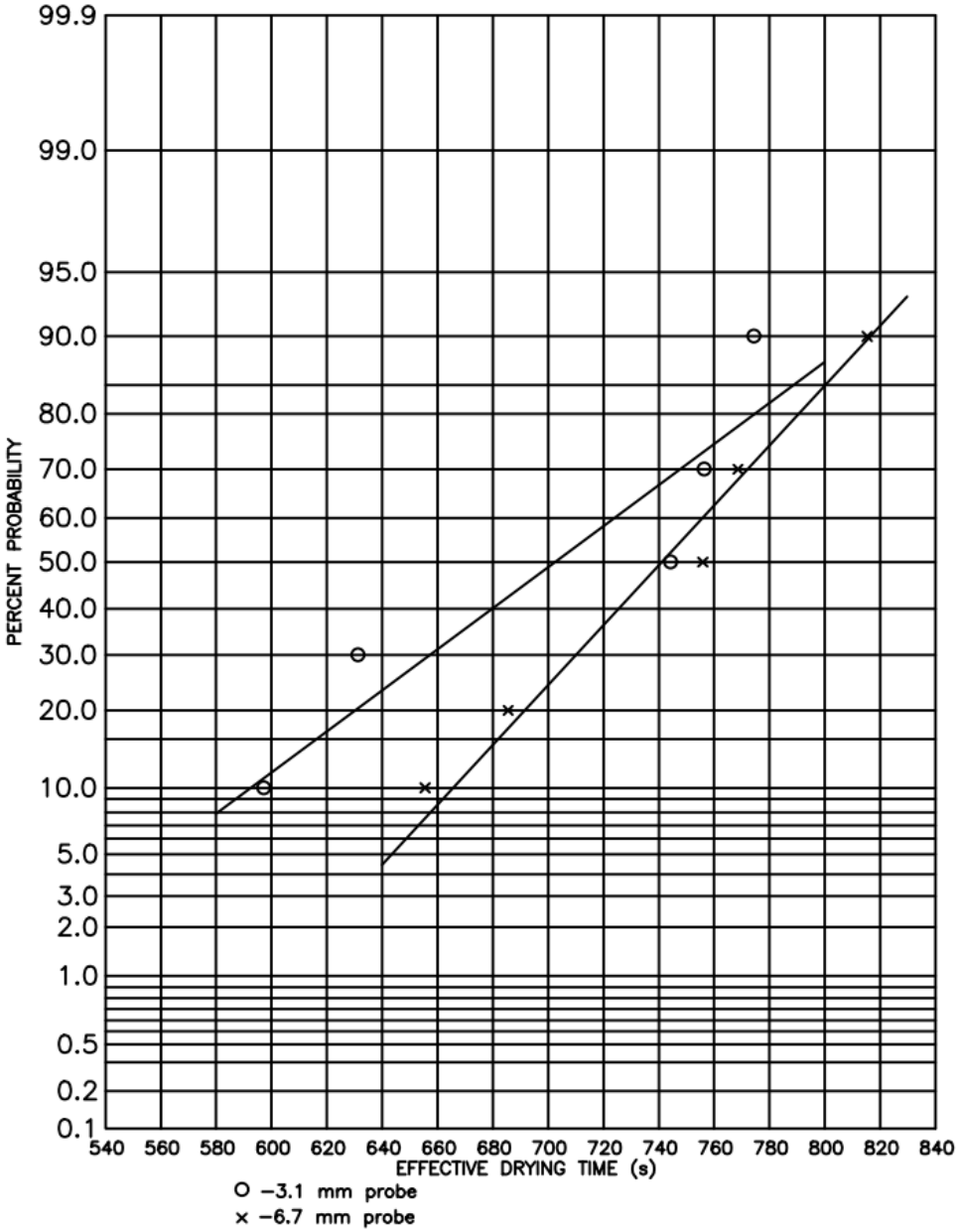

Figure 6.4 Normal distribution plot of the data.

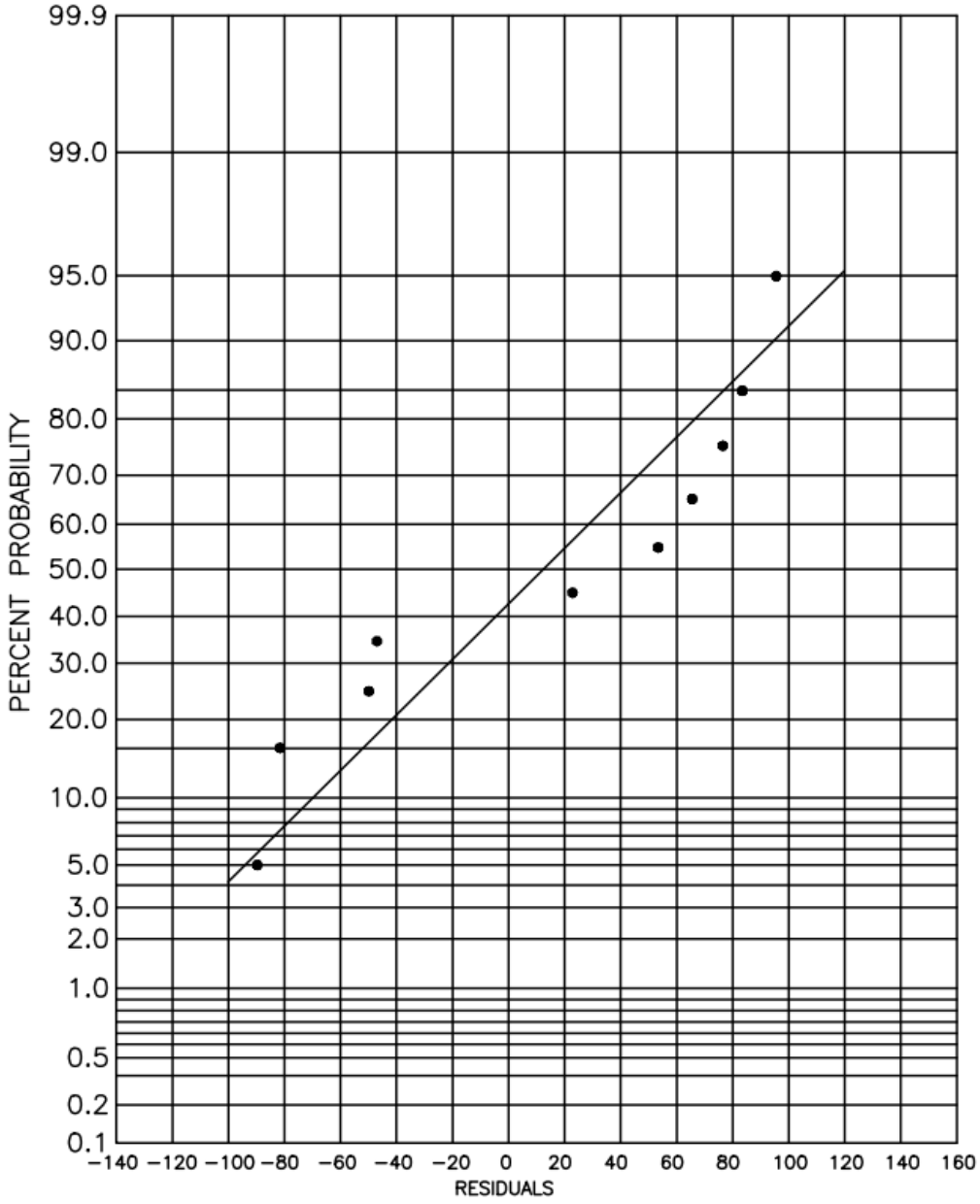

Figure 6.5 Normal distribution plot of residuals from Table 6.3

The drying time measurements were plotted against a variety of abscissas to try to detect any trends in the data due to the experimental method used. A significant trend in the data was discovered and is shown in the plot in Figure 6.6. In this figure, the time to dry values were plotted against the test number. It may be seen that there is a definite downward trend of drying times with the later tests.

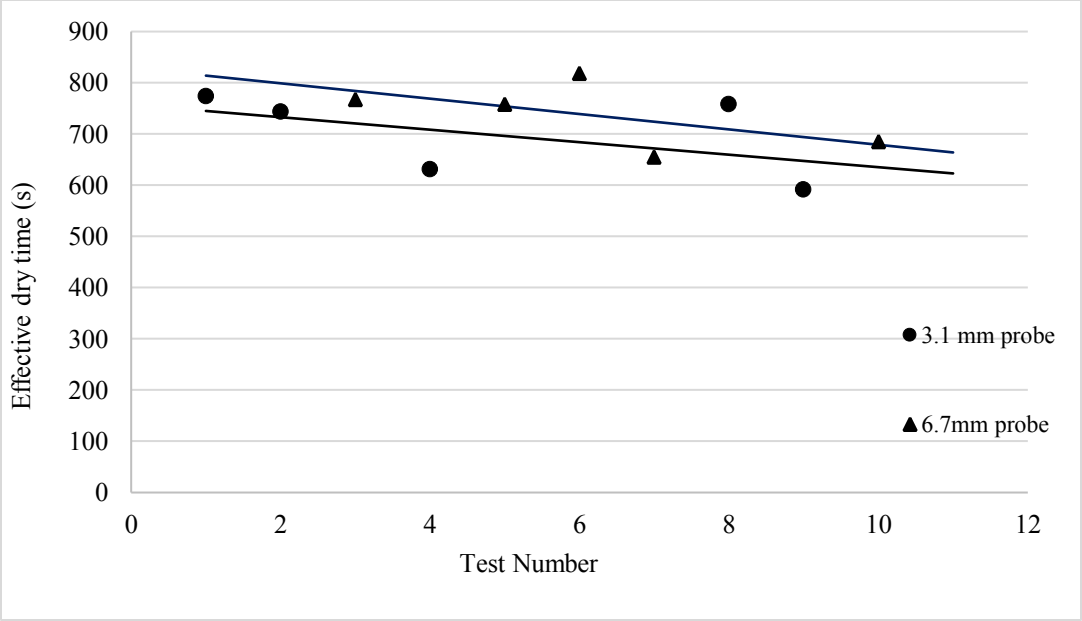

Figure 6.6 Dry times plotted against test number.

The most likely explanation for this trend is that the tests were done over a period of two weeks. The later samples had time to lose some moisture that was not due to the heating from the probes. This decreased the time to dry for the samples tested later since some of their moisture had already evaporated. Even though an effort was made to seal the samples against water loss until they were tested, it is clear from this trend that some water was lost as the samples were stored while waiting for testing.

The trend in the data does not appear to be significant enough to affect the final results. The next step is a statistical analysis of the data to determine whether the Law of Times correctly predicted the change in drying times as the probe diameter changed.

A means comparison t test was performed on the data in Table 6.3. The basic question this experiment is designed to test is whether the drying times are related by the Law of Times. If this were true, the mean of the population of all measurements taken with the 0.122” (3.1mm) probe would be expected to be equal to the mean of the population of all measurements taken with the 0.264” (6.7mm) probe as corrected using the Law of Times. So, the test data that will be compared first will be the values shown in columns 1 and 3 of Table 6.3. If the Law of Times worked as suggested, the mean values of the data in these two columns should be statistically the same.

A two-sample t test was performed on the data in columns 1 and 3 of Table 6.3. The test statistic for this test is shown in Equation (6.4) and (6.5) [67]:

$$t_0 = \frac{\overline{y}_1 - \overline{y}_2}{S_p\sqrt{\frac{1}{n_1} + \frac{1}{n_2}}} \tag{6.4}$$

$$S_p^2 = \frac{(n_1 - 1)S_1^2 + (n_2 - 1)S_2^2}{n_1 + n_2 - 2} \tag{6.5}$$

S_1^2 and S_2^2 are the sample variances found by Equation (6.6):

$$S_x^2 = \frac{\sum_{i-1}^{n}(y_i - \overline{y}_x)^2}{n - 1} \tag{6.6}$$

Where

$\overline{y}_1$ and $\overline{y}_2$ = sample mean drying time for probe 1 or 2 respectively

n = number of samples in each sample set

y_i = individual sample drying time for probe 1 or 2

The null hypothesis H_0 is that the population means of the 0.122" (3.1mm) values in column 1 of Table 6.3 equal the population means of the 0.264" (6.7mm) values adjusted using the Law of Times, in column 3 of Table 6.3. The alternative hypothesis H_1 is that these two population means are not equal.

$H_0: \mu_1 = \mu_2$

$H_1: \mu_1 \neq \mu_2$

Where

μ_1 = population mean of the 0.122" (3.1mm) drying times

μ_1 = population mean of the 0.264" (3.1mm) drying times adjusted using the Law of Times

The test statistic from Equation 6.2 is compared with the reference distribution (the t distribution) $t_{\alpha/2,n1+n2-2}$ where α is the significance level. Using a 95% significance level H_0 is rejected if $t_0 > t_{0.025,8}$ or if $t_0 < -t_{0.025,8}$. From a t distribution table it is found that $t_{0.025,8} = 2.306$.

From Equations (6.4), (6.5), and (6.6), and using the values in Table 6.3:

$S_1^2 = 6854.3$

$S_2^2 = 196.3$

$S_p^2 = 59.37$

$t_0 = 14.43$

Since 14.43>2.306, there is evidence that the null hypothesis should be rejected at the 95% significance level. Applying the P test, there is evidence that the null hypothesis should be rejected for all significance levels less than 99.995%. So, the experiment provides evidence that the mean values of the two data sets are not equal, and the Law of Times did not properly predict drying time values that corresponded to the 0.122” (3.1mm) measurements found experimentally.

If the probe had no effect on the drying times, the population means for the 0.122” (3.1mm) and 0.264” (6.7mm) probes should be identical. If this hypothesis is statistically tested, the mean values in columns 1 and 2 of Table 6.3 should be statistically identical. The null hypothesis for this test is that the population mean of the 0.122” (3.1mm) probe drying times equal the population mean of the 0.264” (6.7mm) drying times (not adjusted using the Law of Times), and the alternative hypothesis is that the two population means are not equal.

$H_0: \mu_1 = \mu_2$

$H_1: \mu_1 \neq \mu_2$

Where

μ_1 = population mean of the 0.122” (3.1mm) drying times

μ_1 = population mean of the 0.264” (3.1mm) drying times

Using (4), (5), and (6) once again and applying the test to the new hypothesis, the following may be found.

$S_1^2 = 6854.3$

$S_2^2 = 4332.3$

$S_p^2 = 74.79$

$t_0 = -0.78$

The t test statistic for this test is again $t_{0.025,8}$ =2.306 at the 95% significance level. The value of t_0 is within the boundaries of the test statistic, i.e. -2.306 < -0.78 < 2.306. Therefore, the null hypothesis is not rejected at the 95% significance level. By applying the P test, the null hypothesis is accepted for all significance levels greater than 54.2%. The experiment appears to support the null hypothesis in this case. The conclusion is that the probe diameter has no effect on the effective drying times of the soil. At a significance level of 95%, there is no reason to believe there is difference between the means of the drying times for the 0.122” (3.1mm) probe and the 0.264” (6.7mm) probe.

A similar analysis was done on the amount of water that was evaporated during the test for each probe size. This data is shown in Table 6.4.

Table 6.4 Water lost during each test

Water Lost 0.122" (3.1mm) probe (g)		Water Lost 0.264" (6.7mm) probe (g)
14.5		10.9
14.9		11.8
12.6		14.6
11.0		12.7
12.2		12.1
AVG.	13.0	12.4

The null hypothesis that will now be tested is that the mean of the water mass that was lost when the 0.122" (3.1mm) probe was used is equivalent to the mean of the water mass that was lost when the 0.264" (6.7mm) probe was used. The alternative hypothesis is that the two means are not equal.

$H_0: \mu_1 = \mu_2$

$H_1: \mu_1 \neq \mu_2$

Where

μ_1 = mean water loss using the 0.122" (3.1mm) probe

μ_1 = mean water loss using the 0.264" (3.1mm) probe

Using Equations (6.4), (6.5), and (6.6), and the measurements in Table 6.4:

$S_1^2 = 2.66$

$S_2^2 = 1.91$

$S_p^2 = 1.51$

$t_0 = 0.63$

Using the 95% significance level, the test statistic is again $t_{0.025,8}$ =2.306 and the comparison of t_0 from the data with the t test statistic results is: -2.306 < 0.63 < 2.306. So, once again there is no evidence that the null hypothesis should be rejected. The P test shows that this is true for any confidence limit above 45.4%. The experiment appears to support the hypothesis that the diameter of the probe has no effect on the amount of drying that occurred in the 14-hour test period.

6.6 Conclusions

The Law of Times has been used in the past to try to determine how quickly soil around a buried cable will dry when the cable is conducting current and generating heat. In the sources recommending its use, it is assumed that the law holds true for all soil types. The method involved obtaining a soil sample and testing it in the laboratory using a heated probe of the same size and type as the 0.122” (3.1 mm) probe used in the experiment reported herein. The time for the soil sample to dry using this probe was measured. The diameter of the cable being considered, the diameter of the probe used in testing, and the time to dry that was measured in the laboratory for the reference probe, are all entered in the Law of Times equation to determine the expected time for the heat generated by the cable to dry out the soil. In this way, an attempt was made to determine the soil thermal stability and its resulting effect on the temperature of the cable.

The empirical evidence obtained in this experiment discredits this method as an accurate predictor of soil stability. This Law of Times is useful when the temperature of the material under consideration is only affected by the conductivity of the material and the material’s specific heat and mass. However, in most underground cable installations significant heat is absorbed and carried away by the movement of moisture through the soil in addition to heat loss by conduction and the absorption of heat. So, the Law of Times would not apply to the case of heat generated in an underground cable which dries the surrounding soil.

The experimental evidence shows that the diameter of the heat source does not influence drying time of the soil or the amount of moisture that is evaporated, in the way predicted by the Law of Times. It is questionable from both experimental and theoretical perspectives that the Law of Times should be applied to predict soil drying times and soil thermal stability. Other methods must be used to include soil thermal stability in cable ampacity calculations [28].

CHAPTER 7
MATERIALS AND METHODS

One goal of the experiment is to compare the calculated values of the Neher-McGrath method to the measured values. Another goal of the experiment is to investigate the extent, if any, of soil drying that occurs due to cable heat. To perform this analysis, the following values must be measured:

1. Cable temperature (measured on the cable jacket)
2. Ambient soil temperature
3. In-situ soil resistivity
4. Lab soil resistivity
5. Soil resistivity directly adjacent (radially) to the cable

The Neher-McGrath method calculates the temperature of the conductor. However, it is difficult to measure the conductor temperature since it is covered by a polyvinyl chloride (PVC) or polyethylene (PE) jacket, providing the protection—and insulation for voltages less than 1000V—for the conductor. If the jacket temperature and thickness is known, the conductor temperature can be calculated using the radial conductive heat transfer equation per unit length as shown in Equation 7.1 [16]:

$$q' = \frac{2\pi\left(T_{jacket} - T_{conductor}\right)}{\ln\left(\frac{r_{conductor}}{r_{jacket}}\right)} \tag{7.1}$$

The following figure illustrates the variables of this equation:

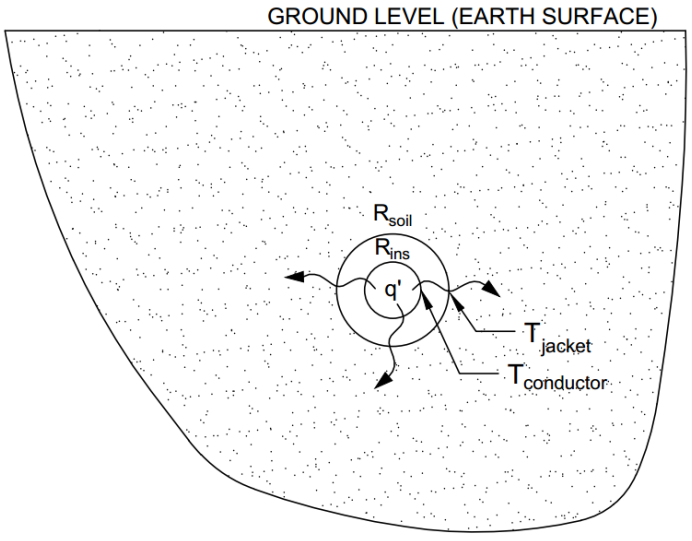

Figure 7.1 Cable conductive heat transfer parameter diagram

The ambient soil temperature is measured by waiting for the temperature sensors to reach thermal equilibrium prior to heating the cable. Most cables are installed at least 2 feet below the earth's surface and medium voltage cables may be installed 4 feet or more below the earth's surface. At this depth, the ambient soil temperature remains fairly constant throughout the year—on the order of a few degrees up or down from the annual mean temperature. So, measuring the temperature just prior to heating the cable provides an accurate reading for the experiment.

The in-situ and lab soil resistivities is measured using IEEE Std 442 [27] and ASTM D5334 [50]. Both the in-situ resistivity measurement and the soil sample for the lab test are taken at the depth of the installed cable. Since soil is not homogenous, multiple measurements are taken. The lab resistivity is measured at various moisture contents, particularly at low moisture contents and fully dried, to produce a soil dry-out curve. IEEE Std 442 [27] and ASTM D5334 [50] define the procedure well, so it is fairly straightforward to determine the value at any given time. The soil resistivity depends on the moisture content of the soil, so additional measurements are taken at the same time as the cable heating experiment using the temperature sensors on the cable jacket and the transient line source method described in [27] and [50].

The soil resistivity radially adjacent to the cable is used to determine how much, if any, soil moisture has been driven away from the cable by heating. Higher resistivities indicate soil drying has occurred. The goal is to determine if the cable heating has caused the soil adjacent to the cable to dry out. Soil resistivity is a bulk property and must be measured over some finite area, so measuring it directly adjacent to the cables is difficult. It is possible to calculate the value using the radial conductive heat transfer equation with 3 variables: heat rate, temperature at two locations, and distance between the two locations. The heat rate is controlled by the input current and the resistance of the conductor. The temperature is measured using temperature sensors. Multiple sensors can be placed radially to determine the resistivity between any two points. The calculated resistivity is an average resistivity between the two temperatures sensors and is valid for steady state conditions.

7.1 Site and Layout

The geographical location for the test is not a factor in this experiment, so the selection was based on convenience. The primary requirements included a level surface, homogenous landscape—at least by observation of the surface—and access to a power source. A homogenous landscape is impossible to guarantee since soil is variable even within a few feet,

but the goal is to avoid locations with known backfill and grading since the material may be dramatically different from the surrounding soil that is a few feet below the surface. The site is located in Boulder, Colorado, 39°57'50.7"N 105°11'16.1"W. The following figures provide the location and the landscape.

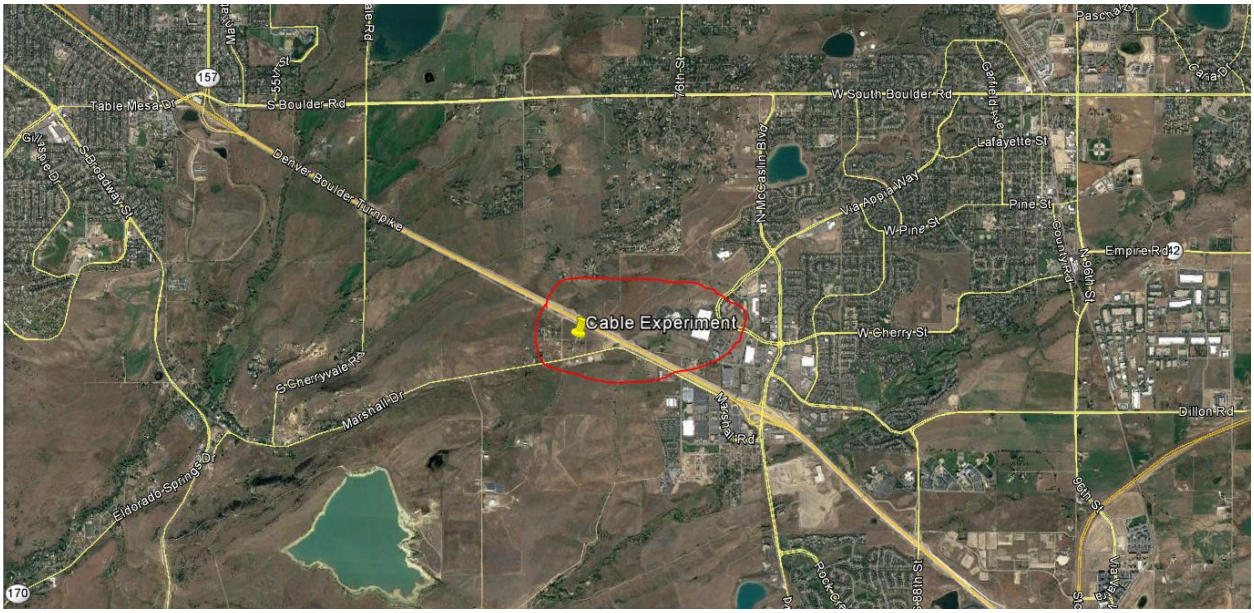

Figure 7.2 Experiment location

Figure 7.3 Trench for experiment

The land is fairly flat but is located near the top of a slight hill extending about a mile around the test location, so it is not subject to water from creeks or floods in heavy rain. This is beneficial because it limits dramatic, transient changes in the soil moisture content due to storms. The land surface consists of prairie grass and is not irrigated. There is a 120VAC power outlet nearby that provides power to the test instruments and the current source.

The cable is buried 31.5” below grade. The NEC specifies minimum cable depths depending on the type of installation. For direct buried cables operating at less than 1000V, the minimum cover (burial depth) is 24 inches [1, Sec. 300.5]. Other installations may involve concrete backfill, such as a duct bank, or conduit and the minimum cover requirement is reduced for these installation types. Medium voltage cables commonly used for utility scale renewable generation projects operate at 34.5kV and require a minimum cover of 36 inches [1, Sec. 300.5]. This experiment is operating at less than 50V, so it’s not subject to these requirements; however, the focus of this experiment is for the installations between 2 and 4 feet since it applies to the majority of cables.

An 11-foot cable (additional detail in Section 7.2.1) was laid in the trench along with the temperature sensors, placed as discussed below. Backfilling was performed by hand with a shovel and a 10” square tamper in 3” lifts. In addition, the soil was lightly wetted to assist in compaction. A yard stick was placed vertically in the trench to determine the height of each lift, the vertical placement of the temperature sensors, and the cable burial depth. A level was used to maintain equal depth along the cable. The final depth of the cable is 31.5” and the installed cable length is 11 feet.

As the cable was installed and covered, the temperature sensors were placed according to the design layout. The layout for the temperature sensors consists of two major measurement cross sections and one minor measurement cross section. These cross sections are oriented along the cable longitudinally and are centered on the cable length. The following figure shows the temperature sensor layout.

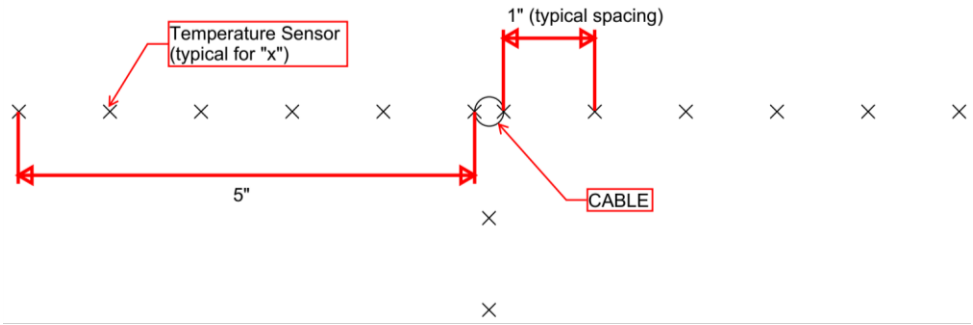

Figure 7.4 Cable and temperature sensor cross section detail

The figure above illustrates the location of the temperature sensors around the cable. There are two other cable cross sections where measurements are made similar to this section. These sections are separated by approximately 2 feet along the cable. The following figure shows all three sections with references, prefixed by a letter, to the sections of soil between temperature sensors.

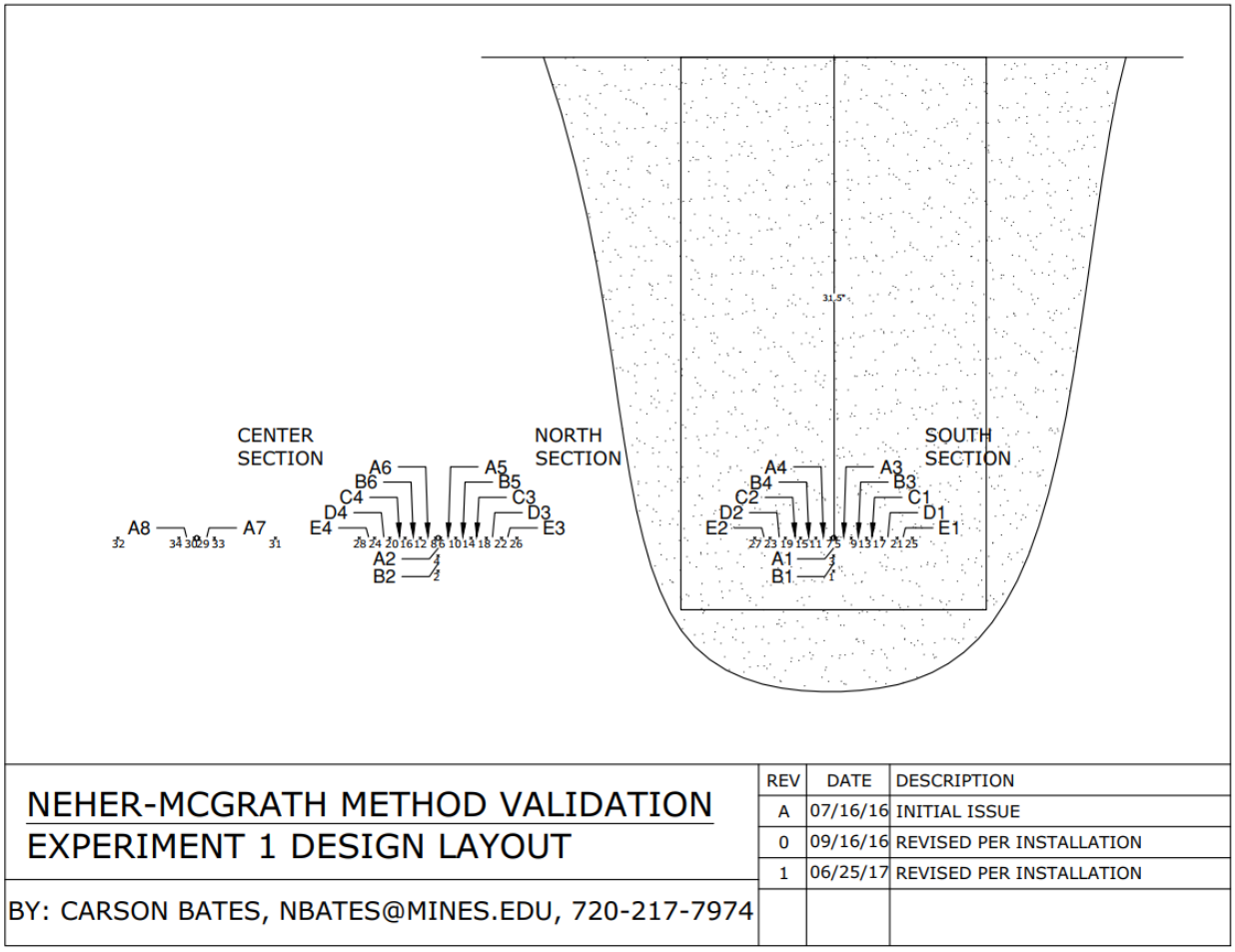

Figure 7.5 Experiment layout detail drawing

The North Section and the South Section were placed approximately 2 feet on either side of the Center Section. All three sections included 2 temperature sensors directly touching the cable jacket, 1 on each side. For the major sections—North and South—there were 5 temperature sensors placed on each side of the cable at 1-inch spacing. In addition, 2 sensors were placed below the cable at 1-inch spacing. For the minor section—Center—there was 1 sensor on each side of the cable spaced 5 inches from the outside diameter of the cable. In

addition, 2 sensors were placed above the cable at 1-inch spacing. A total of 34 sensors were installed.

Achieving the desired spacing was very difficult. The temperature sensor leads, soil granularity, placement of the tape measure—all of this and more made precise placement difficult. The expected tolerance is ⅛” for the placement of the temperature sensors. Once the sensors were placed, a small amount of soil was placed around the sensors and packed down to limit damage to or movement of the sensors. The following figures show the initial setup prior to precisely placing and covering the sensors to maintain the position.

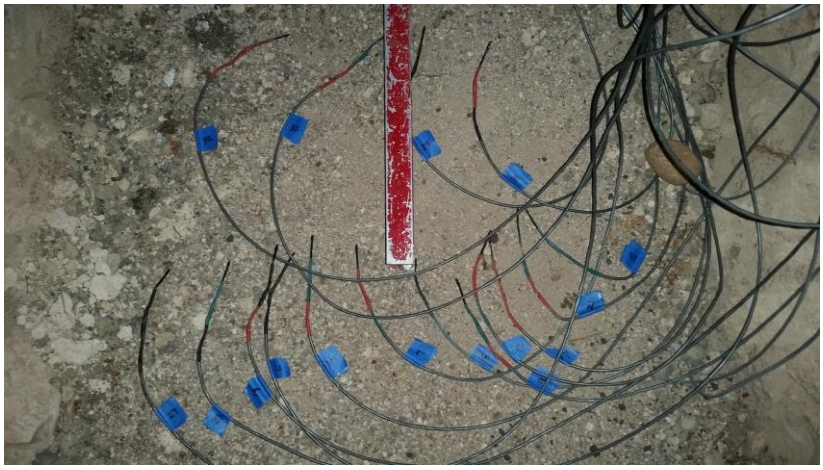

Figure 7.6 Temperature sensor rough placement

Figure 7.7 Temperature sensor precise placement near cable

Figure 7.8 Temperature sensor precise placement

Figure 7.9 Yard stick plumbness verification

7.2 Material and Equipment

Several pieces of material and equipment are required to perform the experiment. These include the cable to be tested (heat source), current source, ammeter (current measuring device), temperature sensors, moisture sensor, and data logger. Selecting the proper material and equipment is important to achieve the goals of the experiment stated above, so an explanation of the selection methodology is provided in the following sections.

7.2.1 Cable and Current Source

In order to dry out the soil around the cable, significant heat must be used. In addition, the heat flux must be high, i.e. the cable diameter must be small relative to the input heat. A 600V, #4 AWG aluminum cable was selected as the test cable because it is readily available and meets these requirements. The cable parameters such as insulation type or thickness are not the focus. Another cable of a different voltage class, conductor type, or conductor size could have been selected. The primary purpose of the cable is to serve as a heat source to the soil. The internal properties or behavior of the cable are not the subject of the research since the purpose of the test is to examine the soil behavior.

Current is applied to the cable using an iron core transformer. The transformer was originally used for a high-pressure sodium light fixture in a parking lot. This type of transformer is readily available and includes multiple taps for power input connection depending on the voltage that is available for the light. It is designed to step-up the input voltage to a high voltage to drive the light ballast. This experiment requires high current, not high voltage, so the high voltage windings were removed, and parallel copper conductors were wound around the core. The parallel conductors consisted of #10 AWG, two-conductor with ground NM cable (10-2 W/G NM). The goal is to maximize the heat dissipated by the test cable, so using large gauge wire (#10 AWG) and running parallel cables reduces the impedance and corresponding losses of the leads to the cable under test. Since the voltage is very low and there is a jacket, the ground can be used to carry current in addition to the standard conductors. This results in parallel cables each with three conductors for a total of six conductors between the transformer and the test cable. The manufacturer windings of the transformer consist of multiple taps: 120V, 208V, 240V, 480V. These allow for adjusting the current circulating in the test cable by adjusting the transformer voltage ratio, i.e. turns ratio, of the transformer. A lower input voltage tap results in a lower turns ratio and a higher output current for a fixed resistance of the test cable. The turns ratio is estimated to be 160:1 for the 120V tap with the modified secondary winding. The following pictures illustrate the installation.

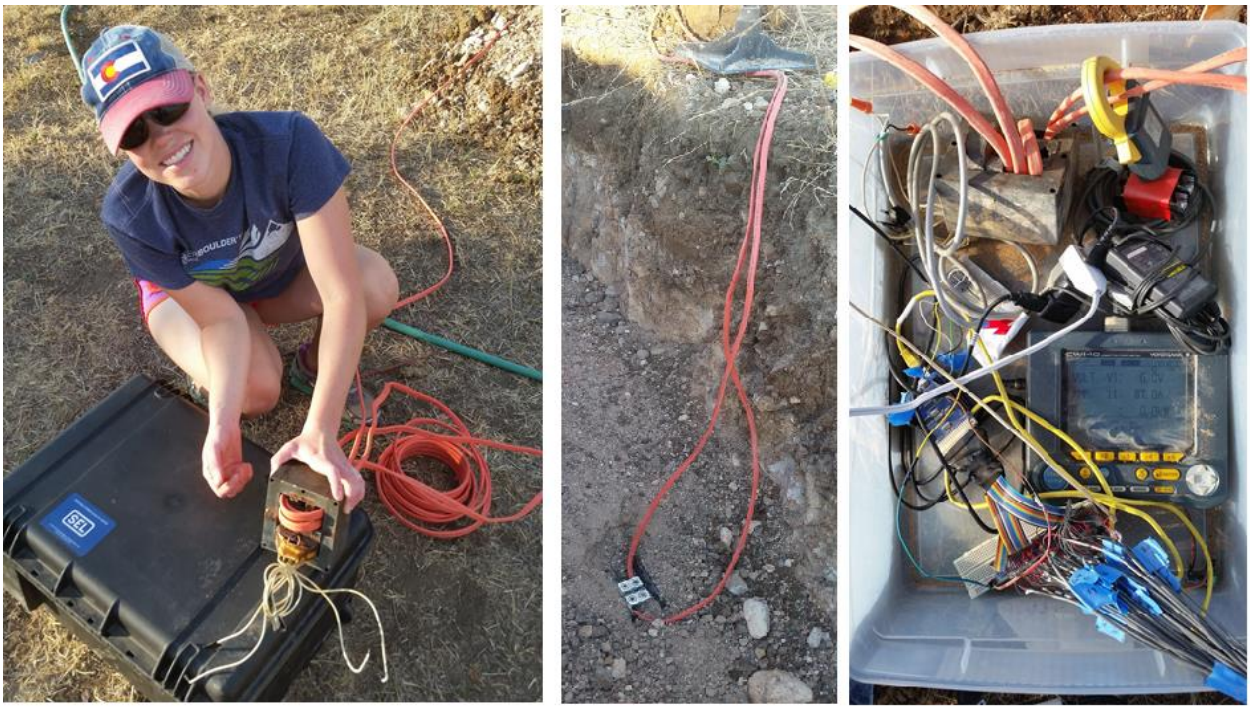

Figure 7.10 Current source and measurement installation

The parallel 10-2 W/G cables wound on the transformer core were connected to a terminal block at each end of the single #4 aluminum cable. With this connection, the only impedance is that of the cable and the transformer. With such a low impedance, it is important to verify that the transformer rating is not exceeded; otherwise, the transformer would overheat and damage the winding insulation. The power rating of the transformer is approximately 400VA. The input power, measured in volt-amperes (VA), is determined by measuring the input current with a clamp-on ammeter and multiplying by the input voltage measured with a voltmeter. The input power is highly inductive because of the transformer winding configuration and the test cable impedance, so a significant portion of the transformer input power and heating is due to eddy and hysteresis losses in the transformer rather than the resistive losses (Joule heating) of the test cable. The following figure is a schematic of the installation:

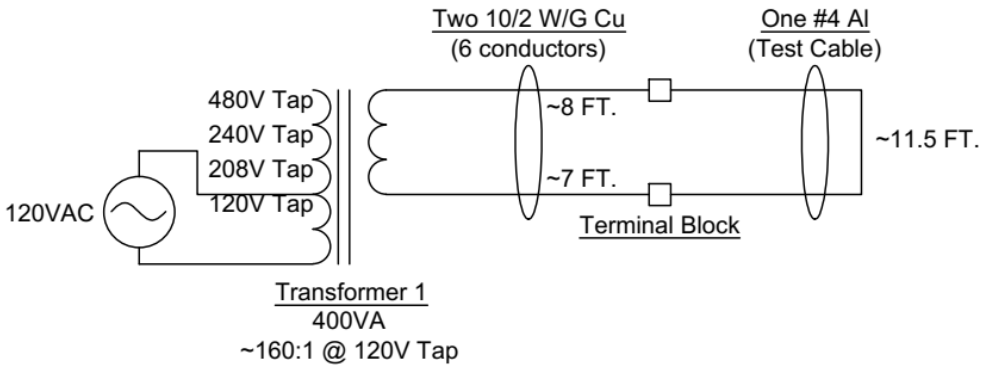

Figure 7.11 Experiment schematic with one transformer

After the initial installation, an additional transformer was added in series to provide additional current through the test cable. It was configured in the same manner as the first transformer. The power rating on the second transformer was 250VA, which was less than the first transformer. Therefore, a higher voltage tap connection was used to reduce the voltage output and corresponding power. The additional transformer after modification had a turns ratio of approximately 520:1 at the 240V tap. This final configuration allowed for a maximum current of approximately 125A on the test cable and allowed for lower currents by utilizing the transformer taps. The following figures illustrate the final configuration:

Figure 7.12 Experiment measurement setup

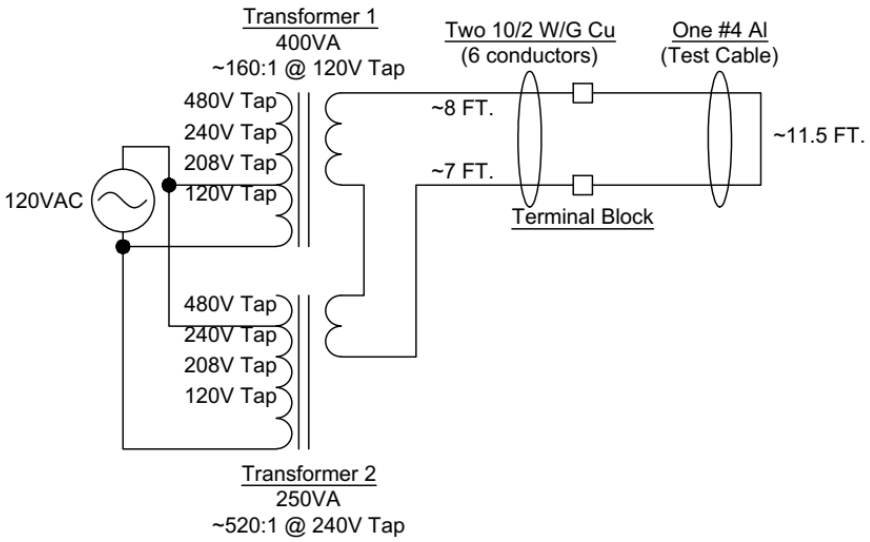

Figure 7.13 Experiment schematic with two transformers

7.2.2 Ammeter

The heat rate of the cable is determined by the current circulating through the cable and the cable resistance, calculated as I^2R. Since the current is squared, the measurement accuracy has a large impact on the overall experiment accuracy. Current was measured using a Yokogawa CW140 with a stated accuracy of ± (0.6% reading + 0.4% range) [68]. The range of the clamp-on is 200 A, so this results in an accuracy of ± (0.6% reading + 0.8 A). During initial testing, an SEL-735 meter was used as a second ammeter to verify the Yokogawa. The results were within 0.1 A, so the remainder of the tests only used the Yokogawa for current measurement.

7.2.3 Temperature Sensors

The temperature sensors are the key components of this experiment. Temperature is commonly measured using one of three devices: resistance temperature detectors (RTDs), thermocouples, and thermistors. Three factors were used to evaluate the selection of the temperature sensors: ease of measurement for a data logger, accuracy, and cost. RTDs are the most accurate; however, they must be measured using an amplifier circuit with high accuracy, and the cost is approximately $5 per sensor. Also, these must be multiplexed into an amplifier or be provided with multiple amplifiers, which adds an additional cost. Thermocouples are relatively inexpensive but are not very accurate and require an amplifier circuit for each sensor or a multiplexed amplifier circuit. Thermistors are relatively inexpensive and can be measured with a simple voltage divider circuit. A comparison of the various sensors is shown below [69].

Sensor Type	Typical Temperature Range (°C)	Accuracy (+/- °C)	Pros	Cons	Applications
Thermistor	• Within ~50°C of a given center temperature • Common range: -40° to 125°	1	• Low cost • Durable • Small size	• Nonlinear output • Slow response time	• Ambient temperature measurements
Thermocouple	-200° to 1450°	2	• High resolution • Small size • High temperature range	• Calibration is highly recommended • Two temperature readings are required: hot junction and cold juntion.	• Industrial use
RTD	-260° to 850°	1	• Linear output • Accurate	• Expensive • Fragile: are often housed in protective probes.	• Industrial use
Analog IC	-40° to 125° (TMP36)	2	• Simple to interface with • Easy to use • Linear output	• More expensive than thermistors. • Limited temperature range.	• Domestic thermostat • Digital thermometer
Digital IC	-55° to 125° (DS18B20)	0.5	• Simple to use with microcontrollers • Accurate • Linear output	• Requries a microcontroller, or something similar. • More expensive than thermistors. • Limited temperature range.	• Domestic thermostat • Digital thermometer • Consumer electronics

Figure 7.14 Temperature sensor comparison [69]

Thermistors accuracy depends on the equation used. Since thermistors are nonlinear, a fitted equation must be used to determine the temperature versus resistance. The Beta equation provides a one parameter logarithmic fit equation while the Steinhart-Hart equation provides a three-parameter logarithmic fit. Using the latter can provide accuracy of 0.02°C [70] if calibrated. The Beta equation is commonly used for its simplicity. Using a data logger with higher processing capability allows for using the Steinhart-Hart equation, so this equation is used for the experiment.

Thermistors were selected as the best option since the measurement accuracy meets the requirements; they are economical, and they are easy to add to a standard data logger—not requiring the use of amplifiers. The measurement range of the experiment is from about 10°C to 90°C. This falls within the preferred measurement range of the thermistors.

7.2.4 Moisture Sensor

The volumetric water content, moisture content, of soil can be measured in multiple ways. Decagon Devices manufacturers the EC-5 sensor that “determines volumetric water content (VWC) by measuring the dielectric constant of the media using capacitance and frequency domain technology” [71]. The volume of measurement is approximately 9 cm in length with a radius of 4 cm in one axis and 5.5 cm in the other. This device is a small volume of measurement compared to other commercially available sensors, which is desirable when determining if the soil adjacent to a cable has dried out. It can also be used to determine ambient soil moisture content. According to the manual, the accuracy is given as: “Generic calibration: ±0.03 m^3/m^3 typical in mineral soils that have solution EC <8 dS/m. Medium specific calibration: ±0.02 m^3/m^3 in any porous medium (± 2%).” Most soil moisture contents for cable ampacity calculation are around 15%, so an accuracy of ± 2% is significant and indicates only general trends can be determined. A 2% moisture content error can result in 10% change in

resistivity depending on the soil. The moisture sensor was used only during the first few experiments to compare with the lab measured moisture content in Section 8.1.

7.2.5 Data Logger

The data logger most commonly measures the raw value of a sensor, converts it to an engineering value, and stores it at a defined interval. Initially, an Arduino Uno was selected to perform this function, but this was subsequently changed to an Arduino Mega 2560 to provide larger memory size for the code. The Arduino platform provides an economical, open source microcontroller [72]. The platform can incorporate a wide variety of sensors and features. Using an Arduino allows for a very tailored solution to a specific application—in this case, a data logger.

Several versions of the data logger were programmed as the experiment was initially developed. The final code provided time stamped temperature measurements to an SD card. Since the thermistors are resistance devices and resistance cannot be measured directly, a voltage divider circuit was used. A 5V power supply was used to power the data logger and provide the source voltage for the voltage divider circuit. The data logger measured the source voltage and the voltage across the thermistor. It used these measurements and the known value of the voltage divider resistance to calculate the thermistor resistance. This resistance was converted to a temperature value using the Steinhart-Hart equation. Oversampling was used to achieve a higher precision. The value was scaled up by 100 and converted to an integer to reduce the memory size required for a floating-point number. The time stamp was provided by a real time clock shield (RTC) using a DS1307 chip.

The temperature logging rate is configurable and was set to five seconds for most of the experiments. Some experiments used one second logging for the first few hours, and then increased to thirty second logging for the first few days, and then five-minute logging for the remaining days. Since the temperature response is logarithmic, increasing the sampling rate with increasing duration reduces the experiment data without loss of information. The data was stored to the SD card located in the SD card shield in CSV format.

Arduino boards have limited capabilities such as limited inputs and outputs, limited storage capabilities, etc. The boards are commonly supplemented by additional boards called shields. These interface with the main Arduino board. This experimental setup used the RTC/SD card shield to provide a clock for time stamping and SD card interface for storage. It also used the MuxShield to provide multiplexing of the thermistors since there are not enough analog inputs on the Arduino Mega2560 board.

Other data loggers were considered for the experiment. There are many pre-built data loggers that can accommodate the required number of inputs, precision, time stamping, and storage; however, the cost was prohibitive. The ability to customize the Arduino data logger was also beneficial. Customization and cost were significant drivers for the selection of an Arduino based data logger. Other researchers may find it is a reasonable alternative to the traditional data loggers, so the source code for this project is provided to assist with the implementation in Appendix B.

7.3 Uncertainty Analysis

The experimental uncertainty was estimated to predict the maximum error and confirm the acceptability of the selected test equipment; it was estimated using the root-mean-square method and the Monte Carlo method. Measuring the cable jacket temperature is relatively straightforward but determining if soil dry-out has occurred around the cable is more difficult. The latter is the focus of the uncertainty analysis.

The root-mean-square method (RSS) is based off the uncertainty in each variable of the resistivity calculation. This error is determined by the derivative in each variable with respect to the variable of interest: the soil resistivity. The following equation is the calculation of resistivity based on pure conduction.

$$\rho = \frac{2\pi(T_1 - T_2)}{\mathrm{q} * \ln\left({}^{r_2}/_{r_1}\right)} = \frac{2\pi(T_1 - T_2)}{\mathrm{I}^2\mathrm{R} * \ln\left({}^{r_2}/_{r_1}\right)} \tag{7.2}$$

Where

ρ=soil thermal resistivity (°C·cm/W)

T=temperature at specified subscript location (°C)

q=heat per unit length (W/cm)

r=radius from cable center at specified subscript (m)

I=current (A)

R=conductor electrical resistance per unit length (Ω/cm)

The following equations are the derivatives for use in the RSS uncertainty analysis:

$$\frac{\partial\rho}{\partial T} = \frac{2\pi}{\mathrm{I}^2\mathrm{R} * \ln\left({}^{r_2}/_{r_1}\right)}$$

$$\frac{\partial\rho}{\partial I} = \frac{-4\pi(T_1 - T_2)}{\mathrm{I}^3\mathrm{R} * \ln\left({}^{r_2}/_{r_1}\right)}$$

$$\frac{\partial \rho}{\partial r_1} = \frac{2\pi(T_1 - T_2)}{\mathrm{I}^2\mathrm{R} * \mathrm{r}_1 * \ln^2\left({}^{r_2}/_{r_1}\right)}$$

$$\frac{\partial \rho}{\partial r_2} = \frac{-2\pi(T_1 - T_2)}{\mathrm{I}^2\mathrm{R} * \mathrm{r}_2 * \ln^2\left({}^{r_2}/_{r_1}\right)}$$

After performing the analysis with best estimates of the values, it was determined that the RSS uncertainty analysis would not provide enough insight into the required design values. This is primarily because there is difficulty in assigning values to the errors. Also, the variables are likely interdependent, so correlation must be considered.

Monte Carlo uncertainty analysis was used to determine the required equipment and installation tolerances. The Monte Carlo technique uses the error and error distribution for each variable in the resistivity equation. The analysis is performed with the expected values plus some random error, which is generated by multiplying a normalized random number by the error distribution. This analysis was performed in a spreadsheet based on an uncertainty analysis by John Denker [73]. The analysis evaluated the selection of the temperature sensor, the bias resistor for the temperature sensor, the sensing voltage, and the analog-to-digital converter (ADC) resolution. The analysis considers the uncertainty in temperature measurement based on the temperature sensor parameter—Steinhart-Hart equations for thermistors—and bias resistor used in the circuit. It also considers the ADC resolution, the conductor resistance and size uncertainty, the current measurement uncertainty, and the probe placement uncertainty. Uncertainties related to products such as temperature sensors, ADCs, and current measurement are based on the manufacturer's datasheets. Probe placement uncertainty is based on an estimate of the installation conditions, which are soil movement and visual placement using a ruler. The independent variables of current and soil resistivity are based on expected values.

The Monte Carlo inputs are shown in the following table:

Table 7.1 Monte Carlo uncertainty analysis inputs

Variable	Calculated Value	Units	Error Description	Error	Units	Notes
T1	313.15	K				
R_T1	5.82E+03	Ohms				
T2	306.65	K				
R_T2	7.32E+03	Ohms				
R_divider	4.75E+03	Ohms	Error R_div	0.1%		
V_s	5	V	Error V_s=	1.0%		only impacts day-to-day comp.
V_o1	2.75	V	Error V_m=	10	bit	ADC resolution
V_o2	3.03	V	Error V_m=	1	bit	LSB error
d1	0.43	cm	Error spacing	0.318	cm	
d2	2.97	cm	Δd	1	in.	
Cable Size	41.70	kcmil	Error Cable	1.0%		
R_cable	1.39E-05	Ω/cm(25°C)			Cu: 10.575, Al:164%Cu	
R_c_temp	1.47E-05	Ω/cm(oper. temp)		5.6%		Cu:0.00385, Al:0.00395
I_cbl	120	A	Error I_cbl	1%		
q'_cbl	0.21	W/cm				
ρ_soil	100.0	°C·cm/W				

The Monte Carlo uncertainty analysis indicates that the largest uncertainty is due to the temperature sensor placement. Using a higher accuracy temperature sensor or lower tolerance resistor or higher bit resolution ADC will not provide significant benefits. The results are shown in the table below.

Table 7.2 Monte Carlo uncertainty analysis results

Variable	No Error Comparison	Monte Carlo Avg	Units	2σ	ppt	Error Contribution
T1	313.15	313.30	K	0.60	0.49	0%
R_T1	5.8249E+03	5.8256E+03	Ohms	1.17E+02	0.12	2%
T2	306.65	306.71	K	0.58	0.20	0%
R_T2	7.3238E+03	7.3221E+03	Ohms	1.47E+02	-0.24	2%
R_div1	4.7500E+03	4.7499E+03	Ohms	9.54E+00	-0.01	0%
R_div2	4.7500E+03	4.7500E+03	Ohms	9.52E+00	0.00	0%
V_s	5.0000	5.0001	V	0.101	0.03	2%
V_ADC1	55.1%	55.1%		0.49%	-0.02	1%
V_ADC2	60.7%	60.7%		0.49%	-0.02	1%
d1	0.434	0.561	cm	0.190	293	34%
d2	2.974	2.970	cm	0.648	-1.15	22%
R_c_temp	1.474E-05	1.473E-05	Ω/cm	2.98E-07	-0.80	2%
I_cbl	120.00	119.99	A	2.42	-0.12	2%
q'_cbl	0.2123	0.2121	W/cm	0.0096	-0.93	5%
Rho	100.0	118.5	°C·cm/W	34.0	185.2	29%

The analysis also indicates a positive bias on the resistivity calculation, “Rho”. This is because the distance “d1” is at the cable jacket, where the thermistor is placed, which cannot have a negative error value. A negative error would represent the thermistor being placed inside of the cable—a physical limitation. The bias towards reduced distance between thermistor 1 on the cable jacket and thermistor 2, approximately one inch away, results in an average value or Rho greater than the expected Rho.

The current supplied through the cable impacts the uncertainty analysis in two ways. The first impact is in the calculation of heat from the cable (I^2R losses). Current is directly in the resistivity equation shown and is obvious. The second impact is on temperature, which occurs indirectly through the temperature difference between two probes. As the temperature

difference decreases, the accuracy of the thermistor and the ADC begin to contribute significant error. In other words, the uncertainty of the temperature measurement beings to exceed the measured temperature difference. Higher current increases the temperature difference thereby overcoming this temperature difference error. The relationship is asymptotic such that current above 60 A no longer contributes significantly to the uncertainty. The graph below illustrates this.

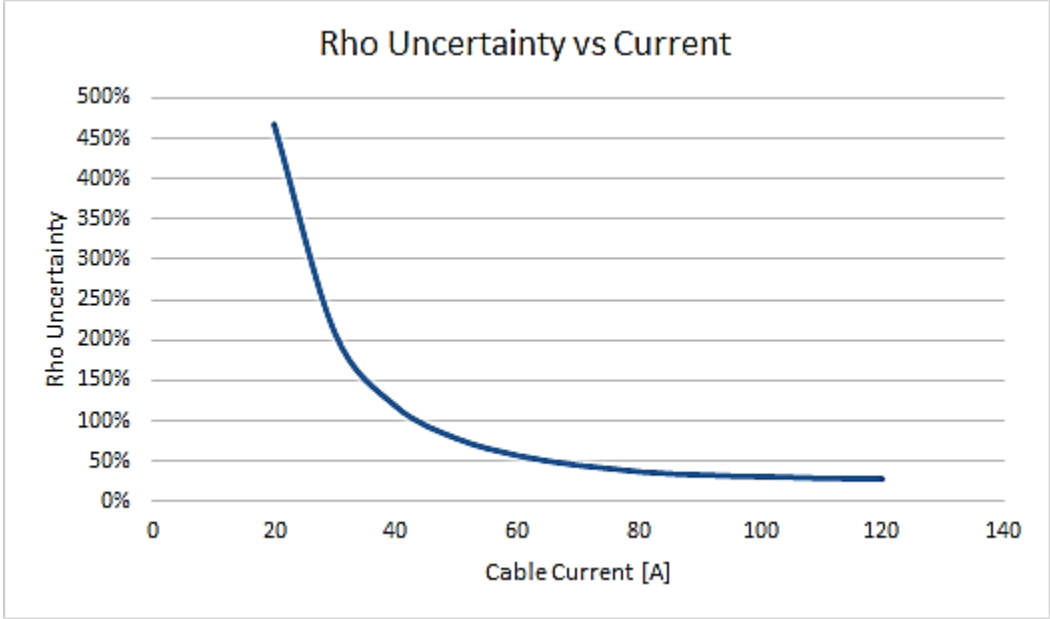

Figure 7.15 Resistivity uncertainty versus cable current

In summary, the results of the uncertainty analysis indicate that the following parts and values are acceptable:

1. Thermistor with 1% tolerance
2. Thermistor bias resistor (voltage divider) with 0.1% tolerance
3. Source voltage of 5V

It also indicates that the thermistor placement is critical. A tolerance of ⅛” is necessary to achieve useful results.

CHAPTER 8
SITE-SPECIFIC DATA COLLECTION

It is important to measure the site-specific parameters for any cable ampacity calculation. These parameters include soil moisture content, density, and thermal resistivity. Without these measurements, it is impossible to accurately compare the measured cable temperature with a calculated temperature from the Neher-McGrath method and software models. This chapter describes the method and results of the measurements. It also illustrates the variability of soil even at a specific location.

8.1 Soil Moisture Content and Density

The soil moisture content and density can be determined using various methods as described by national standards. The most common method is ASTM D6938-17 “Standard Test Methods for In-Place Density and Water Content of Soil and Soil-Aggregate by Nuclear Methods (Shallow Depth)” [74] because of the ease and speed of measurement. The test is performed by inserting a rod connected to the test instrument into the soil, running the test typically lasting a minute or less, and recording the results. Most other methods for determining density and moisture content require digging up a sample of soil and recording the weight before and after drying the sample. ASTM D4643-08 “Standard Test Method for Determination of Water (Moisture) Content of Soil by Microwave Oven Heating” [36] was used for this experiment.

Two soil samples were taken of the soil using the driven cylinder method on July 22, 2017. Three moisture and density tests were performed on both of the samples. The results are shown in the following table.

Table 8.1 Soil moisture content and density

Sample Date	Avg	Stdev
Water Content	14.3%	3.13%
Wet Density (g/cm³)	1.38	0.11
Dry Density (g/cm³)	1.21	0.13

This indicates an in-situ moisture content of 14%. This value is used for comparing the in-situ thermal resistivity measurements with the lab thermal resistivity measurements. If the samples were taken during the expected driest time of the year, the moisture content could be

considered at or near the minimum. July is not the expected driest time for this location, so the measurement is used for adjusting to the minimum expected moisture content based on the thermal resistivity dry out curves.

8.2 In-Situ Soil Resistivity Measurement Theory

The in-situ soil thermal resistivity was measured using 4 thermal resistivity measurement probes at various times during the year. The probes consist of a heating element and temperature sensor contained in a slender tube. There are two standards that are commonly specified for taking soil thermal resistivity measurements: IEEE Std 442 and ASTM D5334 [27] [50]. According to ASTM D5334 [50]:

> "Thermal conductivity is determined by a variation of the line source test method using a needle probe having a large length to diameter ratio to simulate conditions for an infinitely long, infinitely thin heating source…Thermal conductivity is obtained from an analysis of the temperature time series data during the heating cycle and cooling cycle if applicable."

IEEE Std 442 also provides specific details regarding the measurement of soil thermal resistivity and provides construction details for thermal resistivity probes [27]. A simple diagram from this standard is shown in the following figure.

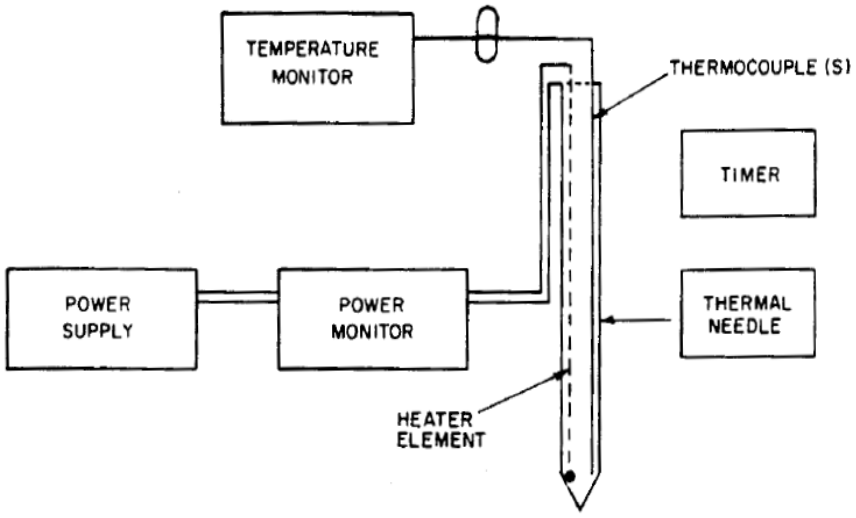

Figure 1—General Schematic Diagram for Test Equipment

Figure 8.1 IEEE Std 442 thermal probe diagram © 1981 IEEE [27]

Measuring soil thermal resistivity is performed using a transient line source analysis technique that assumes an infinite linear heat source embedded in a constant property infinite medium [50]. These assumptions are reasonable for the short durations used for the measurement of soil thermal resistivity. The specific equation is:

$$\rho = \frac{4\pi \cdot (T_2 - T_1)}{q \cdot \ln\left(\frac{t_2}{t_1}\right)}$$

Where

ρ=soil resistivity (°C·cm/W)

T_1=temperature at time t_1 (°C)

T_2=temperature at time t_2 (°C)

q=applied heat (W/cm)

t_1 and t_2 = measurement times from the time heat was applied (s)

The time, t_1, must be selected after the initial transient has settled, which occurs after the probe and the contact resistance from the probe to the soil has exceeded its time constant—typically 10 seconds to 5 minutes depending on the probe diameter. The time, t_2, is selected based on the initial time, t_1, and is typically 7 to 10 times the value (5 minutes to 50 minutes). The basis for the selected times is verified by confirming that the temperature response is approximately linear on a logarithmic x-axis graph [27]. The initial transient, caused by the probe time constant and the influence of the earth's surface at the end of the measurement period, is clearly seen by noting the non-linearity on the graph. Linear regression verifies this visual determination.

To perform the soil thermal resistivity measurement, the probe is inserted into the soil, allowed to reach thermal equilibrium, then heated at a constant rate while temperature measurements are made about every second. These temperature measurements are plotted on a graph with logarithmic time on the x-axis and temperature on the y-axis, called the heating curve. The soil resistivity is equal to the slope of the linear portion of the logarithmic time versus temperature divided by the input heat. An example of this is shown in the following figure.

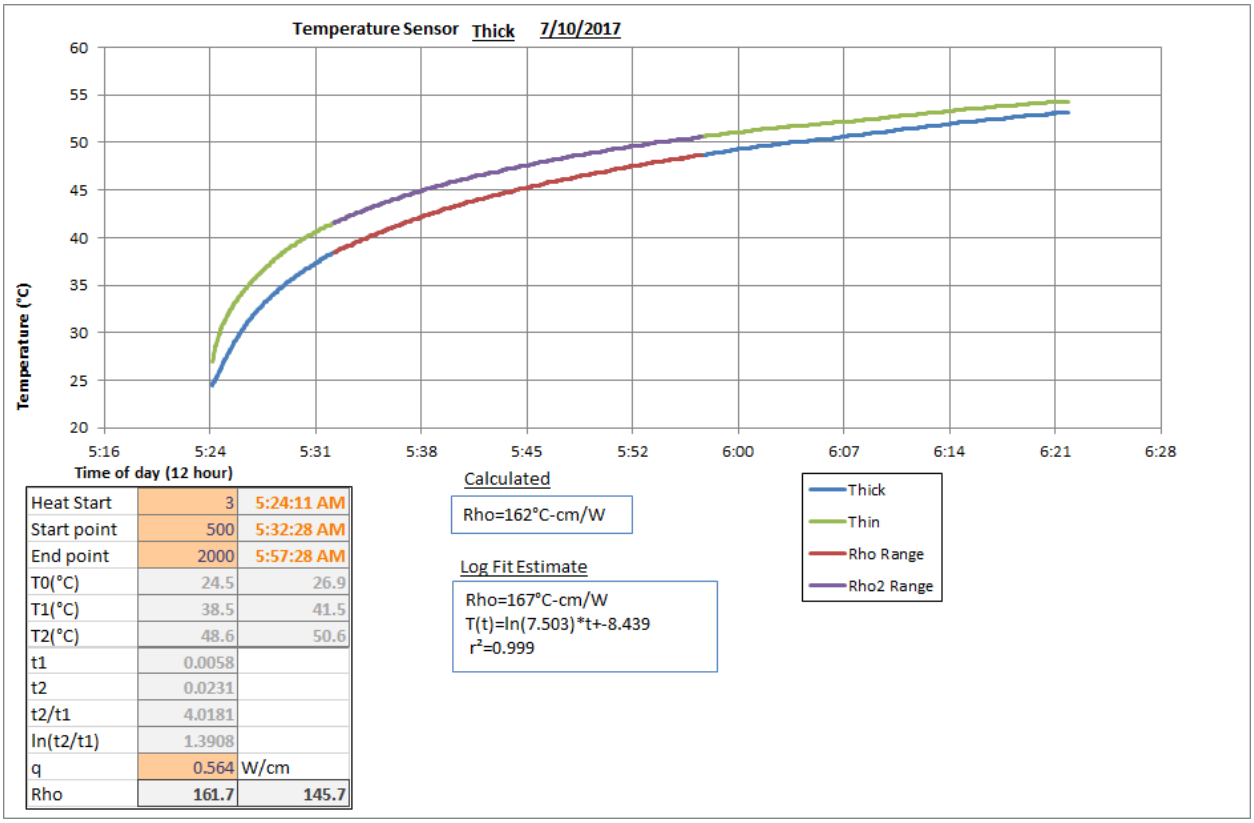

Heat Start	3	5:24:11 AM
Start point	500	5:32:28 AM
End point	2000	5:57:28 AM
T0(°C)	24.5	26.9
T1(°C)	38.5	41.5
T2(°C)	48.6	50.6
t1	0.0058	
t2	0.0231	
t2/t1	4.0181	
ln(t2/t1)	1.3908	
q	0.564	W/cm
Rho	161.7	145.7

Figure 8.2 Soil resistivity calculation on line time scale

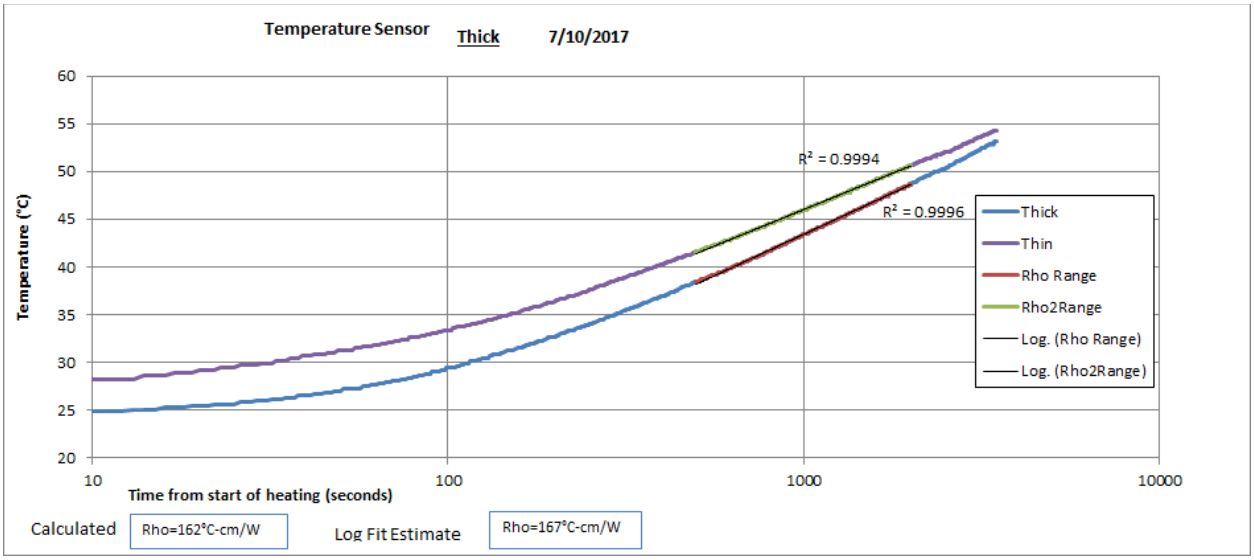

Figure 8.3 Soil resistivity calculation on logarithmic time scale

This same procedure is used on the cooling curve. The probe is heated to approximately steady state, then the heat input is turned off, and the temperature is recorded at 1-second intervals, the same as the heating curve procedure. The resistivity is determined using the same

equation as the heating curve as described in ASTM D5334 [50]. It is proposed that soil drying has occurred if the cooling curve resistivity is higher than the heating curve resistivity.

8.3 Thermal Resistivity Measurement Probes

In order to compare the measurements of 4 thermal resistivity measurement probes, 95 tests were performed. The first probe was constructed using the large probe illustrated and defined in IEEE Std 442 [27], referred to as the Standard Probe in this dissertation. The second probe was constructed using a scaled down version of the large IEEE Std 442 probe, about ⅓ of the size, referred to as the Stainless Probe. The third probe was constructed according to the small laboratory probe of IEEE Std 442, referred to as the Lab Probe. The forth probe was provided by a manufacturer, Decagon Devices, and is similar to the small laboratory probe of IEEE Std 442, referred to as Thermolink. In practice, only one probe is used to measure the soil thermal resistivities, but multiple tests were conducted for this work to compare the results. As described in Chapter 2, part of the difficulty in calculating cable ampacity involves selecting a thermal resistivity. Comparing the resistivities measured by these probes with the temperature calculations in Chapter 9 Experiments provides the data necessary to specify how the thermal resistivity should be measured and used.

8.3.1 Standard Probe

The standard probe is approximately 5 feet long and ¾” diameter. Specific details for the construction are provided in IEEE Std 442, but a brief summary is provided here. The probe consists of a copper pipe containing a heating element (constantan wire) and a temperature sensor (thermocouple). It is filled with thermally conductive powder (boron nitride) to fill the air gaps in the pipe. The probe is difficult to install because subsurface rocks prevent full insertion. The advantage of the probe over the others described in this chapter is that it provides better spatial averaging of the soil conditions, particularly if the probe extends through multiple resistivity layers. Though the standard describes a method for using a sliding hammer to drive the probe into the soil, a drill can also be used with a long drill bit to auger a pilot hole; however, installation is difficult, especially in the rocky soil of this experiment. The following figure illustrates the Standard Probe:

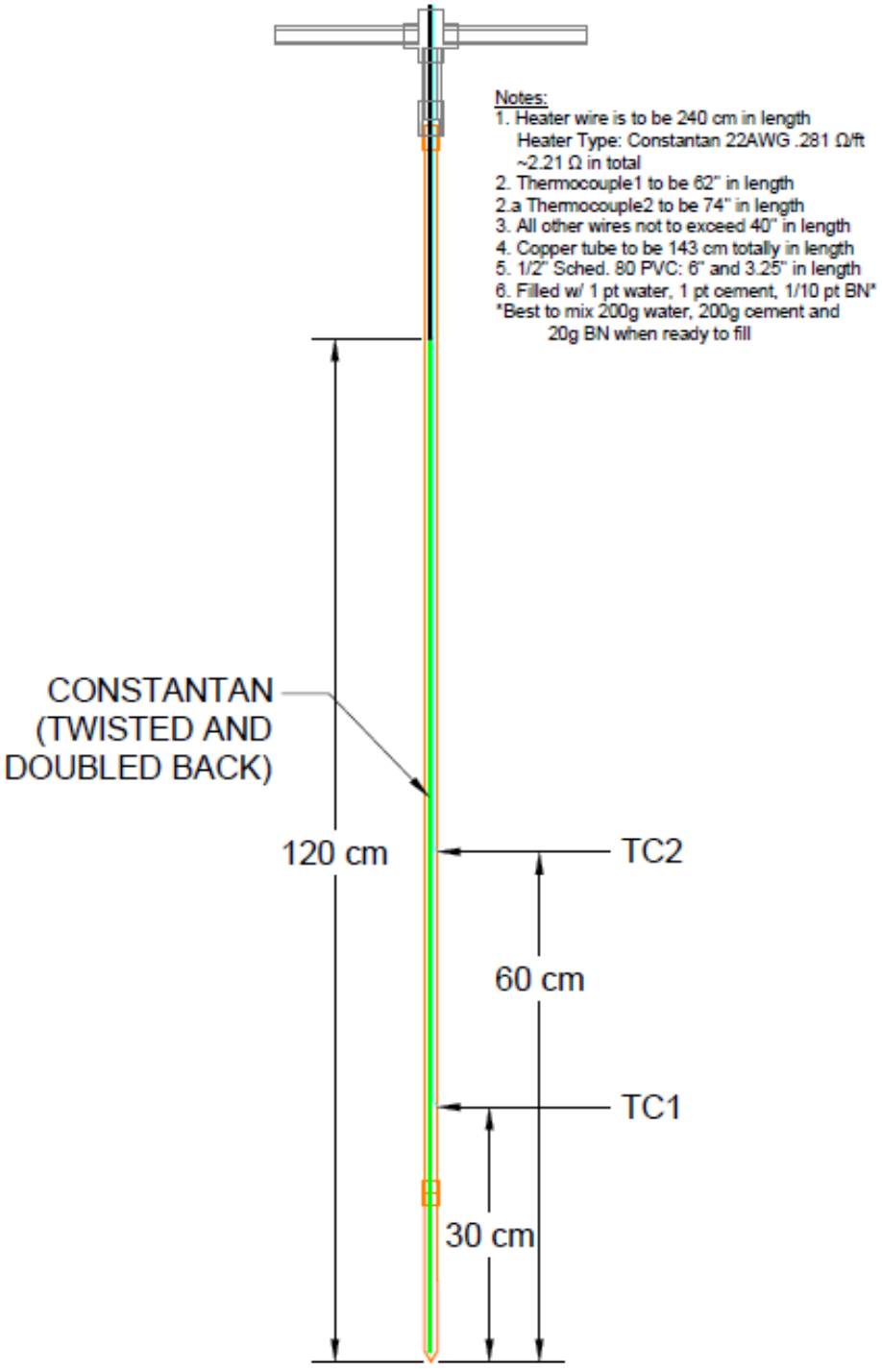

Figure 8.4 Standard Probe construction details

8.3.2 Stainless Probe

The Stainless Probe is approximately 21 inches long and ¼" diameter. The probe is constructed from stainless steel and is the same internal construction as the Standard Probe. Since the probe is narrower and shorter, it permits easier installation than the Standard Probe. It can be installed with a hammer drill because drill bits are available of similar length to the probe—this is not an option for the Standard Probe. In addition to easier installation, the lower thermal mass of the probe reduces the initial transient duration from minutes to seconds. This reduces the total measurement time for determining the thermal resistivity from approximately 45 minutes using the Standard Probe to approximately 15 minutes. The following figure illustrates this probe:

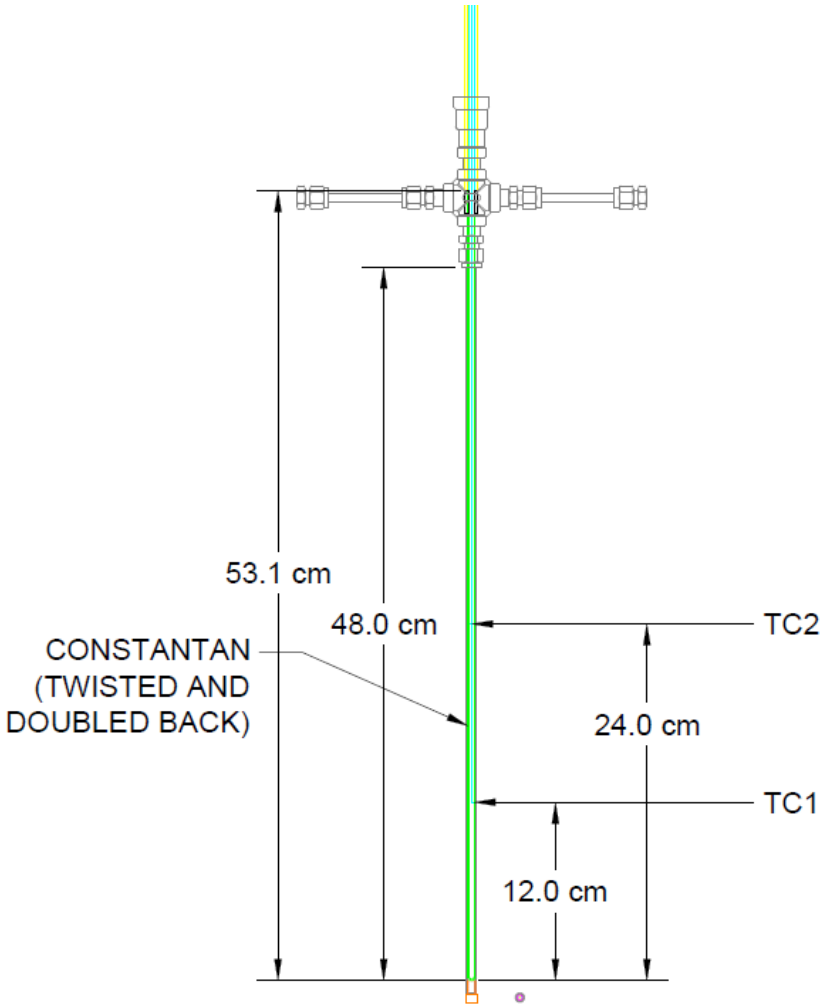

Figure 8.5 Stainless Probe construction details

8.3.3 Lab Probe

The Lab Probe is the smallest probe compared in this experiment. It is intended to be used in the laboratory on soil samples that are extracted during the geotechnical investigation. It can be used in the field; however, it is fragile and is the most sensitive to error caused by large rocks near the probe. Other than requiring a more delicate installation, this probe is the easiest to install. The probe is approximately 4” long and 0.1” diameter. The heater consists of 4 lengths of constantan wire to increase the resistance enough to allow for more accurate control of the heat rate. It contains a thermocouple for measuring the temperature. The following figures illustrate this probe:

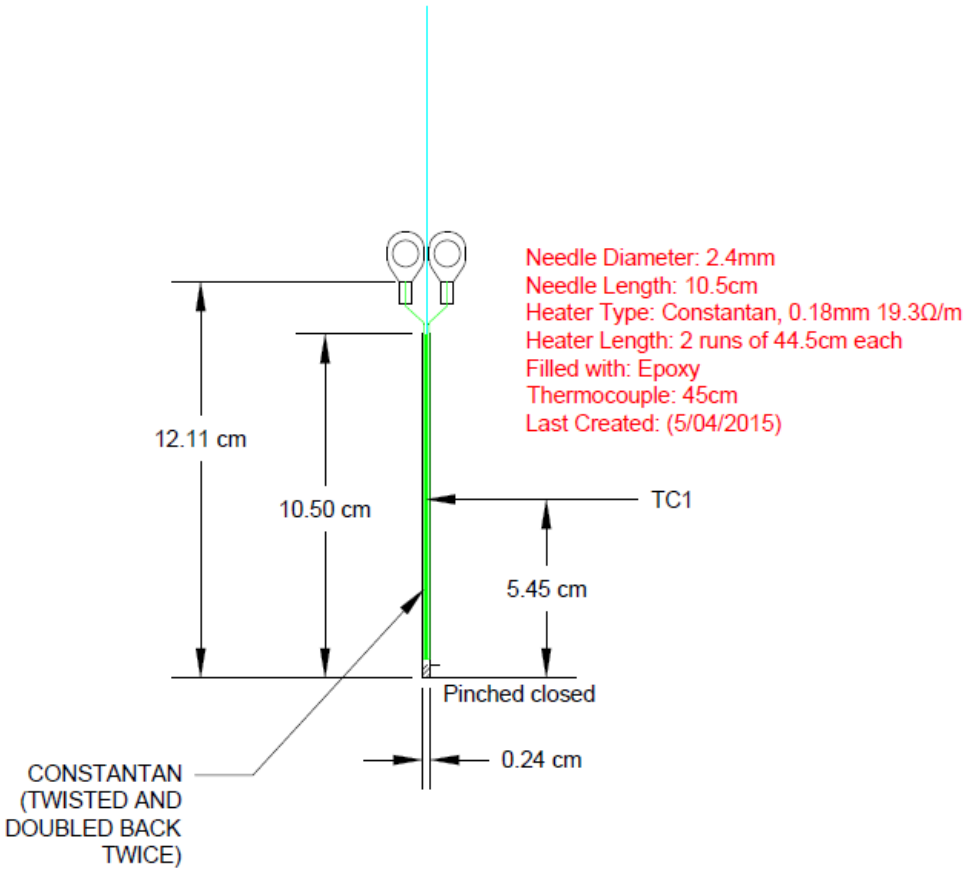

Figure 8.6 Lab Probe construction details

Figure 8.7 Lab Probe testing in-situ soil

8.3.4 Thermolink Probe

The Thermolink Probe was supplied by Decagon Devices now owned by METER Group, Inc [75]. The TR-3 probe dimensions are nearly identical to the Lab Probe. Since it is provided by a manufacturer, the internal composition is unknown, e.g. the heater and temperature measurement probe position. The probe connects to the handheld Thermolink unit: a manufacturer integrated power supply, data logger, and resistivity calculating computer. It is designed to be run as a complete package rather than providing raw temperature data to be analyzed. The device automatically checks for thermal equilibrium of the needle prior to starting the test—a critical condition for the transient line source method [50]. Heat is applied for 1 minute (not user configurable). It analyzes the temperature transient and calculates the thermal resistivity immediately. The resistivity calculation for the other three probes—Standard, Stainless, and Lab probes—is calculated manually by the user after retrieving the data. Calculating the resistivity in the same unit that measures the temperature is very convenient. The unit reports the thermal conductivity, resistivity and error value (indicating the variability of the measurement). All of this data, including the raw temperature measurements, are available for download via USB connection and software. The TR-3 probe and Thermolink measurement unit are shown below.

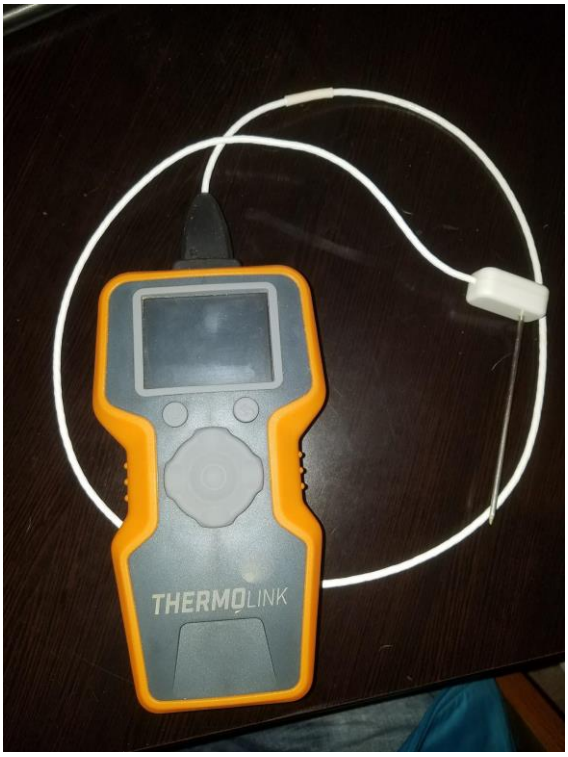

Figure 8.8 Thermolink Probe

8.4 Resistivity Probe Measurements

Several resistivity measurements were performed throughout the year. The results for the Standard Probe are shown in the following figure:

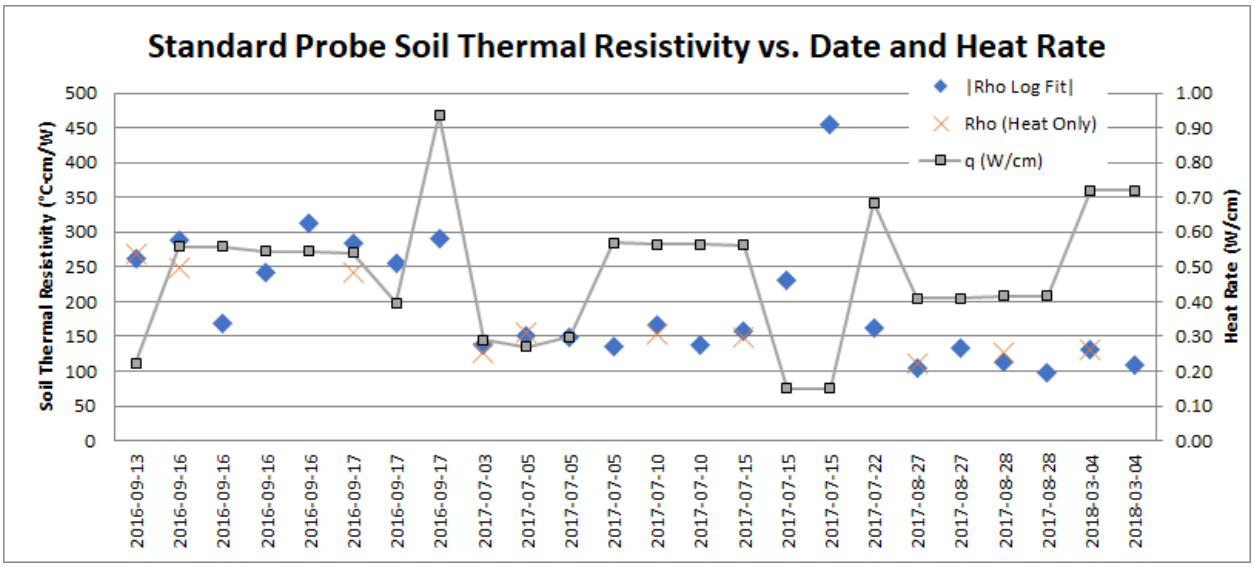

Figure 8.9 Standard Probe soil thermal resistivities and heat rate versus date

The tests were analyzed for the overall mean, the heating only curve, and the cooling only curve. The results are summarized in the following table.

Table 8.2 Thermal probe thermal resistivity measurements

Probe	# Samples, Mean & Std. Dev.	Standard Heating Curve (P1)	Cooling Curve
Standard	47 Samples= 183±77°C·cm/W	10 samples P1= 171±58°C·cm/W	9 samples cooling= 164±51°C·cm/W
Stainless	28 Samples= 296±134°C·cm/W	7 samples P1= 314±133°C·cm/W	6 samples cooling= 301±139°C·cm/W
Lab	6 samples= 307±44°C·cm/W	3 samples P1= 335±37°C·cm/W	3 samples cooling= 279±34°C·cm/W
Thermolink	14 samples= 194±31°C·cm/W		

The following figure illustrates the 95% confidence limit of all the probes:

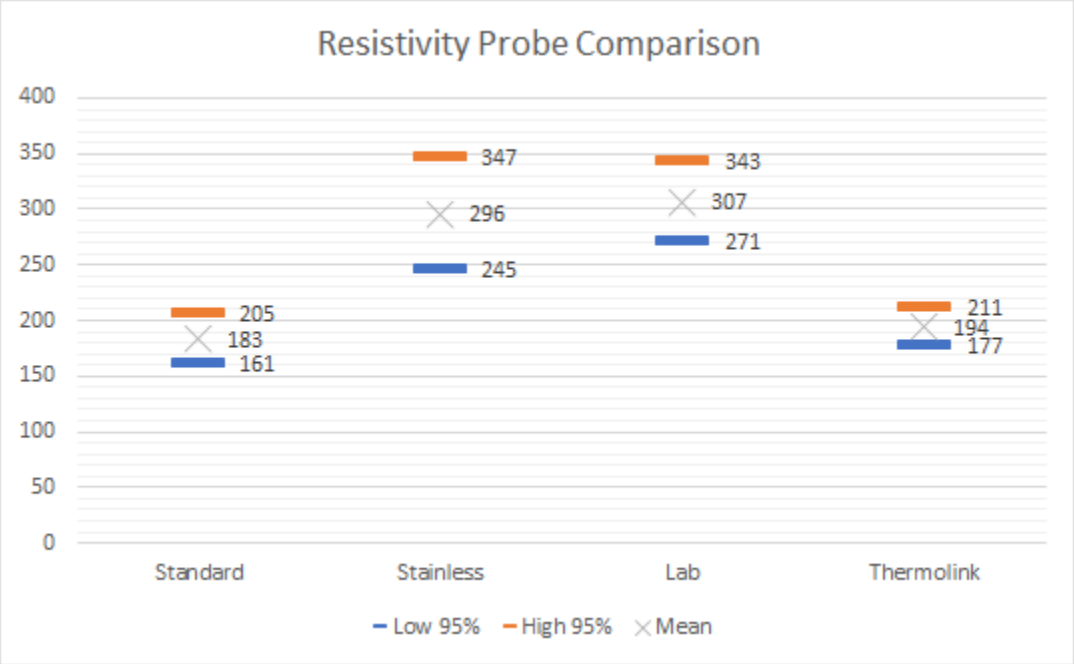

Figure 8.10 95% confidence limit of thermal probe measurements

The standard probe and Thermolink probe are within the same 95% confidence interval, and the stainless steel and lab probes are within the same interval but different than the standard and Thermolink probes. ASTM D5334 defines a calibration procedure for the resistivity

probes [50]. This was performed using a water and agar mixture in a PVC pipe. The results with the calibration are shown in the following figure:

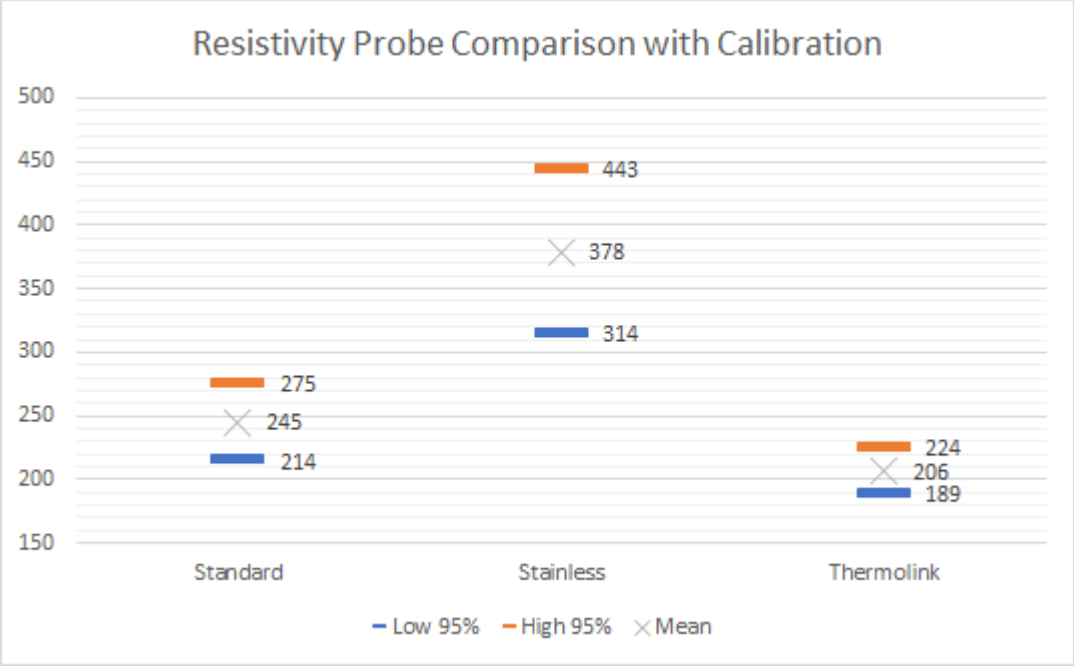

Figure 8.11 Resistivity probe results with calibration

The calibration details are shown in the following table:

Table 8.3 Thermal probe calibration details

Probe	Calibration	Mean	Stdev	#	Low 95%	High 95%
Standard	1.336	245	105	47	214	275
Stainless	1.279	378	172	28	314	443
Thermolink	1.063	206	33	14	189	224

The conclusions are similar with the calibration: the standard and Thermolink probes are effectively the same value when considering the 95% confidence limit. Based on this, the maximum soil resistivity is taken as 220°C·cm/W, which is within the 95% confidence interval of the Thermolink and Standard probes. This ampacity analysis is in Section 9.1.1.

8.5 Non-Drying Heat Rate Measurement

The heating and cooling curve resistivities were compared to determine if the soil dried during the heating measurement. If drying occurs while the probe is heating the soil, the resistivity measurement will be higher for the cooling curve than the heating curve. The Thermolink probe cannot perform this test since it is not manually configurable. The following figures illustrate the results:

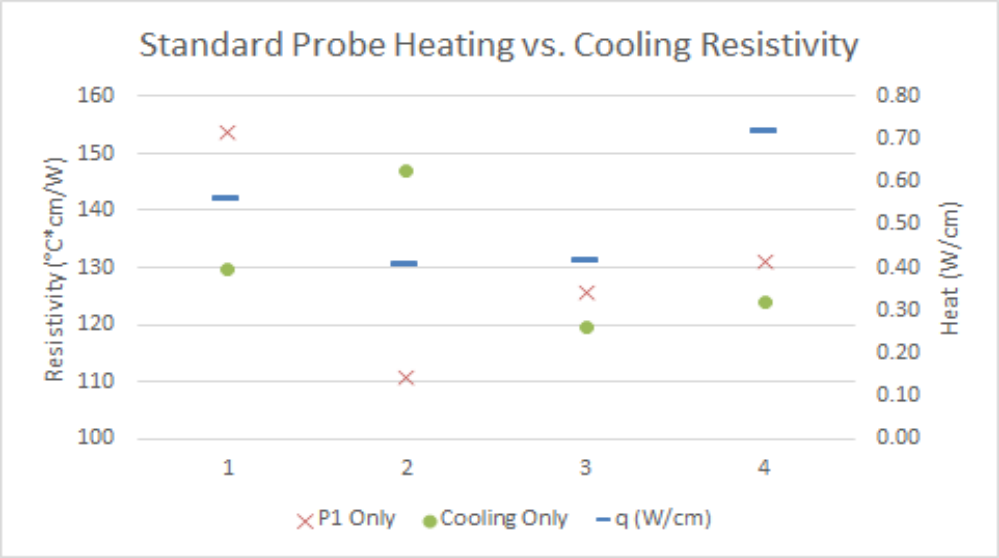

Figure 8.12 Standard Probe heating versus cooling resistivities

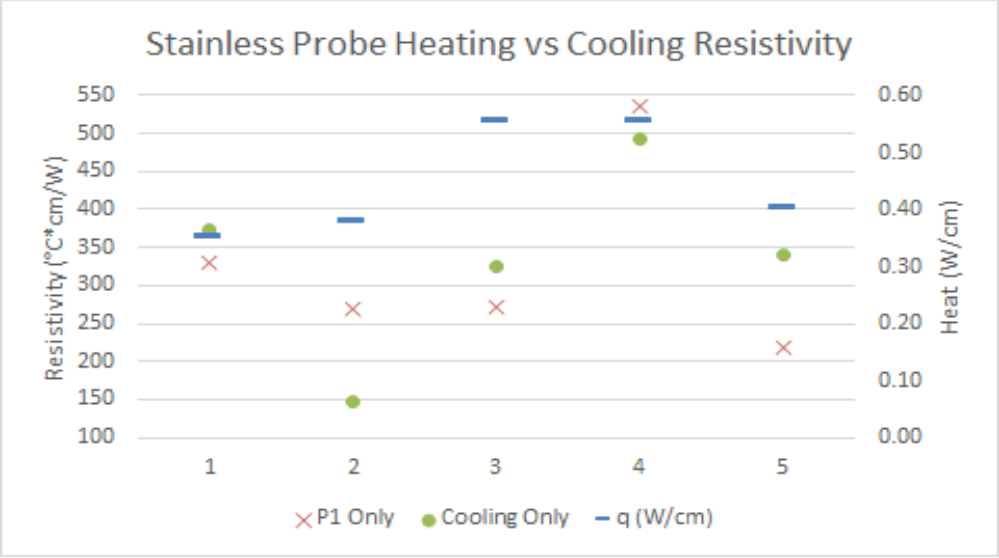

Figure 8.13 Stainless Probe heating versus cooling resistivities

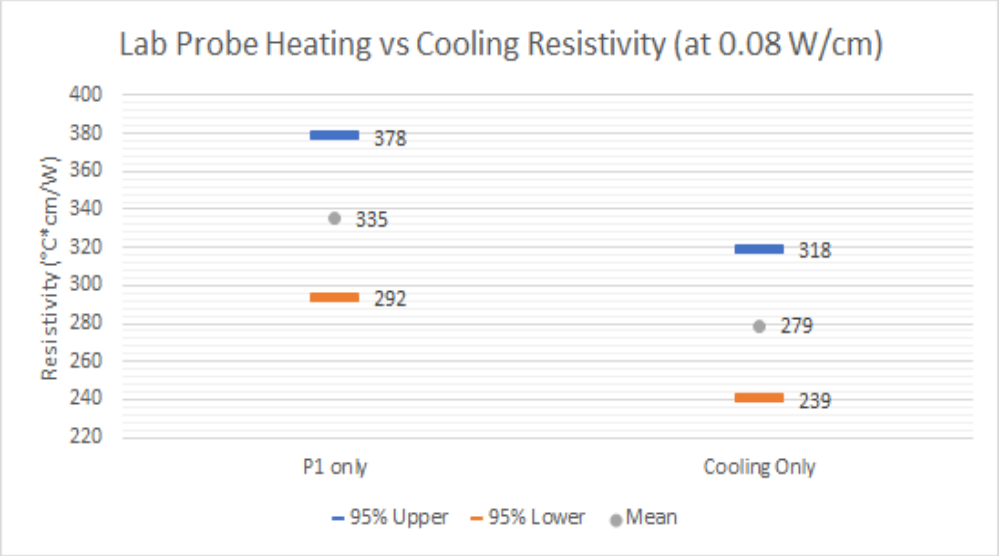

Figure 8.14 Lab Probe heating versus cooling resistivities

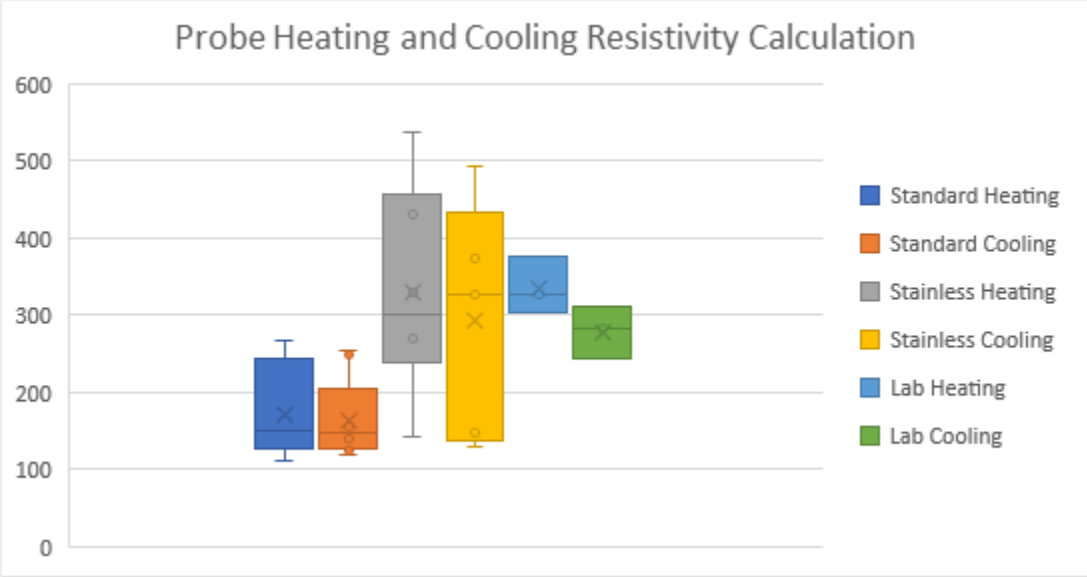

Figure 8.15 Thermal probe heating and cooling resistivities box plot

The cooling resistivity is higher than the heating resistivity for one of the four tests of the Standard Probe and three of the five tests for the Stainless Probe. However, the box and whisker plot does not conclude that the soil dried during soil heating. For the Standard Probe and Stainless Probe, multiple heat rates were used. Higher heat rates are more likely to dry the soil. The non-drying heat rate is determined by finding the heat rate between measurements that show drying and those that do not. No apparent correlation exists between the resistivity and the heat rate. Based on these results, the soil did not dry regardless of heat rate or probe size. The non-drying heat rate is above the tested heat rate of 0.7 W/cm at a diameter of ¾" and

0.55 W/cm at a diameter of ¼" diameter. Most cables operate between 0.2 to 0.4 W/cm at larger diameters of 1 to 3 inches. Based on this, soil drying is unlikely for power cable installations in this soil.

8.6 Lab Soil Resistivity Measurement

The lab soil resistivity measurement was performed using the METER Group Thermolink unit with a TR-3 probe described in Section 8.3.4. It is standard industry practice to measure the soil thermal dry-out curve. This involves testing the soil at a range of moisture contents from dry to optimum (determined by a compaction test). Various methods to perform this test are described in "How to produce thermal dryout curves for buried cable applications" by METER Environment [76]. The thermal dry-out curve was generated for this experiment by using the soil sample from the fully dried state achieved during the moisture content test. It was compacted in 2 plastic cylinders with a 4" diameter and 10" length. The cylinders represented both samples from the in-situ moisture content and density tests.

The fully-dried soil was compacted as much as possible by hand and a thermal resistivity measurement was taken. Since there was minimal moisture content, the compaction was low with a correspondingly high thermal resistivity. The compaction is lower than what is possible in-situ since even light rain would naturally result in a higher compaction. Water was added to increase the moisture content of the samples to 2% by mass and thoroughly mixed in a mixing bowl. The soil was compacted back into the small cylinders and retested. Since the moisture content increased, higher compaction was possible. The goal is to test the samples at the same compaction over a range of moisture contents, so this method of mixing the sample with added water and recompacting would not work. In addition, it is difficult to ensure all of the soil is transferred into the container after mixing, which is required for determining the moisture content based on weight. The best method to ensure consistent compaction over the tests is to compact it once and allow the soil to dry naturally. This was the method used for the tests shown below. Measurements were taken over the course of several weeks to allow the soil to dry naturally.

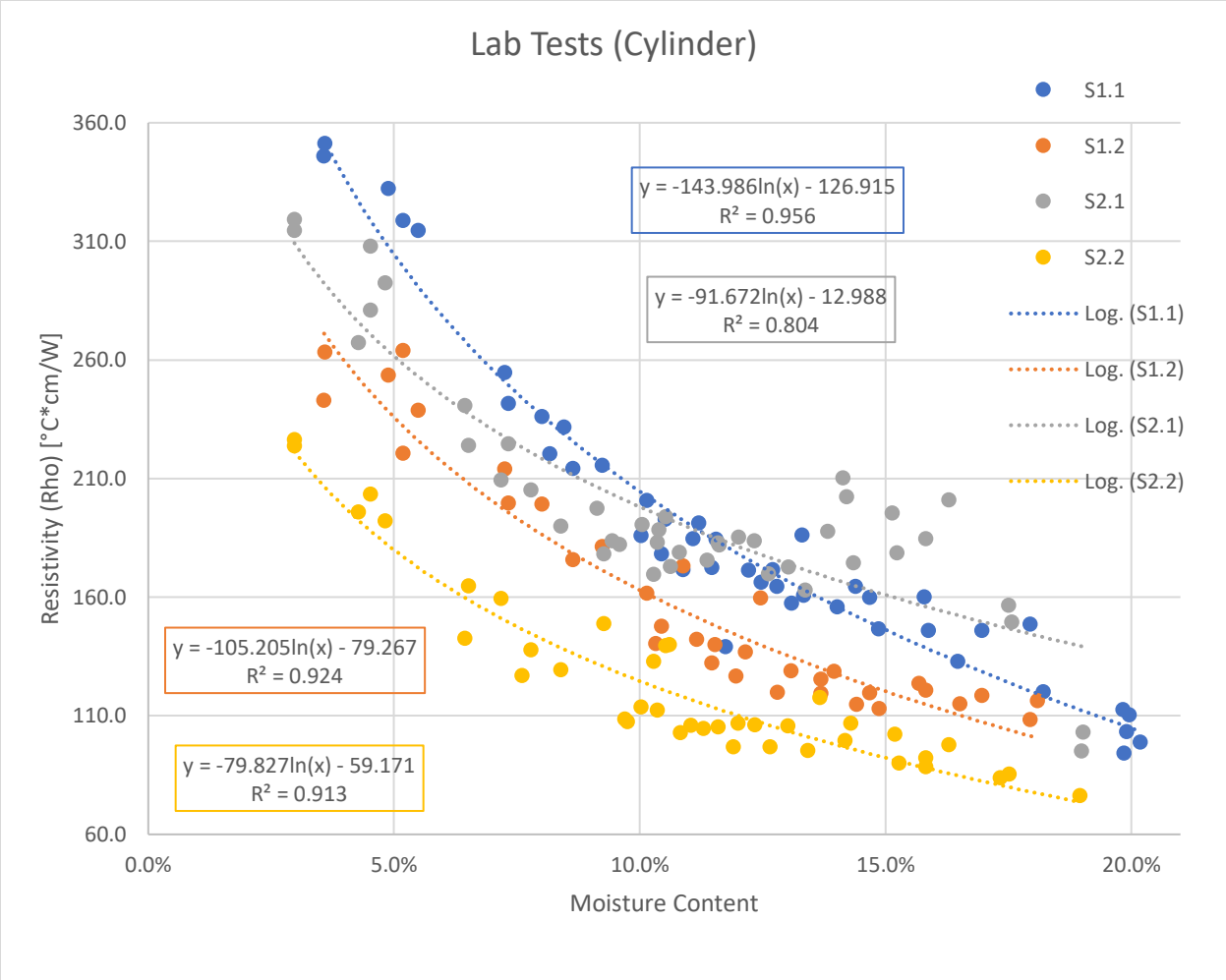

Figure 8.16 Thermal Resistivity Dry-out Curve

Table 8.4 Lab Probe soil sample moist and dry resistivity measurements

Rho	In-situ MC	Std	A	B	Rho@In-situ	Rho-2Std	4%
S1.1	13.6%	1.25%	-143.986	-126.915	160	190	337
S1.2	13.6%	1.25%	-91.672	-12.988	170	189	282
S2.1	12.4%	1.25%	-105.205	-79.267	140	164	259
S2.2	12.4%	1.25%	-79.827	-59.171	107	125	198
Average			A·ln(x)+B		**145**	**167**	**269**
Std					**28**	**30**	**57**

Based on the lab resistivity test, the soil thermal resistivity at in-situ moisture content (14% from Section 8.1) is 145°C·cm/W with a standard deviation of 28°C·cm/W. The resistivity at the lowest expected moisture content of 4% is 269±57°C·cm/W. These results allow for adjustment to the in-situ measurements described in Section 8.4. This is done by multiplying the

in-situ thermal resistivity measurement (220°C·cm/W) by the ratio of the lowest expected moisture content (269°C·cm/W) to the in-situ moisture content (145°C·cm/W). The result (408°C·cm/W) represents the highest expected thermal resistivity and can be used in ampacity calculations to provide conservative results.

8.7 Resistivity Measurement Using Buried Cable

The resistivity of the soil was also determined using the cable jacket temperatures measured during the experiments discussed in Chapter 9 Experiments. Two methods were applied to the measurements to determine resistivity: transient line source and Structure Function. The transient line source method is described in Section 8.2 but is applied to the buried cable as the heat source rather than the thermal probe. The Structure Function method is novel to soil thermal resistance having been previously applied to integrated circuits [77].

The transient line source method is applied to buried cables in the same manner as a vertical probe described in Section 8.2. The slope of the temperature is determined between the temperatures recorded at approximately 3 and 30 minutes after current is applied to the cable. The thermal resistivity was also determined over a sliding window, rather than the typical 30-minute window for the transient line source method. The slope is calculated over a 1-minute range for each timestep over the first couple hours of the measurement of initial cable heating and is referred to hereafter as “sliding window” or “Scilab” since it was calculated using the Scilab computer program [78].

Table 8.5 Resistivity measurements using buried cable

Date (start)	Current (A)	q (W/cm)	Rho Spreadsheet (°C·cm/W)	Rho Scilab (°C·cm/W)
10/09/16	93	0.12	141	110
01/29/17	97	0.13	132	110
07/04/17	120	0.21	122	100
07/15/17	118	0.20	109	120
07/28/17	72	0.07	105	120
08/17/17	71	0.07	95	110
Mean			117	112
Std			17	8

Each row is a test that was initiated on the listed start date and time. “Time” indicates the duration in days that current was applied to the cable. “Current” is the measured current in Amperes applied to the buried cable. “Rho Spreadsheet” is the soil thermal resistivity calculated using the 30-minute window described above. “Rho Scilab” is the soil thermal resistivity calculated using the sliding window method described above. An example of the “Rho Spreadsheet” is shown in the following figures. Note that only two of the jacket temperatures are analyzed in the figures below, and these are averaged with the other analyzed temperatures to produce the resistivity listed in the table above.

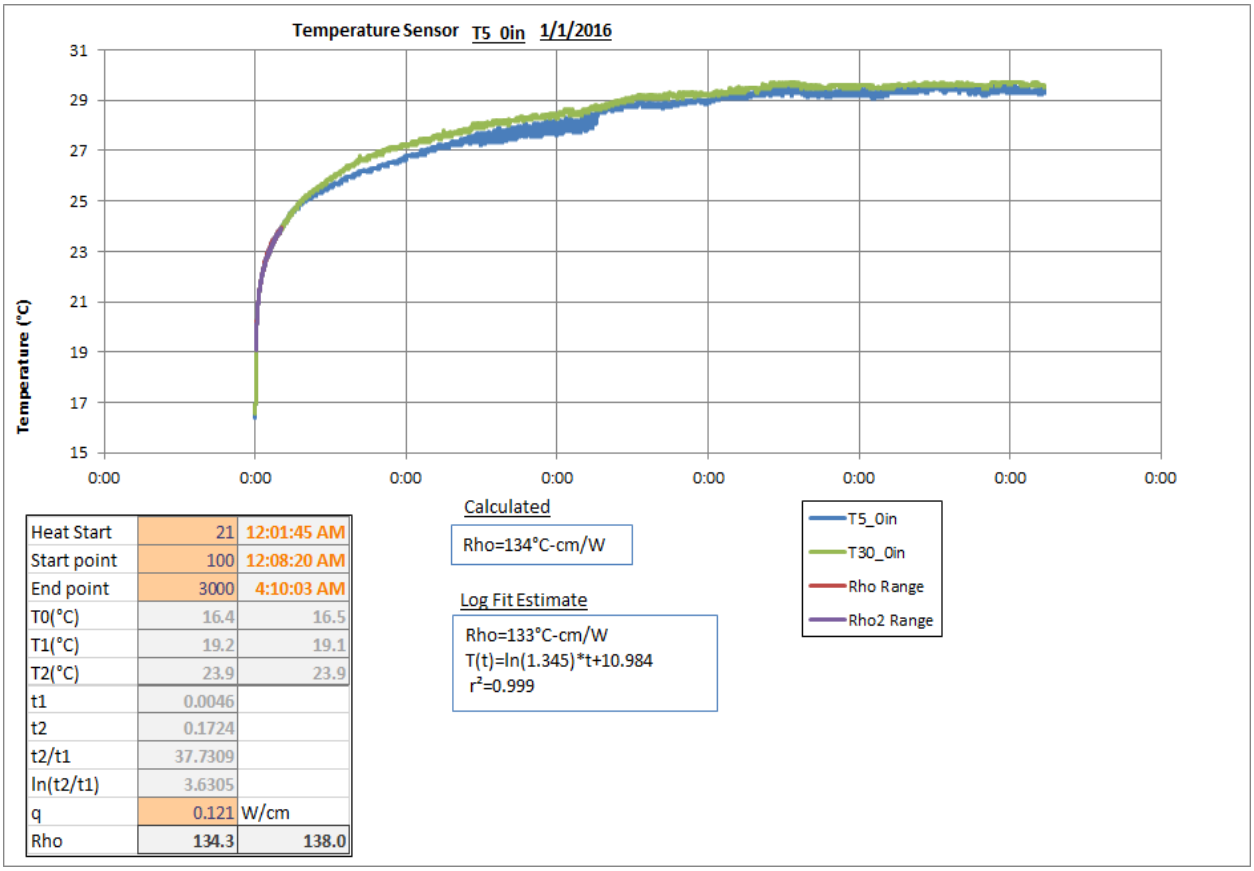

Heat Start	21	12:01:45 AM
Start point	100	12:08:20 AM
End point	3000	4:10:03 AM
T0(°C)	16.4	16.5
T1(°C)	19.2	19.1
T2(°C)	23.9	23.9
t1	0.0046	
t2	0.1724	
t2/t1	37.7309	
ln(t2/t1)	3.6305	
q	0.121	W/cm
Rho	134.3	138.0

Figure 8.17 Resistivity measurement analysis on a linear time scale

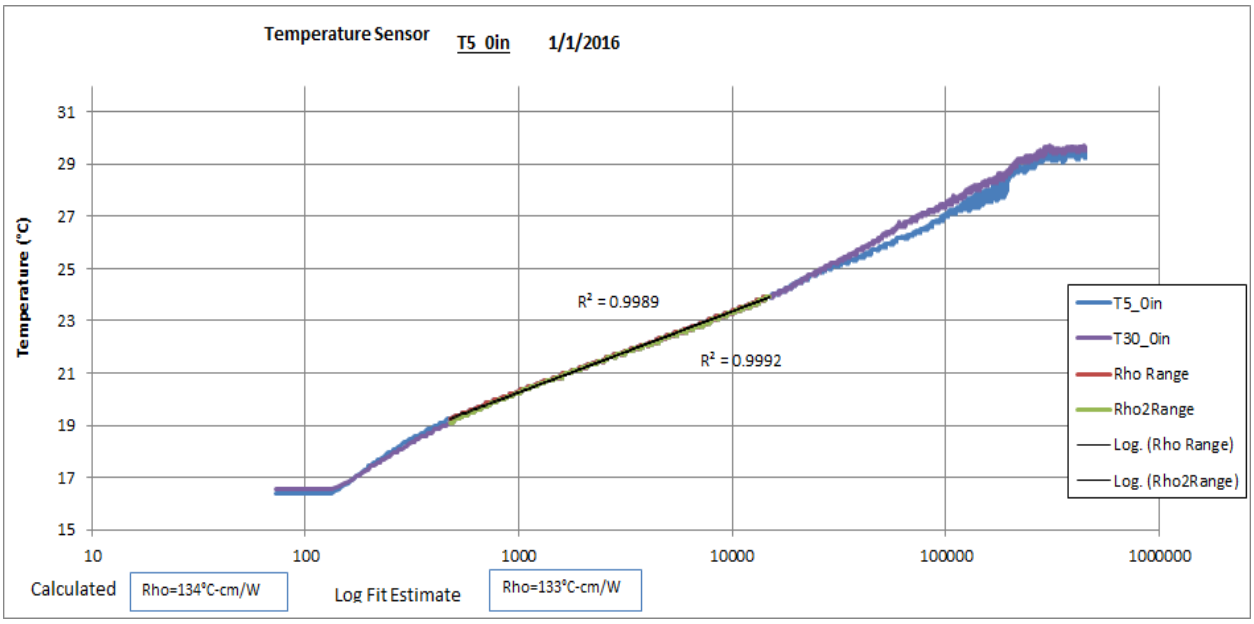

Figure 8.18 Resistivity measurement analysis on a logarithmic time scale

An example of the “Rho Scilab” analysis is shown in the following figure.

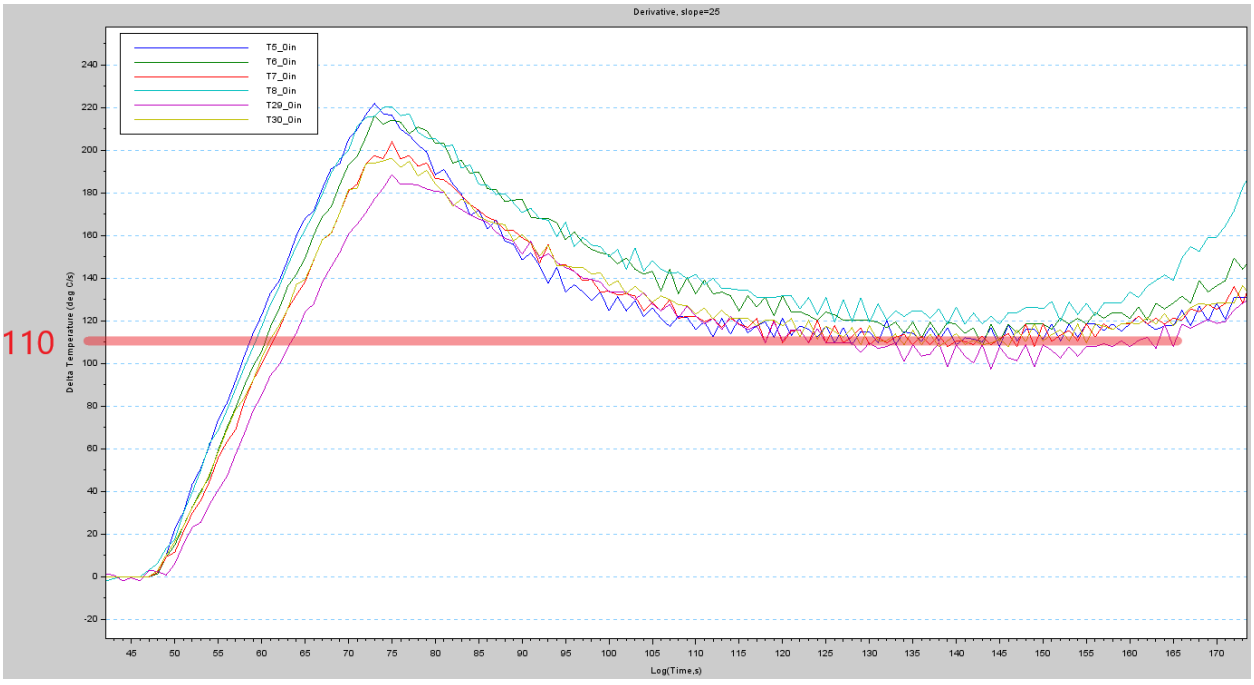

Figure 8.19 Sliding window resistivity analysis

The thermal resistivity is determined by reading the sliding slope window value from the graph at a location where the value is approximately constant. This occurs after the transient due to cable jacket heating and interface thermal resistance has subsided. After several hours,

the slope is no longer constant because the earth surface convective boundary begins to impact the temperature. This deviates from the assumptions used in the transient line source method. Reviewing the results, it is clear that the Scilab resistivity is less precise and provides a type of averaging on the measured resistivity compared to the Spreadsheet resistivity. The Spreadsheet resistivity uses a fixed 30-minute window, so it is more sensitive to error from the recorded temperatures at the window's start and end time. The means are similar for the 6 tests, but the standard deviation is twice as high using the 30-minute window described IEEE Std 442 [27].

8.8 Resistivity from the Structure Function

In addition to the traditional transient line source method, the thermal resistivity can be calculated using a more recently developed method: a deconvolution algorithm that produces a graphical curve referred to as the Structure Function. The Structure Function was pioneered around 1985 by Vladimir Szekely and associates for characterizing thermal layers in an electrical chip assembly [77]. It utilizes the transient temperature response of an object to a heat input, either impulse or step functions, but step functions are most commonly used. The algorithm uses the similarity of electrical circuits to thermal circuits for a resistor and capacitor network, the combination characterized by a time constant. This time constant network of thermal resistance and capacitance is measured in the transient temperature response as a convolution of the heat input and the material thermal properties. So, it can be deconstructed into the components of interest, resistance and capacitance of the soil, by deconvolving the heat input from transient temperature response. This is called the Structure Function.

The method to determine the Structure Function is provided in [77]. The general flow is: acquire temperature data, calculate the numerical derivative, deconvolve the weight function from the temperature response, and perform a Foster/Cauer transformation. The following paragraphs provide some additional detail.

For a unit step heat input to any material surface, the measured temperature is an exponential increase with a time constant of the thermal resistance and capacitance. The equation is $T(t)=P \cdot R \cdot (1-e^{(-t/\tau)})$, where T(t) is the temperature at the surface over time, P is the applied heat, R is the thermal resistance, and τ is the time constant—the product of the thermal resistance and capacitance. Let a(t) equal the temperature response divided by the unit step heat input, P. Let z=ln(t) so that $a(z)=R \cdot (1-e^{(-t/\tau)})$. This formula is derived from the 1-dimensional heat equation into the general form for a single resistance and capacitance (RC) network. The reason for transforming the time domain to the natural log domain is to allow for

mathematical manipulation. Consider that materials, such as soil around a cable, do not have a single discrete thermal resistance or capacitance. Rather, it consists of a continuous spectrum and the temperature response is the sum, or integration, of these values. The equation is then:

$$a(z) = \int_0^\infty R(\zeta) \cdot \left(1 - \exp\left(-\frac{\exp(z)}{\exp(\zeta)}\right)\right) d\zeta$$

Where

ζ = time constant continuous values for the thickness of the entire material or materials.

Taking the derivative allows for further mathematical manipulation.

$$\frac{d}{dz}\, a(z) = \int_0^\infty R(\zeta) \exp(z-\zeta) \cdot (\exp(-\exp(z-\zeta)))d\zeta$$

$$\frac{d}{dz}\, a(z) = \int_0^\infty R(\zeta) \cdot \exp(z - \zeta - \exp(z-\zeta))\, d\zeta$$

This is now the form of a convolution equation:

$$\frac{d}{dz}\, a(z) = R(z) \otimes W(z)$$

Where

a = temperature response

R = time constant spectrum

W = weight function, W=exp(z-exp(z)).

This convolution relationship between the time constant spectrum, R, and the weight function, W, allows for solving for R. A process called the Bayes' iterative process can be used to solve for R because it tolerates noise [79]. The result of the derivation is:

$$R_i^{n+1} = R_i^n \sum_k \frac{W_{k,i} \cdot \frac{dA(jw)}{dz}}{\sum_j W_{k,j} \cdot R_j^n}$$

This formula is convergent as n goes to infinity, and therefore can accurately determine the time constant spectrum with enough iterations. This is to say, the noise tends towards zero as the number of iterations increases. This equation can be further realized into more comprehensible terms using correlation and convolution:

$$R_i^{n+1} = R_i^n \frac{M}{W \otimes R^n} \odot W$$

Where

$\otimes$ = convolution operation

$\odot$ = correlation operation

M = derivative of the temperature response, da/dz.

The application of this was performed in MATLAB. The algorithm for calculating this time constant spectrum is:

1. Input the derivative of the measured response and the time steps
2. Calculate the denominator ($W \otimes R$), using the Fast Fourier Transform (FFT) on each vector, multiply the results, and perform the inverse FFT, where R^0 is equal to M, the derivative of the measured response
3. Divide M by the denominator
4. Calculate the correlation operation using the FFT on the previous division result and W, the weight function, multiply the previous division result by W(-z), or the flipped version of W, and perform the inverse FFT
5. Multiply by the result obtained above by R^n, again, where R^0 is equal to M (the derivative of the measured response)

After calculating the time constant spectrum, the result is discretized into the desired number of time constant segments in order to transform from the Foster network to the Cauer network. Foster networks represent the thermal model in a series combination of parallel RC segments. Cauer networks represent it in a pi-model format in which the thermal capacitance is shunt connected rather than series, and the resistance is a series combination. This allows for direct comparison with the physical order of the thermal circuit. The Foster-Cauer transformation requires very high precision to avoid loss of resolution because it is essentially a partial fraction decomposition. The number discretized RC, or time constant, segments are equal to the number of expanded fractions.

The Structure Function analysis is used to determine if the soil dried around the cable. It is not used to determine the soil resistivity for use in ampacity calculations. Comparing Structure Functions of similar experiments is its primary strength because it highlights the location of the resistivity differences. The transient line source method yields an average of the soil resistivity around the heat source and does not provide any additional detail. Section 9.2.3 provides the results of the analysis using the Structure Function.

8.9 Selecting the Soil Thermal Resistivity

Based on the numerous test results shown in the preceding sections, it is clear that selecting the value to use for thermal resistivity in the ampacity calculations is not trivial. A major

reason for performing multiple tests is to show the variability that can occur if further testing is performed. It illustrates the importance of interpreting a single result with caution. Reviewing results with statistical analysis is the preferred option, but sufficient data must be available. Civil engineers are familiar with specifying the data that is required for designing foundations, which depend on soil properties and its inherent variability. Electrical engineers performing ampacity calculations would be wise to emulate the civil engineers in specifying the method and quantity of soil measurements that are required.

The resistivity measurements obtained with the buried cable are considered the most accurate and are used for the experimental comparisons in Chapter 9 Experiments. They are considered the most accurate because the measurements are made at the soil closest to the cable. Also, the measurements are made at the time of the experiment. These measurements are not available for typical cable installations because temperature sensors are not installed, and the load is not constant.

CHAPTER 9
EXPERIMENTS

Eleven experiments were performed at various heat rates and at various times during the year. The 6 longest duration experiments were selected for the analysis. The first goal of these experiments was to compare the measured temperature with the calculated (modeled) temperature. The second goal was to determine if soil drying had occurred, which was accomplished by performing tests around the non-drying heat rate (NHR). The NHR indicates the maximum heat rate that the soil can withstand without beginning to dry. If the heat rate is above the NHR, the measured cable temperature will be above the modeled temperature that is calculated using the in-situ soil resistivity because the dry soil layer developed around the cable will add thermal resistance. If the heat rate is below the NHR, the cable temperature will be equal to the modeled temperature. In other words, the standard software calculations will match the measured cable temperature unless the heat rate exceeds the non-drying heat rate.

Each experiment began by starting the data logger, energizing the current source (transformer), and measuring the current. After 5 days or more, the current source was disconnected. All of the experiments recorded the temperatures while the current source was energized, and some also recorded temperatures after the current source was disconnected. The data was retrieved from the data logger and analyzed in multiple ways. The first analysis involved comparing the measurement to the calculated/modeled values in two ways:

1. Compare the measured cable temperature to the steady state calculation of CYMCAP software and the Neher-McGrath method
2. Compare the measured cable temperature to the transient calculation of CYMCAP software using a simulation time of five days

The second analysis involved determining if any soil drying had occurred in two ways:

1. Compare the calculated thermal resistance around the cable using the steady state thermal resistance equation: $\rho=2\pi\Delta T/(q\cdot\ln(r_2/r_1))$
2. Compare the calculated thermal resistance before and after heating using the transient line source method

A Scilab software [78] script assisted with data processing since the data size is large, for example, one data set includes over 300,000 rows of data for the 34 temperature sensors. Microsoft Excel was also used for data analysis.

9.1 Temperature Comparison

9.1.1 Steady State

The Neher-McGrath method and CYMCAP software were used to calculate the steady state temperature of the cable for each experiment. The temperature was measured directly on the cable jacket as described in Chapter 7 Materials and Methods. This jacket temperature measurement is logged every five seconds, but only the temperature measured on the fifth day is compared with the calculated temperature—referred to as the five-day temperature. Current was applied to the cable for at least five days. Using the five-day temperature allows for a more consistent comparison between experiments rather than using the maximum temperature because the maximum temperature is impacted by the duration of the experiment. Though the default calculation is the conductor temperature, both CYMCAP and the Neher-McGrath method can calculate the cable jacket temperature for direct comparison with the experimental measurement.

Both CYMCAP and the Neher-McGrath method require numerous inputs as described in Chapter 10 Software Modeling. The soil thermal resistivity is the parameter with the largest uncertainty. For this analysis, the soil thermal resistivity was determined using the transient line source method with the buried cable as described in Section 8.7 Resistivity Measurement Using Buried Cable. The following table compares the five-day temperature with the calculated temperatures from CYMCAP software and Neher-McGrath method spreadsheet:

Table 9.1 Five-day temperature comparison with CYMCAP and Neher-McGrath method

Date (start)	Time (days)	Current (A)	q (W/cm)	5 Day Temp (°C)	CYMCAP SS (°C)	Tj N-M (°C)	CYMCAP % Diff	Tj % Diff
10/09/16	14.2	93	0.12	29.7	32.1	32.1	-8%	-8%
01/29/17	21.0	97	0.13	20.5	20.9	21.6	-2%	-5%
07/04/17	4.9	120	0.21	37.5	46.2	44.9	-23%	-20%
07/15/17	6.6	118	0.20	38.1	42	41.3	-10%	-9%
07/28/17	5.9	72	0.07	27.1	28.9	29.0	-6%	-7%
08/17/17	7.9	71	0.07	27.7	26.8	26.9	3%	3%
Mean							-8%	-8%
Std							8.9%	7.2%

Each row is a test that was initiated on the listed start date and time. “Time” indicates the duration in days that current was applied to the cable. “Current” is the measured current in Amperes applied to the buried cable. The heat input, “q”, is calculated based on the input current and the resistance of the conductor at the maximum operating temperature (I^2R). The “5 Day Temp” is the five-day temperature averaged over all of the jacket temperature sensors. “CYMCAP SS” is the exterior (jacket) temperature result of the CYMCAP steady state calculation. “Tj N-M” is the jacket temperature calculated using the Neher-McGrath method.

The results indicate the calculated values for the CYMCAP software overestimate the temperature with an error of -8%±8.9% (mean and standard deviation) and the Neher-McGrath method to -8%±7.2%. In other words, the calculations predict the correct temperature from -15% (overestimate temperature) to -1% (overestimate temperature) using a 90% confidence interval. The results of CYMCAP steady state analysis and Neher-McGrath spreadsheet calculations are very similar. This is expected because CYMCAP utilizes the Neher-McGrath method for steady state analysis of this type of cable system.

The following table provides additional details comparing the CYMCAP analysis with the measured values:

Table 9.2 CYMCAP steady state comparison details

Date (start)	Soil Amb. Temp (°C)	5 Day Temp (°C)	Temp Rise (°C)	Max. Temp (°C)	Rho Sprdsht (°C·cm/W)	CYMCAP SS (°C)	Delta (°C)	% Diff	Temp Rise (°C)	Temp Rise Diff (°C)	Temp Rise % Diff
10/09	16.5	29.7	13.1	29.9	141	32.1	-2.4	-8%	15.6	-2.4	-18%
01/29	5.7	20.5	15.2	23.4	132	20.9	-0.4	-2%	15.2	-0.1	0%
07/04	22.4	37.5	15.2	37.5	122	46.2	-8.7	-23%	23.8	-8.7	-57%
07/15	21.8	38.1	16.2	38.9	109	42	-3.9	-10%	20.2	-3.9	-24%
07/28	22.1	27.1	5.0	27.1	105	28.9	-1.8	-6%	6.8	-1.8	-35%
08/17	20.8	27.7	6.9	27.7	95	26.8	0.9	3%	6.0	0.9	13%
Mean					117		-2.7	-8%		-2.7	-20%
Stdev					17		3	8.9%		3	25%

The “Soil Amb. Temp” is the average measured temperature of the sensors on the cable jacket. The “Temp Rise” is the difference between the five-day temperature and the initial

temperature. It is calculated individually each jacket temperature sensor and then averaged over all of the jacket sensors. “Max Temp” is the average of the jacket temperatures at the end of the experimental run. “Rho Sprdsht” is the soil thermal resistivity calculated using the 30-minute window described above. “Temp Rise % Diff” is the difference of the measured temperature rise to the CYMCAP calculated temperature rise all divided by the measured temperature rise.

These results show that the maximum temperature at the end of the experiment is similar to the five-day temperature. They also show that that the temperature-rise percent error between the experimental measurements and the CYMCAP steady state simulation (20%) is higher than the percent error for the temperature comparison (8%). This is mostly due to the smaller denominator (temperature difference is smaller than the temperature magnitude). The mean error between the experimental error temperature rise and the CYMCAP steady state is -2.7°C with a standard deviation of 3°C.

The thermal resistivity was also determined using a sliding window as described in Section 8.7 Resistivity Measurement Using Buried Cable. The following table illustrates the results of this analysis:

Table 9.3 Comparison of temperatures calculated using sliding window resistivity

Date (start)	Rho Sprdsht (°C·cm/W)	5 Day Temp (°C)	Rho Scilab (°C·cm/W)	CYMCAP SS (°C)	Delta (°C)	% Diff	Tj N-M (°C)	Tj % Diff
10/09	141	29.7	110	28.3	1.38	5%	29	3%
01/29	132	20.5	110	18.1	2.40	12%	19	8%
07/04	122	37.5	100	41.5	-3.99	-11%	41	-9%
07/15	109	38.1	120	43.9	-5.85	-15%	43	-14%
07/28	105	27.1	120	30.1	-2.96	-11%	30	-11%
08/17	95	27.7	110	26.9	0.80	3%	28	-1%
Mean	117		112		-1.37	-3%		-4%
Stdev	17		8		3	11%		8.5%

“Rho Scilab” is the soil thermal resistivity calculated using the sliding window method described above. Comparing the results of the traditional transient line source method resistivity with the sliding window resistivity indicates a lower average error (-3% versus -8% for CYMCAP) but a higher standard deviation (11% versus 8.9%). The average of the resistivity values is very similar, 117°C·cm/W versus 112°C·cm/W, but the difference is noticeable when

comparing each experimental run. For example, the test on 10/09/16 shows -8% error for the transient line source method whereas the sliding window method shows 5% error. Based on the data, the sliding window method is an acceptable method for determining thermal resistivity for use in ampacity calculations.

Neher-McGrath calculations were also performed with the soil resistivity calculated based on the maximum recorded temperature for each experiment. This resistivity is based on the steady state heat conduction equation for an isothermal cylinder in a semi-infinite medium: $\Delta T \cdot 2\pi/(q \cdot \ln(4 \cdot d/D))$ where ΔT is the difference in temperature between the ambient and the maximum measured, q is the heat rate per unit length, d is the depth of the cable, and D is the diameter of the cable. The equation is valid if the earth surface temperature is equal to the soil ambient temperature, which is not true on an instantaneous basis but can be on a daily basis. It also is based on a uniform (homogenous) soil resistivity. The following table illustrates the results of this calculation:

Table 9.4 Comparison of temperatures calculated using maximum temperature resistivity

Date (start)	Soil Amb. Temp (°C)	5 Day Temp (°C)	Max. Temp (°C)	Rho Spdsht (°C·cm/W)	Tj N-M (°C)	Delta (°C)	Tj % Diff	Rho from Max Temp (°C·cm/W)	Rho from Max T Tj N-M (°C)	Tj % Diff
10/09	16.5	29.7	29.9	141	32.1	-2.4	-8%	114	30.0	-1%
01/29	5.7	20.5	23.4	132	21.6	-1.1	-5%	125	21.7	-6%
07/04	22.4	37.5	37.5	122	44.9	-7.4	-20%	77	37.4	0%
07/15	21.8	38.1	38.9	109	41.3	-3.3	-9%	85	37.9	0%
07/28	22.1	27.1	27.1	105	29.0	-1.9	-7%	74	27.3	-1%
08/17	20.8	27.7	27.7	95	26.9	0.8	3%	103	27.9	-1%
Mean				117		-2.5	-8%	96		-1%
Stdev				17		3	7.2%	21		2.4%

“Rho from Max Temp” is the soil resistivity calculated using the steady state conduction equation and the maximum measured temperature as described above. The results indicate that the calculated temperature is closer to the five-day temperature than the temperature calculated with the transient line source resistivity (“Rho Spdsht”). Interestingly, all of the resistivities are lower for “Rho from Max Temp” than for “Rho Spdsht” except for the last experiment. It is unclear what the cause for this is, but there is correlation between the

experiment duration and “Rho from Max Temp”. Since “Rho from Max Temp” depends on a steady state temperature, it’s likely that this impacted the calculated resistivity.

The following table compares the maximum measured temperature, rather than the five-day temperature, to the calculated values based on the transient line source resistivity:

Table 9.5 Comparison of five-day and max. temperatures using transient line source resistivity

Date (start)	Rho Sprdsht (°C·cm/W)	Max. Temp (°C)	CYMCAP SS (°C)	% Diff 5 day	% Diff Max T	Rho from Spdsht Tj N-M (°C)	Tj % Diff 5 day	% Diff Max T
10/09	141	29.9	32.1	-8%	-7%	32.1	-8%	-7%
01/29	132	23.4	20.9	-2%	11%	21.6	-5%	8%
07/04	122	37.5	46.2	-23%	-23%	44.9	-20%	-20%
07/15	109	38.9	42	-10%	-8%	41.3	-9%	-6%
07/28	105	27.1	28.9	-6%	-7%	29.0	-7%	-7%
08/17	95	27.7	26.8	3%	3%	26.9	3%	3%
Mean	117			-8%	-5%		-8%	-5%
Stdev	17			8.9%	11.5%		7.2%	10%

The following table is the same comparison using the sliding window resistivity:

Table 9.6 Comparison of five-day and maximum temperatures using sliding window resistivity

Date (start)	Rho Scilab (°C·cm/W)	Max. Temp (°C)	CYMCAP SS (°C)	% Diff 5 day	% Diff Max T	Rho from Scilab Tj N-M (°C)	Tj % Diff 5 day	% Diff Max T
10/09	110	29.9	28.3	5%	5%	29	3%	4%
01/29	110	23.4	18.1	12%	23%	19	8%	19%
07/04	100	37.5	41.5	-11%	-11%	41	-9%	-9%
07/15	120	38.9	43.9	-15%	-13%	43	-14%	-11%
07/28	120	27.1	30.1	-11%	-11%	30	-11%	-11%
08/17	110	27.7	26.9	3%	3%	28	-1%	-1%
Mean	112			-3%	-1%		-4%	-1%
Stdev	8			11%	14%		8.5%	12%

The estimated error between the measured maximum temperature and the calculated value is not significantly less than the error between the measured five-day temperature and the

calculated value. In a few cases, the error is worse, such as the “Rho Scilab” (sliding window resistivity) on the experiment on 01/29/17. This indicates the resistivity used in the calculation impacts the error much more than the temperature used, whether the five-day temperature or the maximum. To illustrate this further, a Neher-McGrath calculation was performed using the soil resistivity concluded in Section 8.4 Resistivity Probe Measurements—a resistivity of 220°C·cm/W. The following table provides the results:

Table 9.7 Comparison of temperatures calculated using thermal probe resistivity

Date (start)	5 Day Temp (°C)	Re from Rho= 220 (°C*cm/W)	Rho 220 Tj N-M (°C)	Delta (°C)	Tj % Diff
10/09	29.7	207	41	-11	-38%
01/29	20.5	207	32	-12	-57%
07/04	37.5	207	63	-25	-68%
07/15	38.1	207	61	-23	-60%
07/28	27.1	207	37	-9	-35%
08/17	27.7	207	35	-7	-26%
Mean				-15	-47%
Stdev				8	16%

The results indicate that using the resistivity equal to the upper limit of the 95% confidence interval provides conservative results (a negative difference or percent indicates the calculated temperature is above the measured temperature). This demonstrates that the Neher-McGrath method already provides a significant design margin; additional resistivity should not be added to this resistivity for soil drying or for an additional safety factor.

9.1.2 Transient

CYMCAP transient temperature analysis was used to compare the measured temperatures using an identical test duration. A comparison is made between the five-day temperature and the CYMCAP transient analysis. Another comparison is made between the full experiment duration and CYMCAP transient analysis. The following table provides the result of this comparison:

Table 9.8 Comparison of temperatures calculated with transient analysis using transient line source resistivity

Date (start)	Rho Sprsht (°C·cm/W)	5 Day Temp (°C)	CYMCAP 5d (°C)	Delta (°C)	% Diff		Time (days)	Max. Temp (°C)	CYMCAP Trans (°C)	Delta (°C)	% Diff
10/09	141	29.7	29.6	0.1	0%		14.2	29.9	30.9	-1.0	-3%
01/29	132	20.5	18.5	2.0	10%		21.0	23.4	20.1	3.3	14%
07/04	122	37.5	42.5	-5.0	-13%		4.9	37.5	42.5	-5.0	-13%
07/15	109	38.1	39.1	-1.0	-3%		6.6	38.9	39.6	-0.7	-2%
07/28	105	27.1	28.0	-0.8	-3%		5.9	27.1	28.1	-1.0	-4%
08/17	95	27.7	26.0	1.7	6%		7.9	27.7	26.2	1.5	5%
Mean	117			-0.5	-0.5%					-0.5	-0.4%
Std	17			2.5	8.1%					2.8	9.3%

The five-day transient comparison results indicate the calculated values for the CYMCAP software match the measurements with an error of -0.5%±8.1% (mean and standard deviation). In other words, the calculations predict the correct temperature from -7% (overestimate temperature) to 6% (underestimate temperature) using a 90% confidence interval. The mean error for the transient comparison of -0.5% is less than the mean error of the steady state comparison of -8%. The full experiment duration transient comparison indicates that the CYMCAP results match the measurements with an error of -0.4%±9.3% (mean and standard deviation). Calculations performed using the sliding window resistivity are shown in Table 9.9.

Table 9.9 Comparison of temperatures calculated with transient analysis using sliding window resistivity

Date (start)	Time (days)	Current (A)	5 Day Temp (°C)	Rho Scilab (°C·cm/W)	CYMCAP Trans (°C)	Delta (°C)	% Diff
10/09	14.2	93	29.7	110	27.5	2.18	7%
01/29	21.0	97	20.5	110	17.5	3.00	15%
07/04	4.9	120	37.5	100	38.8	-1.29	-3%
07/15	6.6	118	38.1	120	41	-2.95	-8%
07/28	5.9	72	27.1	120	29.1	-1.96	-7%
08/17	7.9	71	27.7	110	26.2	1.50	5%
Mean				112		0.08	2%
Stdev				8		2	9%

Calculations using the sliding winding resistivities yield a similar mean error to calculations using the transient line source resistivities (2% compared to -0.5%). The sliding window resistivity calculations predict the correct temperature from -6% (overestimate temperature) to 9% (underestimate temperature) using a 90% confidence interval.

9.1.3 Load Factor

The soil time constant appeared to be a factor for some of the results because the error for the CYMCAP transient analysis was smaller than steady state analysis. The Neher-McGrath method does not calculate the temperature for a specific duration as was done in CYMCAP; rather, it uses a load factor. Typically, the load factor is applied based on the number of hours of expected cable load for a 24-hour day. The load factor for a five-day experiment is one based on this definition of daily load factor. If a weekly load factor were considered, it might provide more accurate results similar to the CYMCAP transient analysis. A load factor of 66% was used in the Neher-McGrath calculation below in order to determine if using it reduces the error between the calculation and the measurement.

Table 9.10 Comparison of temperatures calculated with load factor using transient line source resistivity

Date (start)	Time (days)	Soil Amb. Temp (°C)	5 Day Temp (°C)	Max. Temp (°C)	Re from Rho Spreadsheet (°C·cm/W)	Re from Rho Spdsht w/LF (°C·cm/W)	Tj N-M (°C)	Delta (°C)	Tj % Diff
10/09/16	14.2	16.5	29.7	29.9	132	109	29	0	0%
01/29/17	21.0	5.7	20.5	23.4	124	102	19	2	0%
07/04/17	4.9	22.4	37.5	37.5	115	95	41	-3	-3%
07/15/17	6.6	21.8	38.1	38.9	103	85	38	0	0%
07/28/17	5.9	22.1	27.1	27.1	98	81	28	-1	0%
08/17/17	7.9	20.8	27.7	27.7	89	74	26	2	1%
Mean								0.0	-0.3%
Stdev								1.9	1.4%

“Re” is the thermal resistance from the cable jacket to ambient earth and is calculated based on the soil resistivity using the transient line source method with buried cable (Section 8.7 Resistivity Measurement Using Buried Cable). The load factor was selected because it resulted

in the lowest mean error for all six cases. The results demonstrate that using a load factor for continuous cable loading over multiple days is effective at increasing the accuracy of the Neher-McGrath method.

Sources of Error

The possible sources of error for these experiments include soil ambient temperature, soil resistivity, and cable current. These are analyzed prior to the experiment in Section 7.3 Uncertainty Analysis. Soil ambient temperature is affected by the accuracy of the temperature sensor and the time of measurement. If the soil is cooling from a previous experiment or due to seasonal variation, this impacts the calculated temperature results. Examining the experiment on 7/4/2017, the soil ambient temperature consists of a natural variation from the temperature sensor measurements. This is shown in the following figures.

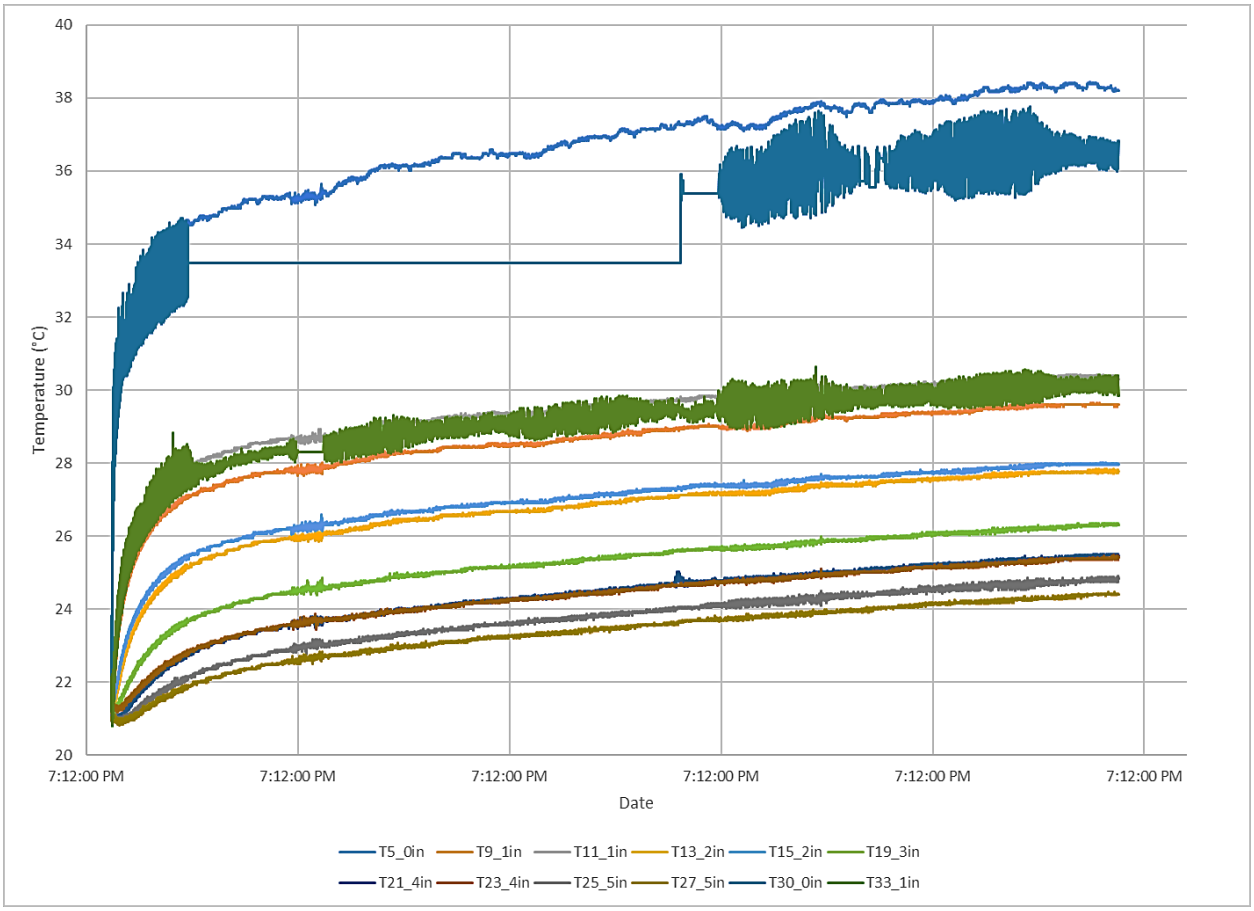

Figure 9.1 Experiment 7/4/17 temperatures

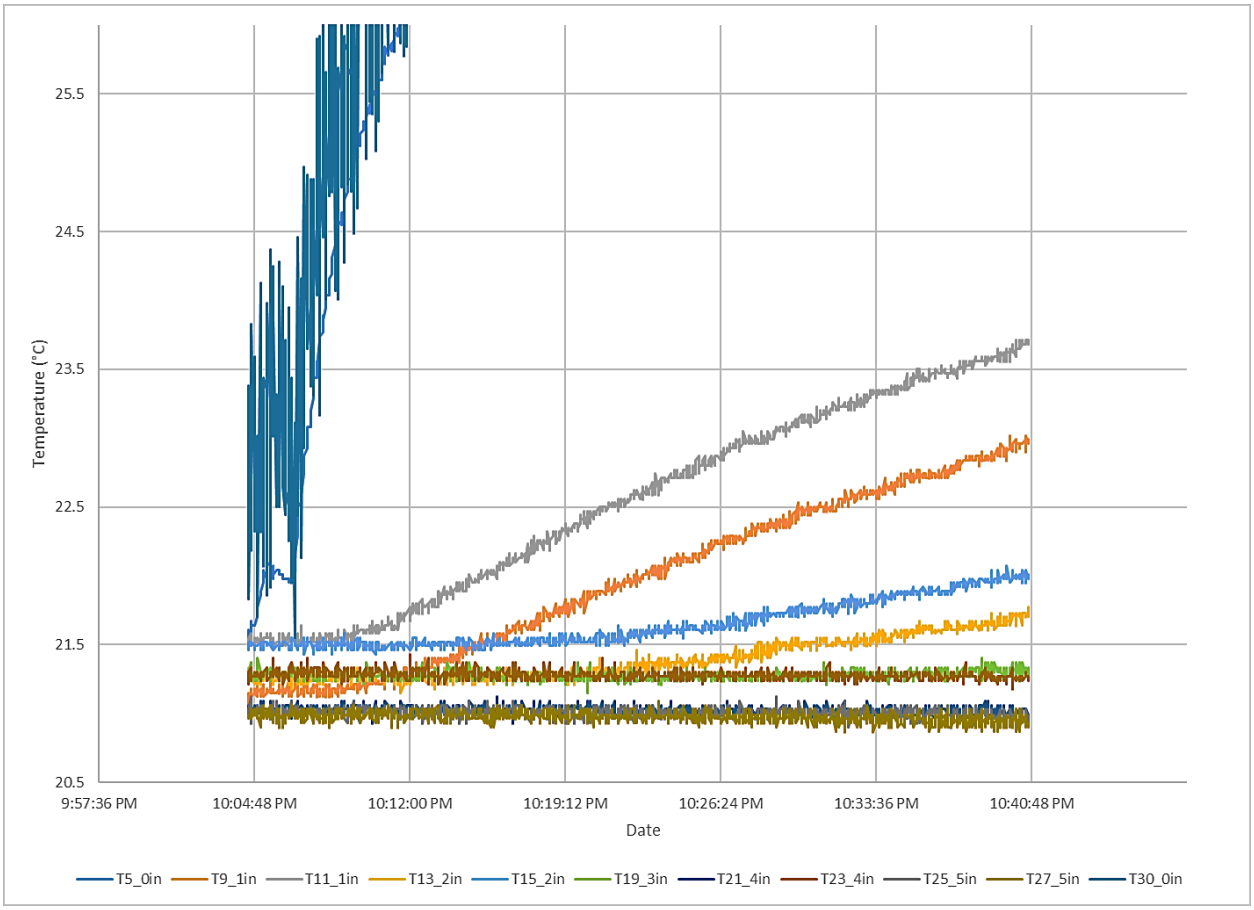

Figure 9.2 Experiment 7/4/17 initial temperatures

If the measured ambient temperature was taken as 21.5°C rather than 22.4°C, the calculated error for the experiment on 7/4/17 reduces by 3%.

The soil resistivity is another source of error. If the soil resistivity varies near the cable due to factors outside of cable heating, such as ambient soil moisture content, this would impact the results. The soil resistivity is proportional to the slope of the temperature response as discussed in Section 8.2 In-Situ Soil Resistivity Measurement Theory. The experiment on 7/4/17 shows a change of slope as shown in the following figure.

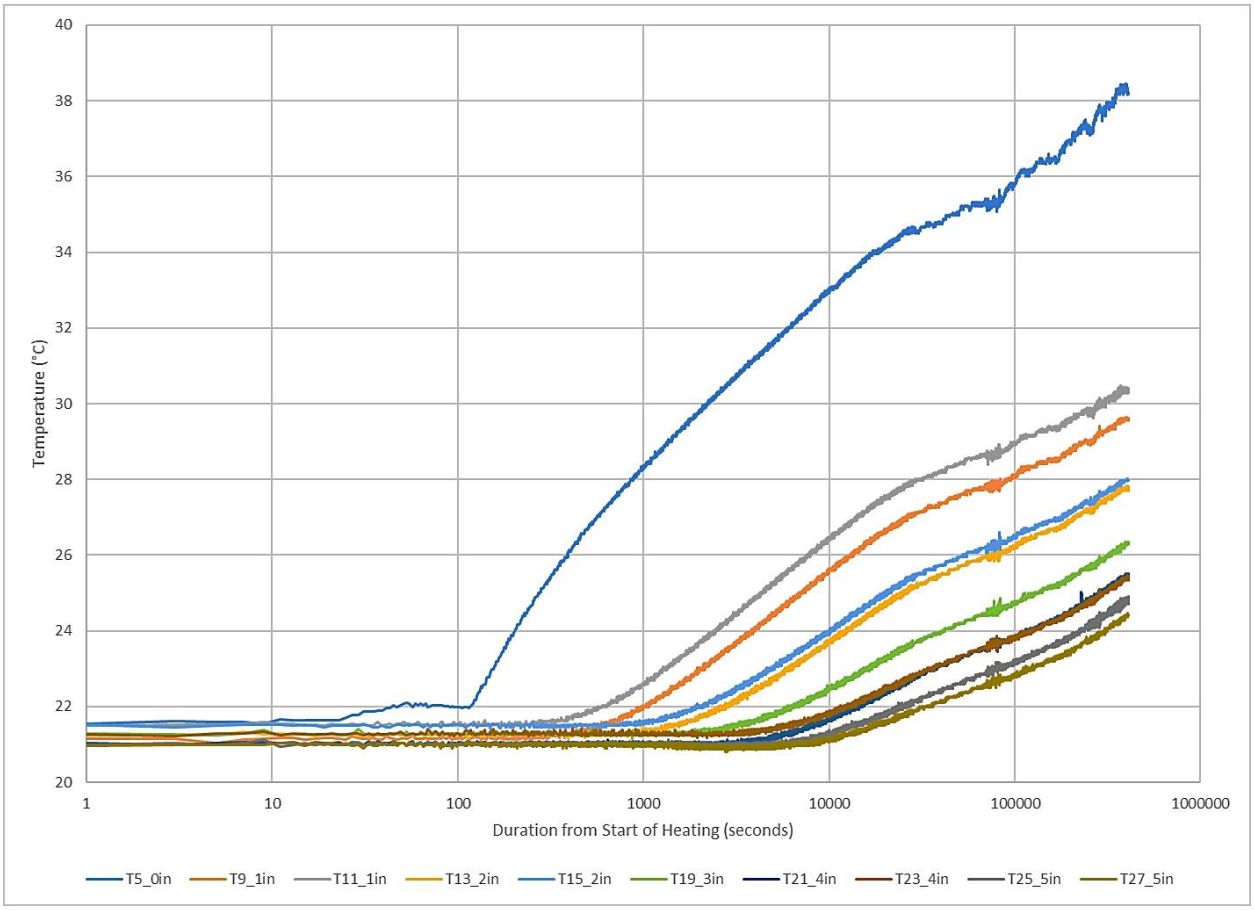

Figure 9.3 Experiment 7/4/17 temperature response slope change (time on logscale)

The slope decreased for the temperatures measured away from the cable jacket (1”, 2”, 3”, and 4”). This could be caused by inaccurate temperature sensor measurements, a change in soil resistivity, or a change in cable current, which was measured with an ammeter periodically during the experiment. This indicates the resistivity may have decreased due to external factors. Error in the resistivity impacts the calculated temperature.

Changing cable current is a third source of error. The current source was dependent on the input voltage, which varies based on the utility source. It is also varies based on ambient temperature because it impacts the resistance of the circuit in the leads to the tested cable and the transformer windings. It’s possible that the cable current changed approximately 20,000 seconds into the experiment (see Figure 9.3). Reduced cable current results would explain the error between the calculated temperature and the measured temperature. For illustration, if the cable current for the experiment on 7/4/17 was 110A instead of 120A that was measured at the start of the test, the error between the calculated and measured temperatures would be reduced by approximately 10%.

The experiment on 7/4/17 showed the highest error from the calculated values for the steady state analysis. It appears the most likely cause for this error is due to an inaccurate soil ambient temperature measurement, inaccurate soil resistivity, and change in cable current. Since the soil resistivity measurement is impacted by the measured current, error in this measurement is compounded in the calculated value. The error for all of the experiments must be considered with the results and particularly for the experiment on 7/4/17.

9.2 Moisture Migration/Soil Dry-out

A common concern for power cable installation is moisture migration or soil dry-out. These terms describe a decrease in soil moisture content as a result of cable heat. This is a problem because a decrease in soil moisture causes an increase in soil thermal resistivity and a corresponding increase in cable temperature. Soil moisture achieves equilibrium based on several factors. The US Geological Survey produced a document entitled, “Fluid Movement in Earth Materials,” which states: “Assuming isothermal conditions and uniform solute concentration, the total force on the soil water would be the sum of the forces due to gravity, hydrostatic pressure, osmosis, and adsorption” [63]. When thermal energy is introduced by cable heating, the vapor diffusion of water becomes a significant driver, as stated in the same document by the US Geological Survey: “moisture flow in response to temperature gradients occurs mainly or completely in the vapor phase” [63]. Dry-out begins near the cable jacket since the cable is the heat source. The extent of drying is limited by the other forces (gravity, hydrostatic pressure, osmosis, and adsorption) as the thermal gradient decreases. The following experimental measurements examine the extent of soil drying by calculating the thermal resistivity in three ways: Fourier’s law, transient line source method, and Structure Function.

9.2.1 Resistance Calculation using Fourier’s Law

In order to determine if moisture migration occurred, a comparison was performed of the resistivity before and after cable heating using Fourier’s Law for resistance of an annulus (or cylindrical shell). Analysis was performed using the initial and maximum temperatures in the standard resistance equation [16]: $\rho=2\pi\Delta T/(q\cdot\ln(r_2/r_1))$. An example of the analysis is shown in the following figure:

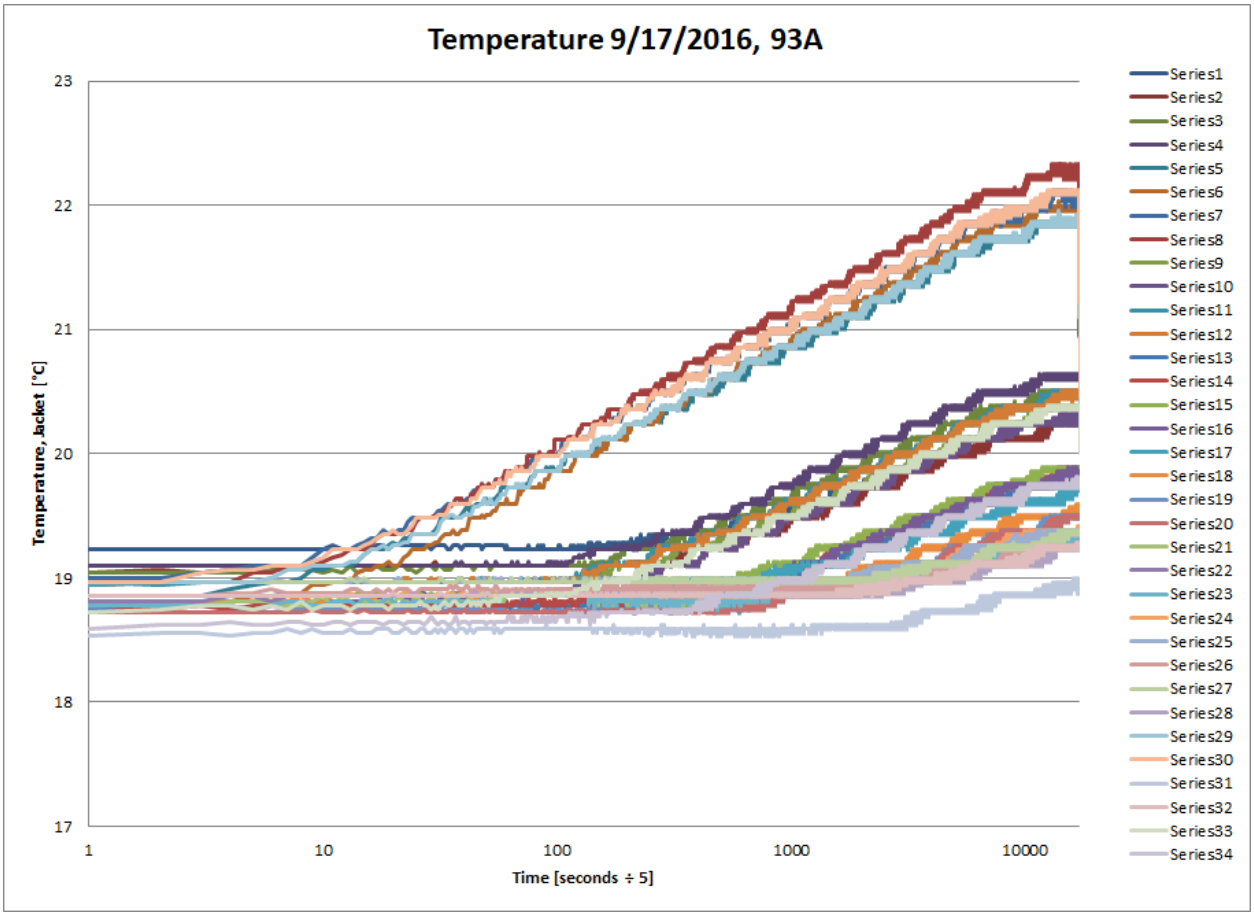

Figure 9.4 Measured temperature (9-17) versus experiment duration on a logarithmic scale

The different temperature measurement locations are noticeable by the smaller slope and lower maximum temperature as the distance from the cable increases. The analysis was performed on several experiments. The resistivity for each 1” soil annulus is shown with increasing letters, where A represents the resistivity between the jacket and 1” from the jacket, B represents the resistivity between 1” from the jacket and 2” from the jacket, etc. Additionally, 2” soil annulus resistivity measurements are indicated with a hyphen between letters, such as A-B representing the resistivity between the jacket and 2” from the jacket, B-C representing the resistivity between 1” from the jacket and 3” from the jacket, etc. For uniform soil resistivity, all of the values will be identical. If the resistivity decreases as the distance increases, it indicates soil drying around the cable, presumably due to the cable heat. The following figure illustrates the results of the analysis:

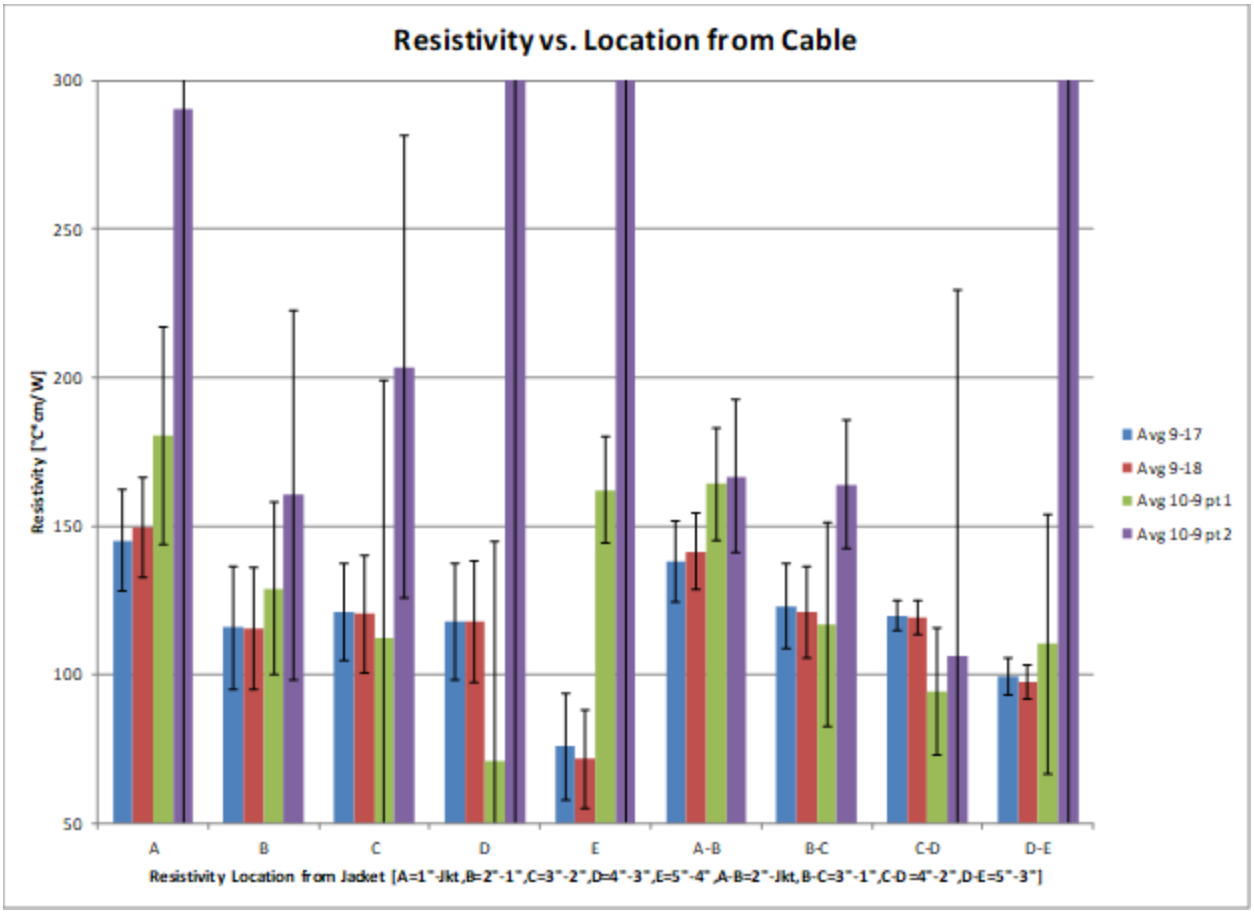

Figure 9.5 Soil dry-out analysis comparing calculated resistivities versus distance from cable

Each color represents the resistivity of the different experiments, where blue is the experiment on September 17, 2016 (0.7-day duration), red is the experiment on September 18, 2016 (0.4-day duration), green is the experiment on October 9, 2016 (6-day duration), and purple is the experiment started on October 15, 2016 (9-day duration). The black lines around the color bars illustrate the error bar of one standard deviation and the color bar is the average of the resistivity calculated for each applicable temperature sensor.

Examining the data, it appears the dataset for 10-9 part two is not helpful because of the large error bars and seemingly nonsensical results. The first three datasets indicate increased resistivity around the cable jacket compared to the soil further away from the jacket. For example, the 9-17 dataset indicates a resistivity of about 150°C·cm/W for the soil adjacent to the cable, 120°C·cm/W for the soil from 1” to 4” and 75°C·cm/W for the soil between 4” and 5” away from the cable jacket. This indicates possible soil drying; however, the error bars indicate that it may not be significant. It is important to consider the accuracy of the thermistor location placement. The formula uses the design spacing, but the measured temperature is dependent

on the actual placement. This is one part of the calculated error, but as previously discussed, is a large factor. The following figure illustrates the measurements at 1” spacing.

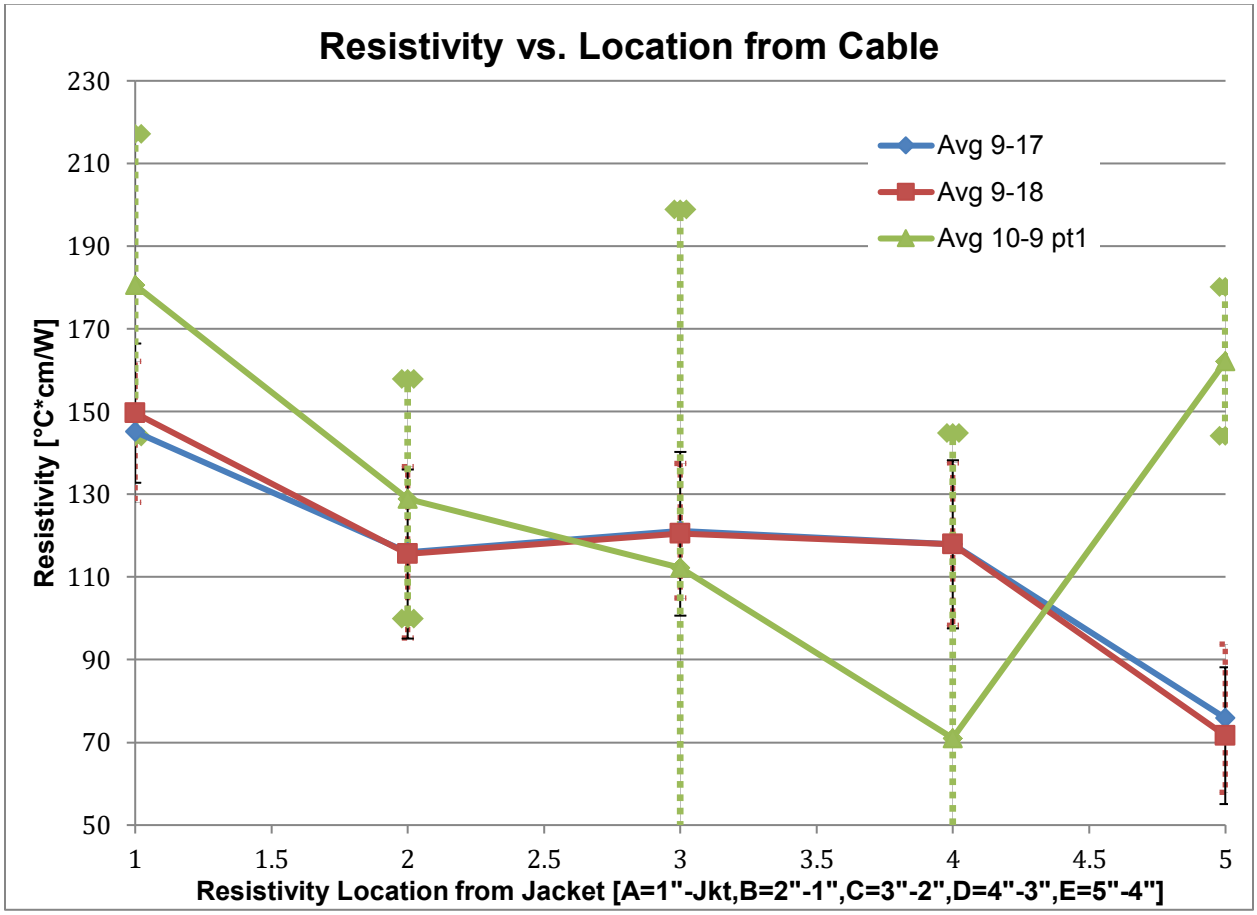

Figure 9.6 Soil dry-out analysis comparing calculated resistivities versus distance from cable

The data should also be considered with consideration of the experiment duration. The data recorded for 9-17 and 9-18 each have a duration of less than a day while the data for 10-9 part one and 10-9 part two each have duration of several days. Since the time constant of the soil is on the order of a few days, this can affect the results. The equation for steady state thermal resistivity of an annulus assumes steady state conditions. If the temperature used for the calculation is approaching steady state, the results will be biased towards a higher resistivity. Additionally, an annulus closer to the cable, such as location A, will be biased more than an annulus further from the cable, such as location E. It appears the temperature measurements for 9-17 and 9-18 are within the measurement error of the steady state temperature based on observation of the data, so it is assumed the presented data is accurate within the stated standard deviation. The linear time plot of 9-17 is shown in the following figure:

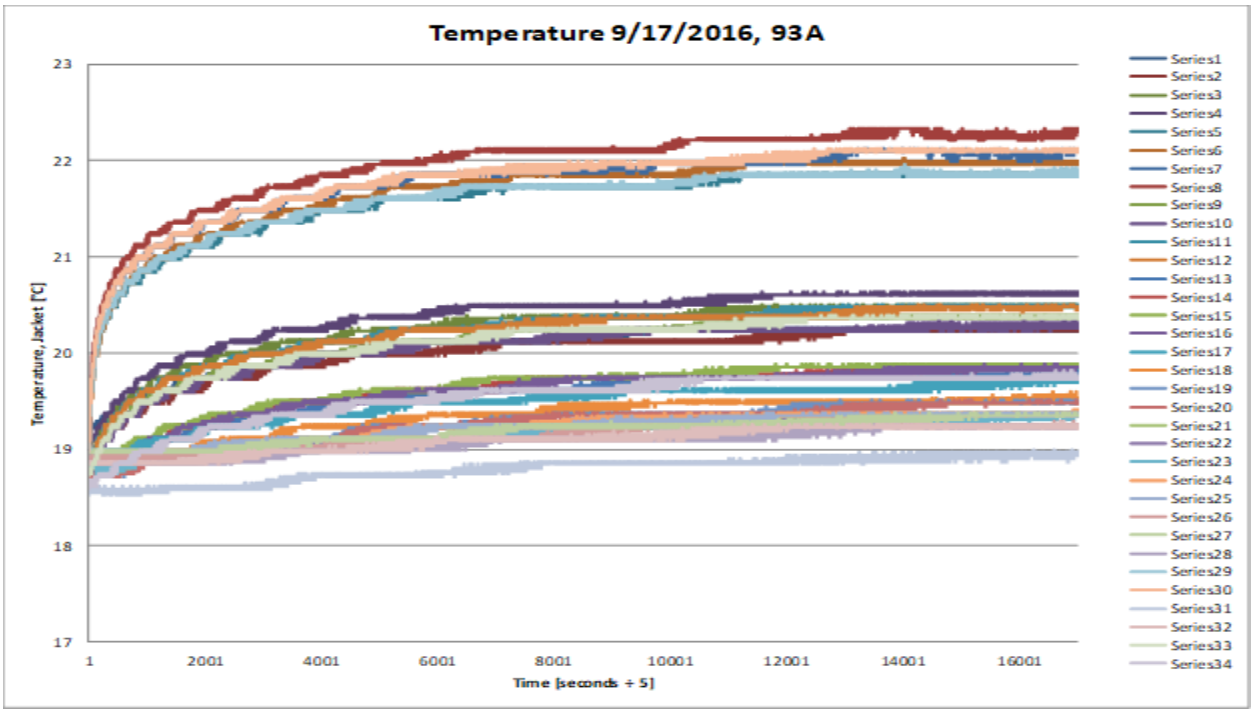

Figure 9.7 Measured temperature (9-17) versus experiment duration on a linear scale

It does appear the temperature approaches the steady state value for the temperature sensors near the cable jacket, but the sensors 3” or more away seem to indicate transient behavior. Since the conduction equation relies on steady state values, the data should be treated with this consideration. The data for 10-9 part one is shown in the following figure:

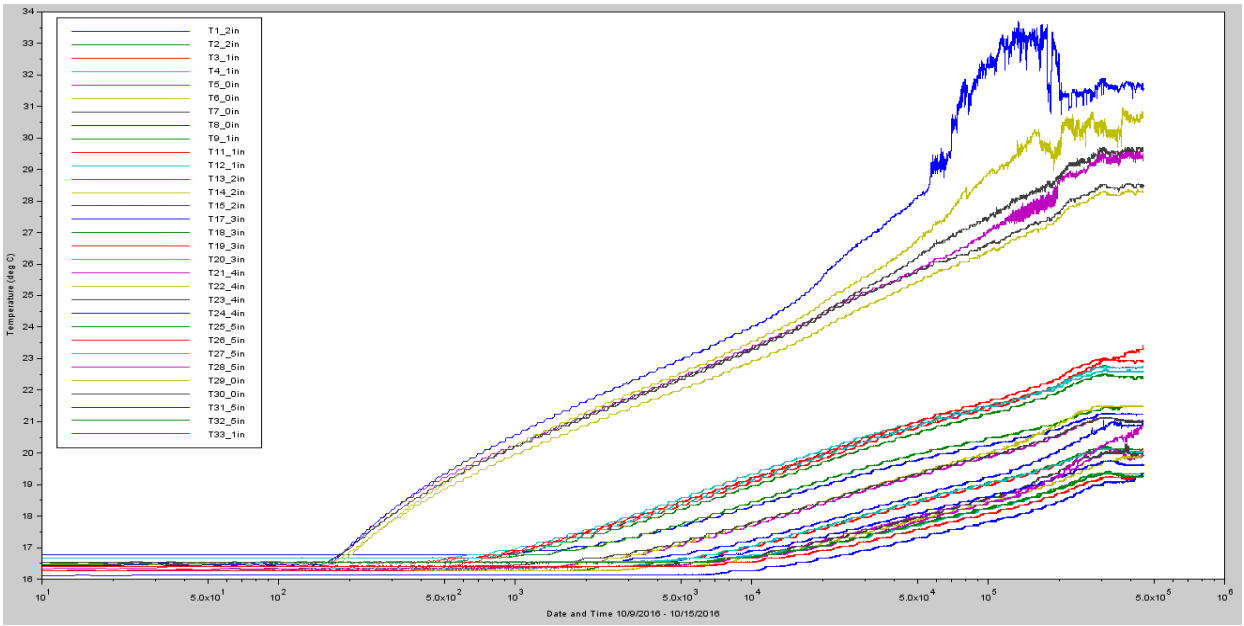

Figure 9.8 Measured temperature (10-9 part one) versus experiment duration on a logarithmic scale

The top two temperature sensors (blue and gold) began to fail towards the end of the experiment as indicated by the erratic measurements. Note the temperature after one day—approximately 10^4 seconds—continues to increase, but the slope remains the same. Considering 10-9 part one resistivity data, some soil drying is possible. The calculated resistivities are shown in the following table.

Table 9.11 Soil dry-out analysis comparing calculated resistivities versus distance from cable

10-9 part one location	Avg 10-9 pt1 [°C-·cm/W]	Stdv 10-9 pt1 [°C·cm/W]	Annulus
A	181	37	0"-1"
B	129	29	1"-2"
C	112	87	2"-3"
D	71	74	3"-4"
E	162	18	4"-5"
A-B	164	19	0"-2"
B-C	117	34	1"-3"
C-D	94	22	2"-4"
D-E	110	44	3"-5"
A-E	151	15	0"-5"

Even though it appears some drying near the cable has occurred, the amount of drying is minor considering the calculated resistivity from the jacket to 5” away from the cable is 151°C·cm/W.

9.2.2 Resistance Calculation using the Transient Line Source Method

A comparison was performed of the resistivity before and after cable heating using the transient line source method for the buried cable (Section 8.7 Resistivity Measurement Using Buried Cable). Not all of the experiments captured the data for both heating and cooling, but the data that did include both is compared in the table below.

Table 9.12 Soil dry-out analysis comparing heating-curve versus cooling-curve resistivities

Date (start)	q (W/cm)	Max. Temp (°C)	Rho Spreadsheet (°C·cm/W)	Rho Spreadsheet Stdev	Rho Off Spreadsheet (°C·cm/W)	Rho Off Spreadsheet Stdev
10/09	0.12	29.9	141	9	181	17
07/04	0.21	37.5	122	13	128	21
07/15	0.20	38.9	109	18	137	18
07/28	0.07	27.1	105	4	104	4

The data indicates that minimal, if any, drying occurs due to the cable heat since the change in resistivity is within one standard deviation for all but the first case. Interestingly, this possible drying occurs for the middle heat rate and temperature. The most likely explanation for this event is that the soil's ability to transport moisture increased over time. This could have occurred due to natural compaction over time around the cable or due to a change in moisture content. Both of these would reduce the likelihood of moisture migration or soil dry-out.

9.2.3 Resistance Calculation using the Structure Function

The extent of soil drying was also evaluated using the Structure Function. Using the Structure Function for soil analysis with buried cables was proposed in 2013 by Chatziathanasiou et. al [80] and followed up in 2016 by the same authors [81]. This method has the advantage of discretizing the thermal network in a spatial context as described in Section 8.8 Resistivity from the Structure Function. The difficulty is that it requires a high precision measurement because the algorithm is very susceptible to noise.

The Structure Functions for three of the experiments were calculated for each temperature sensor. Each curve represents the Structure Function of a particular sensor. The final cumulative resistance, R_c—determined graphically where the cumulative capacitance, C_c, approaches infinite—indicates the thermal resistance from the cable jacket to the ambient air/soil as the heat sink. The final thermal resistance is inversely proportional to the distance from the cable; that is, the temperature sensors measuring from the cable jacket yield a Structure Function with the largest thermal resistance to ambient soil/air whereas the sensors spaced 5" from the cable yield the smallest thermal resistance to ambient soil/air. Cumulative Structure Functions plot cumulative thermal resistance versus cumulative thermal capacitance. Differential Structure Functions plot the plot cumulative thermal resistance versus the ratio of thermal capacitance to thermal resistance. The Differential Structure Function highlights any change in materials or material properties because a change in material results in a change to

either the resistance, capacitance, or both. The Cumulative Structure Functions are shown in the following figures:

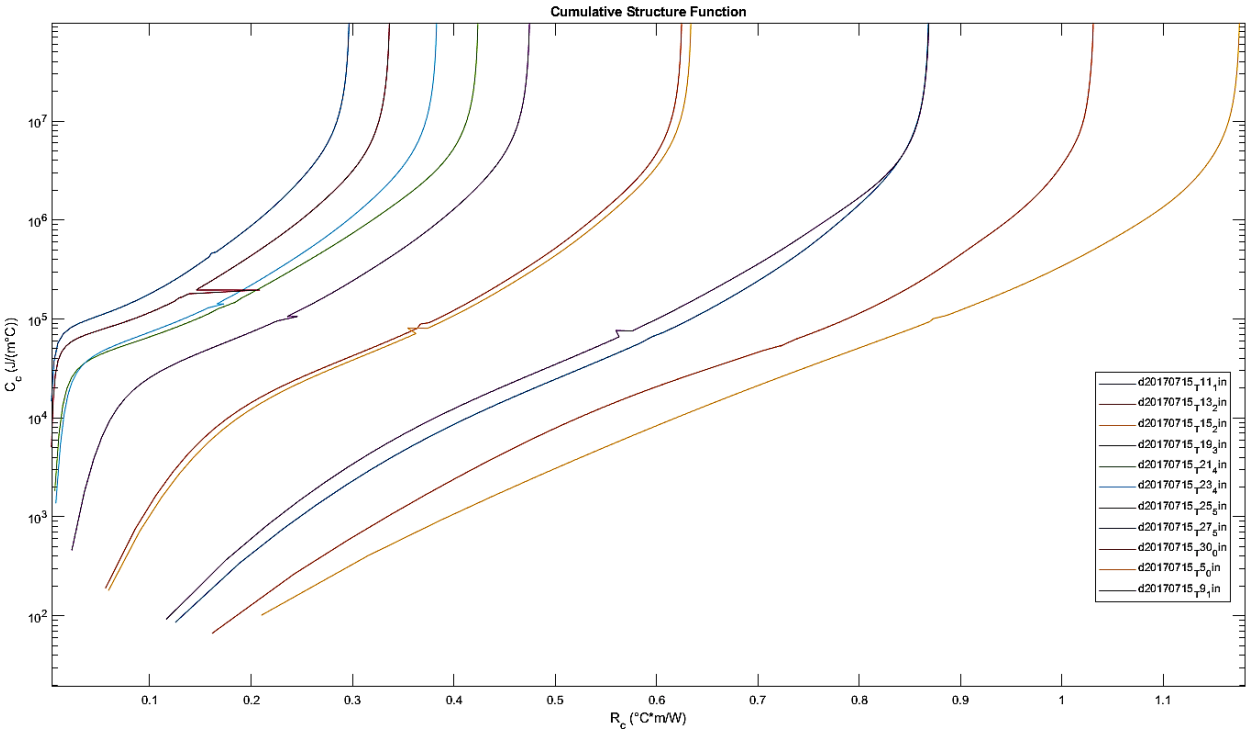

Figure 9.9 Cumulative Structure Functions for experiment on 7-15

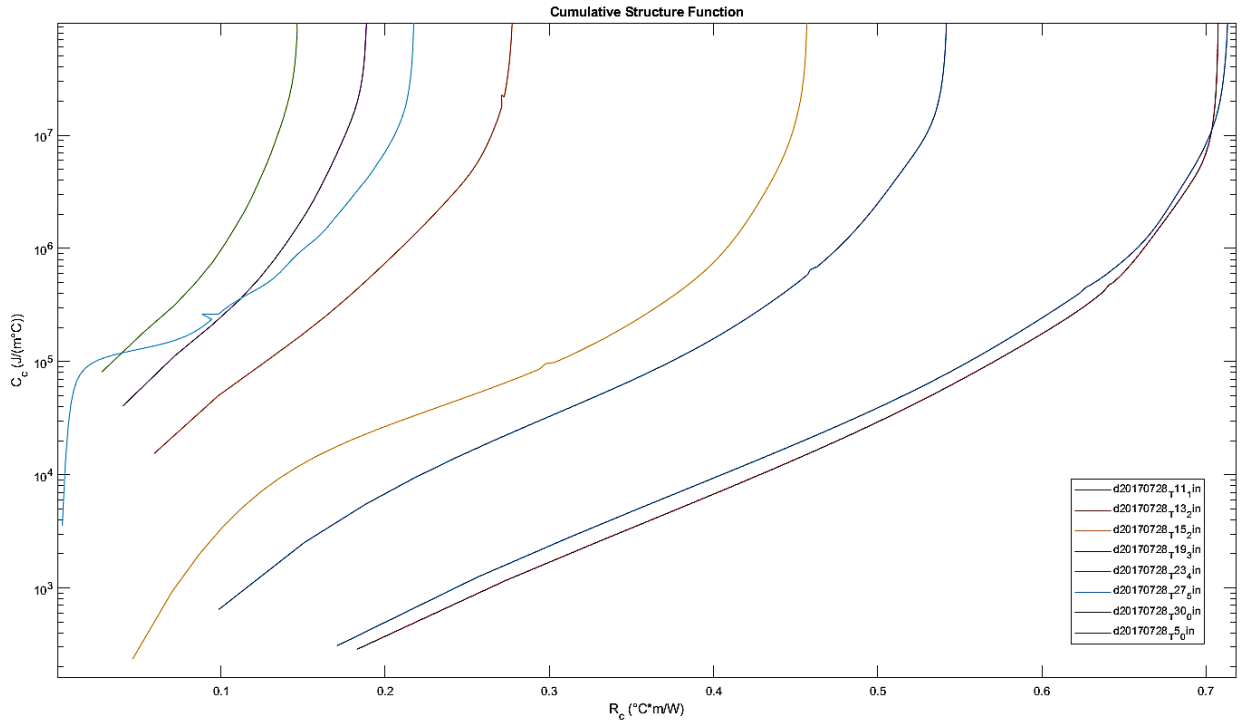

Figure 9.10 Cumulative Structure Functions for experiment on 7-28

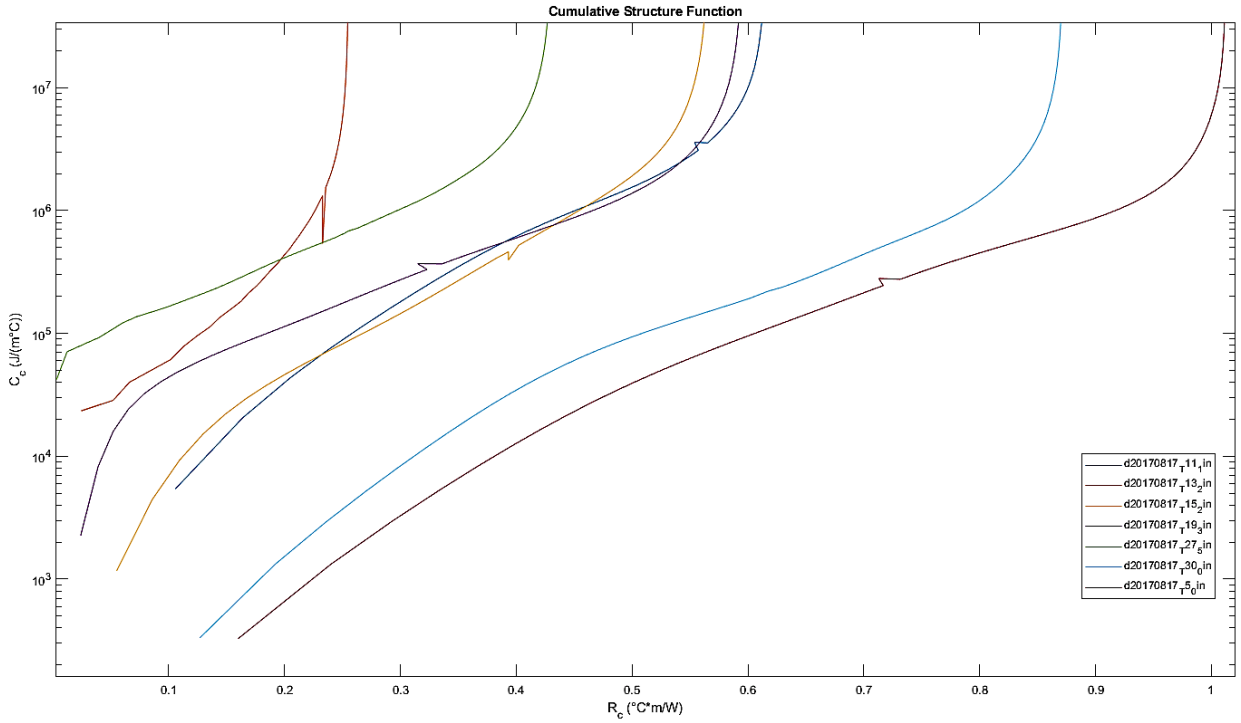

Figure 9.11 Cumulative Structure Functions for experiment on 8-17

The Differential Structure Functions are shown in the following figures:

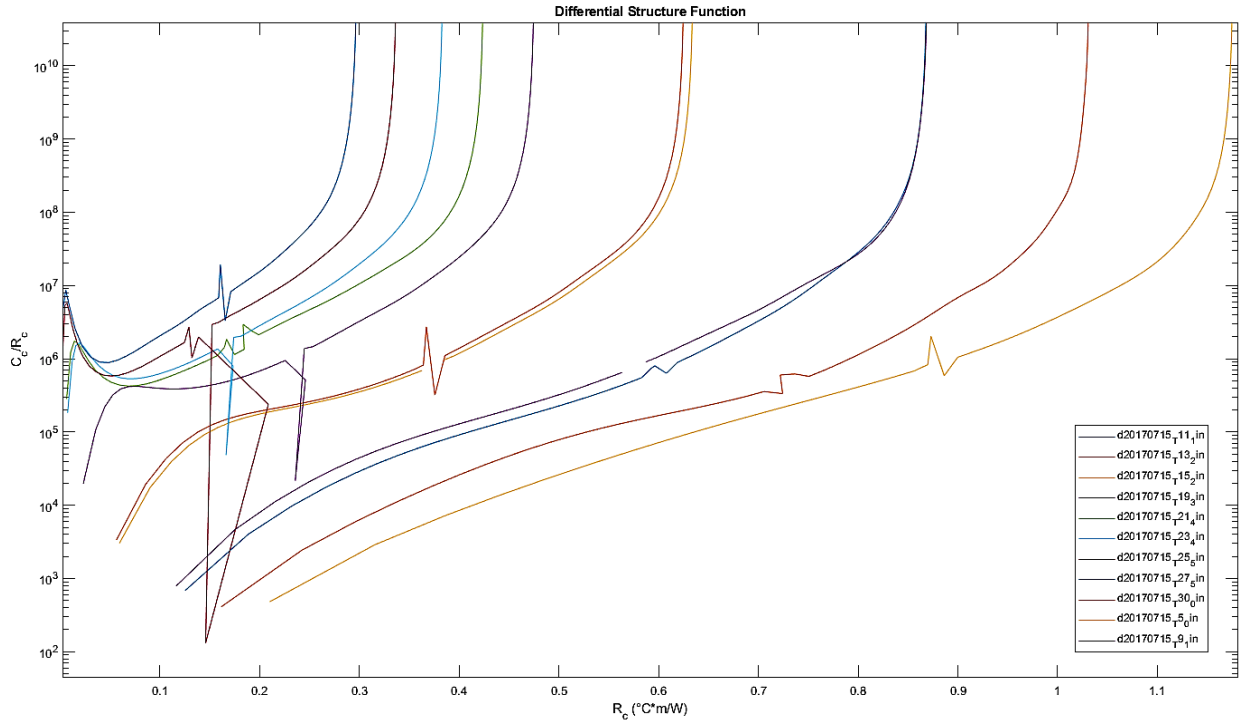

Figure 9.12 Differential Structure Function for experiment on 7-15

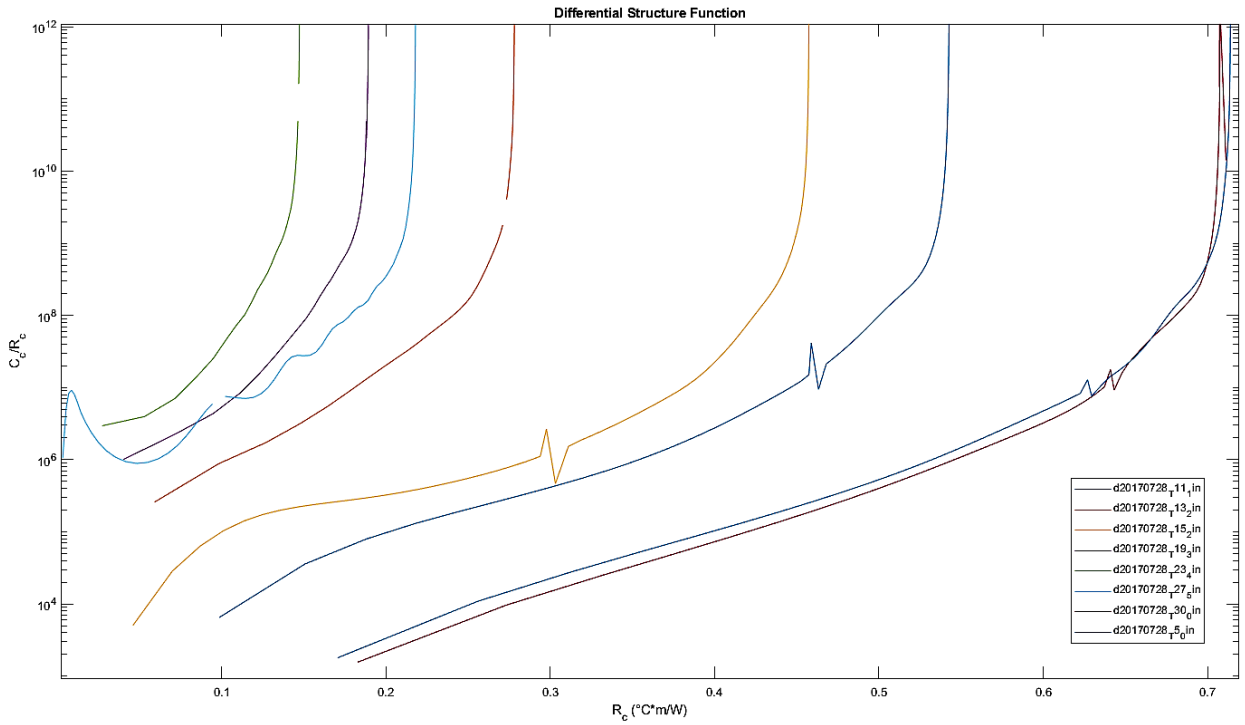

Figure 9.13 Differential Structure Functions for experiment on 7-28

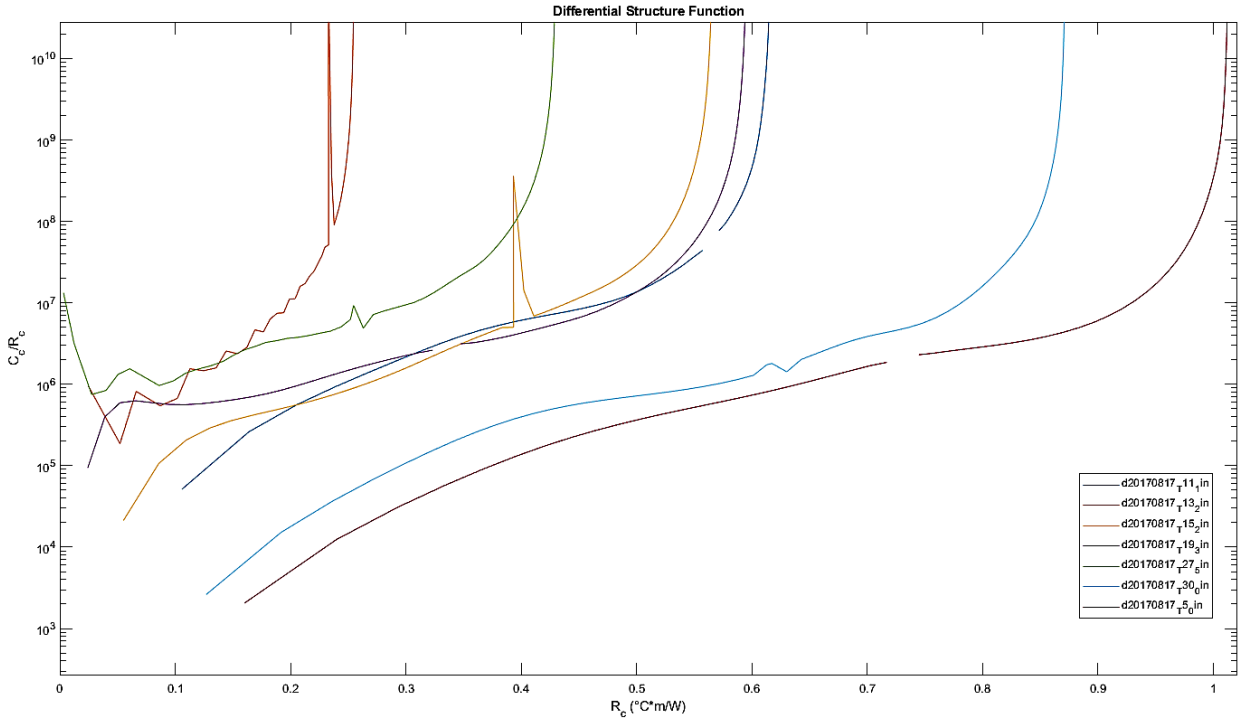

Figure 9.14 Differential Structure Functions for experiment on 8-17

If soil drying were to occur, it would be indicated by a flat cumulative or lower slope differential Structure Function because dry soil has a high resistivity and low specific heat. The

expected location of this flat or lower slope is at the beginning of the Structure Function, i.e. low cumulative resistance. An example of this is shown in the following figure.

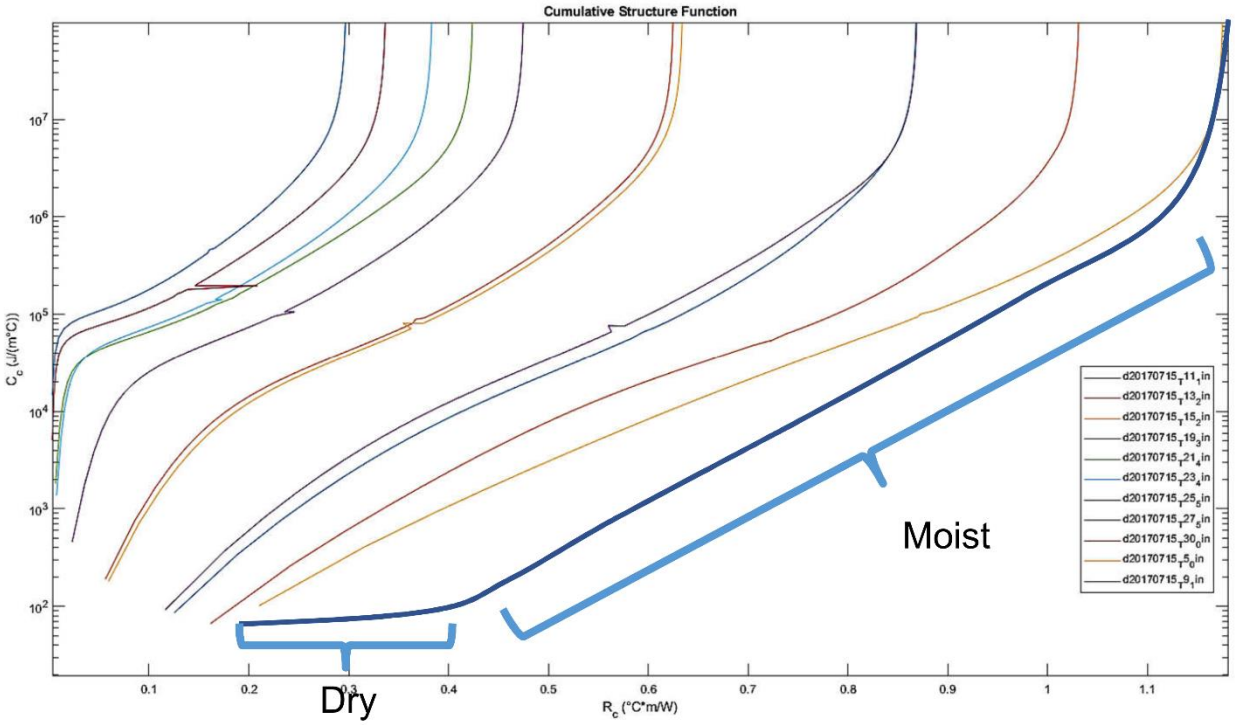

Figure 9.15 Example Structure Function showing dryout around cable

These results do not indicate moisture migration or soil drying. The slope is fairly constant for the cumulative and the differential Structure Functions. Note that the temperature sensors further from the cable jacket do not begin rising in temperature immediately, and this is indicated by a high thermal capacitance.

CHAPTER 10
SOFTWARE MODELING

Cable ampacity calculations involve numerous equations and can be onerous to perform by hand. Software is the most common method for determining ampacity in industry. Several software platforms are described in a previous section with regards to general features and operation. As with any calculation, numerous parameters must be used. The following sections document these parameters. Results that are not previously shown are also included in the following sections.

10.1 CYMCAP

CYMCAP was used to model the cable ampacity for each of the experiments using multiple soil resistivities as shown with the experimental results. It was used for both steady state and transient simulations. The cable was modeled based on the cable manufacturer's datasheet. The relevant parameters are shown in the following figure.

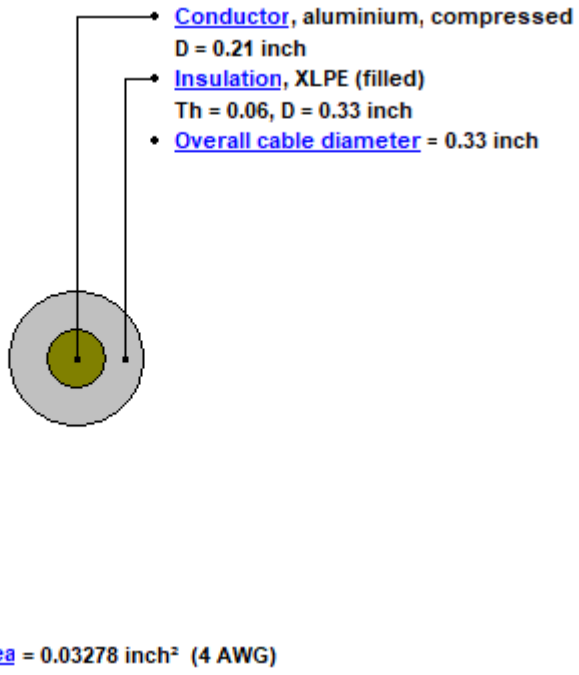

Figure 10.1 CYMCAP cable data entry screenshot

The depth was modeled at 2.63 feet (31.5 inches). The load factor was modeled at 100%. The temperature and soil resistivity were modeled as listed in the experimental comparison tables in the previous section. It is important to note that the transient analysis does not have a parameter for the soil heat capacity or time constant. It has been shown that the

specific heat will vary with moisture content, so this could impact the comparison for the transient calculations [82].

Though the results are shown in the tables in Chapter 8 Experiments, the results of the conductor temperatures are shown below for comparison with the other software results.

Table 10.1 CYMCAP comparison with measured conductor temperature

CYMCAP	Experiment Current (A)	Soil Amb. Temp (°C)	Rho Scilab (°C·cm/W)	Cond. Temp.(°C)	Max Cond Temp (°C)	% Diff
10/09/16	93	16.5	110	32.8	31.2	5%
01/29/17	97	5.7	110	26.5	21.1	20%
07/04/17	120	22.4	100	42.5	46.6	-10%
07/15/17	118	21.8	120	43.8	48.8	-11%
07/28/17	72	22.1	120	28.8	31.8	-10%
08/17/17	71	20.8	110	29.4	28.55	3%
Mean						-3%
Std						15.4%

10.2 ETAP

ETAP was used to model the cable ampacity for steady state conditions. The cable was modeled as a single aluminum conductor with PVC jacket/insulation. As described in Chapter 5 Software Modeling Tools, ETAP provides a cable library for user selection. The cable jacket thickness can be updated by adding a cable to the library, but the jacket resistivity must be adjusted in an underlying file that is not immediately accessible to the user. The selected cable is based on the NEC Table 9 values [1]. The trench detail was modeled by adding a direct burial raceway and direct burial location. The location appears like a 5” conduit, but it is not treated as such and is used for placing the cables. It is not possible to define the depth of the cable, so the depth was approximated by subtracting the measured diameter of the location and the top dimension of the raceway. This is an obvious limitation of the software, but results in a dimension that is close to the actual depth of 31.5 inches. The surrounding soil resistivity and the direct burial raceway were both specified as the same value since no soil drying is expected. The software only provides conductor temperatures, so the measured jacket temperatures were used to calculate the conductor temperature for comparison. ETAP requires the user to place a

single-phase or a three-phase circuit for the cable, so the single cable used for the experiment must be modeled as two cables for a single-phase circuit. This results in twice the heating, i.e. I^2R now equals $2 \cdot I^2R$. In order to properly compare with the experiment, the modeled current was reduced by $\sqrt{2}$. The results are shown in the following table:

Table 10.2 ETAP comparison with measured conductor temperature

ETAP	Experiment Current (A)	Modeled Current (A)	Soil Amb. Temp (°C)	Rho Scilab (°C·cm/W)	Cond. Temp.(°C)	Max Cond Temp (°C)	% Diff
10/09/16	93	65.8	17	110	32.8	30.9	6%
01/29/17	97	68.6	6	110	26.5	21.7	18%
07/04/17	120	84.9	22	100	42.5	46.4	-9%
07/15/17	118	83.4	22	120	43.8	49.7	-14%
07/28/17	72	50.8	22	120	28.8	31.6	-10%
08/17/17	71	50.2	21	110	29.4	29.7	-1%
Mean							-4%
Std							14.6%

10.3 USAmp Prime

USAmp Prime was used to model the cable ampacity for steady state conditions. The cable was modeled as a single aluminum conductor with XLPE jacket/insulation. As described previously, the parameters are easily configured for the proper conductor size, insulation thickness, and thermal resistivities. After the cable was modeled, the trench detail was modeled. The soil thermal resistivity was modeled at 110°C·cm/W based on the sliding window average (Scilab Rho). The depth was modeled at 31.5 inches.

Two operating currents were modeled to compare with the 93 A and 120 A results on 10/9/2016 and 7/4/2017 respectively. The software only provided conductor temperatures because it was a demo version, so the experimental conductor temperature was calculated using the heat conduction equation and the measured jacket temperature. The results are shown below:

Table 10.3 USAmp Prime comparison with measured conductor temperature

USAmp Prime	Soil Amb. Temp (°C)	Rho (°C·cm/W)	Max Cond Temp (°C)	Model Temp (°C)	% Diff
10/09/16	16.5	110.0	32.8	32.1	2%
07/04/17	22.4	110.0	42.5	49.9	-17%

The first experiment compares reasonably well with USAmp modeled temperature. The second experiment, however, does not compare as well. It's speculated that the soil resistivity and the duration of the experiment are the reasons for the difference.

10.4 Finite Element Modeling (FEA)

ANSYS Mechanical was used to perform thermal analysis of the cable using finite element analysis. The cable was modeled as a solid cylinder based on the same geometry as the other software, using the datasheet from the cable manufacturer. The earth was modeled as a rectangular prism with a width of 113 inches and depth of 120 inches. It must be deep enough and wide enough to reduce end effects. The cable and earth were modeled with a length of 12 inches to provide a round number, but this length does not impact the results since it is assumed the actual experimental length of 11 feet provides an infinitely long cable. The cable was modeled in the center of the width of the soil at a depth of 31.5 inches.

After modeling the geometry, the material properties were entered. The earth was modeled with a density of 1390 kg/m^3 and a specific heat of 1000 J/(kg·C) based on typical values. The thermal conductivity of the earth varies based on the experiment time as calculated by the transient line source method. It is a variable for each experiment as described below. The conductor properties do not impact the results since the focus is on the soil temperature, but it was modeled as aluminum with a density of 2689 kg/m^3, a specific heat of 951 J/(kg·C), and a thermal conductivity of 237.5 W/(m·C). The cable jacket properties do not impact the results, similar to the conductor, but it was modeled as hard rubber with a density of 1190 kg/m^3, a specific heat of 1 J/(kg·C), and a thermal conductivity of 0.16 W/(m·C).

After entering the geometry, the model was built. Contact resistance between layers was not modeled since the focus was on the soil temperature. The mesh was automatically generated by ANSYS Mechanical, which produced acceptable results. An adiabatic boundary was applied to the sides and base of the soil rectangular prism as well as to both side of the cross section of the cable and soil. This simulates an infinite length cable, which is the standard assumption for cable ampacity calculations. A convective boundary layer was applied to the top

surface to simulate the air/soil interface with a film coefficient of 10 W/(m^2·C). The convective ambient temperature is a variable for each experiment as described below and is equal to the soil ambient temperature for the compared experiment. It is assumed that the diurnal cycle will result in an approximate temperature equal to the soil ambient temperature based on the time constant of ampacity calculations exceeding a few days.

The results for the steady state analysis were measured by a temperature probe and profile. A temperature probe measuring the maximum value was placed at the jacket to soil interface since this is where the temperature measurements were taken for the experiment. The temperature profile measured the entire cross section of the cable and soil geometry. The steady state measurements were performed with the following variables:

1. Earth thermal conductivity
2. Earth surface convection boundary condition ambient temperature
3. Cable heat rate

Table 10.4 ANSYS resistivity, surface temperature boundary, cable heat rate

Compared Experiment	Earth K [W/(m·C)]	Ambient Temp [°C]	Heat Rate [W]
10/09/16	0.7105	16.5	3.737
01/29/17	0.7571	5.7	3.921
07/04/17	0.8170	22.4	6.411
07/15/17	0.9141	21.8	6.212
07/28/17	0.9565	22.1	2.206
08/17/17	1.0521	20.8	2.161

The maximum measured temperatures on the cable jacket and the steady state temperatures calculated by ANSYS simulation are shown in the following table:

Table 10.5 ANSYS comparison with measured jacket temperature

Compared Experiment	Experiment 5 Day Temp (°C)	Experiment Max. Jacket Temp (°C)	ANSYS Jacket Temp (°C)	% 5d Diff	% Diff
10/09/16	29.7	29.9	34.5	-16%	-15%
01/29/17	20.5	23.4	23.4	-14%	0%
07/04/17	37.5	37.5	49.3	-31%	-31%
07/15/17	38.1	38.9	45.2	-19%	-16%
07/28/17	27.1	27.1	30.0	-11%	-11%
08/17/17	27.7	27.7	27.9	-1%	-1%
Mean				-15%	-11%
Std				11.3%	13.7%

The average difference between the five-day temperature and the ANSYS simulation is -19% with a standard deviation of 9%, where negative indicates that the measured values is less than the ANSYS calculated value. The average difference between the maximum measured and the ANSYS simulation is -15% with a standard deviation of 13%.

10.5 Comparison

Each software program requires different modeling considerations and resulted in different errors from the measured temperatures. A summary of the results is shown in the following table. Negative values indicate that the model calculated a higher temperature than the measurement.

Table 10.6 Software comparison of measured versus calculated temperature difference

Experiment Date	Soil Amb. Temp (°C)	CYMCAP % Diff	ETAP % Diff	USAmp % Diff	ANSYS % Diff
10/09/16	16.5	5%	6%	2%	-15%
01/29/17	5.7	20%	18%	N/A	0%
07/04/17	22.4	-10%	-9%	-17%	-31%
07/15/17	21.8	-11%	-14%	N/A	-16%
07/28/17	22.1	-10%	-10%	N/A	-11%
08/17/17	20.8	3%	-1%	N/A	-1%
Mean		-3%	-4%	N/A	-11%
Std		15.4%	14.6%	N/A	13.7%

CYMCAP and ETAP yield very similar results for all of the experiments. USAmp Prime yields lower error for the experiment on 10/9 and higher error on 7/4 compared to CYMCAP and ETAP. ANSYS yields similar results to CYMCAP and ETAP for the experiments on 7/15, 7/28, and 8/15, but higher error for the experiments on 10/9 and 7/4. ANSYS yields the lowest error for the experiment on 1/29. It is speculated that ANSYS predicts a higher temperature than the CYMCAP analysis due to the convective surface boundary condition and the finite depth and width of the rectangular prism.

CHAPTER 11
SOLAR PV POWER PLANT CASE STUDY

A solar photovoltaic (PV) power plant located in Arizona was studied with the goal of comparing the pre-installation engineering analysis of cable temperature and ampacity with the values measured after PV plant was installed. The rated power output of the PV plant is approximately 10 MW using single axis tracking. In order to provide an optimal design for reliability and cost, the cables were specified using the Neher-McGrath calculation method and designed to operate near their maximum temperature rating. Seven measurements of the soil thermal resistivity were made on soil samples from the installation site. Many of these measurements yielded soil resistivity (RHO) values higher than 90°C·cm/W used to calculate the tables in the National Electrical Code (NEC) [1]. These tables are commonly used by engineers to determine cable ampacity, sometimes without knowledge or consideration of the actual soil resistivity. Many of the measured resistivities also exceed the highest value of RHO, 120°C·cm/W, used in the tables of IEEE Std 835 [11].

The highest thermal resistivity resulting from the testing on-site was 329°C·cm/W, which was given at a soil moisture of 0%. The engineers designing the cable system for the photovoltaic (PV) system used a soil resistivity value of 270°C·cm/W for their design. This was the average of all the tests taken at 0% soil moisture content. Furthermore, the design used a load factor of 53% that was based on measured data from similar projects and calculations from a commercially available software titled PVsyst [83]. These parameters were used by the design engineer in the Neher-McGrath method to specify conductor size and such installation details as cable spacing and depth. The cable was selected based on a maximum operating temperature 75˚C, which is the limit of the cable terminations. Sensors were installed at the site to measure actual cable temperatures, and these measurements were compared with the temperatures anticipated from the design calculations.

11.1 Data Collection

The case study focuses on four sections of installed cable: Section 1-A, 1-B, 2-A, and 2-B. The cable sections and installation details are shown in the following figures:

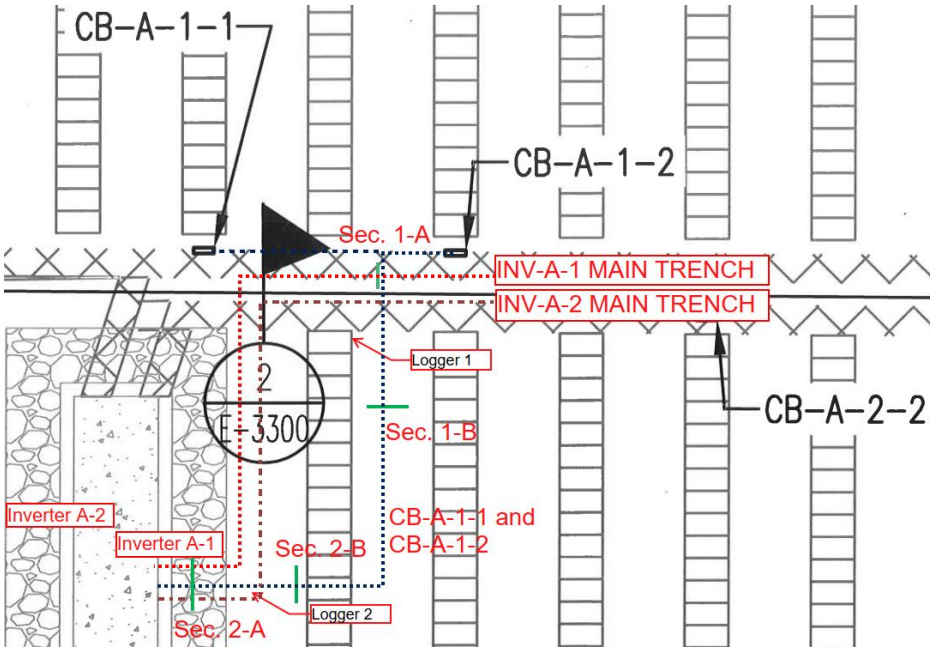

Figure 11.1 Plan view of DC Combiner circuit routing and logger section locations

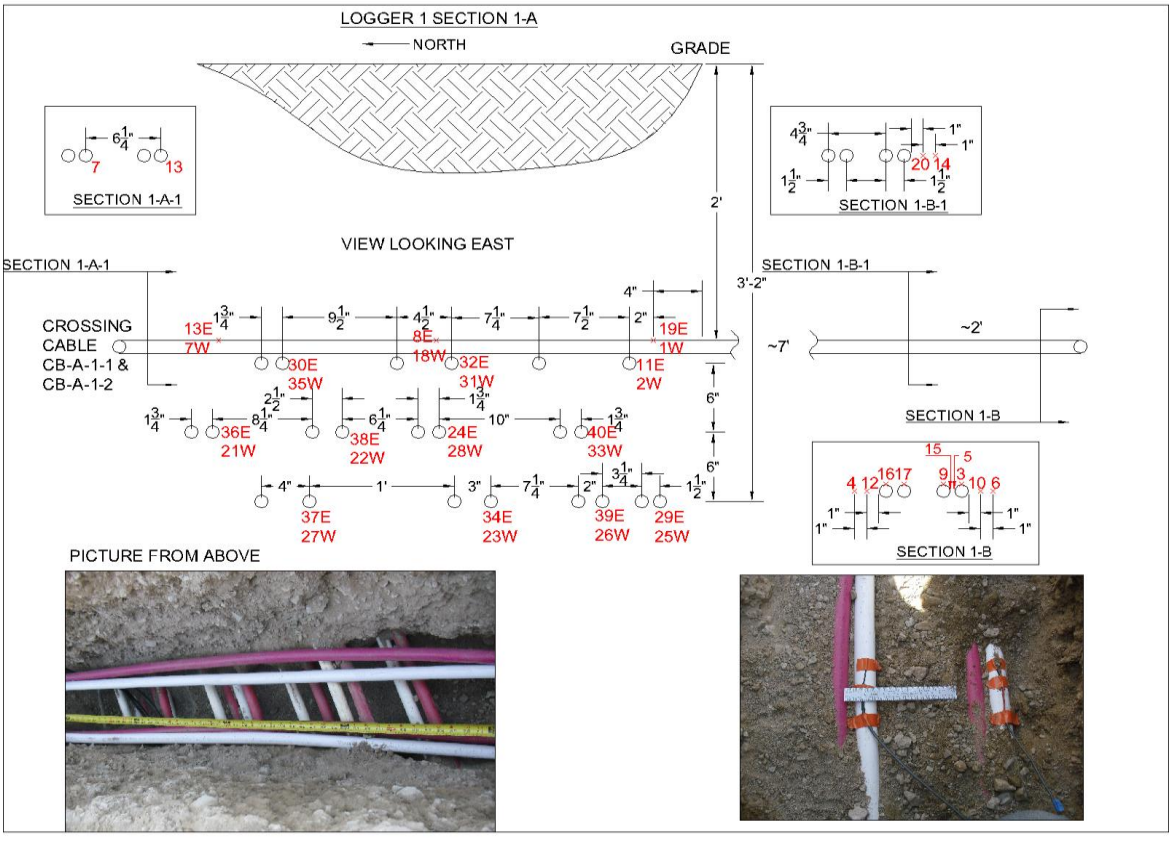

Figure 11.2 Section view of circuit installation detail and sensor locations for logger 1

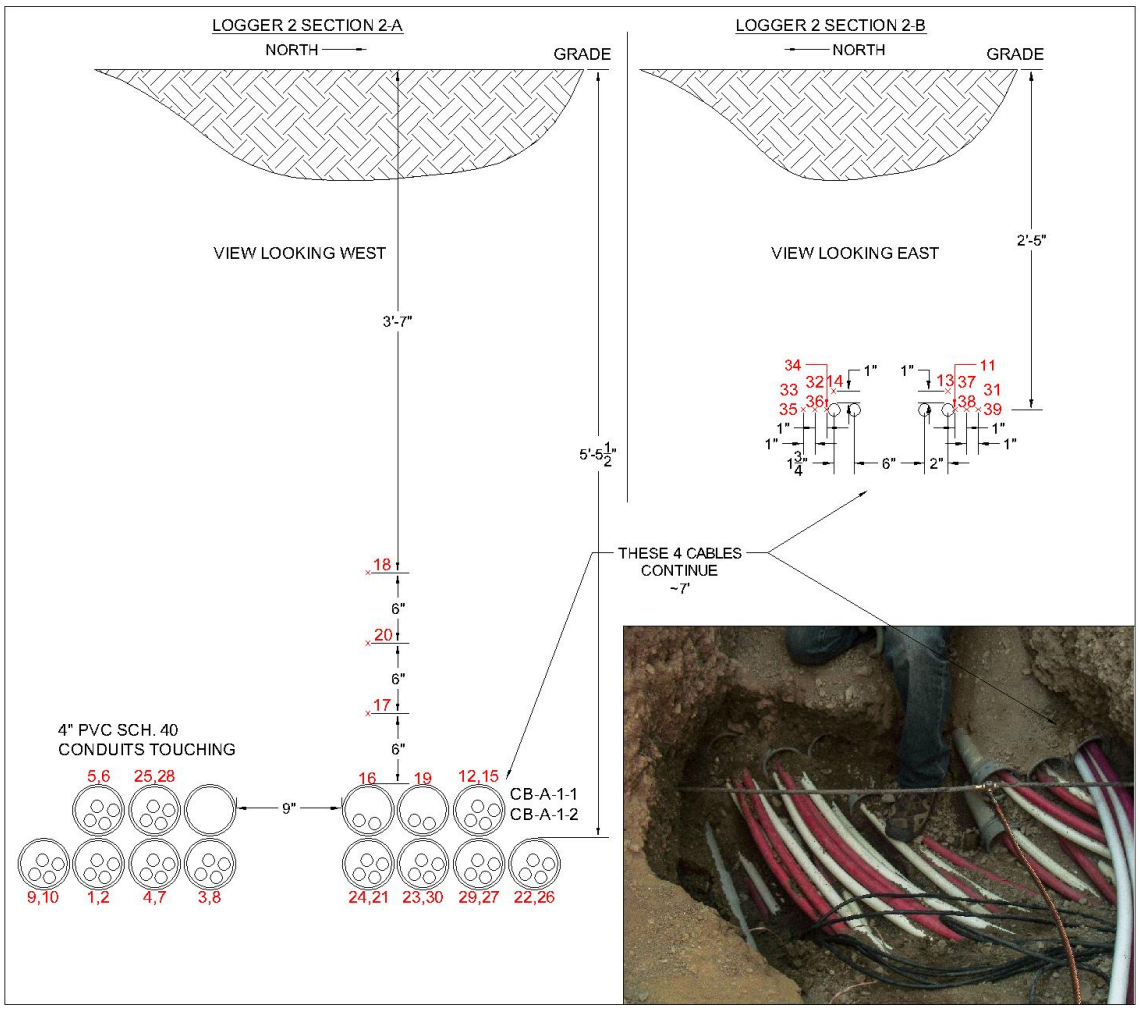

Figure 11.3 Section view of circuit installation detail and sensor locations for logger 2

The data logger and temperature sensors are the same for this case study as for the experimental test setup. In this case, two different setups were used to measure the four sections—two sections for each setup. The data logger stored the measurements on a local Secure Digital (SD) card. Since the PV plant is unmanned, retrieval of this data is difficult. So, a cellular modem was added to the logger to transmit the data to an offsite server for more frequent access. The Arduino boards can interface with a FONA cellular modem to connect to the internet for data transmission. A Ting service contract was purchased to provide cellular access over the T-Mobile network. Since the service contract is based on the amount of data transmitted, it is important to use a protocol with minimal overhead, i.e. maximum data efficiency. According to HiveMQ, “MQTT was developed by Andy Stanford-Clark (IBM) and Arlen Nipper (Eurotech; now Cirrus Link) in 1999 for the monitoring of an oil pipeline through the desert. The goals were to have a protocol, which is bandwidth-efficient and uses little battery

power, because the devices were connected via satellite link and this was extremely expensive at that time" [84]. MQTT has a library implemented in Arduino and a guide is provided by Adafruit [84], [85]. This was implemented into each Arduino data logger.

The recorded temperatures were multiplied by 100 (to maintain two decimal precision), converted to an integer, and combined with a date-time stamp into a packed data structure to further reduce the bandwidth requirements. The transmitted data was received by an MQTT Broker and published to the MQTT subscriber on the same server computer. The received data was processed by a Python script to unpack the data structure into a comma separated value (CSV) file and rescale the integers to decimal values. These values were sent approximately every five minutes; however, cellular data connection often resulted in one or two failed packets and a resulting ten- or fifteen-minute duration between logging. In addition to transmitting data, the loggers could receive commands to adjust the logging frequency and sleep mode (disable logging). These controls were implemented to control energy usage.

The original requirement was to power the data logger with a combination of solar power and battery. In order to size the solar panel and battery pack, some power and energy calculations were performed. Each board—Arduino Mega2560, FONA Cellular GSM, multiplexer, SD Card—required different amounts of power and energy. The supply circuit for the thermistors also required power and energy. First, the power and energies were calculated based on manufacturer provided data and programmed operating times. This indicated a nightly energy use of 5398 mWhr. The solar panel was sized to charge the battery and supply the daytime running power, so the battery was relied on for power only when the solar panel could not. After the required energy was calculated, measurements were made of the actual data logger. These measurements were made with a portable oscilloscope to capture the transient power usage with durations less than a second. A standard ammeter was also used to compare with the portable oscilloscope. The measurements indicated significantly higher energy requirements: about 15,000 mWhr. This is likely due to the extended runtime of the logger from the calculated durations and due to significant energy usage from the thermistors. The following table provides the specific data and calculations:

Table 11.1 Data logger calculated power and energy analysis

	Running (mA)	Sleep (mA)	Duration (s)	Voltage (V)	Power (mW)	Energy (mWhr)
Uno	49	34.5				
Mega2560	68	24				
FONA	53.4		35	3.7	198	1.921
FONA	28	8	99	4.2	118	3.220
>Turn on FONA	99		19.73	4.2	414	1.850
>enable GPRS	159		7.95	4.2	667	0.910
>MQTT (200MB)	157		5.6	4.2	659	0.58
>disable GPRS	167		3.97	4.2	700	0.46
Total			37.25			3.800
# logs/hr	12	log/hr				
standby energy	340	mW				
time w/o sun	14	hr				
total energy	5398	mWhr	V44 Battery = 44,000mWhr			

Table 11.2 Data logger measured power and energy with Fluke 190 including 34 Thermistors (shutoff between logs)

	Running (mA)	Duration (s)	Voltage (V)	Power (mW)	Energy (mWhr)
Startup	320		4.8		
Running	262		4.8	1257.6	
Logging	320	3	4.8	1536	1.28
# logs/hr	12	log/hr			
standby energy	1258	mW			
time w/o sun	14	hr			
total energy	17,821	mWhr			

Table 11.3 Data logger measured power and energy analysis with Fluke 89

	Running (mA)	Duration (s)	Voltage (V)	Power (mW)	Energy (mWhr)
Mega	70				
+SD&MUX	91				
+FONA	236				
Steady State	110	peak at 190 (but very short < 0.5 sec)		5	550
+Thermistors	34		5	5	170
# logs/hr	12	log/hr			
standby energy	550	mW			
time w/o sun	14	hr			
total energy	7740	mWhr			
Uno+Mux+ Ethernet	217			5	1085
standby energy	1085	mW			
time w/o sun	14	hr			
total energy	15,190	mWhr			

Significant power savings can be realized by reducing the Arduino Mega2560 to the bare processor because the USB serial interface and the voltage regulator use significant energy [86]. However, reducing the Arduino to a barebones processor requires additional time and the data logger setup needed to be installed according to the client's timeline, so it was not performed. A 9 W, 44 Watt-hour solar pack and battery provided by Voltaic Systems (www.voltaicsystems.com) exceeded the power and energy requirements. This was installed and configured; however, the controller seemed to shut off even in the "Always On" mode, so the data loggers were connected to a standard 120VAC outlet.

Beyond the temperature sensor data loggers, the current magnitudes for the circuits of each measured section were recorded by the local inverter data logger. The inverter stores the DC current every fifteen minutes for each input module. There are eight parallel input modules for each inverter and the current is measured from the common DC bus to each of the eight

input modules. The DC combiner box circuits are connected in parallel to the common DC bus. So, the current logged by the inverter loses some accuracy from the current for each combiner box, but this is not considered significant since the combiner circuits have similar power output.

The currents measured by the inverter were time-aligned with the temperatures recorded by the data logger since each was measured at a different sample rate. For cable ampacity calculations, the primary factor is maximum current, so the exact time is not critical; however, it is helpful to examine the time constant of the cable/soil system. The following figure shows the recorded data on the hottest day of the year, August 14, for two temperature sensors and the measured current for Inverter A-1:

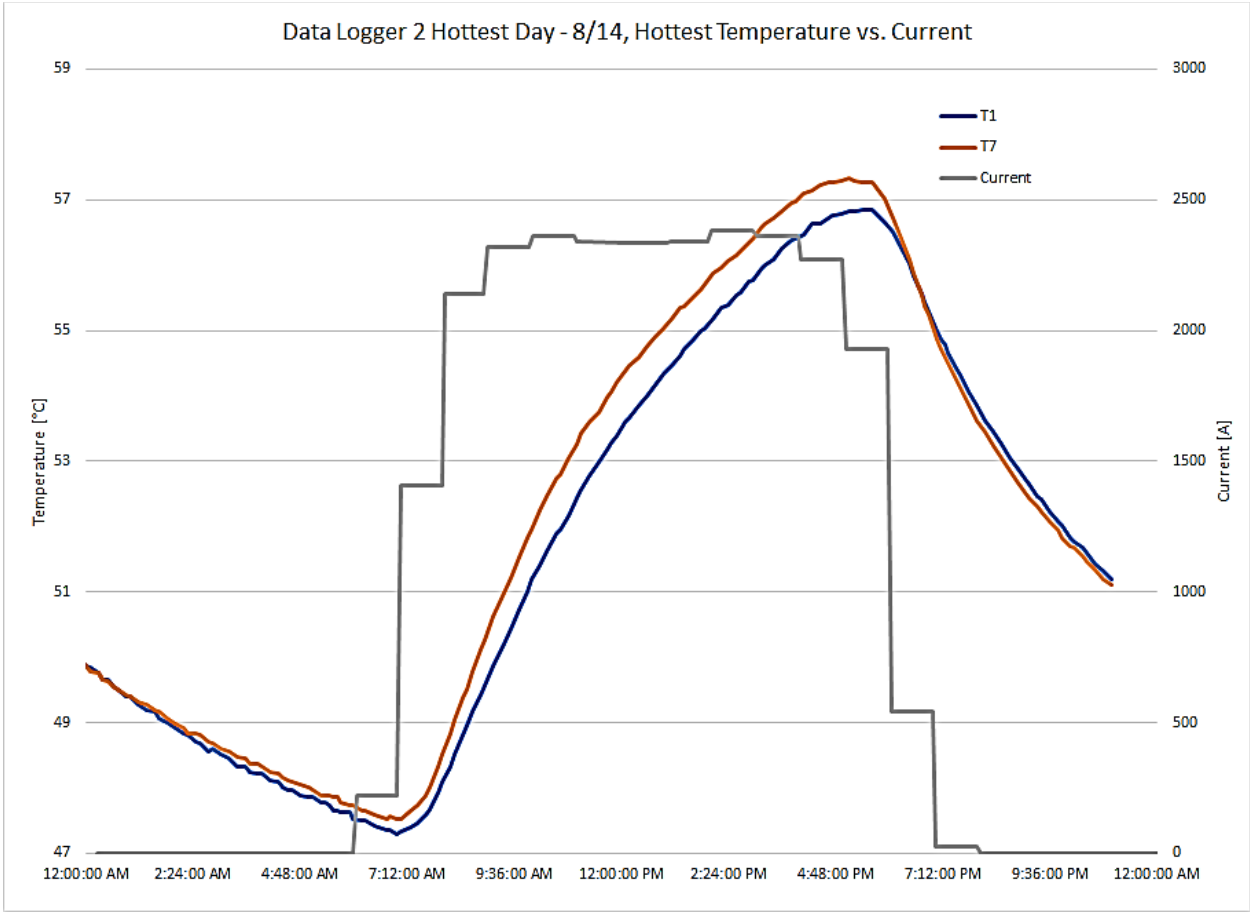

Figure 11.4 Measurements on the hottest day of two temperature sensors and inverter current

11.2 Soil Thermal Resistivity

The soil thermal resistivity is the most important factor for determining cable ampacity and it varies more than any other design parameter. It must be measured at every project site since soil varies by location—it cannot be predicted accurately. However, it is often not measured prior to the design of cable systems in industrial and commercial projects. If it is measured, it is often difficult to determine the appropriate soil resistivity for ampacity calculations. Prior to the design for this case study, the resistivity was measured in a laboratory for seven soil samples taken from the project site. The resistivity was measured seven additional times at the project site (in-situ) after the cables were installed as part of this case study. The first four measurements were performed on native soil in four undisturbed tube samples. The fifth and sixth measurements were performed on native soil that was compacted to 92% modified proctor. The seventh measurement was performed on backfill samples that were lightly tamped, i.e. uncompacted. Seven additional measurement were performed during the initial setup of this experiment using the Stainless Probe described in Section 8.3.2. The results are shown in the following figure:

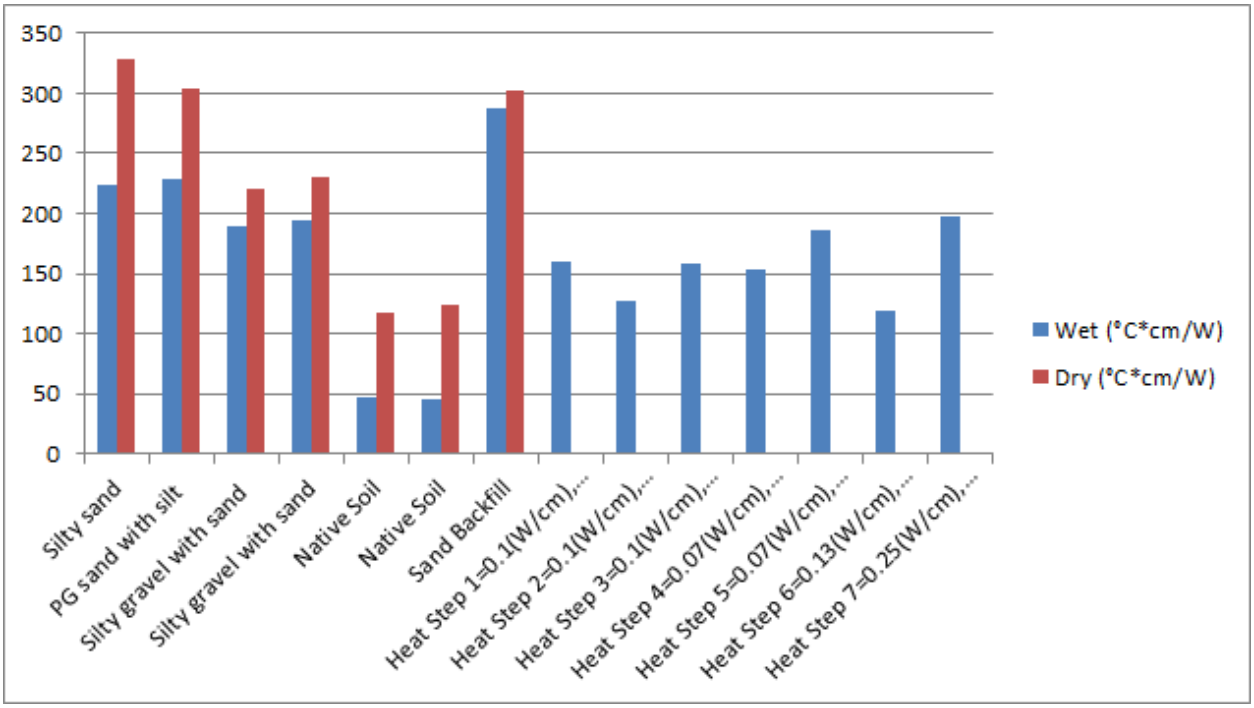

Figure 11.5 Thermal resistivity measurements column graph

Table 11.4 Site-specific wet and dry thermal resistivities

Date	Test Type	Description	Wet (°C·cm/W)	Dry (°C·cm/W)	Moisture Content (%)	Dry Density (lb/ft³)
1/19/2016	Lab	Silty sand	224	329	3	96
1/19/2016	Lab	PG sand with silt	229	304	2	109
1/19/2016	Lab	Silty gravel with sand	190	220	2	118
1/19/2016	Lab	Silty gravel with sand	195	230	2	117
5/20/2016	Lab	Native Soil	47	118	6	120
5/20/2016	Lab	Native Soil	46	124	8.1	119
9/30/2016	Lab	Sand Backfill	287	303	0.5	102
2/1/2017	In-situ	Heat Step 1=0.1(W/cm), total=0.1(W/cm)	160	N/A	unknown	unknown
2/1/2017	In-situ	Heat Step 2=0.1(W/cm), total=0.2(W/cm)	127	N/A	unknown	unknown
2/1/2017	In-situ	Heat Step 3=0.1(W/cm), total=0.3(W/cm)	159	N/A	unknown	unknown
2/1/2017	In-situ	Heat Step 4=0.07(W/cm), total=0.37(W/cm)	153	N/A	unknown	unknown
2/1/2017	In-situ	Heat Step 5=0.07(W/cm), total=0.45(W/cm)	187	N/A	unknown	unknown
2/1/2017	In-situ	Heat Step 6=0.13(W/cm), total=0.57(W/cm)	119	N/A	unknown	unknown
2/1/2017	In-situ	Heat Step 7=0.25(W/cm), total=0.82(W/cm)	197	N/A	unknown	unknown

The values vary significantly, ranging from 46 to 329°C·cm/W. Generally, using the in-situ measurements is the best practice because they represent the most likely operating condition after the installation is complete. The lab values are helpful to provide some adjustment to the in-situ value. Typically, this involves adjustment for moisture content and compaction. These two parameters have a large impact on the resistivity. In this case, the in-situ tests did not include measurement of the moisture content or compaction. However, the geotechnical report indicates the moisture content ranged from 2% to 3% on measurements performed in December 2011. In-situ testing was done in February 2017, and it was assumed that the moisture content of 3% in December was the same in February. Even though the measured resistivity values were much lower, the design engineer used the highest soil resistivity for sizing the cable: a fully dried and minimally compacted soil.

Compaction and moisture content must be determined before selecting a thermal resistivity for use in ampacity calculations. A standard compaction for utility or industrial installations is 85% to 95% of Standard Proctor. This range is primarily determined by the cost of installation with lower compaction requiring less effort and lower cost. Higher compaction reduces the soil thermal resistivity. Commonly, the soil is compacted not for thermal resistivity but to provide a harder surface for vehicular traffic or additional construction above the cables. If vehicle traffic or construction above the cable is not expected, a compaction of 85% of Standard Proctor may allow for better revegetation [87]. Regardless of the amount of compaction, it is common to backfill the cable in one-foot lifts (increments), compacting between lifts using a vibratory or tamping foot compactor. Specifying a higher level of soil compaction for the cable backfill—such as 90% of Standard Proctor—reduces the soil resistivity, allowing the designer to use smaller conductor sizes. Moisture content cannot be specified since it is controlled by site conditions. The soil moisture content should be measured at the project site. If it cannot be measured, soil moisture data is available from various sources on the Internet. This data can assist the designer in determining the minimum moisture content. One source of this data is Soil Climate Analysis Network (SCAN) from USDA's National Resource Conservation Service (NRCS) [30]. If limited data is available, a moisture content of 2% provides a sufficiently conservative design.

11.3 Design Analysis

The design engineer selected the following values for the software program used to perform the Neher-McGrath calculations:

- Soil thermal resistivity = 270°C·cm/W (based on the average of the four thermal resistivities measurements, all at 0% moisture content)
- Ambient soil temperature = 29°C
- Load factor = 53% (based on calculations from PVsyst [83] and measured data from similar projects)
- Conductor temperature limit = 75°C (based on the DC Combiner Junction Boxes terminal temperature, NEC 110.14(C)(1) [1])

A single cable ampacity was used in the design and was determined based on the cable section with the highest temperature. Often, a cable is routed through various environments that consist of different burial depths, number of adjacent cables, ambient temperatures, and soil thermal resistivities. The engineer may choose to calculate the ampacity for every condition along the cable route for every cable, but this is extremely laborious. Alternatively, the engineer limits the number of cable sections to model and considers only the “worst case scenarios” when determining the ampacity.

For this PV plant, one section involved 13 combiner box “home runs” in parallel with another 11 combiner box “home runs” as the cable routes approached the inverter. The physical spacing between parallel circuits is determined by numerous factors such as: installation costs, available area, cable size, and calculated ampacity. The cables were modeled with the spacing shown in the following figure.

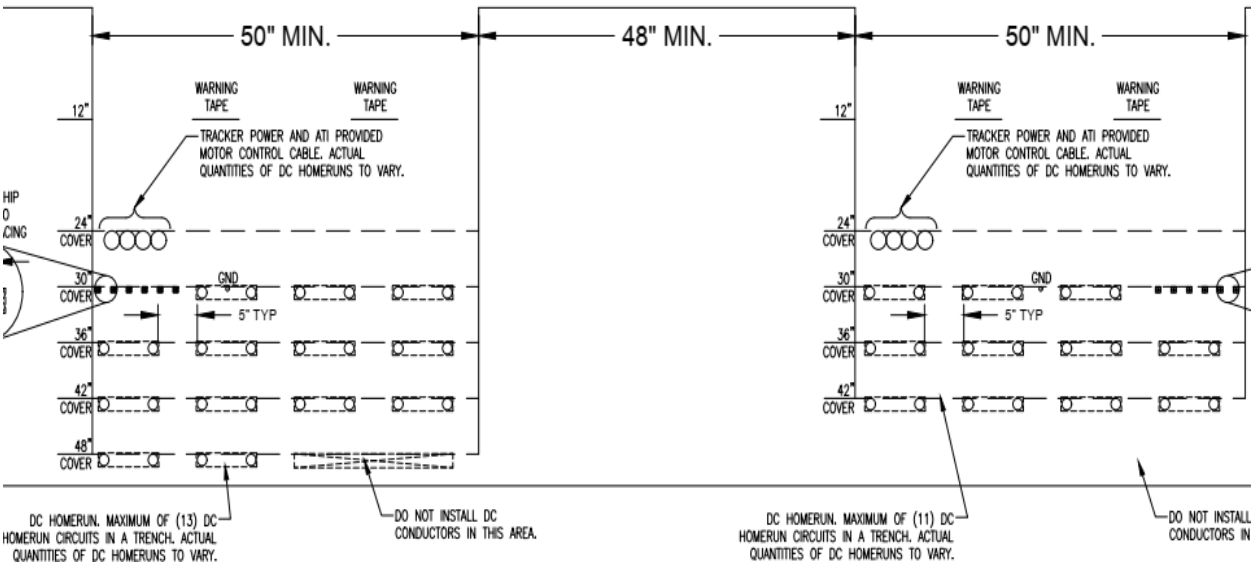

Figure 11.6 DC Combiner circuit section detail

The current in each cable was determined based on the maximum power point current multiplied by 125%. The analysis was performed using commercially available software (AmpCalc). This software utilizes the Neher-McGrath method to determine the conductor temperature for each cable. The results are given in the following table.

Table 11.5 Software calculation results

Trench (separated by 48”)	Number of Circuits	Maximum Cable Temperature	Current
1	13	75°C	220A
2	11	73°C	220A

During the construction of the PV plant, a backfill material was proposed with a dry thermal resistivity that exceeded the modeled thermal resistivity. Backfill material is often selected based on its proximity to the project location. The electrical engineer was called upon to perform the ampacity study based on this proposed backfill. The software model was updated with the backfill thermal resistivity at 0% moisture content (303°C·cm/W). The cable currents were also refined based on the exact number of PV module strings rather than an average for the plant. Some cables in the model increased in current while others decreased, depending on the number of PV module strings. As the ampacity analysis was performed, it was clear the increased soil resistivity posed a problem, so the design engineer proposed moving the routing of two circuits to reduce the cable temperatures. The results are given in the following table.

Table 11.6 Software calculation results with updated backfill resistivity

Trench (separated by 48”)	Number of Circuits	Maximum Cable Temperature	Current
1	11	87°C	258A
2	11	86°C	258A

With the proposed backfill, the software results predicted that the cable temperatures would exceed the design limit of 75°C. Nevertheless, construction moved forward with the intent of measuring the final cable temperatures.

11.4 Temperature Measurement

Temperature sensors were installed on the cables and the backfill was placed in four-inch lifts with manual compaction. After installation and compaction, the solar plant was operated normally, and the temperatures were measured. Installation was completed in February 2017 and measurements from the hottest part of the year, June 24 through August 25, are shown in the following figures. The first figure is from Logger 1, which measures temperatures at locations similar to the software model. The second is from Logger 2, which measures temperatures of the deepest cables (about 5 feet deep, sloping up to 3 feet over a distance of 10 feet).

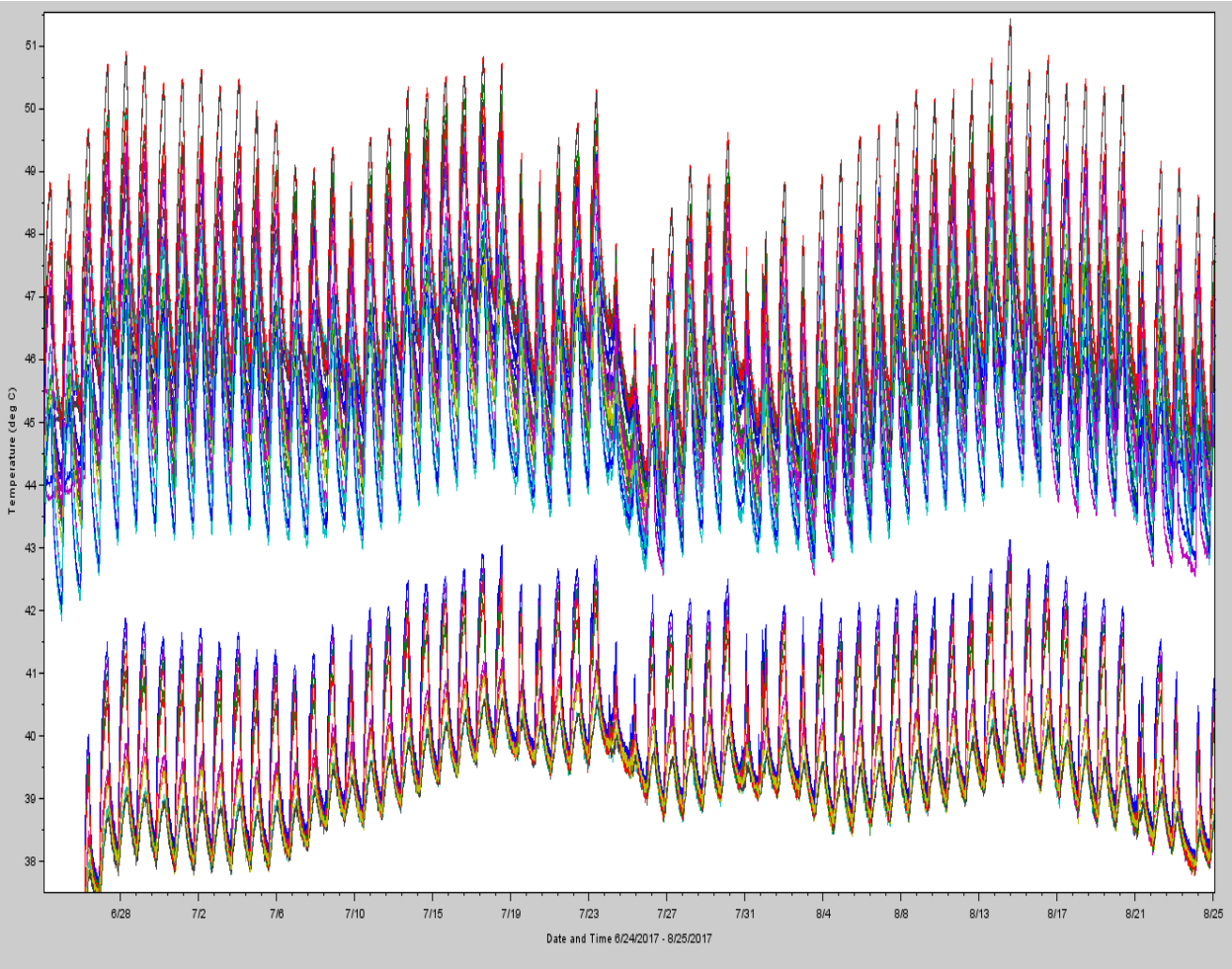

Figure 11.7 Logger 1 cable temperatures from 6/24 to 8/25

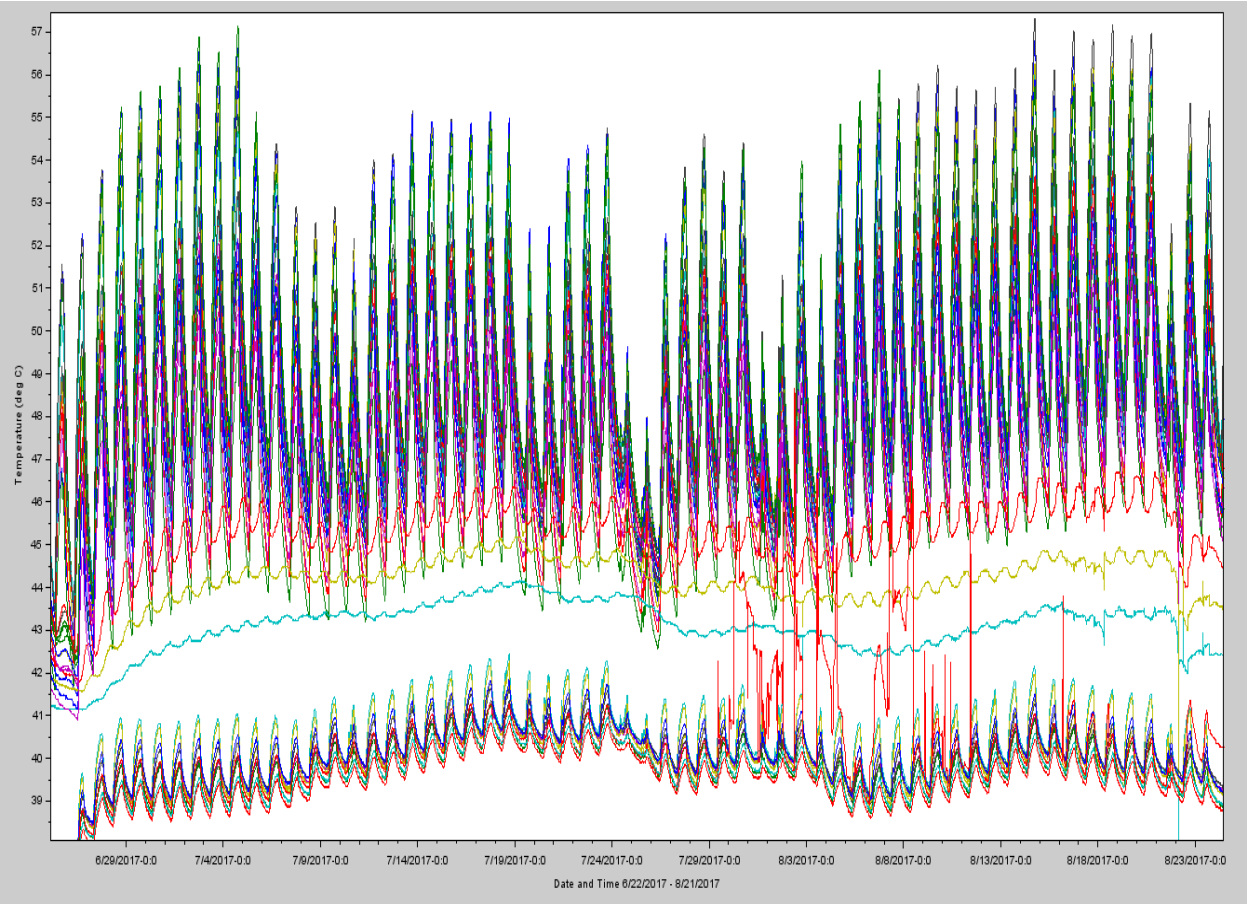

Figure 11.8 Logger 2 cable temperatures from 6/22 to 8/21

Since the temperature sensors were placed on the cable jacket, Fourier's Law was used to determine the conductor temperature across the jacket thermal resistance. The conductor temperature is equal to: $T_c=T_j+I^2R\cdot\rho_j\cdot\ln(r_j/r_c)/(2\pi)$ where $R=8.60\cdot10^{-7}$ Ω/cm (53°C Al), ρ_j=350°C·cm/W, r_c=0.908" (750 kcmil compact), r_j=1.178" (2kV XLPE). The maximum of the measured temperatures over 12 months are listed in the following table:

Table 11.7 Maximum of the measured temperatures

Logger	# of Circuits – separation - # Circuits	Current	Maximum Jacket Temperature	Maximum Conductor Temperature
1 (similar to software)	11 - 48" gap - 11	210A	51.4°C	54.9°C
2 (deeper & closer)	12 - 9" gap - 12	208A	57.3°C	60.7°C

The following table compares the results of the software model, using both values of soil resistivity, with the measurements:

Table 11.8 Software calculated versus measured temperatures

	Maximum Cable Temperature	Current
Software Rho 270	75°C	220A
Software Rho 303	87°C	258A
Logger 1	54.9°C	210A
Logger 2	60.7°C	208A

Clearly, the measurements are lower than either of the software model results. The current is slightly lower for the measurements than for the software model, but this doesn't explain the large difference in maximum temperature. Several other parameters could contribute to this difference: soil thermal resistivity, ambient soil temperature, cable spacing, or load factor. Each of these parameters is discussed in the following paragraphs.

The soil thermal resistivity was measured on-site during the installation of the measurement equipment. The resistivity measurements were significantly lower than the values used for the software model. The mean of the measured values was equal to 157°C·cm/W with a 99% confidence interval of 118 to 197°C·cm/W. Since the in-situ measurements were taken at a single location, the measurements do not account for site variability. The moisture content was not measured during the in-situ testing. Since the measurements were taken in February, it is expected this represents a low moisture content due to lack of rainfall during the winter months. Considering all of this, the upper limit of the 99% confidence interval, 197°C·cm/W, is lower than either of the resistivities used in the design calculations (270°C·cm/W and 303°C·cm/W). This is the most likely explanation for the difference between the maximum measured temperature and the calculated maximum temperature.

The ambient soil temperature was not measured at site. The closest measurement that could be considered ambient was the sensor located 18" above the top of the cables for data logger 2. It seemed to vary with cable current rather than accurately measuring ambient temperature but was suggestive of the maximum possible ambient temperature at the site. The measurements from this sensor for the hottest day are shown in the following figure:

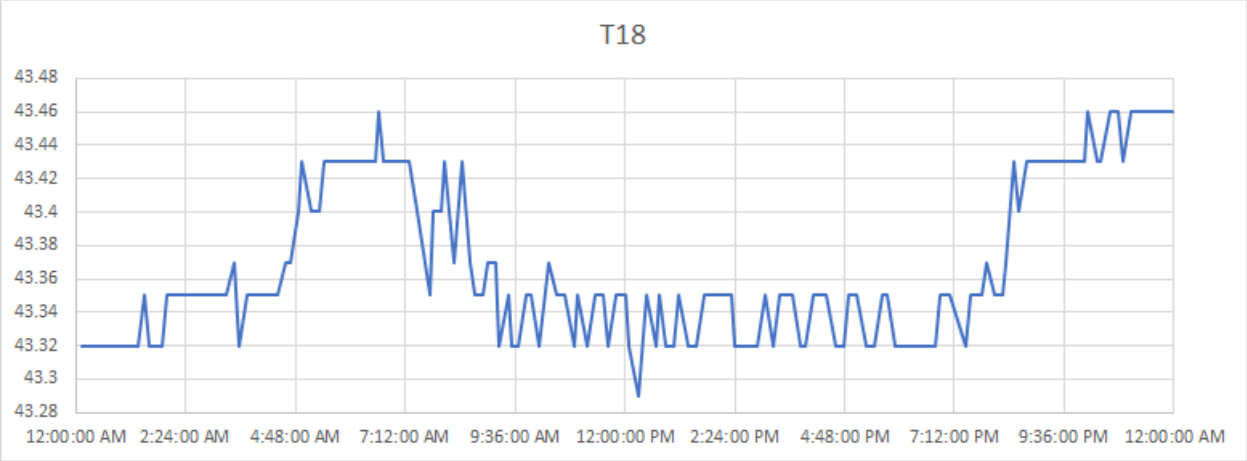

Figure 11.9 Suggestive soil ambient temperature on the hottest day

The measurements suggest a maximum temperature of 43.46°C. One common method for estimating the maximum temperature of the site is to use nearby SCAN data from the NRCS [30]. The nearest recording site to the installation site is recording station 2185, named Essex, and located in San Bernardino County, CA. The site has been recording data since 2012. Data from 2012 to 2017 was compiled and analyzed for the maximum temperature and minimum moisture content. The following figures are the summary of this data analysis:

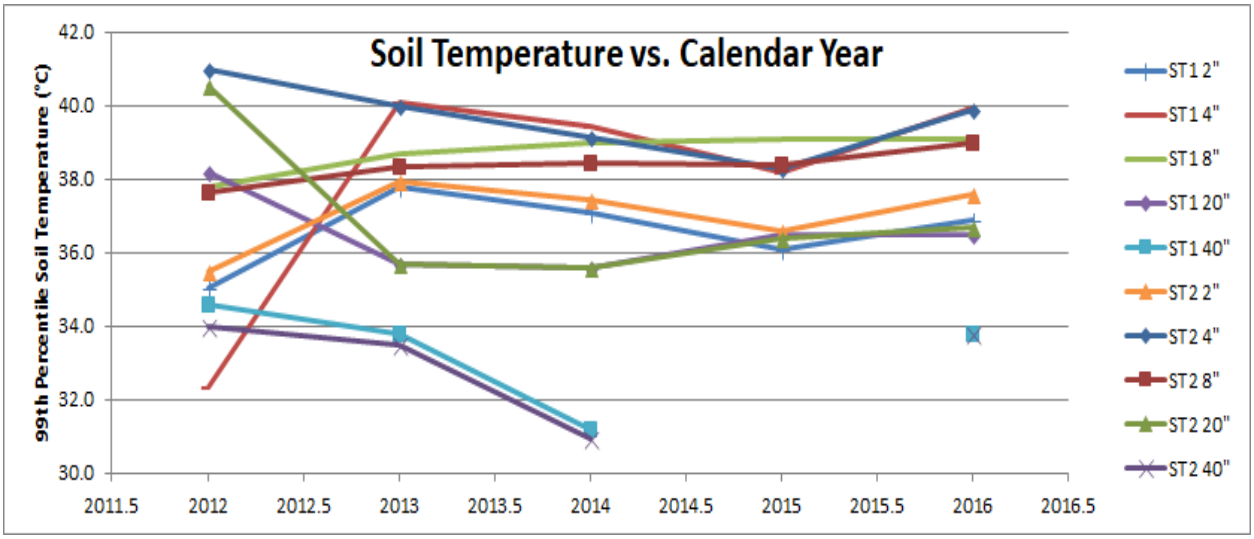

Figure 11.10 Historical maximum soil temperature at five depths

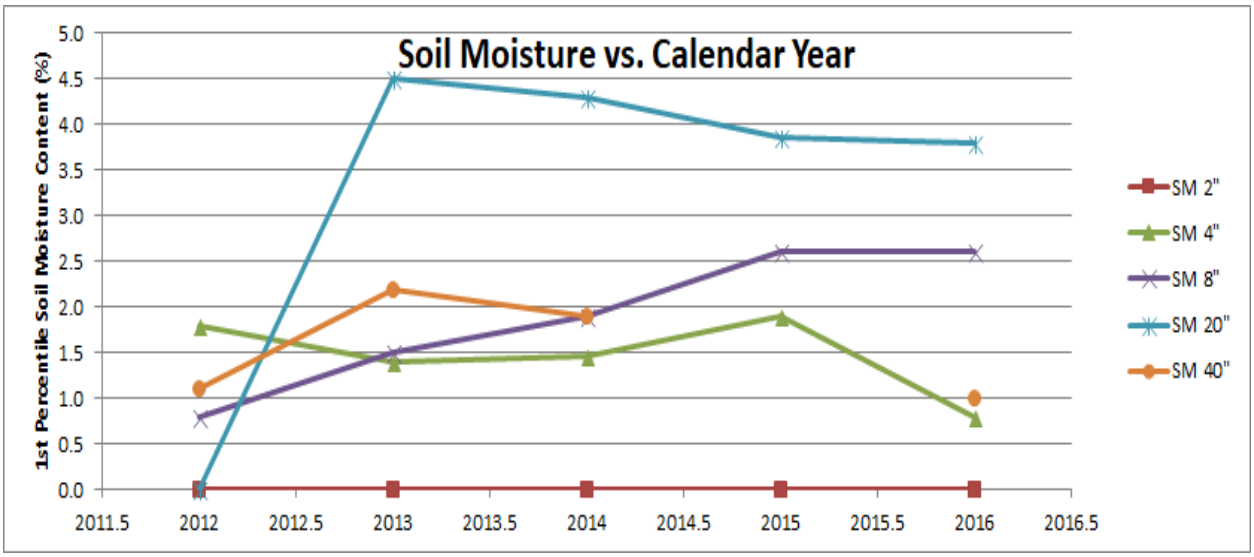

Figure 11.11 Historical maximum soil moisture content at five depths

“ST” stands for Soil Temperature, and “SM” stands for Soil Moisture. Both prefixes are followed by the soil depth in inches where the measurement was made as listed in the legends of the graphs.

The primary value of interest is the maximum temperature near the depth of the installed cables, which is 40” since the middle of the trench is approximately 36” below grade. When modeling cable ampacity, the design must account for the highest temperature at the lowest moisture content, because it is associated with the highest thermal resistivity/ambient temperature combination of the soil. From the SCAN site data, the highest yearly 99th percentile soil temperature is 34.6°C and the lowest yearly 1st percentile moisture content is 1%. To summarize, the maximum measured temperature 18” above the cables is 43.5°C, the maximum temperature from a nearby SCAN site is 34.6°C, and the software modeled temperature is 29°C. Since the modeled ambient temperature was less than the actual ambient temperature, the resulting cable temperature should have been greater than the calculated temperature. The cable temperature was not greater, so the ambient temperature cannot be the reason for the discrepancy between the measured and calculated cable temperatures.

Cable spacing could also explain the difference between the measured temperature and the calculated temperature. The spacing between cables and between circuits is specified by the engineer in the form of drawing details. These details are used during construction by the tradesperson. It is difficult to maintain the specified cable spacing in direct-buried cable installations since the tradesperson must visually place the cables and avoid disturbing their spacing while backfilling. Installations in conduit or duct banks reduce the variability in cable

spacing. The project utilized direct-buried cable, and the spacing deviated from the design by more than the expected tolerance of two inches. This is shown in the following figure:

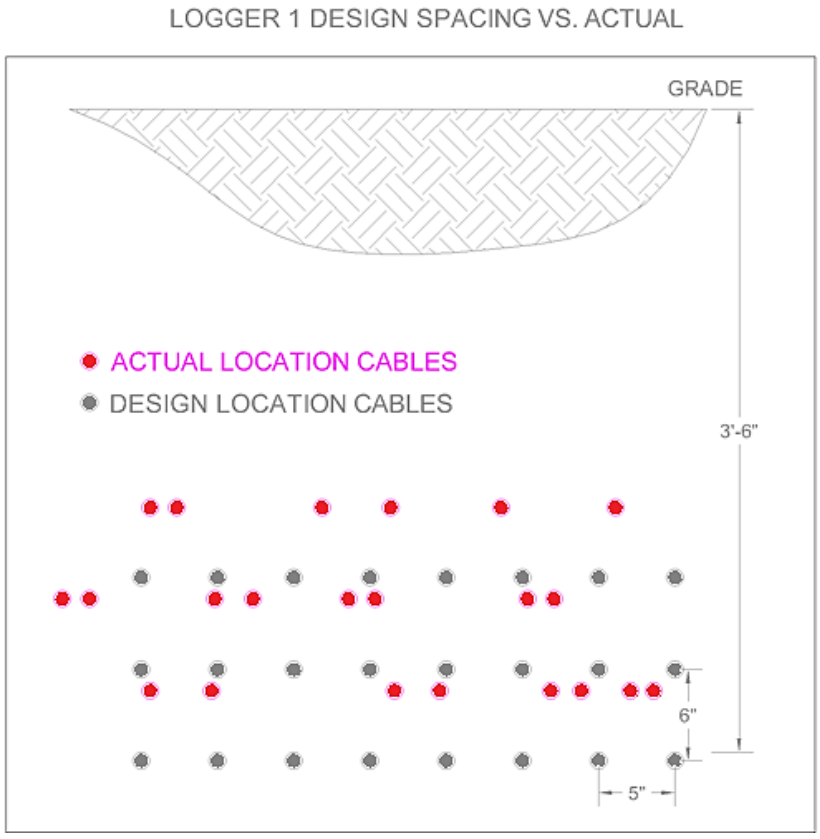

Figure 11.12 Specified cable spacing versus installed location

The installed depth was shallower than the designed depth. This will result in lower temperatures than expected. The spacing was not consistent—some cables were closer than five inches and others were farther. Many cables of the same DC circuit have a spacing of only two-inches. Additionally, the center cables are closer than the specified spacing. It is expected that the net result of the spacing discrepancies would be higher operating temperatures than calculated. Since these installation deviations counteract each other in temperature effects, it is difficult to determine whether the resulting temperature will be higher or lower than the calculated temperature. The assumed result is neutral. Neither a higher nor lower temperature should result from these deviations that occurred during installation.

Regardless of the net temperature impact resulting from these deviations, the installation practices can result in a final installation that varies from the engineer's design. This possibility should be evaluated by the design engineer. It may be prudent to evaluate the installation at a

more conservative condition, such as closer spacing and deeper burial depth, than the specified installation. Any critical spacing should be emphasized to the installer.

Load factor is another parameter that could result in differences between the measured and the expected cable temperature. Its impact is nonlinear, so an exact ratio between load factor and ampacity is not possible. However, ampacity is more sensitive to soil resistivity when using lower load factors. That is, an increase in soil resistivity at 100% load factor affects the ampacity less than the equivalent increase in soil resistivity at 50% load factor. The design load factor is 53% based on PVsyst analysis and measured data from similar projects. The actual load factor can be calculated for the experimental data by dividing the average current by the maximum current for a given period. The daily and weekly load factors are shown in the following figure. The number of daylight hours divided by 24 hours is also shown. The daylight hours are calculated based on the latitude and day of the year.

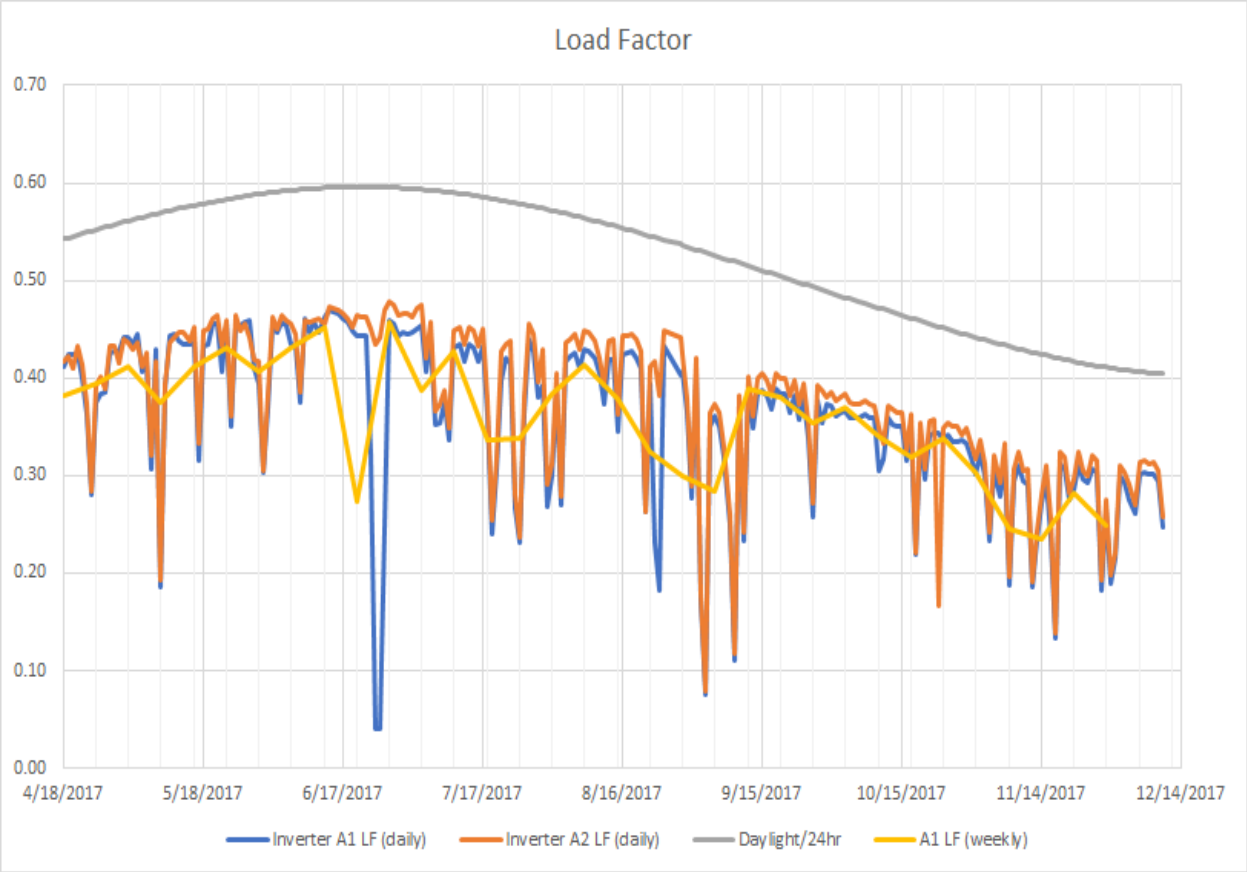

Figure 11.13 Measured daily and weekly load factor

The measured data indicates a maximum daily load factor of 48% and weekly load factor of 46%. This is 10% less than the design load factor. The expected operating temperature should be correspondingly lower.

11.5 Conclusion

In summary, the installation differed from the design parameters. The following table compares the differences and predicts the impact on cable temperature.

Table 11.9 Installation differences and their impact on temperature

Parameter	Design	Measured	Temperature Impact from Design to Measured
Soil thermal resistivity	270 and 303°C·cm/W	197°C·cm/W	Lower
Ambient soil temperature	29°C	34.6°C	Higher
Cable spacing	5” horizontal, 6” vertical	Varies from 2” to 12”	Neutral
Load factor	53%	48%	Lower

The measured temperature is lower than the calculated temperature, so it is clear that the differences between the design parameters and the actual site conditions resulted in a net impact of lower cable temperatures. The design engineer did not include any additional safety factors or design margins. Had he done so, there would have been an even greater over-estimation of temperature and over-sizing of the cables, resulting in unnecessary expense. It appears that the Neher-McGrath method provides an already conservative design and does not require additional safety factors or design margins.

The original design analysis indicated the cables would operate near their temperature rating. Following that, backfill soil with a soil resistivity higher than the original design was installed. Ampacity calculations using this higher soil resistivity predicted operation above the temperature rating of the cables. The measurements revealed that the actual operating temperature was much lower than the temperature calculated using the Neher-McGrath method.

CHAPTER 12
CONCLUSIONS & RECOMMENDATIONS

The purpose of this work is to investigate underground cable ampacity calculation methodology with a focus on the surrounding soil. The motivation of this work comes from personal difficulty in determining the value of soil resistivity for calculating cable ampacity. Currently, there are standard values for the details of the cable type and installation geometry. The soil properties, however, are far from standard and vary based on location and time of year. There is no clear industry standard, and there is significant misunderstanding of soil properties. One engineer may choose a value for soil resistivity that results in a cable that is ⅓ the size of a cable specified by another engineer and both may have justification for their analysis. The goal of this research is to address these topics with experiments and analyses.

The first 3 chapters provide the background and compare the existing options for determining cable ampacity. Chapter 4 provides a new method for addressing the difficulty of soil thermal stability, i.e. soil dry-out, by supplementing the existing methods. Chapter 5 examines software packages that assist with determining cable ampacity. Chapter 6 addresses the issue of soil dry-out related to time. Experiments and a case study were performed to compare the calculations of cable ampacity with measured values in the remaining chapters.

12.1 Chapter Summaries

Chapter 1 Introduction to Cable Ampacity provides an historical overview of cable ampacity. It's clear that underground power cables have been studied for over 100 years. Despite this long history, there is still misapplication of the equations in calculating ampacity. The principles of ampacity are provided to define the problem. The failure modes of underground power cables are briefly addressed to illustrate the need for properly determining ampacity.

Chapter 2 Ampacity Calculation Methods provides details of the cable ampacity method that is commonly used. Ampacity is a problem of heat generation and thermal resistance. Reducing either will increase the cable ampacity. Reviewing these details illustrates that many parameters are a function of material properties that are not easily adjusted. The largest parameter for most designs is the soil around the cable, not the cable itself. Commonly, the soil thermal resistance is more than half of the total conductor to ambient resistance, and soil thermal resistivity is the most variable resistivity in the thermal circuit. For these reasons, it is important to accurately characterize the soil thermal properties in order to determine the cable ampacity. The difficulty in selecting the soil thermal resistivity as a result of the soil thermal

stability is illustrated through an example. This concept is developed further in the remainder of the dissertation.

Chapter 3 Standard Industry Practice describes various methods that are currently used to determine cable ampacity. An example cable ampacity study is used to compare the methods. The results illustrate that the different methods yield significant differences that have cost implications—about 25% increase or a $2 million increase for a typical wind farm. While it is possible to select cables out of the ampacity tables, the user should understand the underlying assumptions. The table-selected cable will not be optimized for the design, so either the cost or reliability will be impacted. This may be acceptable for shorter or smaller cables because the cost of a larger cable or the cost of replacing an undersized cable is low. However, the time spent on performing the calculations with a more detailed method is beneficial for longer or larger cables.

Chapter 4 Ampacity Calculation Method Including Soil Thermal Stability introduces a method for addressing soil thermal stability in ampacity calculations. The water transportation within soil is examined as it relates to the underground power cable as a heat source. A new parameter is introduced called the non-drying heat rate (NHR). The NHR is the heat rate where the water repelled from the cable due to cable heating is equal to the water attracted to the cable due to the hydraulic gradient. Using the equations for the driving potential of water, it is possible to calculate an effective dried soil area. In addition, it is proposed that soil dry-out will not occur if the expected cable heat rate is less than non-drying heat rate. The ampacity calculation does not need to include a dry soil layer but can use the thermal resistivity at the minimum moisture content independent of cable heating. This results in favorable ampacity results. If the cable heat rate is greater than the non-drying heat rate, the amount of equivalent dried area can be calculated and used in the design. The additional thermal resistance due to the dried area is added to the traditional Neher-McGrath method.

Soil thermal stability, the metric for soil dry-out and thermal runaway, is a concern for an engineer performing ampacity calculations. Some engineers mitigate the risk of soil thermal instability by assuming an arbitrarily large dried soil area around the cables. The size of the area is based on engineering judgement. More critical cables may assume a larger dried area based on the risk, not on any calculation or metric. Other engineers use an increased value from the measured thermal resistivity based on intuition. Many do not consider thermal stability due to lack of ability to characterize its impact or lack of knowledge. Using the method presented in Chapter 4, an engineer can quantitatively address the risk of soil dry-out.

Though thermal stability is not addressed in commonly used standards in the United States, such as IEEE, it is addressed by IEC 60287-1. This standard uses a critical temperature rise as the metric for determining the extent of soil drying. The difficulty in using the critical temperature rise of a soil is the difficulty in measuring it. As with thermal resistivity, the critical temperature varies for different types of soil, so it must be measured at the cable installation location. According to Anders, “Determination of the temperature, and, hence, the position of the critical isotherm, is a complicated matter, but examples of theoretical and experimental derivations are given in the literature (Donnazi et al., 1979; Brakelmann, 1984; Groeneveld et al., 1984; Black et al., 1932)” [14]. Anders follows this quote by providing an example of how to determine the critical temperature rise using critical degree of saturation and a migration parameter. He then states, “In closing this section, we would like to point out that the crucial assumption used in the above developments, that the critical temperature rise is independent of the heat flux at the surface of the cable, may not be valid when the soil becomes thermally unstable. In fact, developments presented by Hartley and Black (1982) suggest that the heat flux at the surface of the cable is an important factor in determining the time required for a soil to become unstable” [14]. This statement is consistent with the original development of the critical temperature rise that states, “Until further information is available, it is proposed in this report to use a simple temperature rise above ground ambient as the critical factor” [31]. Additional information is available to address soil thermal stability in this dissertation and other works [62] [32] [88].

Chapter 5 Software Modeling Tools reviews some common software packages used for determining cable ampacity. Most are based on the Neher-McGrath method. CYMCAP includes some extensions to the Neher-McGrath method including the IEC 60287-1 critical temperature rise. It also includes a finite element method for calculation of multiple duct banks. CYMCAP has been developed over many years to perform ampacity calculations, and the number of features beyond other commercially available software is evidence of this. The other software packages provide standard features for ampacity calculations. ETAP provides an integrated solution with other power system design such as power flow simulations. USAmp Prime provides a focused and detailed ampacity calculation for a reduced price compared to CYMCAP. ANSYS allows for the most detailed simulations but requires significant data entry since it is not customized for ampacity calculations.

Chapter 6 Soil Thermal Stability investigates the details of soil moisture theory and the impact on soil resistivity. A method for correlating the time to dry for a laboratory probe test to a cable installation, called the “Law of Times,” is experimentally tested. The results show that the

“Law of Times” is not the proper ratio. However, the results do indicate some correlation between the probe diameter and the time to dry. All the results are based on laboratory tests, not cables installed in a trench. As described in the beginning of the chapter, soil thermal stability involves many factors. Many of these factors are not applicable in a smaller scale test performed in a laboratory. Therefore, an experiment is performed in Chapter 8 Experiments.

Chapter 7 Materials and Methods describes the apparatuses used for the experiment. The data logger setup provides a low-cost alternative to the more commonly used data loggers. More effort is required to use an Arduino as the microcontroller as opposed to a more integrated data logger such as a Campbell Scientific CR1000. However, the Arduino can be customized to meet the specific experimental requirements. It is possible to use this setup as a template for other experiments, particularly when cost is a major consideration. The selected apparatuses were analyzed for the expected uncertainty in the measurement. This analysis highlights the parts of the experiment that require a better instrument or attention to detail. In the case of this experiment, the largest error stems from the placement of the temperature sensors. So, extreme care was used when placing them.

Chapter 8 Site-Specific Data Collection describes the measurement of the site-specific data. This step should be performed for any cable ampacity study. Assuming a soil temperature or soil thermal resistivity will likely result in inaccurate ampacity results and at the very least results in larger uncertainty in the result. In-situ soil thermal resistivity measurements were made using multiple probes at various dates. The measured soil resistivities for this experiment vary throughout the year and based on the probe. Statistical analysis indicates the IEEE Std 442 “standard” probe and the METER Group Thermolink TR-3 probe measure the same resistivity within a 95% confidence interval. The “stainless” probe and the “lab” probe measure the same resistivity within a 95% confidence interval but higher than the measurement of the “standard” and TR-3 probes. Lab soil thermal resistivity measurements were made in addition to the in-situ measurements. Because of cost and simplicity, lab measurements are commonly used in ampacity studies as the only resistivity measurement. The results are similar between the lab tests and the in-situ tests.

While performing the in-situ thermal resistivity tests, the data was reviewed for increased resistivity after heating the soil. This would indicate soil drying and correlation with higher heat rates would determine the non-drying heat rate. The soil for this experiment did not show any drying for the tested heat rates. Typical heat rates for cables do not exceed 0.4 W/cm at diameters of 1 to 3 inches. The highest heat rate for the ⅝ inch diameter probe was 0.9 W/cm. Based on this, the soil will not dry due to cable heating.

Chapter 8 Site-Specific Data Collection also presents a novel technique for determining soil thermal resistivity: the Structure Function. This concept was developed by Vladimir Szekely for electronic packages [77] but is applied to cable heating for this work. The purpose of the Structure Function is to determine the thermal resistance and thermal capacitance of a system correlated with physical distance from the heat source. Discontinuities in the soil due to soil drying can be identified with the Structure Function. The results of the Structure Function analysis in Chapter 9 Experiments do not indicate any drying.

Chapter 9 Experiments presents the results of the experiment. The results were analyzed in two ways: comparison of the measured versus the calculated temperature and evaluation to determine if any soil drying occurred adjacent to the cable. Comparing measured temperatures with calculated temperatures consisted of several subparts. Calculations were performed using two different thermal resistivities with CYMCAP software and Neher-McGrath equations to compare with the measurements. Though the Neher-McGrath method is implemented in CYMCAP, references to Neher-McGrath refer to equations implemented in a spreadsheet.

Steady state calculations indicate the calculated values for the CYMCAP software and the Neher-McGrath method overestimate the temperature with an error of 8%±8.9% (mean and standard deviation) and 8%±7.2% respectively. Using the proposed sliding window resistivity instead of the transient line source resistivity yields a lower average error (-3% versus -8% for CYMCAP) but a higher standard deviation (11% versus 8.9%). Transient calculations for a duration of five days indicate the calculated values for the CYMCAP software match the measurements with an error of -0.5%±8.1% (mean and standard deviation). This indicates that using the transient calculation results in reduced error compared to the steady state calculation.

An additional calculation was performed using a load factor with the Neher-McGrath method to determine its impact. Using a load factor of 66% for a five-day continuous run reduces the mean error from -8% to -0.3% and the corresponding 90% confidence interval from (-14%,-2%) for 100% load factor to (-1.4%, 0.8%) for 66% load factor. Clearly, using a load factor results in reduced error.

The second experimental analysis examined soil drying. This analysis consisted of three subparts. First, the resistance calculation using Fourier's Law indicated minor drying near the cable for the test on 10/9. The resistivity within the first inch of soil adjacent to the cable was calculated at 181 ± 37°C·cm/W whereas the resistivity within the first 5 inches was calculated at 151 ± 15°C·cm/W. Second, the resistance calculation using the transient line source method indicated possible drying for the test on 10/9, but the tests on 7/4, 7/15, and 7/28 did not show

any drying. Third, the resistance calculation using the Structure Function did not show any drying. Based on this analysis, drying is considered negligible for the experiments. This matches the prediction of the non-drying heat rate in Sections 8.5 Non-Drying Heat Rate Measurement.

Chapter 10 Software Modeling describes the modeling assumptions and results of CYMCAP, ETAP, USAmp Prime, and ANSYS software. CYMCAP and ETAP yielded similar results and compared well with the experimental results. Using software designed for cable ampacity appears to be the best option rather than using a full-finite element analysis software such as ANSYS. In addition, it is more likely to make a mistake in modeling using a full FEA software program. This modeling was relatively simple compared to most ampacity projects that involve numerous cables and cross sections. However, ANSYS may be useful for small cable segments involving complex boundary conditions that are not easily addressed by cable ampacity software.

Chapter 11 Solar PV Power Plant Case Study is a specific example of the cable design process. It illustrates how the project schedule and limited information cause difficulty in determining cable ampacity. Though the operating temperatures were anticipated to be above the maximum permissible temperature, the actual measurements were well under this temperature. It appears that the Neher-McGrath method provides an already conservative design and does not require additional safety factors or design margins. The case study also reveals how installation practices can result in a final installation that varies from the engineer's design. This possibility should be evaluated by the design engineer. It may be prudent to evaluate the installation at a more conservative condition, such as closer spacing and deeper burial depth, than the specified installation. Any critical spacing should be emphasized to the installer.

12.2 Contributions

This dissertation provides analytical, experimental, and operational test results for underground cables. Publicly available cable temperature measurements and associated comparisons with ampacity methods are scarce—six experiments were performed to alleviate this. In addition, rigorous analysis of cable ampacities at three different soil thermal resistivities is provided. The results show that the Neher-McGrath method overestimates cable temperature. This contribution assists engineers in evaluating how to select the soil thermal resistivity for use in cable ampacity calculations.

This dissertation also investigates soil thermal stability. Experimental results show that the soil did not dry out around the cable at three heat rates run for at least five days. A

theoretical method is proposed to address soil thermal stability using the non-drying heat rate. This method did not predict drying for the experiments, which agreed with the measurements. This work proposes a method to measure and account for soil thermal stability.

12.3 Recommendations

Underground power cables are designed and used according to external factors. They provide the connection between the source and the load. If the cable fails, due to overheating or other factors, the load no longer operates. Some loads require high reliability. Designing a cable system for such a load should be based on the best information available and utilize methods that reduce risks. One aspect of the design involves determining the cable size or cable ampacity. The recommended approach is:

1. Determine the in-situ soil thermal resistivity 90% confidence interval using in-situ measurements at multiple locations along the cable route processed using statistical analysis. IEEE Std 442 provides the details on measuring soil thermal resistivity [27]. The frequency should be determined by the desired results from the statistical analysis and expected geological features along the route. One study measured the resistivity every 20 meters [59].
2. Measure the soil moisture content and soil density at the same time in-situ soil thermal resistivity measurements are made (step 1). Collect soil samples for laboratory thermal resistivity testing (step 5).
3. Determine the 99th percentile of soil temperature and the 1st percentile soil moisture content at the cable burial depth by statistically analyzing several years of data at or near the cable route. Data may be obtained using NRCS SCAN sites [30].
4. Determine the extent, if any, soil drying that may occur. This can be calculated by measuring the non-drying heat rate described in Chapter 4 and in [54].
5. Determine the soil dry-out curve, i.e. soil thermal resistivity versus moisture content. Compute the ratio of the thermal resistivity at the 1st percentile moisture content (step 3) over the resistivity at the in-situ moisture content (step 2). Multiply the upper limit of the 90% confidence interval of the in-situ soil thermal resistivity (step 1) by this ratio. This is defined as the modeled soil resistivity.
6. Model the cable installation details based on a cable manufacturer data sheet. Use the 99th percentile of soil temperature (step 3) for the soil temperature and the modeled soil resistivity (step 5). If the cable heat rate exceeds the non-drying

heat rate, determine the dried soil radius, add the layer to the ampacity model using the dried soil resistivity from the dry-out curve (step 5), and re-run the ampacity calculation. If the cable heat rate changes significantly, the dried soil radius can be adjusted, and the ampacity can be recalculated iteratively until the heat rate converges.

If the cable route consists of different burial depths, ambient soil temperatures, moisture contents, external heat sources, or different cable installation details, it may be beneficial to break the ampacity calculation into segments of the cable route. This will provide the results necessary to determine the controlling segment. It has been shown that a change in soil conditions can have an impact of 5-10% on the cable ampacity within 5 times the length to conduit diameter ratio (for a cable installed in conduit) and achieves a fixed derating value of 5-20% within 15 times the length to conduit diameter ratio [60].

IEEE has published numerous guides for performing electrical studies for the power system, but there is not a guide for performing ampacity calculations that addresses soil thermal stability. IEEE Std 835 [11] is the closest standard to an ampacity calculation guide, but its primary purpose is the ampacity tables. It does not address the considerations an engineer must make such as selecting a thermal resistivity from numerous tests or even how to specify such tests. Publishing a guide would reduce confusion and variability in designs such as is demonstrated in Chapter 11. This dissertation is proposed as a basis to such a guide.

12.4 Future Work

There are several areas that can be investigated as future work. One area to continue research is the soil time constant and the impact on maximum cable temperature. The analysis in Section 9.1.3 Load Factor revealed that it is beneficial to consider load factor, traditionally applied based on number of hours operating in a 24-hour day, over multiple days. Wind generation sites commonly use a load factor of 100% since it is possible for the wind to blow for 24 hours. Since soil time constants are longer than one day, additional studies should be performed to determine how to handle multiple-day events that do not reach steady state temperature. Transient analysis appears to be a reasonable solution based on Section 9.1.2 Transient. Some analysis has been done in [25].

Performing the soil resistivity measurements for this dissertation revealed the need for additional studies comparing soil thermal resistivity measurements and probe sizes. Small probes are commonly used in industry rather than larger standard IEEE Std 442 field probes. Additional experimentation could be performed evaluating the smaller probe in a variety of soil

types. It is suspected that the small probes will be more sensitive to any large rocks in the vicinity of the probe than the larger probes. This may be remedied by performing more measurements and removing outliers.

Future work could investigate an ampacity method using multiple soil layers similar to how multiple layers are used in ground grid design. Many soils have multiple layers that could result in different soil thermal resistivity layers. Though the depth of influence for thermal analysis is much less than for electric ground current analysis, it is possible this could have an impact on the calculated ampacity.

REFERENCES CITED

[1] National Fire Protection Association, *NFPA 70 National Electrical Code 2014*. 2013.

[2] A. E. Kennelly and E. R. Shepard, “The Heating of Copper Wires by Electric Currents,” *Transactions of the American Institute of Electrical Engineers*, vol. XXVI, no. 2, pp. 969–995, 1907.

[3] C. Holyk and G. J. Anders, “Power Cable Rating Calculations - A Historical Perspective [History],” *IEEE Ind. Appl. Mag.*, vol. 21, no. 4, pp. 6–64, 2015.

[4] A. E. Kennelly, “On the carrying capacity of electric cables, submerged, buried or suspended in air,” *Proc. Minutes 9th Annual Meeting Association Edison Illuminating Companies*, pp. 79–92, 1893.

[5] D. M. Simons, “Cable geometry and the calculation of current-carrying capacity,” *Journal of the American Institute of Electrical Engineers*, vol. 42, no. 5, pp. 525–539, 1923.

[6] S. W. Melsom and H. C. Booth, “The rating of cables for intermittent or fluctuating loads,” *Journal of the Institution of Electrical Engineers*, vol. 61, no. 316, pp. 363–368, 1923.

[7] S. Whitehead and E. E. Hutchings, “Current rating of cables for transmission and distribution,” *Journal of the Institution of Electrical Engineers*, vol. 83, no. 502, pp. 517–557, 1938.

[8] J. H. Neher and M. H. McGrath, “The calculation of the temperature rise and load capability of cable systems,” *Transactions of the American Institute of Electrical Engineers. Part III: Power Apparatus and Systems*, vol. 76, no. 3, pp. 752–764, 1957.

[9] D. M. Simmons, *Calculation of the Electrical Problems of Underground Cables*. The Electric Journal, 1932.

[10] J. H. Neher *et al.*, *Power cable ampacities*, vol. 81. IEEE, 1962.

[11] IEEE Std 835™-1994, “Standard Power Cable Ampacity Tables,” The Institute of Electrical and Electronics Engineers, 1994.

[12] G. J. Groeneveld, A. L. Snijders, G. Koopmans, and J. Vermeer, “Improved method to calculate the critical conditions for drying out sandy soils around power cables,” *IEE Proceedings C Generation, Transmission and Distribution*, vol. 131, no. 2, p. 42, 1984.

[13] IEC 60287-1, “Electric cables—Calculation of the current rating—Part 1: Current rating equations (100% load factor) and calculation of losses,” International Electrotechnical Commission, 2006.

[14] G. J. Anders, *Rating of Electric Power Cables: Ampacity Computations for Transmission, Distribution, and Industrial Applications*. McGraw Hill Professional, 1997.

[15] C. Bates, B. Carson, M. Keith, and C. David, “Cable Ampacity Calculations: A Comparison of Methods,” *IEEE Trans. Ind. Appl.*, vol. 52, no. 1, pp. 112–118, 2016.

[16] T. L. Bergman, F. P. Incropera, and A. S. Lavine, *Fundamentals of Heat and Mass Transfer*. John Wiley & Sons, 2011.

[17] T. Arnold and D. Mercier, Eds., *Southwire Power Cable Manual 3rd Edition*. Southwire, 2006.

[18] I. Sarajcev, M. Majstrovic, and I. Medic, “Calculation of losses in electric power cables as the base for cable temperature analysis,” *WIT Trans. Eng. Sci.*, vol. 27, 2000.

[19] IEEE Std™ 575-2014, “Guide for Bonding Shields and Sheaths of Single-Conductor Power Cables Rated 5 kV through 500 kV,” The Institute of Electrical and Electronics Engineers, 2014.

[20] W. Thue, Ed., *Electrical Power Cable Engineering, Third Edition*. CRC Press, 2011.

[21] R. Hartlein *et al.*, “Diagnostic testing of underground cable systems (Cable Diagnostic Focused Initiative),” NEETRAC at Georgia Institute of Technology, DOE Award No. DE-FC02-04CH11237, 2010.

[22] K. Summers, T. Popkiss, D. Frost, T. Czaskejko, “Cable System Failure Experience in Wind Farms,” in *AORC Technical Meeting*, 2014.

[23] M. A. Mozan, M. A. El-Kady, and A. A. Mazi, “Advanced thermal analysis of underground power cables,” in *Record of the Fifth International Middle East Power Conference MEPCON’97*, Alexandria, Egypt, 1997.

[24] G. C. Stevens, A. Pye, A. S. Vaughan, C. D. Green, and J. Pilgrim, “High performance thermoplastic cable insulation systems,” in *2016 IEEE International Conference on Dielectrics (ICD)*, 2016, vol. 1, pp. 272–275.

[25] “Cableizer - Blog post about ‘Cyclic loading with daily, weekly, and yearly load factors.’” [Online]. Available: https://www.cableizer.com/blog/post/cyclic-loading-daily-weekly-yearly-load-factors/. [Accessed: 18-Sep-2018].

[26] S. M. Sellers and W. Z. Black, “Refinements to the Neher-McGrath model for calculating the ampacity of underground cables,” *IEEE Trans. Power Delivery*, vol. 11, no. 1, pp. 12–30, 1996.

[27] IEEE Std™ 442-1981, “Guide for Soil Thermal Resistivity Measurements,” The Institute of Electrical and Electronics Engineers, 1981.

[28] K. Malmedal, C. Bates, and D. Cain, “The measurement of soil thermal stability, thermal resistivity, and underground cable ampacity,” in *2014 IEEE Rural Electric Power Conference (REPC)*, 2014, pp. C5–1–C5–12.

[29] O. Hyunjun, “Thermal Resistivity Dry-Out Curve for Thirteen Sandy Soils,” Master of Science, University of Wisconsin-Madison, 2014.

[30] “NRCS National Water and Climate Center - Soil Climate Analysis Network.” [Online]. Available: https://www.wcc.nrcs.usda.gov/scan/. [Accessed: 26-Oct-2018].

[31] Working Group 02 (Cable Ratings) of Study Committee 21 (HV Insulated Cables), “Current ratings of cables buried in partially dried-out soil Part 1,” in *Electra No. 104*, 1986, pp. 11–22.

[32] M. A. Martin, R. A. Bush, W. Z. Black, and J. G. Hartley, “Practical Aspects of Applying Soil Thermal Stability Measurements to the Rating of Underground Power Cables,” *IEEE Power Engineering Review*, vol. PER-1, no. 9, pp. 35–35, 1981.

[33] R. A. Hartlein, “Factors to Consider Before Operating Extruded Cables at Elevated Temperatures,” in *IEEE Insulated Conductors Committee 74th Meeting*, 1984, p. Appendix F–3.

[34] International Electrotechnical Commission, *IEC 60502-2: 1998. Power Cables with Extruded Insulation and Their Accessories for Rated Voltages from 1 KV (Um*. International Electrotechnical Commission, 1998.

[35] R. A. Bush, W. Z. Black, and M. A. Martin, “Soil Thermal Properties And Their Effect On Thermal Stability And The Rating Of Underground Power Cables,” in *Proc. 7th IEEE/PES Transmission and Distribution Conf. and Expo.*, 1979, pp. 275–280.

[36] ASTM D4643-08, “Standard Test Method for Determination of Water (Moisture) Content of Soil by Microwave Oven Heating,” ASTM International, West Conshohocken, PA, 2008.

[37] K. Malmedal, C. Bates, and D. K. Cain, “The Heat and Buried Cable Conundrum: A Method to Help Determine Underground Cable Ampacity,” *IEEE Ind. Appl. Mag.*, vol. 22, no. 5, pp. 20–31, 2016.

[38] V. V. Mason and M. Kurtz, “Rapid measurement of the thermal resistivity of soil,” *Transactions of the American Institute of Electrical Engineers. Part III: Power Apparatus and Systems*, vol. 71, no. 1, pp. 570–577, 1952.

[39] J. H. Neher, “The Temperature Rise of Buried Cables and Pipes,” *Transactions of the American Institute of Electrical Engineers*, vol. 68, no. 1, pp. 9–21, Jul. 1949.

[40] G. W. N. Fitzgerald and J. W. Newall, “Seasonal Variation in Soil Thermal Resistivity,” *Transactions of the American Institute of Electrical Engineers. Part III: Power Apparatus and Systems*, vol. 3, no. 79, pp. 892–897, 1960.

[41] J. W. Cary, “Soil Moisture Transport Due to Thermal Gradients: Practical Aspects,” *Soil Sci. Soc. Am. J.*, vol. 30, no. 4, pp. 428–433, 1966.

[42] S. H. Don, *Soil Physics*. Ames, IA: Iowa State University Press, 2000.

[43] A. S. Mickley, “The thermal movement of moisture in soil,” *Trans. Amer. Inst. Elect. Engineers*, vol. 68, no. 1, pp. 330–335, 1949.

[44] C. Liu and J. B. Evett, *Soils and Foundations, 4th ed*. Pearson/Prentice Hall, 1998.

[45] ASTM D2937-10, “Standard Test Method for Density of Soil in Place by the Driven-Cylinder Method,” ASTM International, West Conshohocken, PA, 2010.

[46] ASTM D1556-07, “Standard Test Method for Density and Unit Weight of Soil in Place by Sand-Cone Method,” ASTM International, West Conshohocken, PA, 2007.

[47] ASTM D7759-14, “Standard Guide for Nuclear Surface Moisture and Density Gauge Calibration,” ASTM International, West Conshohocken, PA, 2014.

[48] ASTM D2216-10, “Standard Test Methods for Laboratory Determination of Water (Moisture) Content of Soil and Rock by Mass,” ASTM International, West Conshohocken, PA, 2010.

[49] ASTM D4959-07, “Standard Test Method for Determination of Water (Moisture) Content of Soil by Direct Heating,” ASTM International, West Conshohocken, PA, 2007.

[50] ASTM D5334-14, “Standard Test Method for Determination of Thermal Conductivity of Soil and Soft Rock by Thermal Needle Probe Procedure,” ASTM International, West Conshohocken, PA, 2014.

[51] “CYMCAP Software, Power Cable Ampacity Rating,” *CYME Power Engineering Software*. [Online]. Available: http://www.cyme.com/software/cymcap/. [Accessed: 03-Nov-2018].

[52] F. de Leon, “Major factors affecting cable ampacity,” in *2006 IEEE Power Engineering Society General Meeting*, Montreal, Que., Canada, 2006.

[53] “ETAP | Electrical Power System Analysis Software | Power Management System.” [Online]. Available: http://etap.com. [Accessed: 03-Nov-2018].

[54] C. Bates, K. Malmedal, and D. Cain, “How to include soil thermal instability in underground cable ampacity calculations,” in *2016 IEEE Industry Applications Society Annual Meeting*, 2016, pp. 1–8.

[55] USi, “USAmp Prime Insulated Cable Ampacity Software.” [Online]. Available: http://www.usi-power.com/software-applications-usamp/. [Accessed: 31-Mar-2018].

[56] B. Sjodin, “What’s The Difference Between FEM, FDM, and FVM?,” *Machine Design*, 18-Apr-2016. [Online]. Available: http://www.machinedesign.com/fea-and-simulation/what-s-difference-between-fem-fdm-and-fvm. [Accessed: 13-Nov-2017].

[57] “Simulation Capabilities | ANSYS Mechanical Pro.” [Online]. Available: https://www.ansys.com/products/structures/ansys-mechanical-pro/mechanical-pro-capabilities. [Accessed: 13-Oct-2018].

[58] “Glossary of Soil Science Terms,” *Soil Science Society of America*. [Online]. Available: https://www.soils.org/publications/soils-glossary/#. [Accessed: 01-Nov-2017].

[59] Andreas Lilliestierna and Johan Utas, “Thermal classification of cable route,” Master’s Degree, Chalmers University of Technology, 2015.

[60] R. Hartlein and W. Black, “Hot-Spots in Underground Power Cable Systems,” in *PES ICC Fall 2006 Meeting Minutes*, 2006.

[61] J. V. Schmill, “Variable Soil Thermal Resistivity - Steady-State Analysis,” *IEEE Transactions on Power Apparatus and Systems*, vol. PAS-86, no. 2, pp. 215–223, Feb. 1967.

[62] H. S. Radhakrishna, F. y. Chu, and S. A. Boggs, “Thermal Stability and its Prediction in Cable Backfill Soils,” *IEEE Transactions on Power Apparatus and Systems*, vol. PAS-99, no. 3, pp. 856–867, 1980.

[63] I. Remson and J. R. Randolph, “Review of some elements of soil-moisture theory,” *USGS Numbered Series*, 1962.

[64] K. Malmedal, C. Bates, and D. Cain, “On the Use of the Law of Times in Calculating Soil Thermal Stability and Underground Cable Ampacity,” *IEEE Trans. Ind. Appl.*, vol. 52, no. 2, pp. 1215–1220, Mar. 2016.

[65] J. G. Hartley and W. Z. Black, “Predicting Thermal Stability And Transient Response Of Soils Adjacent To Underground Power Cables,” in *1979 7th IEEE/PES Transmission and Distribution Conference and Exposition*, 1979, pp. 316–320.

[66] L. Ingersoll, O. J. Zobel, and A. C. Ingersoll, *Heat Conduction: With Engineering Geological And Other Applications*. University of Wisconsin Press, 1954.

[67] D. C. Montgomery, *Design and Analysis of Experiments*, Eighth Ed. John Wiley & Sons, 2013.

[68] “Yokogawa CW140 Manual,” ATE Corp, Jul. 2001.

[69] N. Davis, “Introduction to Temperature Sensors: Thermistors, Thermocouples, RTDs, and Thermometer ICs.” [Online]. Available: https://www.allaboutcircuits.com/technical-articles/introduction-temperature-sensors-thermistors-thermocouples-thermometer-ic/. [Accessed: 30-Jun-2017].

[70] Keysight Technologies, “Practical Temperature Measurement,” 02-Aug-2014. [Online]. Available: http://literature.cdn.keysight.com/litweb/pdf/5965-7822E.pdf.

[71] “EC-5 | Soil Moisture Sensor | METER Environment,” *METER*. [Online]. Available: https://www.metergroup.com/environment/products/ec-5-soil-moisture-sensor/. [Accessed: 26-May-2018].

[72] Arduino: The world’s leading open-source hardware and software ecosystem, “Arduino.” [Online]. Available: http://www.arduino.cc/. [Accessed: 05-Nov-2018].

[73] “Uncertainty as Applied to Measurements and Calculations.” [Online]. Available: www.av8n.com/physics/uncertainty.htm. [Accessed: 19-May-2018].

[74] ASTM D6938-17a, “Standard Test Methods for In-Place Density and Water Content of Soil and Soil-Aggregate by Nuclear Methods (Shallow Depth),” ASTM International, West Conshohocken, PA, 2017.

[75] M. Environment, “Thermal Properties Analyzer.” [Online]. Available: https://www.metergroup.com/environment/products/tempos/. [Accessed: 04-Nov-2018].

[76] G. Campbell, “How to produce thermal dryout curves for buried cable applications,” *METER*. [Online]. Available: https://www.metergroup.com/environment/articles/produce-thermal-dryout-curves-buried-cable-applications/. [Accessed: 04-Nov-2018].

[77] V. Székely and T. Van Bien, “Fine structure of heat flow path in semiconductor devices: A measurement and identification method,” *Solid State Electron.*, vol. 31, no. 9, pp. 1363–1368, Sep. 1988.

[78] Scilab Enterprises © ESI Group - 2017, “Scilab: Open source software for numerical computation.” [Online]. Available: https://www.scilab.org/. [Accessed: 04-Nov-2018].

[79] W. H. Richardson, “Bayesian-based iterative method of image restoration,” *JOSA*, vol. 62, no. 1, pp. 55–59, 1972.

[80] V. Chatziathanasiou, P. Chatzipanagiotou, I. Papagiannopoulos, G. De Mey, and B. Więcek, “Dynamic thermal analysis of underground medium power cables using thermal impedance, time constant distribution and structure function,” *Appl. Therm. Eng.*, vol. 60, no. 1, pp. 256–260, Oct. 2013.

[81] P. Chatzipanagiotou, V. Chatziathanasiou, G. De Mey, and B. Więcek, “Influence of soil humidity on the thermal impedance, time constant and structure function of underground cables: A laboratory experiment,” *Appl. Therm. Eng.*, vol. 113, pp. 1444–1451, Feb. 2017.

[82] R. Olsen, G. J. Anders, J. Holboell, and U. S. Gudmundsdóttir, “Modelling of dynamic transmission cable temperature considering soil-specific heat, thermal resistivity, and precipitation,” *IEEE Trans. Power Delivery*, vol. 28, no. 3, pp. 1909–1917, 2013.

[83] “PVsyst Photovoltaic Software.” [Online]. Available: http://www.pvsyst.com/en/. [Accessed: 22-Oct-2018].

[84] “MQTT 101 - How to get started with the lightweight IoT protocol,” *HiveMQ*, 22-Oct-2014. [Online]. Available: http://www.hivemq.com/blog/how-to-get-started-with-mqtt. [Accessed: 09-Jul-2017].

[85] “MQTT, Adafruit IO & You!” [Online]. Available: https://learn.adafruit.com/mqtt-adafruit-io-and-you/overview. [Accessed: 09-Jul-2017].

[86] “Gammon Forum : Electronics : Microprocessors : Power saving techniques for microprocessors.” [Online]. Available: http://www.gammon.com.au/power. [Accessed: 09-Jul-2017].

[87] “Optimizing Soil Compaction and Other Strategies - Forester Network,” *Forester Network*, 01-Sep-2004. [Online]. Available: https://foresternetwork.com/daily/construction/optimizing-soil-compaction-and-other-strategies/. [Accessed: 11-Mar-2018].

[88] D. S. Freitas, A. T. Prata, and A. J. de Lima, “Thermal performance of underground power cables with constant and cyclic currents in presence of moisture migration in the surrounding soil,” *IEEE Trans. Power Delivery*, vol. 11, no. 3, pp. 1159–1170, 1996.

Additional publications for reference but not cited in the body

C. Bates, D. Cain, and K. Malmedal, “Including Soil Drying Time in Cable Ampacity Calculations,” *IEEE Trans. Ind. Appl.*, vol. 52, no. 6, pp. 4646–4651, Nov. 2016.

K. Malmedal, C. Bates, and D. Cain, “Engineering the thermal resistivity of concrete duct banks,” in *2015 IEEE-IAS/PCA Cement Industry Conference (IAS/PCA CIC)*, 2015, pp. 1–10.

C. Bates, D. Cain, and K. Malmedal, “The effect of raw material source on concrete duct bank thermal resistivity,” in *2018 IEEE-IAS/PCA Cement Industry Conference (IAS/PCA)*, 2018, pp. 1–5.

APPENDIX A
NEHER-MCGRATH CALCULATIONS

Table A.1 AIEE-IPCEA (Black Book) calculation. 3 cables direct buried, 15kV, 90C conductor, 20C ambient, 350kcmil, 100LF, Rho 90

Variable		Units	Notes	Ref. in Neher-McGrath Paper
DC Resistance				
ρ	10.371	cmil·Ω/ft at 20C	resistivity of conductor (copper=10.371)	Table 1
τ	234.5	°C	inferred temp of zero resistance (copper = 234.5)	Table 1
T_c	90	°C	temperature of conductor	
ρ_T	13.22	cmil·Ω/ft at T_c	not explicitley calculated in N-M	
CI	0.35	circular inches	Conductor Size	
Lay Factor	1.02		Included by N-M to account for estimated conductor length	
R_dc	38.54	μΩ/ft	DC resistance	10
Tape Shield or Concentric Neutral Resistance (Sheath in N-M)				
ρ_s	10.371	cmil·Ω/ft at 20C	resistivity of shield (copper=10.371)	Table 1
τ	234.5	°C	inferred temp of zero resistance (copper = 234.5)	Table 1
T_s	75	°C	temperature of shield	
ρ_T	13	cmil·Ω/ft at T_s	not explicitley calculated in N-M	
t	0.11	inches	shield thickness	
D_sm	1.265	inches	mean diameter of shield	
R_s	23	μΩ/ft	DC resistance of shield	11
Conductor Skin Effect				
k_s	1		Conductor skin effect	Table 2
x_s	1.09		Skin effect function	22
R_dc/k	39			
Y_cs	0.0074		Conductor skin effect, divide table by 100	Table 3
k_p	0.8		Proximity coefficient	Table 2
x_p	0.98		Proximity effect function	24
R_dc/k	48			
F(x_p)	0.0047		Divide table value by 100	Table 3
D_c	0.616	inches	Conductor diameter	
S	7.5	inches	Axial spacing between conductors	

Table A.1 Continued

Variable		Units	Notes	Ref. in Neher-McGrath Paper
Y_cp	0.000		Conductor skin effect due to proximity	
1+Y_c	1.008		Total conductor losses	
R_ac	38.83	μΩ/ft	ac resistance of conductor including skin and proximity only	
Shield Skin Effect (Sheath)				
Short circuited shields				
X_m	56.84	μΩ/ft	Shield mutual inductance	28
Y_sc	0.51		Shield circulating current effect	27
T	0.297	inches	insulation thickness	
s	0.70	inches		32
Y_se	0.67		Shield eddy current effect, may need to multiply by 12/1000	31
	0.14		Sheath eddy loss reduction, multiply open-circuit shield eddy	
Open circuited shields				
Y_se	0.002		Shield eddy current effect	30
Total Shield Losses				
Y_s	0.002		Total shield losses (Y_se+Y_sc if shield is shorted)	
R_ac/R_dc	1.010		AC/DC ratio of cable system, include Y_c, Y_s, and Y_p	14
q_s	1.002		ratio of sum of losses in conductors and sheaths to losses in conductors	18
q_e	1.002		ratio of sum of losses in conductors, sheaths, and conduit to losses in conductors	
Dielectric Loss				
E	8.66	kV	Phase to neutral voltage	
e_r	4.5		specific inductive capacitance of insulation	Table 5
cos Phi	3.5%		insulation power factor	Pg. III Blk bk
W_d	0.111	W/ft	Dielectric loss per foot at 60Hz	

Table A.1 Continued

Variable		Units	Notes	Ref. in Neher-McGrath Paper
Thermal Resistance				
Insulation				
D_i	1.21	inches	Diameter to outside of insulation	
p_i	500	C*cm/W	Insulation thermal resistivity	Table 6
G_i	191.57		Cable geometric factor (3 conductor cable), single=191.57	Ref. 1 Fig 2
R_i	1.759	thermal ohm feet	Single conductor resistance in conduit	38
Jacket				
t_j	0	inches	thickness of jacket	
D_j	1.43	inches	Diameter to outside of jacket	
p_j	100	°C*cm/W	resistivity of jacket	Table 6
R_j	0.00	thermal ohm feet		
Duct Air				
A	17			Table 7
B	2.3			Table 7
C	0.024			Table 7
A'	4.6			Table 7
B'	0.27			Table 7
T_m	58	C	Temperature of duct air	
n_d	1	cables	number of cables per duct	
D_s	1.43	inches	outside diameter of sheath or cable jacket	
R_sd	0.00	thermal ohm feet	Resistance from jacket surface to duct inner wall	41
Duct				
t_d	0.25	inches	thickness of pipe (PVC)	
D_e	1.43	inches	outside diameter of pipe or cable if direct buried	
p_d	480	°C*cm/W	resistivity of pipe	Table 6
R_d	0.00	thermal ohm feet	Resistance of pipe to earth	40
Concrete and Earth				
p_c	90	°C*cm/W	resistivity of concrete duct bank	Table 6
p_e	90	°C*cm/W	resistivity of earth	
N	3	cables	number of cables in duct bank	

Table A.1 Continued

Variable		Units	Notes	Ref. in Neher-McGrath Paper
F	93		Mutual heating factor	46
a	2.75	in^2/hour	diffusivity of medium (earth)	
lf	100%		daily load factor	
LF	1.00		loss factor	3
D_x	8.29	inches		45
L	36	inches	depth to hottest cable	
L_b	36	inches	depth to center of duct bank	
x	2.5	inches	dimension of short side	
y	18	inches	dimension of long side	
r_b	1.71	inches		
G_b	1.62		Geometric factor (square term dropped?)	57
R_e'	4.29	thermal ohm feet	effective resistance from pipe to remote earth	44A
R_e'@1	4.29	thermal ohm feet	effective resistance at unity load factor	44A
R_se	0.00	thermal ohm feet	resistance between sheath and start of earth	
R_ca'	6.06	thermal ohm feet	effective resistance between conductor and ambient	8
T_d	0.57	°C	temperature rise due to dielectric rise	6
T_a	20	°C	ambient temperature at depth of hottest cable	
T_c	90	°C	maximum conductor temperature	
I	543	A	maximum current	9
	534	A	Black book value, pg 210	
	98.29%		Ratio of calculated to book value	
Total cable heating				
W_c	11.46	W/ft		
W_s	0.02	W/ft		
W_d	0.11	W/ft		
W_total	11.59	W/ft		
	0.38	W/cm		

Table A.1 Continued

Variable		Units	Notes	Ref. in Neher-McGrath Paper
Soil stability with NHR				
q_nhr	0.1	W/cm		
T1	25	°C		
T2	20	°C		
q_c	0.061	W/cm		
m_nhr	3.76E-08	lb/(sec*cm)		
q_w+q_v	0.148	W/cm		
D1	0.625	inches		
D2	2.377	inches		
p_dry	350			
R_ds	0.93	thermal ohm feet		
R_e'	4.05	thermal ohm feet		
R_e'@1	4.05	thermal ohm feet		
R_se	0.93	thermal ohm feet		
R_ca'	6.75	thermal ohm feet		
I	515	A		

APPENDIX B
ARDUINO DATA LOGGER SOURCE CODE

```
/*************************************************
 Arduino Data Logger 1 - MQTT published Temperature Measurements
 Carson Bates, carsonbates@gmail.com
 04/04/2017

  Adafruit invests time and resources providing this open source code,
  please support Adafruit and open-source hardware by purchasing
  products from Adafruit!

  Written by Limor Fried/Ladyada for Adafruit Industries.
  MIT license, all text above must be included in any redistribution

Muxshield = 2,4,6,7, a0,a1,a2 (cut traces to eliminate 8,10,11,12)
SD & RTC (Adafruit Data Logger) = 10 (can cut a trace to re-assign), ICSP SCK - SPI clock,
ICSP MISO - SPI MISO, ICSP MOSI - SPI MOSI
FONA = 11,12,{7} (must rewire from 2,3 and cut trace on 4 to remove)
FONA_KEY = 13
VCC_ON = 3 (used to turn on 5V to thermistor voltage dividers only when req'd to reduce
power)
VCC_ON2 = 5 (used to turn on 5V to thermistor voltage dividers only when req'd to reduce
power)
 *************************************************/
#include <Adafruit_SleepyDog.h>
#include <SoftwareSerial.h>
#include "Adafruit_FONA.h"
#include "Adafruit_MQTT.h"
#include "Adafruit_MQTT_FONA.h"
#include <MuxShield.h>
#include "SdFat.h"
#include <Wire.h>
#include <RTClib.h>

//Initialize the clock
RTC_PCF8523 rtc;

//Initialize the Mux Shield
MuxShield muxShield;

//Initialize the SD shield
SdFat SD;

/************************** Sleep ***********************************/
#define time_wakeup 6   //hour of day to start logging
#define time_sleep 19   //hour of day to sleep

/************************** Thermistors ***********************************/
#define vcc_on 3      //used to supply 5V to thermistor circuit--turn on/off for power savings
#define vcc_on2 5     //used to supply 5V to thermistor circuit--turn on/off for power savings
```

```
#define anlg_cnt 40
#define oversample 16 //amount of oversampling, result of 4^n, i.e. 4^0: 1 = 10 bit, 4^1: 4 = 11
bit, 4^2: 16= 12 bit, etc.
#define oversample_bitshift 2 //exponent (n) of 4^n, i.e. 0 for 4^0, 1 for 4^1, 2 for 4^2, etc.
#define ADC_bit (pow(2, 10 + oversample_bitshift) - 1)
#define r_divider 4750 //may need to use float if decimals are required

/************************** FONA Pins *********************************/
#define FONA_RX 11
#define FONA_TX 12
#define FONA_RST 14
#define FONA_KEY 13
SoftwareSerial fonaSS = SoftwareSerial(FONA_TX, FONA_RX);

Adafruit_FONA fona = Adafruit_FONA(FONA_RST);

/************************* FONA Login Info ********************************/
/*Optionally configure a GPRS APN, username, and password.
  You might need to do this to access your network's GPRS/data
  network.  Contact your provider for the exact APN, username,
  and password values.  Username and password are optional and
  can be removed, but APN is required.*/
#define FONA_APN       ""
#define FONA_USERNAME  ""
#define FONA_PASSWORD  ""

/************************* MQTT Setup *********************************/
#define MQTT_SERVER      "***.com"
#define MQTT_SERVERPORT  1883
#define MQTT_CID         "mohavelog1"
#define MQTT_USERNAME    "mohavelog1"
#define MQTT_KEY         "***"

/************ Global State (you don't need to change this!) ******************/
// Setup the FONA MQTT class by passing in the FONA class and MQTT server and login
details.
Adafruit_MQTT_FONA mqtt(&fona, MQTT_SERVER, MQTT_SERVERPORT, MQTT_CID,
MQTT_USERNAME, MQTT_KEY);

// You don't need to change anything below this line!
#define halt(s) { Serial.println(F( s )); while(1);  }

// FONAconnect is a helper function that sets up the FONA and connects to
// the GPRS network. See the fonahelper.cpp tab above for the source!
boolean FONAconnect(const __FlashStringHelper *apn, const __FlashStringHelper *username,
const __FlashStringHelper *password);

/****************************** Feeds ***************************************/
// Setup a feed for publishing.
//publish as CSV (array) of data
Adafruit_MQTT_Publish mohave_publish = Adafruit_MQTT_Publish(&mqtt, "/mohave1");
```

```
Adafruit_MQTT_Subscribe sleep_onoff = Adafruit_MQTT_Subscribe(&mqtt, "/mohave1/sleep");
//set to "ON" for deep sleep enable or "OFF" to disable
Adafruit_MQTT_Subscribe log_rate_cmd = Adafruit_MQTT_Subscribe(&mqtt,
"/mohave1/logctrl"); //value in seconds between logs

boolean sleep_enable = false;
uint8_t log_rate = 35;   //number of 8 second sleeps, i.e. =4 corresponds to 4*8=32 seconds
/************************ Arbitrary Payload ********************************/
// Union allows for easier interaction of members in struct form with easy publishing
// of "raw" bytes
typedef union {
  //Customize struct with whatever variables/types you like.

  struct __attribute__((__packed__)) { // packed to eliminate padding for easier parsing.
    uint32_t sec_since_2000;
    int temperature[anlg_cnt];
  } s;

  uint8_t raw[sizeof(s)];                  // For publishing

  /*
     // Alternate Option with anonymous struct, but manual byte count:
     struct __attribute__((__packed__)){  // packed to eliminate padding for easier parsing.
        char charAry[10];       // 10 x 1 byte  =   10 bytes
        int16_t val1;           // 1 x  2 bytes =   2 bytes
        unsigned long val2;     // 1 x  4 bytes =   4 bytes
        uint16_t val3;          // 1 x  2 bytes =   2 bytes
                                 ------------------
                                 TOTAL =    18 bytes
     };
     uint8_t raw[18];                  // For publishing
  */

} packet_t;

packet_t dataPacket;    //initialize arbitrary payload

void setup() {
  while (!Serial);

  Serial.begin(57600);

  //  start SD card
  if (!SD.begin(4)) { //pin 4 used for Adafruit SD card datalogger with RTC
    //    //      Serial.println("ERROR-SD card");    // init failed
    //  }
    //  //  Serial.println("SUCCESS-SD card");
    //  // check for index.htm file
    //  //  if (!SD.exists("index.htm")) {
    //  //      Serial.println("ERROR-No index.htm");  // can't find index file
    return;
```

```
  }

  //start RTC
  if (! rtc.begin()) {
    //    Serial.println("Couldn't find RTC");
    return;
  }

  mqtt.subscribe(&sleep_onoff);
  mqtt.subscribe(&log_rate_cmd);

  //set analog ref to external for Muxshield (thermistors)
  analogReference(EXTERNAL);
  pinMode(vcc_on, OUTPUT);
  pinMode(vcc_on2, OUTPUT);

//log one set of data in case FONA has trouble connecting
//Initialize string for SD card data logging in CSV format
  String dataString = "";
  digitalWrite(vcc_on, HIGH);   //turn on 5V to thermistor voltage divider (uses max of 0.85mA
per thermistor), must limit to 40mA per output
  digitalWrite(vcc_on2, HIGH);   //turn on 5V to thermistor voltage divider (uses max of 0.85mA
per thermistor), must limit to 40mA per output
  delay(50);      //allow circuit to stabilize
  //get current time and place as first column
  DateTime time_now = rtc.now();
  uint32_t time_secs = time_now.secondstime();
  uint8_t time_hour = time_now.hour();
  dataString += time_secs;

  //read thermistors through Muxshield
  int analog_val = 0;

  for (int feed_ind = 0; feed_ind < anlg_cnt; feed_ind++) {
    dataString += ",";
    analog_val = ReadTemp(feed_ind);
    dataString += String(analog_val);
  }

  digitalWrite(vcc_on, LOW);
  digitalWrite(vcc_on2, LOW);

  Serial.println(dataString);
  //log data to SD card
  File logFile;
  logFile = SD.open(F("log.txt"), FILE_WRITE);
  logFile.println(dataString);
  logFile.close();

  /************ MQTT FONA ******************/
  pinMode(FONA_KEY, OUTPUT);
```

```
  Watchdog.enable(8000);
  fona_connect();
}

void loop() {
  // Make sure to reset watchdog every loop iteration!
  Watchdog.reset();

  //Initialize string for SD card data logging in CSV format
  String dataString = "";
  digitalWrite(vcc_on, HIGH);   //turn on 5V to thermistor voltage divider (uses max of 0.85mA
per thermistor), must limit to 40mA per output
  digitalWrite(vcc_on2, HIGH);   //turn on 5V to thermistor voltage divider (uses max of 0.85mA
per thermistor), must limit to 40mA per output
  delay(50);      //allow circuit to stabilize
  //get current time and place as first column
  DateTime time_now = rtc.now();
  uint32_t time_secs = time_now.secondstime();
  uint8_t time_hour = time_now.hour();
  dataPacket.s.sec_since_2000 = time_secs;
  dataString += time_secs;

  //read thermistors through Muxshield
  int analog_val = 0;

  for (int feed_ind = 0; feed_ind < anlg_cnt; feed_ind++) {
    Watchdog.reset();
    dataString += ",";
    analog_val = ReadTemp(feed_ind);
    //publish as individual feeds for each temperature
    //    Serial.print(F("\nSend T"));
    //    Serial.println(feed_ind+1);
    //    if (! t[feed_ind].publish(analog_val)) {
    //      Serial.println(F("FAIL"));
    //      txfailures++;
    //    } else {
    //      Serial.println(F("OK"));
    //      txfailures = 0;
    //    }

    dataString += String(analog_val);
    dataPacket.s.temperature[feed_ind] = analog_val;
  }

  digitalWrite(vcc_on, LOW);
  digitalWrite(vcc_on2, LOW);
  Watchdog.reset();

  Serial.println(dataString);
  //log data to SD card
  File logFile;
```

```
logFile = SD.open(F("log.txt"), FILE_WRITE);
logFile.println(dataString);
logFile.close();

Watchdog.reset();
MQTT_connect();
Watchdog.reset();

Serial.println(char(dataPacket.raw));
//publish to MQTT Broker
if (! mohave_publish.publish(dataPacket.raw, sizeof(packet_t))) {
  Serial.println(F("FAIL"));
} else {
  Serial.println(F("OK"));
}

Watchdog.reset();

// this is our 'wait for incoming subscription packets' busy subloop
Adafruit_MQTT_Subscribe *subscription;
while ((subscription = mqtt.readSubscription(3000))) {
  if (subscription == &sleep_onoff) {
    Serial.print(F("Got: "));
    Serial.println((char *)sleep_onoff.lastread);
    if (strcmp((char *)sleep_onoff.lastread, "ON") == 0) {
      sleep_enable = true;
      Serial.println("sleep enable=ON");
    }
    if (strcmp((char *)sleep_onoff.lastread, "OFF") == 0) {
      sleep_enable = false;
      Serial.println("sleep enable=OFF");
    }
  }
  Watchdog.reset();
  if (subscription == &log_rate_cmd) {
    Serial.print(F("log_rate_cmd: "));
    Serial.println((char *)log_rate_cmd.lastread);
    uint8_t test_log_rate = atoi((char *)log_rate_cmd.lastread);  // convert to a number
    if (test_log_rate > 0 && test_log_rate < 7200) {
      log_rate = test_log_rate / 8;
    }
  }
}

Serial.print(F("sleep status = "));
Serial.println(sleep_enable);
Serial.println(time_hour);
Serial.print(F("log rate = "));
Serial.println(log_rate);
//check if we're in the hours for deep sleep
```

```
  if (sleep_enable && (time_hour < time_wakeup || time_hour >= time_sleep)) {  //for
time_wakeup > time_sleep
    Serial.println(F("entering sleep mode"));
    fona_sleep(time_hour);
    fona_connect();
  } else {    //normal delay between data logging
    for (int sleep_ind = 0; sleep_ind < log_rate; sleep_ind++) {
      Watchdog.sleep();   //default wait period without closing cell connection, 8 seconds per sleep
    }
  }
}

// Function to connect and reconnect as necessary to the MQTT server.
void MQTT_connect() {
  int8_t ret;

  // Stop if already connected.
  if (mqtt.connected()) {
    return;
  }

  Serial.print(F("Cnctng MQ"));

  while ((ret = mqtt.connect()) != 0) { // connect will return 0 for connected
    Serial.println(mqtt.connectErrorString(ret));
    Serial.println(F("Retry MQ 5 sec"));
    mqtt.disconnect();
    Watchdog.sleep(5000);  // wait 5 seconds
    Watchdog.reset();
  }
  Serial.println(F("MQ Cnctd"));
}

//Read temperatures (thermistor values) through Mux II Shield by Mayhew Labs
int ReadTemp(int anlg_index)  {
  //read thermistors through Muxshield
  float analog_val = 0;

  //    Serial.print("oversample ");
  //    Serial.println(oversample);
  //    Serial.print("oversample_bitshift ");
  //    Serial.println(oversample_bitshift);
  //    Serial.print("ADC_bit ");
  //    Serial.println(ADC_bit);
  //    Serial.print("r_divider ");
  //    Serial.println(r_divider);


  int row_ind = anlg_index / 16 + 1;
  int col_ind = anlg_index % 16;
  analog_val = muxShield.analogReadMS(row_ind, col_ind);
```

```
  //  Serial.print("analog_val before scale");
  //  Serial.println(analog_val);
  unsigned int oversample_val = 0;
  for (int over_ind = 0; over_ind < oversample; over_ind++) {
    oversample_val += muxShield.analogReadMS(row_ind, col_ind);
  }
  analog_val = oversample_val >> oversample_bitshift;
  //convert to temperature
  analog_val = log(r_divider / ((ADC_bit / analog_val - 1) * 10E3)); //pull-up configuration
  //  analog_val = log(4750 / ((1024 / analog_val - 1) * 10E3)); //pull-up configuration
  analog_val = 1 / (3.354016E-3 + analog_val * (3.001308E-4 + analog_val * (5.085165E-6 +
analog_val * 2.18765E-07)));
  analog_val -= 273.15;           // Convert Kelvin to Celsius
  //  Serial.print("analog_val after scale");
  //  Serial.println(analog_val);
  analog_val *= 100;
  analog_val = (int) analog_val;
  return analog_val;
}

//turn on FONA with KEY pin and connect to cell network
void fona_connect() {
  digitalWrite(FONA_KEY, LOW);  //toggle FONA power ON
  delay(2000);
  digitalWrite(FONA_KEY, HIGH);

  Watchdog.reset();
  // Initialise the FONA module
  while (! FONAconnect(F(FONA_APN), F(FONA_USERNAME), F(FONA_PASSWORD))) {
    Serial.println(F("Rtry FONA"));
  }

  Serial.println(F("Cnctd Cell"));

  Watchdog.reset();
  delay(1000);  // wait a few seconds to stabilize connection
  Watchdog.reset();
}

//turn off FONA and use Watchdog sleep
void fona_sleep(uint8_t time_hour) {
  Serial.println(F("going to sleep"));
  mqtt.disconnect();
  uint8_t sleep_duration;

  if (time_hour > time_wakeup) {
    sleep_duration = 24 - time_hour + time_wakeup;
  } else {
    sleep_duration = time_wakeup - time_hour;
  }
```

```
  int sleep_ind_duration = 60 / 8 * 60 * sleep_duration + 30; //add 30*8 seconds to ensure next
hour
  Serial.print(sleep_ind_duration);
  Serial.println(" index");
  Serial.print(sleep_duration);
  Serial.println(" hour");
  digitalWrite(FONA_KEY, LOW);  //toggle FONA power OFF
  delay(2000);
  digitalWrite(FONA_KEY, HIGH);
  for (int sleep_ind = 0; sleep_ind < sleep_ind_duration; sleep_ind++) {
    //for (int sleep_ind = 0; sleep_ind < (60 / 8 * sleep_duration); sleep_ind++) {
    //while (time_hour <= time_wakeup || time_hour >= time_sleep) {
    Watchdog.sleep();
    //DateTime time_now = rtc.now();
    //uint8_t time_hour = time_now.minute();
  }
}
```

APPENDIX C
COPYRIGHT PERMISSIONS

Copyright Clearance Center RightsLink®

Account Info | Help

Title:	Standard Test Method for Determination of Thermal Conductivity of Soil and Soft Rock by Thermal Needle Probe Procedure
Article ID:	D5334-14
Publication:	Publication1
Publisher:	CCC Republication
Date:	Jun 1, 2014

Logged in as:
Nick Bates
Account #:
3001358030
LOGOUT

Order Completed

Thank you for your order.

This Agreement between Nick C Bates ("You") and ASTM International ("ASTM International") consists of your order details and the terms and conditions provided by ASTM International and Copyright Clearance Center.

License number	Reference confirmation email for license number
License date	Nov, 05 2018
Licensed content publisher	ASTM International
Licensed content title	Standard Test Method for Determination of Thermal Conductivity of Soil and Soft Rock by Thermal Needle Probe Procedure
Licensed content date	Jun 1, 2014
Type of use	Thesis/Dissertation
Requestor type	Academic institution
Format	Print
Portion	excerpt (up to 400 words)
Number of excerpts requested	1
The requesting person/organization	Carson Bates
Title or numeric reference of the portion(s)	section 4.1 "Thermal conductivity is determined by...and cooling cycle if applicable."
Title of the article or chapter the portion is from	n/a
Editor of portion(s)	n/a
Author of portion(s)	n/a
Volume of serial or monograph	n/a
Issue, if republishing an article from a serial	n/a
Page range of portion	2
Publication date of portion	2014
Rights for	Main product
Duration of use	Life of current edition
Creation of copies for the disabled	no
With minor editing privileges	no
For distribution to	United States
In the following language(s)	Original language of publication

With incidental promotional use	no
Lifetime unit quantity of new product	Up to 499
Title	PhD student
Institution name	Colorado School of mines
Expected presentation date	Nov 2018
Order reference number	2
Requestor Location	Nick C Bates 491 CRAWFORD ST Golden, CO 80401 United States Attn:
Billing Type	Invoice
Billing address	Nick C Bates 491 CRAWFORD ST Golden, CO 80401 United States Attn: Nick C Bates
Total (may include CCC user fee)	0.00 USD
Total	0.00 USD

CLOSE WINDOW

Title: Cable Ampacity Calculations: A Comparison of Methods
Author: Carson Bates
Publication: Industry Applications, IEEE Transactions on
Publisher: IEEE
Date: Jan.-Feb. 2016

Thesis / Dissertation Reuse

The IEEE does not require individuals working on a thesis to obtain a formal reuse license, however, you may print out this statement to be used as a permission grant:

Requirements to be followed when using any portion (e.g., figure, graph, table, or textual material) of an IEEE copyrighted paper in a thesis:

1) In the case of textual material (e.g., using short quotes or referring to the work within these papers) users must give full credit to the original source (author, paper, publication) followed by the IEEE copyright line © 2011 IEEE.
2) In the case of illustrations or tabular material, we require that the copyright line © [Year of original publication] IEEE appear prominently with each reprinted figure and/or table.
3) If a substantial portion of the original paper is to be used, and if you are not the senior author, also obtain the senior author's approval.

Requirements to be followed when using an entire IEEE copyrighted paper in a thesis:

1) The following IEEE copyright/ credit notice should be placed prominently in the references: © [year of original publication] IEEE. Reprinted, with permission, from [author names, paper title, IEEE publication title, and month/year of publication]
2) Only the accepted version of an IEEE copyrighted paper can be used when posting the paper or your thesis on-line.
3) In placing the thesis on the author's university website, please display the following message in a prominent place on the website: In reference to IEEE copyrighted material which is used with permission in this thesis, the IEEE does not endorse any of [university/educational entity's name goes here]'s products or services. Internal or personal use of this material is permitted. If interested in reprinting/republishing IEEE copyrighted material for advertising or promotional purposes or for creating new collective works for resale or redistribution, please go to http://www.ieee.org/publications_standards/publications/rights/rights_link.html to learn how to obtain a License from RightsLink.

If applicable, University Microfilms and/or ProQuest Library, or the Archives of Canada may supply single copies of the dissertation.

BACK CLOSE WINDOW

Gmail Carson Bates <car333son@gmail.com>

CYMCAP Screenshots in Academic Dissertation

Evangelista, Umberto <UmbertoEvangelista@eaton.com> Mon, Nov 5, 2018 at 11:58 AM
To: Carson Bates <nbates@mymail.mines.edu>

Hello Carson,

Yes you are free to use this and the extract that you sent previously in your academic dissertation at the Colorado School of Mines.

Kind regards,

Umberto (Bert) Evangelista , P. Eng.

Regional Sales Manager

CYME International T&D Inc.

Eaton

1485 Roberval, Suite 104

St.Bruno-de-Montarville, Quebec

Canada J3V 3P8

Office: +1 450 461-6193

Fax: +1 450 461-0966

UmbertoEvangelista@eaton.com

www.eaton.com/cyme

From: Carson Bates [mailto:nbates@mymail.mines.edu]
Sent: November 5, 2018 1:53 PM
To: Evangelista, Umberto
Subject: Re: [EXTERNAL] CYMCAP Screenshots in Academic Dissertation

Bert,

Thank you. I have updated it to read:

CYMCAP is focused on calculating cable ampacity. Other products of Eaton's CYME Power Engineering Software are available for performing additional power system design calculations such as power flow analysis, coordination studies, or other studies. Because of the focus of CYMCAP is cable ampacity, it lends itself to quickly beginning the underground cable analysis. It also steps the user through entering the required cable data rather than relying on typical values.

Based on this edit, do I have your permission to use this and the extract I sent previously (including this modified first paragraph) in my academic dissertation at the Colorado School of Mines?

Thank you,

Carson

On Mon, Nov 5, 2018 at 7:05 AM Evangelista, Umberto <UmbertoEvangelista@eaton.com> wrote:

> Hello Carson,
>
> Given that we don't have the full context of the dissertation and since it sounds a bit limitative, we would like the first paragraph to mentioned that the other studies/analysis could be performed by other modules.
>
> Here's our suggestion:
>
> "CYMCAP is focused on calculating cable ampacity. Other products of Eaton's CYME Power Engineering Software are available for performing additional power system design calculations such as power flow analysis, coordination studies, or other studies."
>
> Hope this helps.
>
> Regards,
>
> Bert
>
> ---
>
> **From:** Evangelista, Umberto
> **Sent:** November 5, 2018 8:09 AM
> **To:** 'Carson Bates'
> **Subject:** RE: [EXTERNAL] CYMCAP Screenshots in Academic Dissertation

Hi,

I am working on my doctoral dissertation and would like to use a few screenshots from your software. I have attached the section from my dissertation.

"CYMCAP Software, Power Cable Ampacity Rating," *CYME Power Engineering Software*. [Online]. Available: http://www.cyme.com/software/cymcap/. [Accessed: 03-Nov-2018]

Is it acceptable to include these in my dissertation with the proper citation listed above?

Thank you,

Carson Bates

ELSEVIER LICENSE
TERMS AND CONDITIONS

Nov 01, 2018

This Agreement between Nick C Bates ("You") and Elsevier ("Elsevier") consists of your license details and the terms and conditions provided by Elsevier and Copyright Clearance Center.

License Number	4460000598870
License date	Nov 01, 2018
Licensed Content Publisher	Elsevier
Licensed Content Publication	Solid-State Electronics
Licensed Content Title	Fine structure of heat flow path in semiconductor devices: A measurement and identification method
Licensed Content Author	Vladimir Székely,Tran Van Bien
Licensed Content Date	Sep 1, 1988
Licensed Content Volume	31
Licensed Content Issue	9
Licensed Content Pages	6
Start Page	1363
End Page	1368
Type of Use	reuse in a thesis/dissertation
Intended publisher of new work	other
Portion	excerpt
Number of excerpts	1
Format	both print and electronic
Are you the author of this Elsevier article?	No
Will you be translating?	No
Title of your thesis/dissertation	PhD student
Publisher of new work	Colorado School of mines
Expected completion date	Nov 2018
Estimated size (number of pages)	1
Requestor Location	Nick C Bates 491 CRAWFORD ST Golden, CO 80401 United States Attn:
Publisher Tax ID	98-0397604
Total	0.00 USD

Gmail

Carson Bates <car333son@gmail.com>

NON RIGHTSLINK Request Permission to reuse excerpts from T. L. Bergman, F. P. Incropera, and A. S. Lavine, Fundamentals of Heat and Mass Transfer. John Wiley & Sons, 2011.

Wiley Global Permissions <permissions@wiley.com> Tue, Nov 6, 2018 at 4:59 AM
To: Carson Bates <nbates@mymail.mines.edu>

Dear Nick,

Thank you for your email.

Permission is granted for you to use the material requested for your thesis/dissertation subject to the usual acknowledgements (author, title of material, title of book/journal, ourselves as publisher) and on the understanding that you will reapply for permission if you wish to distribute or publish your thesis/dissertation commercially.

You should also duplicate the copyright notice that appears in the Wiley publication in your use of the Material. Permission is granted solely for use in conjunction with the thesis, and the material may not be posted online separately.

Any third-party material is expressly excluded from this permission. If any material appears within the article with credit to another source, authorisation from that source must be obtained.

Many thanks,

Orla Davies

Rights Assistant

John Wiley & Sons Ltd

WILEY

From: Carson Bates <nbates@mymail.mines.edu>
Sent: 01 November 2018 02:52
To: Wiley Global Permissions <permissions@wiley.com>
Subject: NON RIGHTSLINK Request Permission to reuse excerpts from T. L. Bergman, F. P. Incropera, and A. S. Lavine, Fundamentals of Heat and Mass Transfer. John Wiley & Sons, 2011.

[Quoted text hidden]

RightsLink®

Home | Create Account | Help

Standard: IEEE Guide for Soil Thermal Resistivity Measurements
Publisher: IEEE
Issue Date: 12 May 1981

Thesis / Dissertation Reuse

The IEEE does not require individuals working on a thesis to obtain a formal reuse license, however, you may print out this statement to be used as a permission grant:

Requirements to be followed when using any portion (e.g., figure, graph, table, or textual material) of an IEEE copyrighted paper in a thesis:

1) In the case of textual material (e.g., using short quotes or referring to the work within these papers) users must give full credit to the original source (author, paper, publication) followed by the IEEE copyright line © 2011 IEEE.
2) In the case of illustrations or tabular material, we require that the copyright line © [Year of original publication] IEEE appear prominently with each reprinted figure and/or table.
3) If a substantial portion of the original paper is to be used, and if you are not the senior author, also obtain the senior author's approval.

Requirements to be followed when using an entire IEEE copyrighted paper in a thesis:

1) The following IEEE copyright/ credit notice should be placed prominently in the references: © [year of original publication] IEEE. Reprinted, with permission, from [author names, paper title, IEEE publication title, and month/year of publication]
2) Only the accepted version of an IEEE copyrighted paper can be used when posting the paper or your thesis on-line.
3) In placing the thesis on the author's university website, please display the following message in a prominent place on the website: In reference to IEEE copyrighted material which is used with permission in this thesis, the IEEE does not endorse any of [university/educational entity's name goes here]'s products or services. Internal or personal use of this material is permitted. If interested in reprinting/republishing IEEE copyrighted material for advertising or promotional purposes or for creating new collective works for resale or redistribution, please go to http://www.ieee.org/publications_standards/publications/rights/rights_link.html to learn how to obtain a License from RightsLink.

If applicable, University Microfilms and/or ProQuest Library, or the Archives of Canada may supply single copies of the dissertation.

BACK | CLOSE WINDOW

RightsLink®

Home | Create Account | Help

Standard: IEEE Standard Power Cable Ampacity Tables
Publisher: IEEE
Issue Date: 30 Dec. 1994

LOGIN
If you're a copyright.com user, you can login to RightsLink using your copyright.com credentials.
Already a RightsLink user or want to learn more?

Thesis / Dissertation Reuse

The IEEE does not require individuals working on a thesis to obtain a formal reuse license, however, you may print out this statement to be used as a permission grant:

Requirements to be followed when using any portion (e.g., figure, graph, table, or textual material) of an IEEE copyrighted paper in a thesis:

1) In the case of textual material (e.g., using short quotes or referring to the work within these papers) users must give full credit to the original source (author, paper, publication) followed by the IEEE copyright line © 2011 IEEE.
2) In the case of illustrations or tabular material, we require that the copyright line © [Year of original publication] IEEE appear prominently with each reprinted figure and/or table.
3) If a substantial portion of the original paper is to be used, and if you are not the senior author, also obtain the senior author's approval.

Requirements to be followed when using an entire IEEE copyrighted paper in a thesis:

1) The following IEEE copyright/ credit notice should be placed prominently in the references: © [year of original publication] IEEE. Reprinted, with permission, from [author names, paper title, IEEE publication title, and month/year of publication]
2) Only the accepted version of an IEEE copyrighted paper can be used when posting the paper or your thesis on-line.
3) In placing the thesis on the author's university website, please display the following message in a prominent place on the website: In reference to IEEE copyrighted material which is used with permission in this thesis, the IEEE does not endorse any of [university/educational entity's name goes here]'s products or services. Internal or personal use of this material is permitted. If interested in reprinting/republishing IEEE copyrighted material for advertising or promotional purposes or for creating new collective works for resale or redistribution, please go to http://www.ieee.org/publications_standards/publications/rights/rights_link.html to learn how to obtain a License from RightsLink.

If applicable, University Microfilms and/or ProQuest Library, or the Archives of Canada may supply single copies of the dissertation.

BACK | CLOSE WINDOW

RightsLink®

Home | Create Account | Help

Title: Including Soil Drying Time in Cable Ampacity Calculations
Author: Carson Bates
Publication: Industry Applications, IEEE Transactions on
Publisher: IEEE
Date: Nov.-Dec. 2016

Thesis / Dissertation Reuse

The IEEE does not require individuals working on a thesis to obtain a formal reuse license, however, you may print out this statement to be used as a permission grant:

Requirements to be followed when using any portion (e.g., figure, graph, table, or textual material) of an IEEE copyrighted paper in a thesis:

1) In the case of textual material (e.g., using short quotes or referring to the work within these papers) users must give full credit to the original source (author, paper, publication) followed by the IEEE copyright line © 2011 IEEE.
2) In the case of illustrations or tabular material, we require that the copyright line © [Year of original publication] IEEE appear prominently with each reprinted figure and/or table.
3) If a substantial portion of the original paper is to be used, and if you are not the senior author, also obtain the senior author's approval.

Requirements to be followed when using an entire IEEE copyrighted paper in a thesis:

1) The following IEEE copyright/ credit notice should be placed prominently in the references: © [year of original publication] IEEE. Reprinted, with permission, from [author names, paper title, IEEE publication title, and month/year of publication]
2) Only the accepted version of an IEEE copyrighted paper can be used when posting the paper or your thesis on-line.
3) In placing the thesis on the author's university website, please display the following message in a prominent place on the website: In reference to IEEE copyrighted material which is used with permission in this thesis, the IEEE does not endorse any of [university/educational entity's name goes here]'s products or services. Internal or personal use of this material is permitted. If interested in reprinting/republishing IEEE copyrighted material for advertising or promotional purposes or for creating new collective works for resale or redistribution, please go to http://www.ieee.org/publications_standards/publications/rights/rights_link.html to learn how to obtain a License from RightsLink.

If applicable, University Microfilms and/or ProQuest Library, or the Archives of Canada may supply single copies of the dissertation.

BACK | CLOSE WINDOW

Gmail Carson Bates <car333son@gmail.com>

IEEE Paper Reuse in Dissertation

Keith Malmedal <keithmalmedal@msn.com> Sun, Nov 4, 2018 at 1:08 AM
To: David Cain <dcain@neieng.com>, Carson Bates <nbates@mymail.mines.edu>

Fine with me.

Keith

On November 3, 2018, at 10:00 PM, David Cain <dcain@neieng.com> wrote:

Yup, that looks good to me!

David Cain
NEI Electric Power Engineering
Electrical Engineer | dcain@neieng.com
(p) 303-431-7895 x 406

On Nov 3, 2018, at 9:56 PM, Carson Bates <nbates@mymail.mines.edu> wrote:

Hi Keith and David,

I would like to use 3 of the papers we coauthored in my dissertation in their entirety. According to IEEE copyright policy, this is acceptable if I receive permission from the coauthors. Do I have your permission to use these papers as appropriately cited below?

C. Bates, K. Malmedal, and D. Cain, "Cable Ampacity Calculations: A Comparison of Methods," *IEEE Trans. Ind. Appl.*, vol. 52, no. 1, pp. 112–118, 2016.

K. Malmedal, C. Bates, and D. K. Cain, "The Heat and Buried Cable Conundrum: A Method to Help Determine Underground Cable Ampacity," *IEEE Ind. Appl. Mag.*, vol. 22, no. 5, pp. 20–31, 2016.

K. Malmedal, C. Bates, and D. Cain, "On the Use of the Law of Times in Calculating Soil Thermal Stability and Underground Cable Ampacity," *IEEE Trans. Ind. Appl.*, vol. 52, no. 2, pp. 1215–1220, Mar. 2016.

Thank you,
Carson

RightsLink®

Home | Create Account | Help

Title: Power Cable Rating Calculations - A Historical Perspective [History]
Author: C. Holyk
Publication: IEEE Industry Applications Magazine
Publisher: IEEE
Date: July-Aug. 2015

LOGIN

If you're a copyright.com user, you can login to RightsLink using your copyright.com credentials.

Already a RightsLink user or want to learn more?

Thesis / Dissertation Reuse

The IEEE does not require individuals working on a thesis to obtain a formal reuse license, however, you may print out this statement to be used as a permission grant:

Requirements to be followed when using any portion (e.g., figure, graph, table, or textual material) of an IEEE copyrighted paper in a thesis:

1) In the case of textual material (e.g., using short quotes or referring to the work within these papers) users must give full credit to the original source (author, paper, publication) followed by the IEEE copyright line © 2011 IEEE.
2) In the case of illustrations or tabular material, we require that the copyright line © [Year of original publication] IEEE appear prominently with each reprinted figure and/or table.
3) If a substantial portion of the original paper is to be used, and if you are not the senior author, also obtain the senior author's approval.

Requirements to be followed when using an entire IEEE copyrighted paper in a thesis:

1) The following IEEE copyright/ credit notice should be placed prominently in the references: © [year of original publication] IEEE. Reprinted, with permission, from [author names, paper title, IEEE publication title, and month/year of publication]
2) Only the accepted version of an IEEE copyrighted paper can be used when posting the paper or your thesis on-line.
3) In placing the thesis on the author's university website, please display the following message in a prominent place on the website: In reference to IEEE copyrighted material which is used with permission in this thesis, the IEEE does not endorse any of [university/educational entity's name goes here]'s products or services. Internal or personal use of this material is permitted. If interested in reprinting/republishing IEEE copyrighted material for advertising or promotional purposes or for creating new collective works for resale or redistribution, please go to http://www.ieee.org/publications_standards/publications/rights/rights_link.html to learn how to obtain a License from RightsLink.

If applicable, University Microfilms and/or ProQuest Library, or the Archives of Canada may supply single copies of the dissertation.

BACK | CLOSE WINDOW

Copyright Clearance Center

Confirmation Number: 11760728
Order Date: 10/29/2018

Customer Information

Customer: Nick Bates
Account Number: 3001358030
Organization: Nick Bates
Email: nbates@mines.edu
Phone: +1 (720) 217-7974
Payment Method: Credit Card ending in 2003

This is not an invoice

Order Details

Course: DOCTORAL DISSERTATION

University/Institution: COLORADO SCHOOL OF MINES **Instructor:** Pankaj Sen
Start of term: 08/01/2018 **Your reference:**
Course number: **Accounting reference:**
Number of students: 1 **Order entered by:**

Rating of electric power cables : ampacity computations for transmission, distribution, and industrial applications

Billing Status: **Charged to Credit Card**

Order detail ID: 71635405
ISBN: 9780070017917
Publication Type: Book
Publisher: MCGRAW-HILL
Rightsholder: MCGRAW-HILL EDUCATION
Author/Editor: ANDERS, GEORGE J. ; Institute of Electrical and Electronics Engineers

Permission Status: **Granted**
Permission type: Use in electronic course materials
Page range(s): 14,60,62,63,296,417
Total number of pages: 6
Number of students: 1
Payment Method: CC ending in 2003 **$4.58** **($4.58 per student)**

Total order items: 1 **Order Total: $4.58**

Gmail Carson Bates <car333son@gmail.com>

USAmp Prime Screenshot Publication

Wael Moutassem <wmoutassem@usi-power.com> Mon, Nov 5, 2018 at 11:54 AM
To: Carson Bates <carsonbates@gmail.com>

Hey Carson,

I took a look at it during the weekend. Yes, you can go ahead with it.

Good luck with your dissertation!

Regards,

Wael

From: Carson Bates <carsonbates@gmail.com>
Sent: Monday, November 5, 2018 1:48 PM
To: Wael Moutassem <wmoutassem@usi-power.com>
Subject: Re: USAmp Prime Screenshot Publication

Hi Wael,

I don't mean to rush you, but I do need to finalize the dissertation soon. Is it acceptable to include this in my dissertation?

Thank you,

Carson

On Thu, Nov 1, 2018 at 3:20 PM Wael Moutassem <wmoutassem@usi-power.com> wrote:

> Thanks Carson. I will review and get back to you.
>
> Regards
>
> Wael
>
> Get Outlook for Android
>
> ---
>
> **From:** Carson Bates <carsonbates@gmail.com>
> **Sent:** Thursday, November 1, 2018 11:15:08 AM
> **To:** Wael Moutassem
> **Subject:** Re: USAmp Prime Screenshot Publication

Hi Wael,

Yes, I missed this year due to other conferences and finishing my PhD. I really wanted to attend, and I'm looking forward to being there in the spring.

Please see attached extract. I'd be happy to receive any comments/corrections you may have on it.

Thank you,

Carson

On Thu, Nov 1, 2018 at 9:01 AM Wael Moutassem <wmoutassem@usi-power.com> wrote:

> Hi Carson,
>
> Thanks for your enquiry. Can you share with me the screenshots that you plan to use.
>
> I missed you at the conference this week. I believe you informed Dave that you won't be able to make it.
>
> Best regards,
>
> Wael
>
> Get Outlook for Android
>
> ---
>
> **From:** Carson Bates <carsonbates@gmail.com>
> **Sent:** Thursday, November 1, 2018 12:05:00 AM
> **To:** Wael Moutassem
> **Subject:** USAmp Prime Screenshot Publication
>
> Hi Wael,
>
> Thanks for your willingness to let me use a trial version of your software for my doctoral pursuit. Is it acceptable for me to use about 5 screenshots of the program in my dissertation? I have cited your website for additional info as follows:
>
> [35] "USAMP PRIME: INSULATED CABLE AMPACITY SOFTWARE - USi," *USi*. [Online]. Available: http://www.usi-power.com/software-applications-usamp/. [Accessed: 31-Mar-2018].
>
> Thank you,
>
> Carson Bates

Gmail

Carson Bates <car333son@gmail.com>

Follow Up

David Dunkin <DDunkin@wrightsmedia.com> Fri, Nov 2, 2018 at 3:54 PM
To: Carson Bates <carsonbates@gmail.com>

Carson,

Yes, that is acceptable. You are cleared for usage.

Regards,

-Sent From My iPhone-

David Dunkin | Licensing & Content Manager
Wright's Media
2407 Timberloch Place, Suite B
The Woodlands, Texas 77380
O: 281-419-5725 x113
Toll: 877-652-5295

From: Carson Bates <carsonbates@gmail.com>
Sent: Friday, November 2, 2018 4:03:08 PM
To: David Dunkin
Subject: Re: Follow Up

Hi David,

Thanks for the response. The school does publish the dissertation for academic purposes. Is this acceptable? It will be cited in the dissertation and listed in the references. The attached document shows the quote cited in IEEE format as [37].

B. Sjodin, "What's The Difference Between FEM, FDM, and FVM?," *Machine Design*, 18-Apr-2016. [Online]. Available: http://www.machinedesign.com/fea-and-simulation/what-s-difference-between-fem-fdm-and-fvm. [Accessed: 13-Nov-2017]

Thank you,
Carson

On Fri, Nov 2, 2018 at 2:47 PM David Dunkin <DDunkin@wrightsmedia.com> wrote:

> Hi Carson,
>
> As long as it is not going to be published, you may use the content in your dissertation free of charge.
>
> Regards,
>
> **David Dunkin | Licensing & Content Manager**
>
> **Wright's Media**
> 2407 Timberloch Place, Suite B
> The Woodlands, Texas 77380
> O: 281-419-5725 x113

Cigre ELT 104 Current ratings of cables Copyright Permission

Central Office
21, rue d'Artois
75008 Paris
France

T: +33 (1) 53 89 12 90
F: +33 (1) 53 89 12 99
W: cigre.org

Carson Bates
491 Crawford St
Golden,
CO 80401
USA

Our reference: Copyright CIGRE 2018-11

7 november 2018

Dear **Mr. Bates**,

I am authorized to grant permission to use the material from CIGRE publications in connection with the project below:

- ***Title:*** Academic doctoral dissertation "*Underground Cable Ampacity: A Fresh Look at Addressing the Future Electric Grid*"
- ***Author:*** *Carson Bates*
- ***Publisher:*** *Colorado School of Mines 1500 Illinois St Golden, CO, USA 80401*
- ***Date of publication:*** *December 2018*

The specific material, text and figures, from CIGRE publications to be included in this project is described in the attached appendix.

Non-exclusive, irrevocable, royalty-free permission to use this material is granted for world rights distribution, with permission to modify the text, including figures and photographs to fit the needs of the new document and to reprint in all future revisions and editions of the resulting book.

It is required to include an acknowledgment in the front matter and use the standard attribution footnote as shown: <*Material*> reprinted with permission from CIGRE, <*title of work from which material is excerpted*>, © <*copyright year*>.

Best regards,

Philippe ADAM
Secretary General

Association Loi 1901 TVA : FR 784330201 Siret : 78433020100038 APE : 7219Z

Appendix to the letter

Copyright CIGRE 2018-11 of 7th november 2018

ELECTRA Article Ref. ELT_104_2
Current ratings of cables buried in partially dried-out soil Part 1
WG 21.02 (1986)

Quotes

"The external thermal resistance of a buried cable plays an important part in the determination of its current carrying capacity, the temperature difference between a cable surface and ambient being in the region of 50 to 70 percent of the conductor temperature rise. Of all the factors which can influence the thermal resistivity of soil, its moisture content is one of the most important, particularly so because serious changes of moisture content in soil around a cable can be caused by heat from the cable itself. A reliable value of current carrying capacity can be allocated to a cable only if the thermal behaviour of its surrounding soil is taken into account."

"A simple approach to the problem is to limit cable surface temperatures so that soil temperatures do not rise to levels at which significant migration is expected. This tends towards under-utilisation of cable materials and its economic justification usually depends on the relative value placed on the effort needed to obtain more complete soil information"

The working group states, "Workers in this subject have proposed various critical parameters such as temperature gradient, temperature difference, and heat flux density,", and follows up by stating, "Until further information is available, it is proposed in this report to use a simple temperature rise above ground ambient as the critical factor which gives the position of the dry/moist boundary and to assume that the boundary is circular in shape"